Terms and Conditions of Use of Digitised Theses from Trinity College Library Dublin

Copyright statement

All material supplied by Trinity College Library is protected by copyright (under the Copyright and Related Rights Act, 2000 as amended) and other relevant Intellectual Property Rights. By accessing and using a Digitised Thesis from Trinity College Library you acknowledge that all Intellectual Property Rights in any Works supplied are the sole and exclusive property of the copyright and/or other IPR holder. Specific copyright holders may not be explicitly identified. Use of materials from other sources within a thesis should not be construed as a claim over them.

A non-exclusive, non-transferable licence is hereby granted to those using or reproducing, in whole or in part, the material for valid purposes, providing the copyright owners are acknowledged using the normal conventions. Where specific permission to use material is required, this is identified and such permission must be sought from the copyright holder or agency cited.

Liability statement

By using a Digitised Thesis, I accept that Trinity College Dublin bears no legal responsibility for the accuracy, legality or comprehensiveness of materials contained within the thesis, and that Trinity College Dublin accepts no liability for indirect, consequential, or incidental, damages or losses arising from use of the thesis for whatever reason. Information located in a thesis may be subject to specific use constraints, details of which may not be explicitly described. It is the responsibility of potential and actual users to be aware of such constraints and to abide by them. By making use of material from a digitised thesis, you accept these copyright and disclaimer provisions. Where it is brought to the attention of Trinity College Library that there may be a breach of copyright or other restraint, it is the policy to withdraw or take down access to a thesis while the issue is being resolved.

Access Agreement

By using a Digitised Thesis from Trinity College Library you are bound by the following Terms & Conditions. Please read them carefully.

I have read and I understand the following statement: All material supplied via a Digitised Thesis from Trinity College Library is protected by copyright and other intellectual property rights, and duplication or sale of all or part of any of a thesis is not permitted, except that material may be duplicated by you for your research use or for educational purposes in electronic or print form providing the copyright owners are acknowledged using the normal conventions. You must obtain permission for any other use. Electronic or print copies may not be offered, whether for sale or otherwise to anyone. This copy has been supplied on the understanding that it is copyright material and that no quotation from the thesis may be published without proper acknowledgement.

Hypothesis testing of glenoid component innovation in total shoulder arthroplasty

Linda Ann Murphy, B.A., B.A.I.

A thesis submitted to the University of Dublin in partial fulfilment of the requirements for the degree of

Doctor in Philosophy

Trinity College Dublin

June 2002

Prof. Patrick J. Prendergast
Supervisor

Prof. dr. Frans van der Helm
External examiner

Dr. Kevin O'Kelly
Internal examiner

Contents

List of Figures

List of Tables

Declaration

I declare that the present work has not previously been submitted for a degree at any University. It consists entirely of my own work, except where references indicate otherwise.

The Trinity College Dublin Library may lend or copy this thesis on request.

Linda A Murphy

12th June 2002

List of publications and presentations

PAPERS:

LA Murphy, PJ Prendergast, H Resch, Structural analysis of an offset-keel design glenoid component compared to a centre keel design. *J Shoulder Elbow Surg,* 10: 568-579, 2001.

D Lacroix, LA Murphy, PJ Prendergast, Three-dimensional finite element analysis of glenoid replacement prostheses: a comparison of keeled and pegged anchorage systems. *J Biomech Eng*, 122: 430-436, 2000.

PJ Prendergast, LA Murphy, Selection of glenoid prosthesis-type based on an assessment of glenoid bone. *Proc 3rd Conference of the International Shoulder Group,* 83-86, DUP Science: Delft, 2000.

PRESENTATIONS BY THE AUTHOR:

LA Murphy, PJ Prendergast, Similarity of strain data between finite element models and photoelastic models of the scapula, *13th Conference of the ESB,* in press, 2002.

LA Murphy, PJ Prendergast, Analysis of acromial fixation of glenoid components using a 3D finite element model of the scapula with comparison to results using the photoelastic technique. *4th World Congress of Biomechanics,* in press, 2002.

LA Murphy, PJ Prendergast, Can acromion fixation prevent loosening of the glenoid component in TSA? *Trans 48th ORS Annual Meeting,* 2002.

LA Murphy, PJ Prendergast, Similarity of strain data between finite element models and photoelastic models of the scapula. *Proc 8th Bioengineering in Ireland,* p 82, 2002.

LA Murphy, PJ Prendergast, R Christie, H Resch, Finite element analysis predicts lower cement stresses for an offset-keel glenoid component compared to a centre-keel design. *Trans 47th ORS Annual Meeting,* p 787, 2001.

LA Murphy, PJ Prendergast, R Christie, An evaluation of acromion fixation of glenoid components in TSA. *Proc 7th Bioengineering in Ireland,* p 16, 2001.

LA Murphy, D Lacroix, PJ Prendergast, 3D Finite element analysis of pegged and keeled glenoid replacement components. *Proc 4th Sir Bernard Crossland Symposium,* p 144, 2000.

LA Murphy, PJ Prendergast, R Christies, H Resch, Finite element analysis of an offset keeled glenoid prosthesis compared to a centre keeled design. *Proc 12th Conference of the ESB,* p 160, 2000.

LA Murphy, PJ Prendergast, A finite element stress analysis of a centre-keel prosthesis compared to an anterior offset-keel prosthesis in normal and Rheumatoid Arthritic bone. *Proc 3rd International Shoulder Conference,* 2000.

LA Murphy, D Lacroix, PJ Prendergast, 3D Finite element analysis of pegged and keeled glenoid replacement components: an analysis of cement stresses. *Proc 9th Conference of the EORS,* 1999.

LA Murphy, D Lacroix, PJ Prendergast, 3D Finite element analysis of pegged and keeled glenoid replacement components. *ULBMI Annual Research Day,* 1999.

LA Murphy, D Lacroix, DP Fitzpatrick, PJ Prendergast, Stress in glenoid bone with pegged versus keeled glenoid components: a finite element study. *J Bone Joint Surg [Br],* 81-B, p 94, 1999.

LA Murphy, D Lacroix, BP Murphy, PJ Prendergast, Comparison of pegged and keeled glenoid components: a probability of failure analysis using FE data. *Proc Bioengineering in Ireland,* p10, 1999.

PRESENTATIONS BY OTHERS OF THE WORK MADE IN THIS THESIS:

D Lacroix, LA Murphy, PJ Prendergast, DP Fitzpatrick, Replacement of the glenoid in total shoulder arthoplasty: a finite element analysis. *Ir J Med Sc Vol,* 167 (4), p 275, 1998.

TC Lee, D Lacroix, LA Murphy, PJ Prendergast, Form and function – a three-dimensional finite element analysis of the scapula. *J Anatomy,* 193, p 303, 1998.

H Resch, PJ Prendergast, LA Murphy, Structural analysis of an offset-keel design glenoid component compared to a centre keel design. *Proc 1st closed meeting European Society for Surgery of the Shoulder and the Elbow,* p 33, 2001.

H Resch, PJ Prendergast, LA Murphy, Structural analysis of an offset keel glenoid component compared to a centre keel design. *Proc. 8th International Congress on Surgery of the Shoulder.* p 98, 2001.

Acknowledgements

I would like to thank my supervisor, Prof. Patrick Prendergast, for his constant guidance and help throughout my research and also for the many opportunities he has provided me with.

At the start of my research I received a lot of valuable guidance and help from Damien Lacroix, thanks Damien. Also, I would like to thank Alex for his help with the temperamental biostation, Suzanne for her general advice. Many thanks to Peter for his assistance using the Instrons and to the other technicians for their help.

During the course of my work here in Trinity College Dublin, I have made many great friends. I have particularly enjoyed working with the Bioengineering group, Damien, Suzanne, Peter, Bruce, Alex, Adriele, Seosamh, Danny, John, Laoise, Triona, James and Laura and have enjoyed watching the development of the group into various interesting research areas over the past couple of years. More importantly, I have thoroughly enjoyed their company and the great time we've had, mainly over a few pints. Much of which is down to Prof. Prendergast who has a particular talent in selecting students who "fit right in". I have also enjoyed working amongst the many other postgrads, including Fergal, Richard, Mary and Kevin. I will see you all at the Garden party next year.

Finally, many thanks to my parents for all their support over the years and to my family, Susan, Martin and Tony. Also to my friends, particularly Bruce and Helen, who have sponsored my social life for the past few weeks! I owe you all lots of money when I get a job.

Abstract

A glenoid component with reliable long-term performance does not exist for total shoulder arthroplasty. Poor glenoid component durability may be explained by the huge variability that exists at the shoulder joint pre-operation. Furthermore, factors such as the *ageing population* and the low average age associated with total shoulder arthroplasty patients can only highlight the necessity to increase glenoid component durability. Despite this need, designs introduced to the market continue to lack rigorous biomechanical testing, and the problem of glenoid component loosening is far from solved. The author proposes that glenoid component durability can be imporved by pre-clinical testing eliminating weak designs before continuing to costly clinical trials. The specific mode of investigation persued in this thesis is "hypothesis-based" research. From the universal statement that glenoid component performance weakens total shoulder arthroplasty, statements of a lesser universiality ("hypotheses") regarding glenoid component designs are deduced and tested.

A complex geometry, three-dimensional muscle and joint loading, and range of materials exist at the shoulder joint. In addition the joint experiences huge variability depending on the pathology, this makes bench testing problematic, and therefore, the method of three-dimensional finite element analysis is used. With adequate representation of the real situation, three hypotheses on glenoid component design are tested.

The results corroborate the hypotheses showing that (i) greater durability to prevent glenoid loosening is provided by a pegged prosthesis in normal bone and a keeled prosthesis in compromised glenoid bone: (ii) an anterior offset keel provides better durability than a centre keel design: and (iii) attachment of the scapular-side component to the acromion may lead to component failure. Clinically significant deductions are then made on the basis of these three hypotheses showing that: Glenoid material property distribution plays an essential role in glenoid component design; it is essential to use *good* quality bone to its best advantage; removal of *bad* quality bone and replacement with better quality material, results in a decrease of cement stresses and essentially a lower probability of failure for the implant; remaining *good* bone is left to provide good support to the prosthesis.

Chapter 1

Introduction

1.1 Total shoulder arthroplasty

Total joint replacement has become a common surgical procedure, with high expectation for both immediate and long-term benefits by the general population. It is performed to alleviate pain and debilitation caused by osteoarthritis (OA)*, rheumatoid arthritis (RA)†, fractures, dislocations, congenital deformities, and other joint related problems. In most uncomplicated cases, pain is eliminated or very much relieved and considerable mobility is re-established. However, complications can occur and improvements can always be made. Replacement surgery of joints, such as the hip and knee, has improved immensely over the past thirty years. Unfortunately, shoulder arthroplasty has not followed the same trend. This may be partly attributed to the lower number of shoulder arthroplasties performed and the corresponding slower development rate. Furthermore, the complicated geometry of the shoulder, and the very complex range of muscle and joint forces, results in many design challenges. These, and other related issues, are developed in this introductory chapter.

Total shoulder arthroplasty or TSA is the name given to a procedure where both sides of the glenohumeral joint are replaced, i.e. the glenoid of the scapula and the head of the humerus, see Fig.1.1. The primary indications for TSA include pain and loss of normal glenohumeral articulation and the most common diagnoses for patients who receive a TSA are OA, RA, osteonecrosis, acute fracture and post-traumatic arthritis (Cofield, 1994).

An active range of motion may not be reliably restored with shoulder replacement, especially in cases of long-standing joint disease, such as RA. This fact is particularly important when we consider that up to 90% of patients hospitalized with RA have problems relating to the shoulder (Petersson, 1986).

---

* *Osteoarthritis* ("wear and tear" arthritis): This type of arthritis is produced by degeneration of the cartilage found at the joint surfaces and by overgrowth of bone at the margin of the joint.

† *Rheumatoid arthritis* is characterized by swelling of the joint capsule, progressive joint destruction, which also extends to the surrounding muscles, and fibrous and osseous fusion of bones across the joint space.

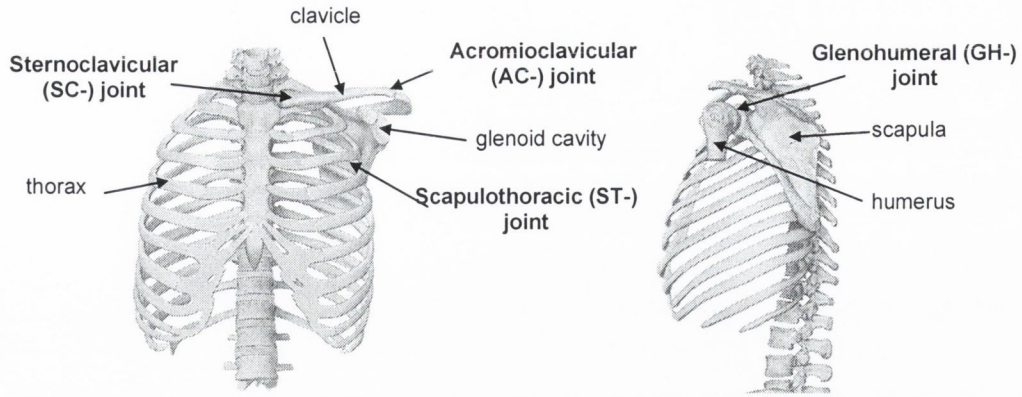

Figure 1.1 *Anatomy of the shoulder joint, with the four joints of the shoulder mechanism in bold. Adapted from Shier et al., 1999.*

The main stabilizing muscles of the shoulder joint are collectively known as the "rotator cuff" which consists of the supraspinatus, infraspinatus, subscapularis and teres minor, see Fig. 1.2. The scapula extends up and around the shoulder joint to form the acromion and at the front to form the coracoid process. Normal motion of the humerus results from the simultaneous motions of the sternoclavicular (SC-) joint, the scapulothoratic joint (ST-), the acromioclavicular (AC-) joint and the glenohumeral (GH-) joint, as shown in Fig. 1.1. A large array of muscles exist at the joint which contribute to its large range of motion. The major muscles include the trapezius, which runs from the neck area down to the top of the shoulder blade and the deltoid, which runs from that point downward into the upper arm. These particular muscles contribute mainly to raising and lowering of the arm.

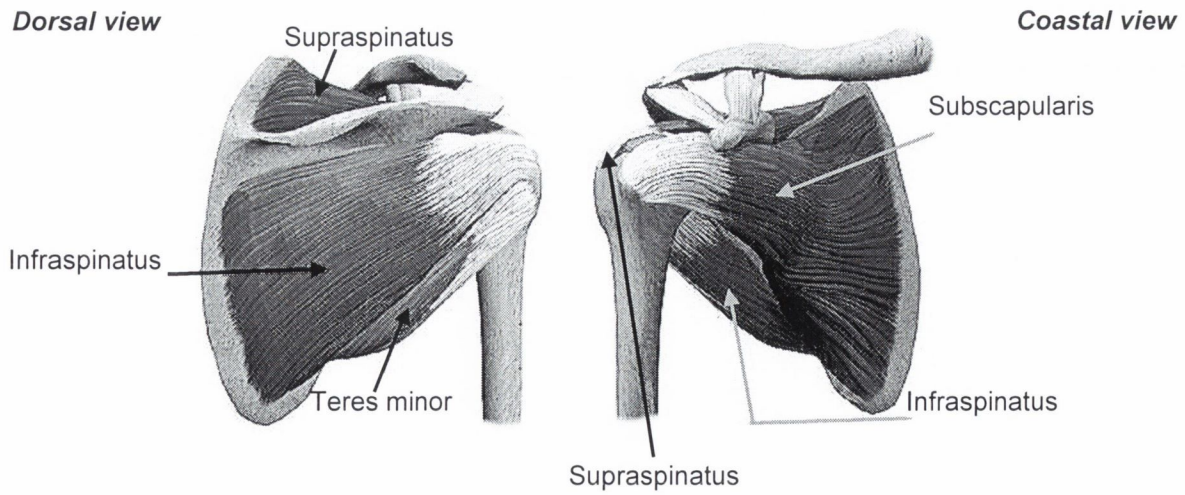

Figure 1.2 *Rotator cuff muscles. Adapted from the Medical Multimedia Group, 1999 (www.medicalmultimediagroup.com).*

Surgically TSA has been described as "the most technically demanding of current joint replacement procedures" (Neer and Morrison, 1988). This is mainly due to the difficulty in gaining sufficient exposure of the joint when performing surgery and the shoulder's reliance on soft tissue for stability. The surgical procedure of TSA, illustrated schematically in Fig. 1.3, involves removal of the humeral head with accurate reaming of the medullary canal of the humerus. This is followed by insertion of a humeral component, generally fixated with polymethylmethacrylate (PMMA) bone cement. The glenoid of the scapula is then replaced to provide an articulating surface for the humeral component.

A lower number of shoulder arthroplasties and a slower development rate have been mentioned in comparison to the hip and knee. Regarding this statement, statistics show that in the USA (population approximately 286 million) about 15,000 shoulder replacements (TSA or hemiarthroplasty) are carried out each year compared to 500,000 hip and knee operations (AAOS, 2001), see Fig. 1.4. In comparison, Norway, with a population closer to that of the Republic of Ireland ($\approx$ 4.5 million and $\approx$ 3.8 million respectively), has an average of 133 shoulder arthroplasties each year, see Table 1.1. Similar published data does not exist for the Republic of Ireland. However, Table 1.2 shows the number of shoulder replacements carried out in the Republic of Ireland in the years 1998 to 2000 (received by personal communication, Hospital in patient enquiry 1999 and Voluntary Health Insurance 2000, Ireland). This shows that, in the year 2000, a total of 200 shoulder arthroplasties were carried out in the Republic of Ireland. With this in mind, and noting that the ageing population is a well-known demographic trend, it is essential that shoulder arthroplasty becomes a more successful procedure.

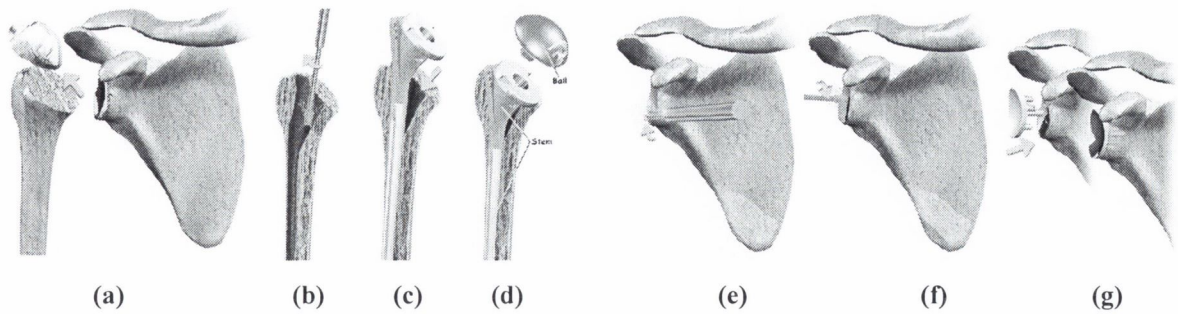

Figure 1.3 *TSA Surgical technique,* ***(a)*** *removal of the humeral head,* ***(b)*** *reaming of the humeral canal,* ***(c)*** *insertion of a humeral component,* ***(d)*** *humeral component with a modular head,* ***(e)*** *burring of the glenoid,* ***(f)*** *reaming of the glenoid and* ***(g)*** *insertion of a glenoid component. Adapted from the Medical Multimedia Group, 1999 (www.medicalmultimediagroup.com).*

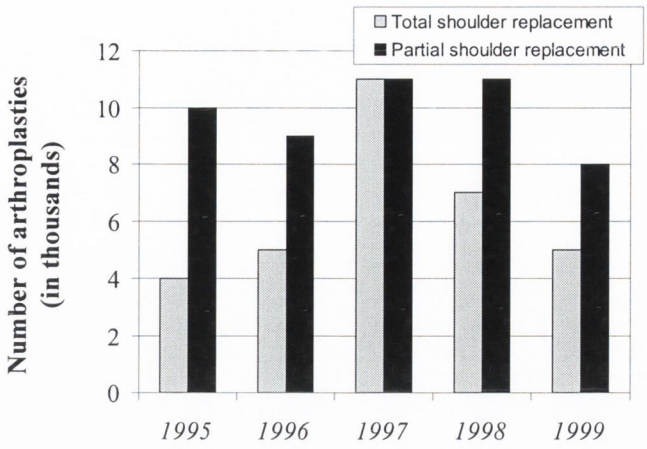

Figure 1.4 *Arthroplasty and total joint replacement procedure figures from the American Academy of Orthopaedic Surgeons (2001). USA population is approximately 286 million.*

Table 1.1 *Total shoulder arthroplasty and hemiarthroplasty statistics from the Norwegian Register.*

Arthroplasty	*1994*	*1995*	*1996*	*1997*	*1998*	*1999*	*2000*
Total shoulder replacement	28	31	29	15	10	24	26
Hemiarthroplasty	93	85	92	133	119	134	111

Table 1.2 *Total shoulder arthroplasty and hemiarthroplasty statistics from the Republic of Ireland with the HIPE Scheme (public sector) and VHI Healthcare (private sector).*

Sector	*1998*	*1999*	*2000*
Public	29	36	57
Private	54	96	143

1.2 The problem of glenoid component loosening

Considering design and durability of glenoid components, many factors must be taken into account; these include the large forces at the glenoid surface and the small amount of bone for fixation. Other factors include selecting appropriate materials, shape of the subchondral contact surface, radius of curvature of the articulating surface, surface area of articulation, component thickness, type of anchorage system, and the method of fixation. Adequate durability is imperative given that the average age for shoulder replacement is the lowest among those for all major joint replacements (Wirth and Rockwood, 1996). As it stands, nearly half of all young patients who have a shoulder arthroplasty have an unsatisfactory result (Sperling *et al.*, 1998) and follow-up studies have shown that glenoid component loosening is still the most frequently encountered

long-term complication in TSA (Wirth and Rockwood, 1994). Consequently, one of the critical questions to be addressed in this thesis is simply: "Can the rate of loosening of glenoid prostheses be reduced?"

It has been proposed that the complications associated with loosening are hastened by tears of the rotator cuff, by conforming prostheses, and by incorrect prosthesis positioning (Ibarra *et al*, 1998). In addition, the small amount of glenoid bone available for fixation may be diminished further by the effects of RA, increasing the probability of loosening. It is clear, therefore, that a pre-clinical comparison of glenoid prosthesis performance in *healthy* shoulder joints is unsatisfactory since the majority are, in fact, placed in quite unhealthy RA joints.

In this thesis, the author will argue that it is imperative that TSA durability is improved by testing the biofunctionality of glenoid components with rigorous engineering methods prior to clinical use. Testing must include analysis of prosthesis durability with the various glenoid bone and muscle qualities which are observed clinically. To date, the author believes that pre-clinical testing of glenoid prostheses has not been performed to a sufficiently high level, resulting in a plethora of designs available to the orthopaedic surgeon. Many of these designs have no rigorous biomechanical basis. Trial and error approaches to prosthesis implantation is not sufficient, particularly where patient pathologies are so variable. It is worthwhile to quote Brems (1993): "The surgeon should not alter the bone to fit the implant morphology; rather, the bone morphology should dictate the choice of implant used".

1.3 Three hypotheses regarding glenoid component design

As discussed above, there are many glenoid component designs on the market – perhaps too many. Figure 1.5 shows some of these components. Glenoid component designs may be broadly classified as either "pegged" or "keeled". It is the contention of this thesis that glenoid component fixation can be very much improved if rigorous design assessment is carried out. This design assessment will be based fundamentally on the pre-clinical testing platform suggested by Prendergast and Maher (2001) where computational and experimental testing procedures are used. To defend this thesis, the author proposes to test three hypotheses. These are:

1.3.1 Hypothesis 1

"A pegged prosthesis provides greater potential durability to prevent glenoid loosening in normal bone whereas a keeled prosthesis is recommended when there is compromised glenoid bone", i.e. destruction of the bone due to OA or RA. This hypothesis has been proposed in commercial marketing brochures (Rockwood and Matsen, 1992) but has never been scientifically tested.

1.3.2 Hypothesis 2

"An anterior offset keel provides better durability than a centre keel design due to its more central alignment in the glenoid bone". This hypothesis was put to the author by Professor Herbert Resch, University of Salzburg, Austria.

1.3.3 Hypothesis 3

"Secure fixation is difficult to achieve for glenoid components, additional attachment to the acromion reduces loosening rates". This hypothesis is the basis of a prosthesis used by Professor Oliver Gagey, University of Paris, France.

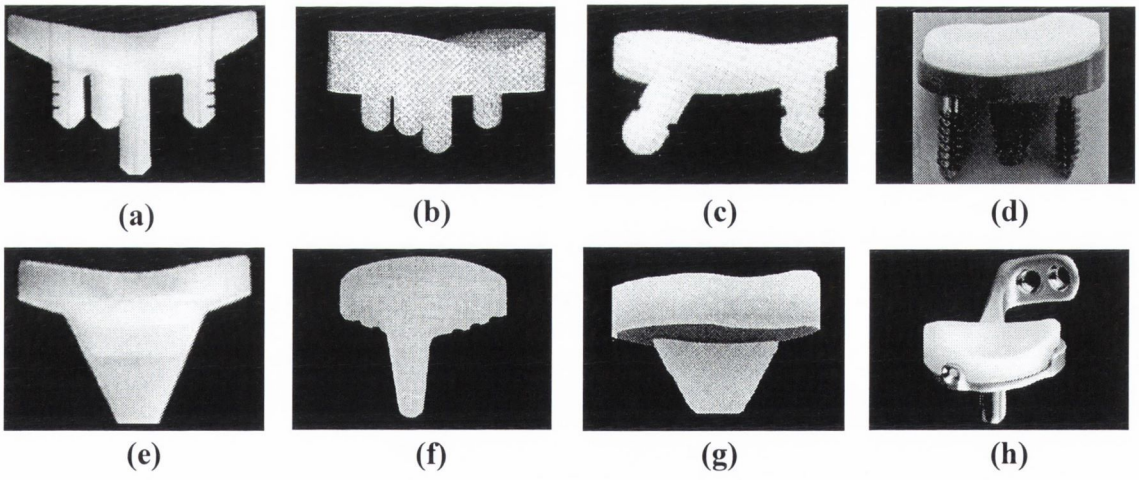

Figure 1.5 *Various glenoid component designs,* ***(a)*** *an all-polyethylene five pegged component with a curved back,* ***(b)*** *an all-polyethylene five pegged component with a flat back,* ***(c)*** *an all-polyethylene two pegged component with a curved back and one angled peg,* ***(d)*** *pegged component with metal-backing, polyethylene liner and screw fixation,* ***(e)*** *an all-polyethylene center-keeled component,* ***(f)*** *an all-polyethylene anterior offset-keeled component,* ***(g)*** *a polyethylene center-keeled component with metal-backing and* ***(f)*** *an acromion fixated design with metal-backing and screw fixation.*

1.4 Conclusion

Replacement surgery of joints such as the hip and knee has improved immensely over the past thirty years whereas shoulder arthroplasty has not shared this success. Glenoid component fixation is the weak link in TSA. This is why there is continued interest and design activity taking place with respect to it. However, a question posed in 1979 by Clarke *et al.,* was:

> "Why are new designs being considering for surface replacement of the shoulder when so many designs already exist?"

The author would like to revisit this question. In the twenty years since this was first posed, a constant introduction of new innovative designs (without rigorous scientific testing) has continued apace. As a result, and perhaps it is to be expected, an abundance of relatively ineffective TSA systems exist and the situation seems to have been reached where problematic glenoid component loosening has become an accepted fact in TSA. The author suggests, therefore, that prosthetic durability must be enhanced by testing the biofunctionality of glenoid components with rigorous engineering methods prior to clinical use. Thus allowing the surgeon to select glenoid prostheses pre-operation which have been passed through meticulous pre-clinical, and subsequently, clinical trials. If prosthesis functionality is better understood, appropriate selection of prostheses based on the individual patient pathology can be achieved with the ultimate objective of reducing glenoid component loosening rates. Therefore, it is the authors thesis that a pre-clinical testing method used to test clear-cut hypotheses regarding a joint arthroplasty (such as the three above) can give the correct direction for further development of high performance devices.

Chapter 2

Literature Review

2.1 Introduction

The objective of this chapter is to present a description of the shoulder joint and to review the development of total shoulder arthroplasty (TSA). The chapter concludes with an analysis of the differences in the published work and an analysis of the requirements necessary to enhance the performance of glenoid components.

2.1.1 Anatomy of the shoulder joint

The shoulder mechanism is a chain of bones connecting the upper extremity to the trunk. The four bony elements include the thorax, clavicle, scapula and humerus. The scapula is a flat, triangular bone possessing three bony processes: the coracoid, the spine, and the acromion. With the arm at the side, the scapula overlaps the second to seventh ribs, its long axis being nearly vertical, see Fig. 1.1. The bone consists of costal and dorsal surfaces, and medial and lateral borders, see Fig. 2.1. Most of the scapula consists of a thin layer of cortical bone with the three processes and the thickened lateral border consisting of cancellous bone. The prominent bony processes and thickened areas serve as muscle attachment sites (Pegington, 1991). The clavicle is located between the sternum and the acromion. Functionally, it serves to connect the upper extremity to the axial skeleton. The shape of the glenoid itself is shown in Fig. 2.2.

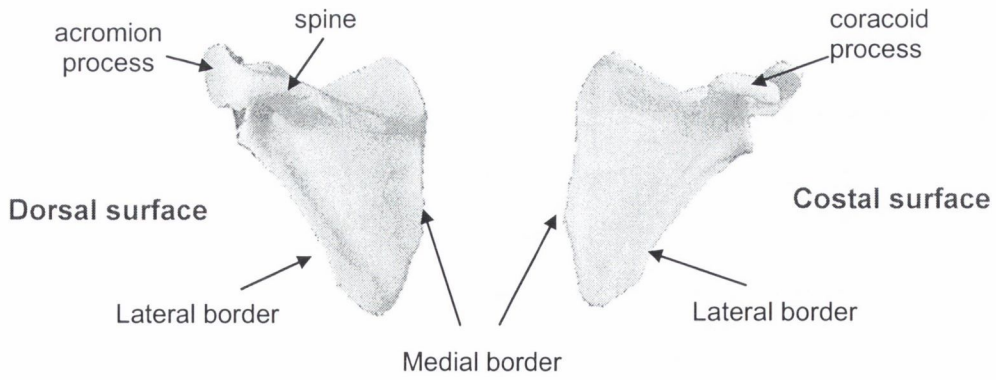

Figure 2.1 *Anatomy of the scapula, adapted from Shier et al., 1999.*

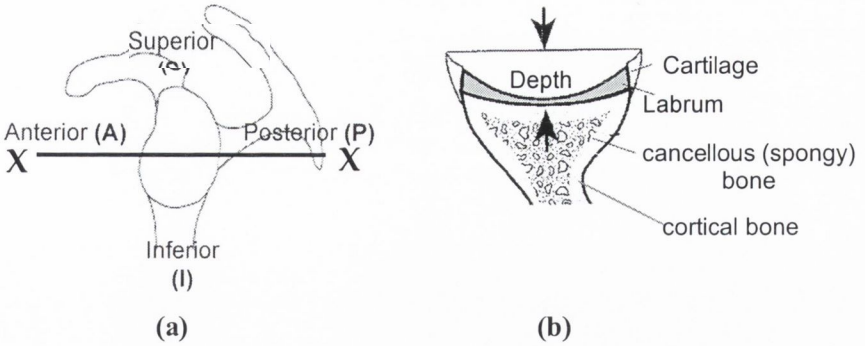

Figure 2.2 ***(a)*** *Superior, anterior, posterior and inferior aspects of the glenoid of a left scapula. X-X is a cross-section taken through the glenoid and is shown in figure* ***(b)*** *identifying the labrum etc. of the glenoid.*

The interaction of the muscles (Fig. 2.3) and four bony elements of the shoulder mechanism achieve a large range of motion for the upper extremity. This results in the most mobile of all limbs in the human body. It is also unique in that it is a three degree-of-freedom system with abduction or adduction about the anterior-posterior axis, flexion or extension about the transverse axis and internal or external rotation about the humeral axis, see Fig. 2.4. The muscle origin and insertions are given in Table 2.1.

The muscles can be broadly classified either as primary movers or primary stabilisers. The primary movers consist of the deltoid, pectoralis major, latissimus dorsi, and teres major. They are largely responsible for rotating the glenohumeral joint. The primary stabilisers include the supraspinatus, infraspinatus, teres minor and subscapularis, collectively termed the "rotator cuff", see Fig. 1.2. Their function is to hold the head of the humerus into the glenoid cavity and to stabilize against subluxation or dislocation; this is illustrated in Fig. 2.5. However, progression of diseases such as RA can lead to weakening of this fundamental stabilizing mechanism by deterioration of the surrounding cartilage and rotator cuff muscles, resulting in impingement and instability of the shoulder joint, see Fig. 2.5.

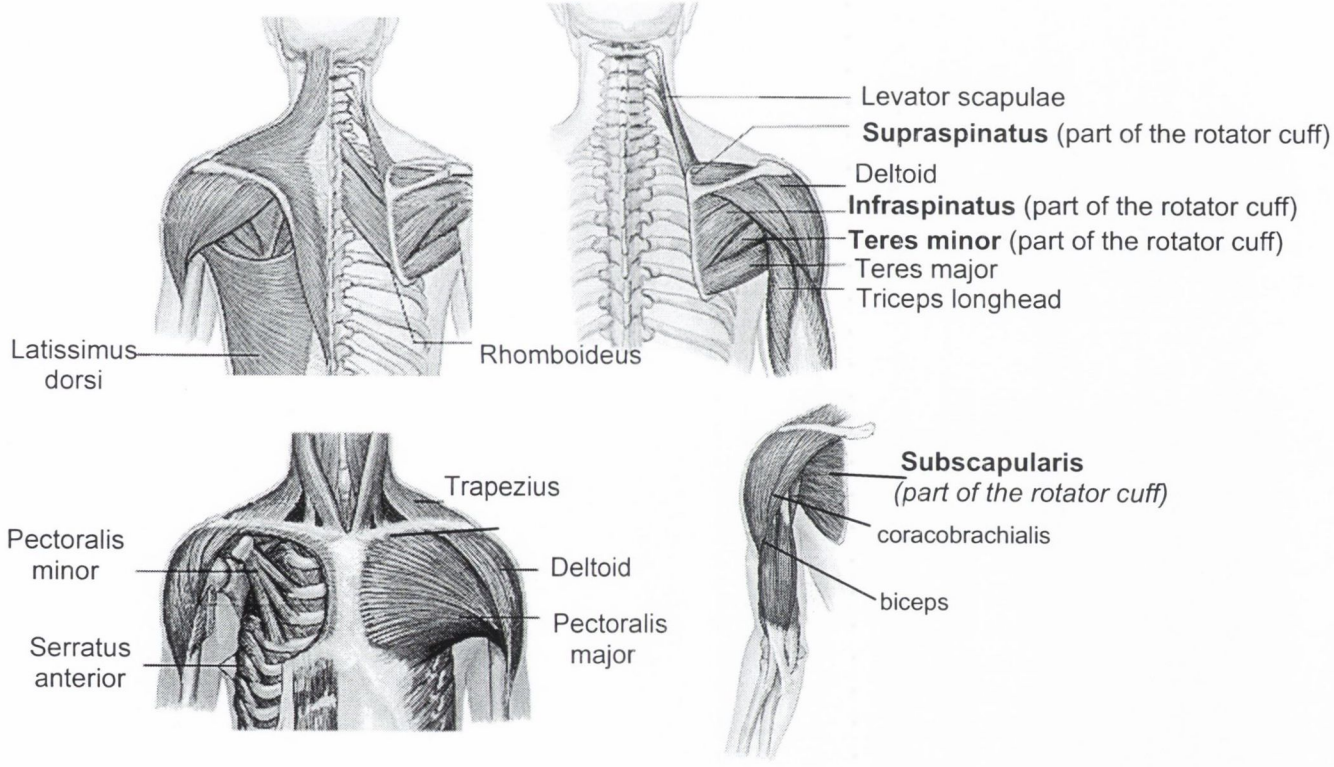

Figure 2.3 *Interaction of the muscles and the four bony elements of the shoulder mechanism achieve a large range of motion for the upper extremity. The rotator cuff muscles are shown in bold. Adapted from Shier et al., 1999.*

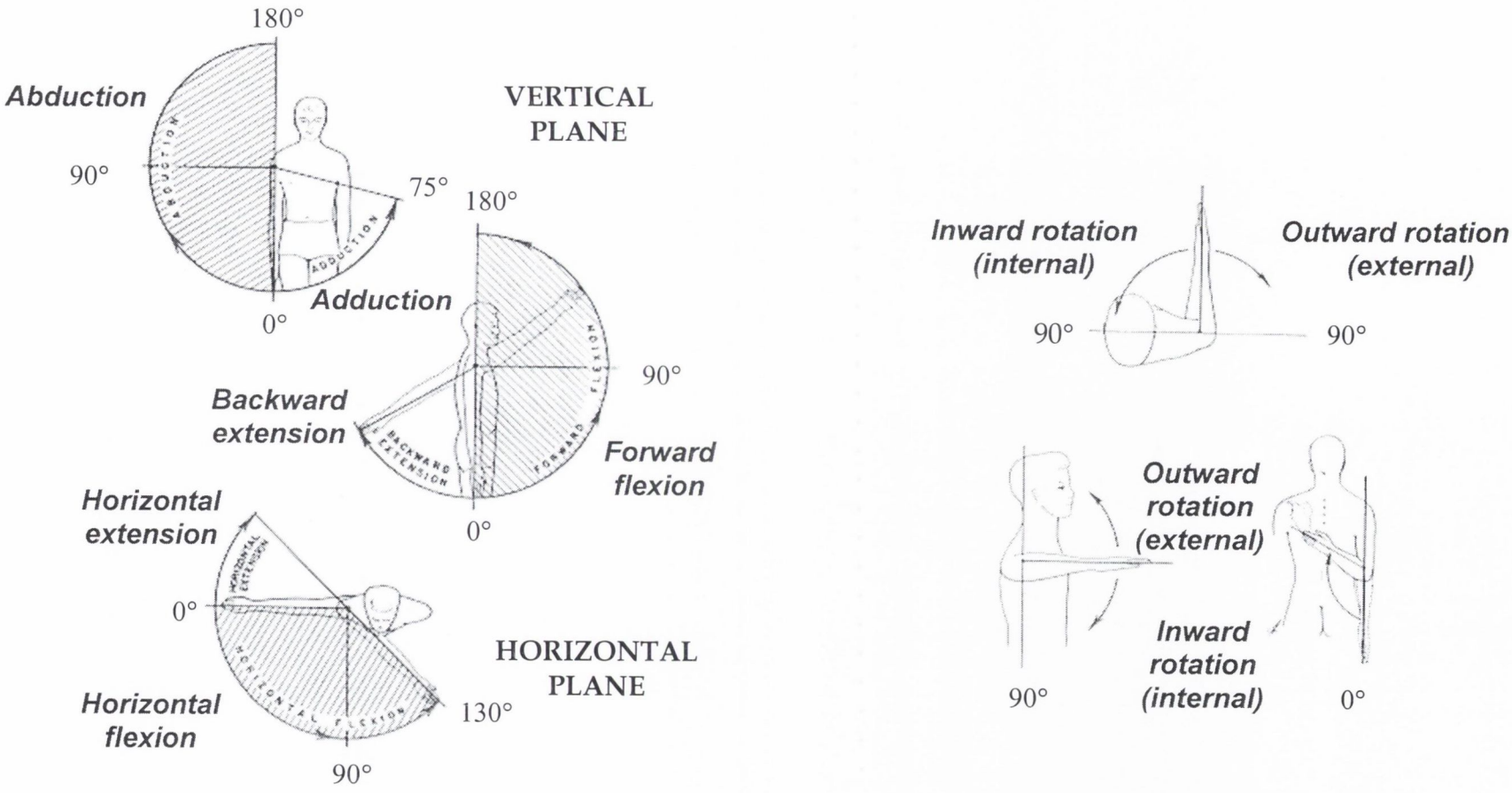

Figure 2.4 *Planes and angles of motion occurring at the shoulder, after the American Academy of Orthopaedic Surgeons, 1965.*

Table 2.1 *Origin and insertion of the muscles at the bones of the shoulder mechanism, after van der Helm (1994).*

Origin	*Insertion clavicula*	*Insertion scapula*	*Insertion humerus*
Thorax	Trapezius, clav. part Subclavius	Trapezius, scap. part Serratus anterior Levator scapulae Rhomboideus Pectoralis major	Pect. Major, thor. part Latissmus dorsi
Clavicula			Deltoidus, clav. part Pect. Major, clav. part
Scapula			Deltoidus, scap. part Subscapularis Supraspinatus Infraspinatus Teres minor Teres major Coracobrachialis Biceps, shorthead Biceps, longhead Triceps, longhead

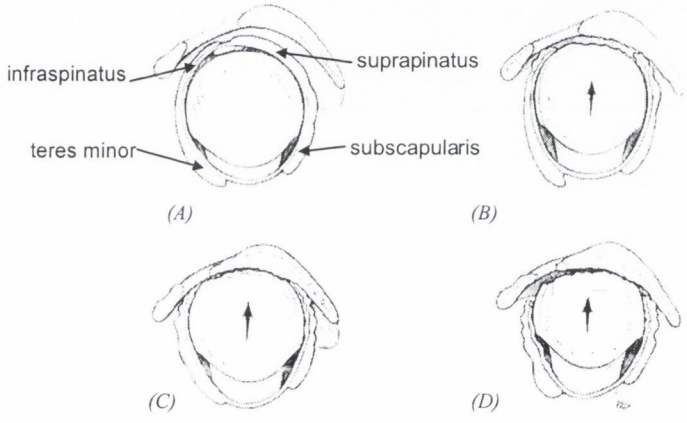

T

Figure 2.5 *(A) Normal anatomy. (B) Progressive cuff fiber failure with upward displacement of the humeral head and loading of the undersurface of the acromion. (C and D) Further cuff failure.*

The glenoid cavity is slightly deepened and enlarged by a cartilaginous rim termed the glenoid labrum, see Fig. 2.2 (b). It is believed that it also assists in lubrication and bone protection at the glenohumeral joint. Maintaining stability at this joint is complex where the large head of the humerus articulates against the glenoid surface of one-third its size. This has been likened to keeping a ball on a saucer, preventing it from revolving while applying significant forces directing its displacement from the saucer. Therefore, any weakening of the rotator cuff increases the risk of instability.

2.1.2 Pathology of the shoulder joint

Up to 90% of patients hospitalised with RA have problems with the shoulder joint, (Petersson, 1986). Moreover, most RA patients referred for shoulder arthroplasty are at the late stage of the disease with severe pathological changes including both rotator cuff tearing and degenerative glenoid bone stock (Sneppen *et al.,* 1996). Progression of RA weakens the fundamental stabilizing mechanism of the shoulder joint by deteriorating the surrounding cartilage and rotator cuff muscles. Furthermore, collapse of dead bone at the glenohumeral joint results in incongruity of the articular surfaces and joint destruction (Waldman *et al.,* 1998). Patients with RA generally have poorer functional results after TSA than those with OA.

There is a large variation in RA patient shoulder pathologies. However, it has been argued that there is a reliable pattern of progression with a pre-determined course even though all cases may not reach the final stage of disruption (Kelly, 1994). So what exactly happens in the RA patient? This may be explained as follows (Miller and Keane, 1997):

1) Inflammation of the synovium at the joint.
2) Formulation of a layer of granulation tissue that erodes and destroys the cartilage and eventually spreads to neighbouring areas, causing destruction of the bone membrane and parts of the muscles that control the joint.
3) Fibrous fusion across the joint space, resulting in invasion of the granulation tissue by tough fibrous tissue.
4) Bony fusion as the fibrous tissue becomes calcified. Also, wasting of the muscles and bones adjacent to the affected area may occur.

Evaluation of the rheumatoid shoulder, from a clinical point of view, can be carried out using the Larsen classification system. This system is based on radiographic findings ranging from zero: a normal shoulder, to Grade V: severe bony destruction, implies that a patient will go through these grades of destruction progressively. In patients with Larsen Grade IV and V, the pain source is usually from the glenohumeral joint and shoulder replacement should be considered. Indications for surgery are severe pain and limited function where the pain is emerging from the glenohumeral joint. According to Kelly

(1994) Crossan and Vallance studied 100 shoulders to obtain their five stage grading system, which focuses on the sphericity of the humeral head (preserved until the end stages), see Fig. 2.6.

Neer has described two forms of rheumatoid disease, the 'dry' type and the 'wet' type. The 'dry' type (similar to OA) is progressively slow and the bone quality remains good, with minimal erosion. In the 'wet' type the bone-quality is poor, resorption may occur and progression may be very rapid (Kelly, 1994).

This merely shows that not only is there a large variation in the degree to which patients are affected and the rate of progression of RA; there are also large variations in the classification of the stages of the disease. As a result accurate biomechanical modelling of this pathology may prove to be quite difficult.

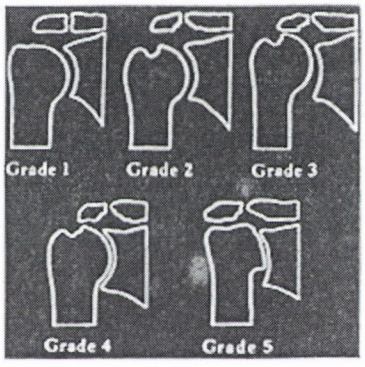

Figure 2.6 *Crossan and Vallance classification of the rheumatoid shoulder. After Kelly (1994).*

2.1.3 Kinematics and forces at the glenohumeral joint

Although the glenohumeral joint has previously been considered as a "non-weight bearing surface" (Poppen and Walker, 1978), large forces are encountered. It has been reported that one of the major activities required after shoulder arthroplasty is abduction (McCullagh, 1995) with the maximum glenohumeral load occurring for 90 degrees arm abduction angle. In a study by Davis (1977), the number of glenohumeral motions and ranges of these motions are reported showing that even the mere task of getting up requires large glenohumeral movements, see Tables 2.2 and 2.3. Table 2.2 does not include television watching, bathing, using the toilet etc., which implies that actual

movement frequency is more of the order of 1,000 movements per day. The average person walks two to four miles per day, which is equivalent to 2,500+ shoulder swings. The total is now equal to 3,500 glenohumeral motions. However, this also varies for different occupations. Therefore, for the average so-called "healthy/active" human, an approximate total of 10,000 glenohumeral movements occur per day.

Accurate measurements of the forces occurring at the shoulder joint are hard to obtain because of the difficulty involved in accurately simulating the complex system. Poppen and Walker, (1978) estimated that when the arm is positioned at 90 degrees of abduction (empty handed) the joint reaction force is approximately 0.89 times body weight. This force is greatly magnified if a weight is held or if there is sudden movement e.g. throwing or falling. More recently, Van der Helm (1994) included an analysis of the magnitude and direction of joint reaction forces occurring at the glenohumeral joint for various arm positions. In this study a description of the motion of the bones and muscles were quantified using a 3D inverse dynamic model in which the attachments of all the muscles of an average cadaver were digitised and combined to describe and quantify multiple force equivalents for each muscle. Positions and motions of the bones for loaded and unloaded abduction and flexion of the humerus were recorded for input into a FEM. The FE musculoskeletal model of the shoulder mechanism, consists of the thorax clavicle, scapula and humerus and was generated for a kinematic (analysis of the rotation of the bones) and dynamic (analysis of the muscle and joint forces) analysis. The model included seventeen muscles, three ligaments and three joints. The morphological structures were represented by elements whose mechanical behaviour was known. Therefore, an analysis of the force and moments exerted by individual muscles to maintain the desired humeral position and to counterbalance the external load was carried out.

All input and output were represented with respect to a global co-ordinate system, as in Fig. 2.7 (a). Local co-ordinate systems were also used to define the orientation of each of the bones. This allows for the muscle data to be easily applied to other FE models of the system. For the scapula, the x_s-axis of the scapula is along the scapular spine AC-TS (where AC is the most dorsal point of the acromio-clavicular joint and TS is the trigonum spinae) pointing to the TS. The y_s-axis is in the scapular plane defined by AC-TS-AI,

where AI is the angulus inferior, pointing caudally. Finally, the z_s-axis is perpendicular to the scapular plane, pointing dorsally.

The location of the resultant joint vectors intersecting the glenoid cavity are shown in Fig. 2.7 (b). The pole co-ordinates ϕ and θ, represent the angle with the frontal plane and with the transverse plane, respectively. For the rest position, zero degrees humeral elevation, the humerus hangs on the glenoid rim. As the arm position increases the intersection point on the glenoid cavity moves inferior following the paths shown. During abduction the intersection points are on the anterior side of the glenoid and during flexion they are positioned on the posterior side. Fig. 2.8 shows the magnitude of the resultant force at the glenohumeral joint. The x-axis shows the humeral elevation (degrees) and the y-axis shows the corresponding force (Newtons). The x, y and z components are given allowing the total force to be calculated using Eqn. 2.1. From this we can clearly show that the largest reaction force is indeed for 90 degrees arm abduction angle.

$$\text{sum of forces} = \sqrt{(\text{fx})^2 + (\text{fy})^2 + (\text{fz})^2} \qquad (2.1)$$

Table 2.2 *Glenohumeral motions for daily activities, after Davies (1977).*

Activity	*Number of movements*	*Range of motion (flexion to extension)*
Getting up	210	+40° → -30°
breakfast	60	+30° → 0°
lunch	90	+30° → 0°
dinner	120	+30° → 0°
To bed	140	+50° →-35°
Total	**620**	

Table 2.3 *Glenohumeral motions for "working" daily activities, after Davies (1977).*

Occupation	*Number of movements*	*Range of motion (flexion to extension)*
Brick layer	5,700	+55° → -45°
Wall plasterer	7,800	+80° → -50°
Scaffolder	1,100	+80° → -20°
Laborer	6,200	+45° → 0°

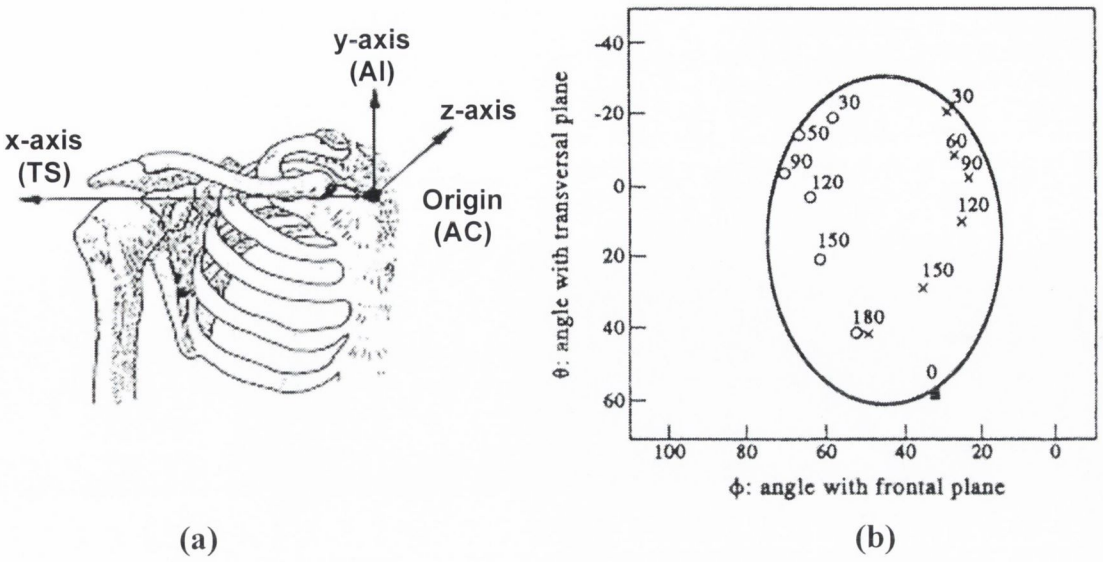

Figure 2.7 ***(a)*** *The global co-ordinate system used in van der Helm's model. The origin is at the Incisisura Jugularis, X-axis pointing from medial to lateral, Y-axis from caudal to cranial and Z-axis from ventral to dorsal (for a right shoulder). Adapted from Veeger (1991).* ***(b)*** *Intersection of the joint reaction force vector and the articular surface of the glenoid, x: Intersection points for abduction unloaded, o: Intersection points for flexion unloaded. After van der Helm (1994).*

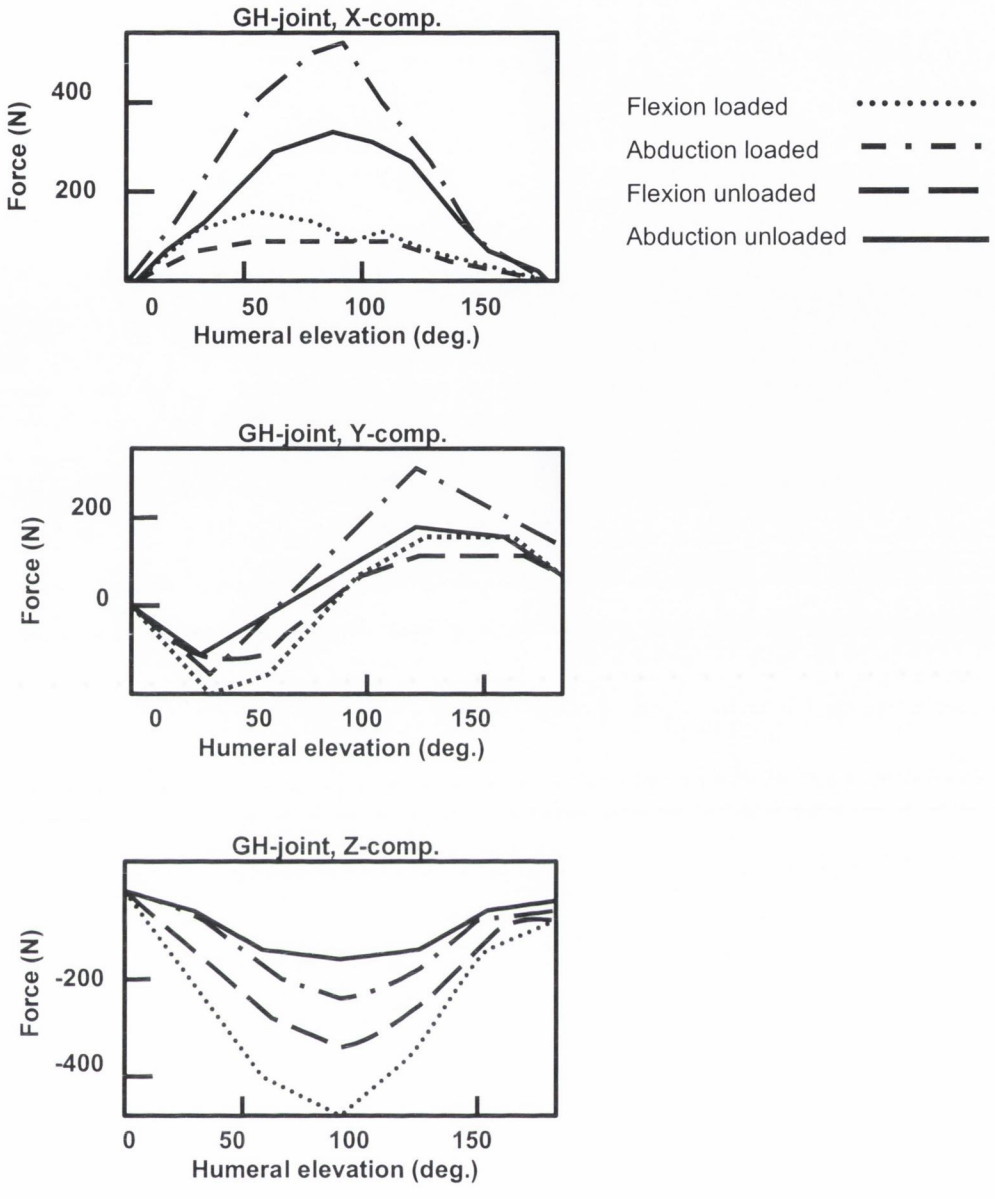

Figure 2.8 *Magnitude of the resultant force at the glenohumeral joint. The x, y and z components are given allowing the total force to be calculated. The x-axis shows the humeral elevation (degrees) and the y-axis shows the corresponding force (Newtons), from van der Helm (1994).*

2.2 Development of shoulder joint replacement

During the 19th century, animal bone and ivory were used for the fabrication of prostheses for humans. The French surgeon, Jules Emile Péan, performed the first documented prosthetic arthroplasty of the shoulder in the International Hospital of Paris in 1893. Under the commission of Péan, a French dental surgeon, J. Porter Michaels, designed the prosthesis (Lugli, 1978). The design consisted of a prosthesis with a platinum shaft with holes placed distally for screw fixation to the humeral shaft. The metal tube contained two longitudinal ridges with small holes drilled proximally to allow for reattachment of muscles, see Fig. 2.9. The head of the humerus was replaced with a large hardened rubber ball boiled in paraffin for 24 hours for insertion into the body. Two thick platinum wires were placed in the deep circumferential grooves, with one screwed to the side of the glenoid and the other attached to the platinum shaft. The prosthesis was inserted in a young man with tuberculosis that involved the glenohumeral joint. The implant functioned relatively well for two years but had to be removed due to recurrent infection.

Despite this early development in shoulder arthroplasty, the next step toward a modern shoulder arthroplasty occurred much later in 1950. Frederick Krueger implanted the first modern shoulder arthroplasty with an anatomic shape. It consisted of a stemmed design; see Fig. 2.10 (a). The prosthesis was implanted in a young sailor with aseptic necrosis of the humeral head and it achieved a "well functioning and painless shoulder" (Emery, 1998). This was followed by the design of a prosthesis for the treatment of fracture dislocations of the proximal humerus, by Neer. At this time only replacement of the humeral head was being carried out. The prosthesis was made of cast cobalt-chrome alloy (Vitallium), which was recognized at the time as being a strong and inert material for internal fixation of fractures (Neer, 1990). Initial modifications of the design included addition of varying diameters of the stem for a better press-fit. Also, holes were added in the flanges for bone ingrowth, see Fig. 2.10 (b). Replacement of the shoulder for arthritic problems was the next step and commenced in the late 1960's with constrained designs (Neer, 1990) such as the Stanmore, Beuchel and Reese designs.

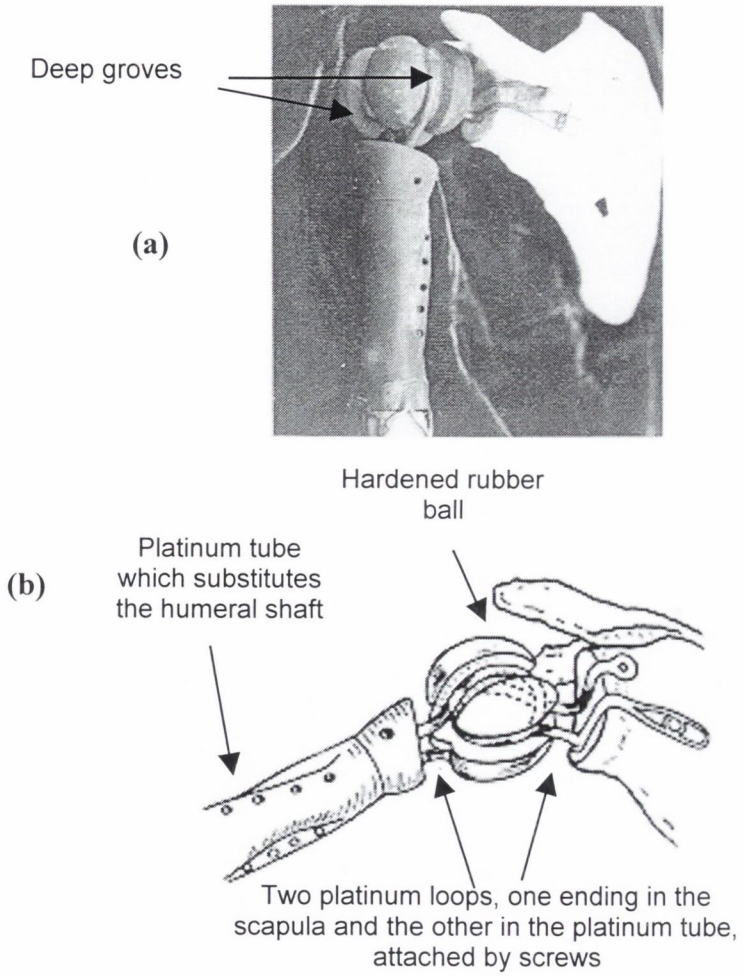

Figure 2.9 ***(a)*** *The Péan shoulder (adapted from Wallace, 1998).* ***(b)*** *Schematic of the Péan shoulder (adapted from Lugli, 1978).*

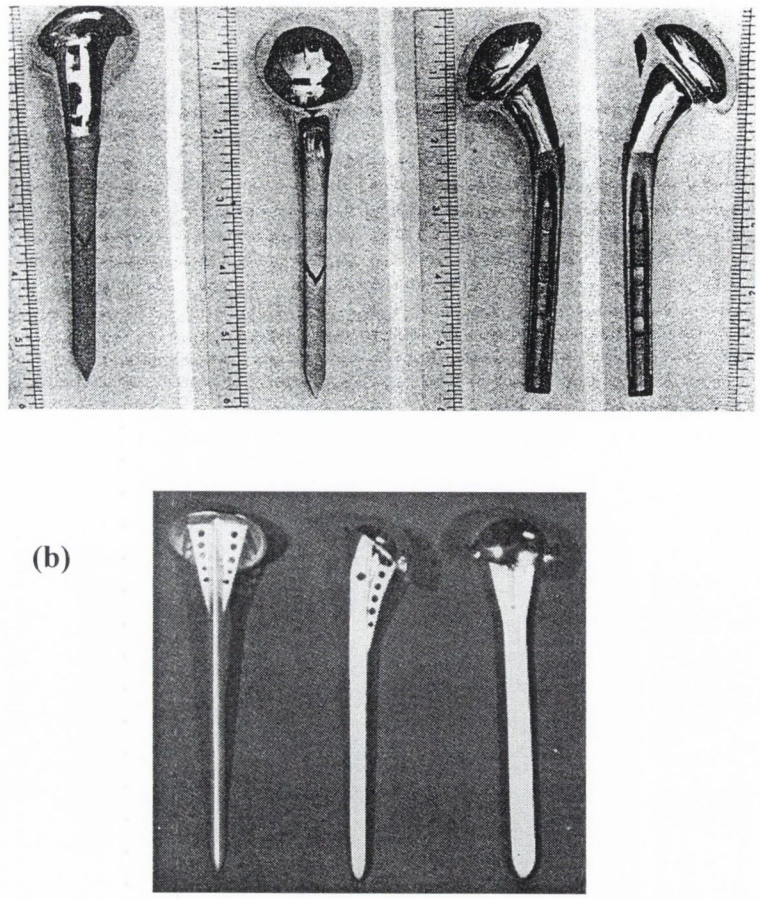

Figure 2.10 ***(a)*** *Kruger's humeral prosthesis showing medial and posterior offset, after Emery, 1998.* ***(b)*** *Initial design modifications included flange holes for bone ingrowth, after Neer, 1990.*

2.2.1 Constrained devices

Functional results of humeral head arthroplasty, i.e. replacement of the humeral side only, were poor for arthritis at the shoulder joint. This was due to abnormal function or degeneration of the rotator cuff, deltoid muscles or the glenoid articular surface. In the 1970's the use of an acrylic bone cement for prosthesis anchorage was introduced by Charnley. This was applied to a new Neer "fixed fulcrum" design, which consisted of a cemented glenoid component, attached to a humeral component, see Fig. 2.11. This was the first step towards a "Total shoulder arthroplasty" (TSA) system. Several of these fixed fulcrum designs were introduced between 1970 and 1973 (Neer, 1990). The rationale for their design was based on the belief that glenohumeral instability resulted from a weakened or torn rotator cuff. Therefore, these designs would eliminate the need for reconstruction of the rotator cuff and stability would be restored. However, since the normally functioning joint has such a large range of motion, the basic "constraint" of the device resulted in a number of complications. These complications consisted of failure of the implant due to loss of osseous fixation, bending or breakage of the implant and dysfunction related to joint stiffness and non-physiological tensioning of the surrounding tissues. Furthermore, in some cases reconstruction of the rotator cuff was still required by surgeons with this design (Neer, 1990), removing its basic design objective. The rate of complications in 13 series reported between 1975 and 1992 ranged form 8% to 100% (Wirth and Rockwood, 1996). Re-operation for constrained prostheses was quite common with report rates ranging from 4% (3 of 71) to 54% (13 of 24). Prostheses such as the Stanmore had failure rates of 44%, the Bickel design had failure rates of 50%, and the Reese design had similar high failure rates of 30% (Brems, 1993).

2.2.2 Unconstrained devices/ total shoulder arthroplasty systems

Before 1973, surgeons such as Kenmore and Zippel (Neer, 1990) had begun using unconstrained devices, which involved implanting a separate glenoid component along with the Neer humeral component (non fixed fulcrum device). In 1973 Neer redesigned his original humeral component to conform to a polyethylene glenoid component for the Neer-II system. The stem of the humeral component was also redesigned for cemented

fixation. This resulted in numerous unconstrained systems being developed from then until the present date.

Ultimately the fundamental difference between these unconstrained and constrained designs is that the unconstrained device allows for physiological tensioning of the surrounding soft tissues with less restriction of motion, see Fig. 2.12 (a). Constrained devices, on the other hand, tend to force a certain motion with non-physiological tensioning of the soft tissues, see Figure 2.12 (b). This may lead to overstressing of the fixation and subsequent loosening.

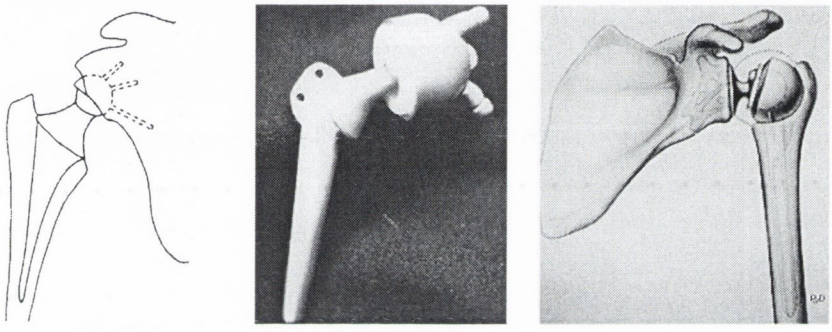

Figure 2.11 *Several fixed fulcrum (constrained) TSA designs were developed between 1970 and 1973 in the hope that they would solve the problem of a deficient rotator cuff or damaged glenoid.* ***(a)*** *Stanmore design of Lettin and Scales. After Wolff, Shoulder replacement.* ***(b)*** *Neer designs. After Neer, 1990.*

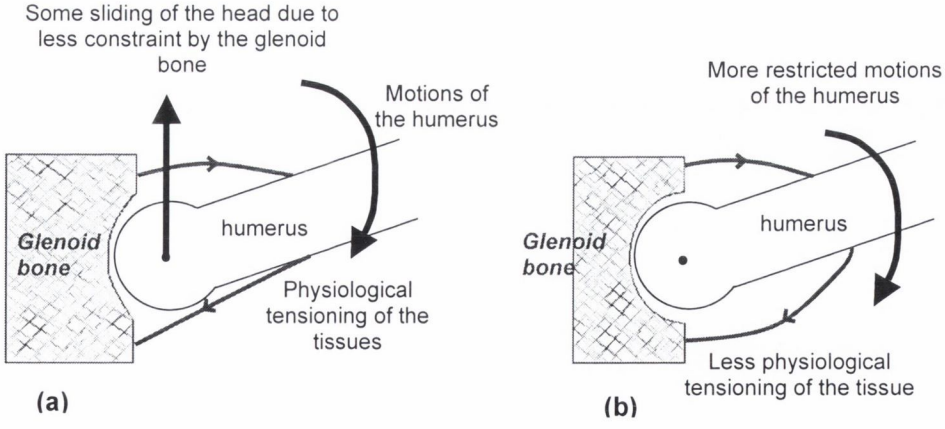

Figure 2.12 ***(a)*** *Non-constrained device allows some "sliding" with a more physiological tensioning of the tissues.* ***(b)*** *Constrained device which restricts motion resulting in non physiological tensioning of the soft tissue.*

2.2.3 The humeral and glenoid prosthesis

(I) Humeral component: Further advances in humeral prostheses design have included modularity of the humeral head. This comprises of a humeral head, which is dissociable from the stem, allowing for better access if revision surgery is required. Also smaller inventory is required due to mixing and matching of stem and head sizes and flexibility of placement of the humeral component with respect to the rotator cuff is facilitated. Generally, the same basic design of humeral prostheses exists with the type of material used varying between chrome-cobalt, cobalt-chromium-molybdenum and titanium. The humeral component is usually fixated with bone cement. Cofield (1994) recommend that the humeral component should be press-fit for hemiarthroplasty and cemented for TSA for improved results. It is also recommended for an improved outcome that the lateral humeral offset is reconstructed to within 2-3mm of the anatomical position (McCullagh, 1995) see Fig. 2.13. This will result in maximum rotator cuff function. Therefore, for adequate reconstruction a range of different sized humeral components is required during surgery, which further validates the use of modular systems.

(II) Glenoid component: It has been well documented that loosening of the glenoid component is the main complication associated with TSA (Wirth and Rockwood, 1996). As a result, further investigation of their design is important. For glenoid component design several factors need to be considered. These include: accommodating the large glenohumeral forces, selecting appropriate materials, shape of the subchondral contact surface, radius of curvature of the articulating surface, surface area of articulation, component thickness, type of anchorage system, method of fixation and, as we will discuss later, glenoid bone architecture and muscle function. Practically all early designs of glenoid components were cemented (Brems, 1993). This was due to the small amount of bone available for fixation. In the case of bone stock degeneration, due to RA, the bone available for fixation is even more limited; i.e. there is a smaller amount of bone and it is weaker. Furthermore, cysts may be present due to underlying pathological processes, which further excavate the bone. As a result adequate fixation becomes even more difficult to achieve. This must be considered in glenoid prosthesis design as the small volume of glenoid bone allows for little room for modification of designs.

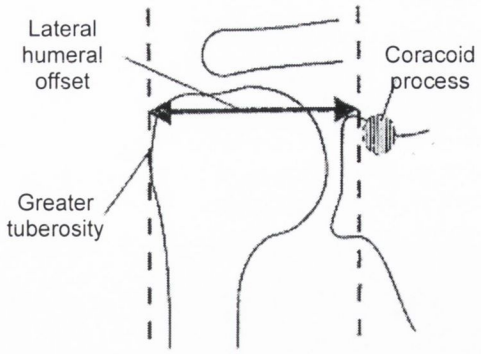

Figure 2.13 *Lateral humeral offset, after Ianotti et al., (1992).*

Two types of polyethylene are used for glenoid component manufacture. These are ultra high molecular weight polyethylene, UHMWPE, and Hylamer. Hylamer possesses a higher molecular weight, a higher crystallinity, and is therefore denser than UHMWPE; as a result it has better wear characteristics. The glenoid flange thickness varies with manufacturer from three to ten millimetres.

Considering metal-backing, case studies from Driessnack *et al.,* (1990), Kirk *et al.,* (1997) and Feldman *et al.,* (1999) have showed problems with dissociation of the plastic liner from the metal tray. Finite element studies by Friedman (1992) and Lacroix and Prendergast (1997) found very high stresses in surrounding bone and bone-cement produced by metal-backing. Furthermore, metal-backing can also increase the lateral distance of the joint, see Fig. 2.14. As a result, impact on the rotator cuff may occur, thus increasing the risk of impingement.

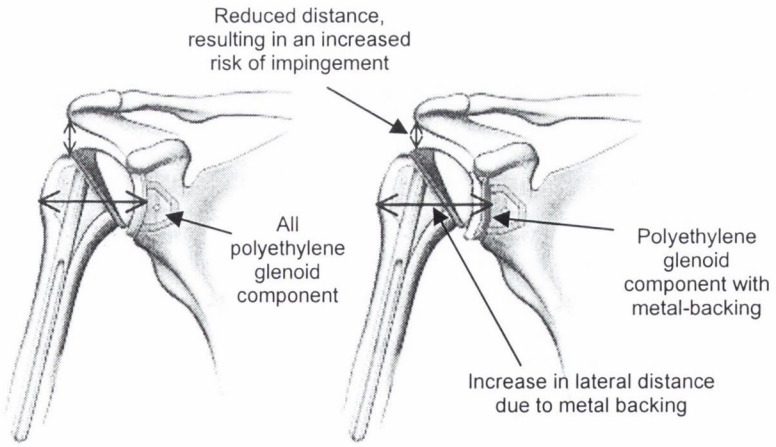

Figure 2.14 *Metal backing of the glenoid component increases the "lateral" distance and may result in an increased risk of impingement. Adapted from Neer (1990).*

2.2.4 Design options for glenoid prostheses

At present there are a wide range of glenoid components on the market. Broadly speaking, they fall into either pegged or keeled designs; the first which is discussed is the pegged design. Giori *et al.,* (1990) carried out a study to determine the optimum peg fixation. Their study indicated that prostheses with multiple smaller fixation pegs better conserves bone stock and distributes stress more evenly with stronger and stiffer shear fixation than fewer larger pegs. Anglin *et al.,* (1999) simulated the "rocking horse" effect mechanically in order to compare prosthesis stability. The procedure involved applying physiological eccentric loads at the glenoid surface and measuring the relative displacement of the prostheses and the surrounding glenoid bone. She determined that convex backing of prostheses is superior to plane backing: a direct comparison of pegged and keeled prostheses was not possible but Anglin stated that the use of a pegged design is preferable. Her argument was that pegs can be placed on the periphery of the component where they will provide greater resistance to eccentric loads than would a keel. Furthermore, Anglin believed that the associated surgical technique is more precise than for a keeled design. Finally, there is little published information specifically comparing the various types of stem designs on the stability of the prosthesis and comparing their performance in various bone-stock qualities and under varying strengths of surrounding musculature.

Previous studies have analyzed the effect of offsetting the keel inferiorly. These include the UCLA total shoulder arthroplasty, which consists of an inferiorly placed keel and aims to facilitate anatomical insertion of the glenoid component. Amstutz *et al.,* (1981) report that (from clinical observation) glenoid bone stock is slightly more geometrically "spacious" in the inferior region. Their design aimed at more closely fitting this available glenoid bone, and eliminating the need for trimming the keel due to cortex perforation. In a further study, Amstutz *et al.,* (1988) proposed the DANA (Designed After Natural Anatomy) total shoulder arthroplasty, which again consists of an inferiorly placed keel and is similar to the UCLA design. Clinical results reported on the performance of 46 DANA prostheses implanted between 1976 and 1984 (with introduction of the inferior keel design in 1979). At a minimum of two years follow-up (2-10 years), five glenoid components required revision surgery. Orr *et al.,* (1988) carried

out a two-dimensional finite element study on the performance of a centre-keel and an inferior offset-keel with and without metal-backing and metal keels, see Table 2.6. They found that an inferiorly placed keel may provide better resistance to bending. Figgie *et al.,* (1992) reported on the clinical results of a metal-backed glenoid component with an inferior keel, which was implanted in 27 patients with rheumatoid arthritis. Follow-up studies of five years (range, 3-7 years) showed that two patients required re-operation and six glenoid components had glenoid radiolucency of which two were "progressive".

In conclusion, an array of keeled and pegged fixation systems have been developed, variations continue to appear but the biomechanical advantages of any new design are not apparent.

2.2.5 Semi-constrained devices and acromial fixated designs

Continued interest in generating new designs is largely due to the fact that, when arthritis exists, the unconstrained system still requires adequate repair of the rotator cuff. Several "alternative" type designs have used the acromion to aid in fixation of the glenoid prosthesis and to reduce impingement of the humeral head. These designs consist of subacromial spacers and buttons, bipolar systems and glenoid components with acromial fixation.

During the 1970s, designs of subacromial spacers were introduced; again this was to aid patients with irreparable rotator cuff tears. In theory, they would hold the humeral head down during the early stages of abduction, until the remainder of the rotator cuff could stabilize the head while the deltoid continued to produce elevation. According to Redfern and Wallace (1998) Welsh and Mcnab described the first design in 1977. Around the same time a similar design was produced in Liverpool, U.K. and is shown in Fig. 2.15 (Redfern and Wallace, 1998). This design consisted of a spacer which is cemented to the under surface of the acromion at its anterior end. It has not been used much clinically and is reported to allow a modest gain in abduction in totally rotator cuff deficient patients. Furthermore, loosening of the spacer has not been reported.

Clayton *et al.,* (1982) also designed a subacromial prosthesis which consisted of a block of high-density polyethylene sutured to the under surface of the of the coracoacromial ligament with four non-absorbable sutures, shown in Fig. 2.16. They

reported on the comparative performance of these all-polyethylene sub-acromial components and all-polyethylene glenoid components inserted with Neer humeral prostheses. Eight patients had Neer glenoid and humeral components alone, seven had a subacromial spacer and humeral prosthesis alone and seven patients had hemi-arthroplasties. Spacers were inserted into five OA patients and two RA patients. At two years post-operation eleven patients had no pain and eight had mild pain. Two complications occurred with anterior subluxation of one spacer and recurrent subluxation (where revision was advised) in another patient with a spacer.

Neer has suggested problems with subacromial spacers; he states that they do prevent ascent of the humeral head and contact between the head and the acromion. However, Neer reports that they do not eliminate pain from the glenohumeral incongruity, and they can dislocate if there is not sufficient cuff to provide stability for the glenohumeral joint (1990).

The Acropole prosthesis from Grammont described by Redfern and Wallace (1998) consisted of a curved shaped prosthesis made of metal screwed into the coracoid (one pin) and bolted into the inferior surface of the acromion (two pins) in the line of the coracoacromial ligament, with a small amount of cement also used for fixation, see Fig. 2.17. It articulated with a curved prosthetic insert in the form of a curved strip arching over the superior pole of the humeral head. Again, the prosthesis was not widely used even though pain relief was reported to be good. However, gains in power and range of movement were poor.

In 1977 Mcnab reported on the experimental development and use of uncemented bipolar shoulder prostheses. The design consisted of a screw fixation to the scapula with additional fixation to the acromion. Twenty-nine replacements in the cases of OA or of failed replacement with a Neer prosthesis were carried out. Functional gain was reported to be good with abduction ranging from 120 to 140 degrees in 25 patients. However, no long-term results or complications were given.

Apoil (1983) states that if a functioning rotator cuff is present then an unconstrained system will perform well. However, if the rotator cuff is damaged then, with time, the humeral head will impinge on the acromion. Therefore, Apoil's semi-constrained glenoid prosthesis aims at stabilizing the prosthetic joint against subluxation when a damaged

rotator cuff exists. The glenoid component consists of two upward extensions, one to the acromion and the other to the coracoid process, see Fig. 2.18. In this study, Apoil also carried out an anatomical review of scapulae geometry. By analysing twenty different scapulae he found that the variation of the position of the acromion (with respect to the glenoid) is small whereas the variation of the position of the coracoid (with respect to the glenoid) is larger. This was taken into account in the prosthetic design and methods of fixation. The glenoid section is cemented in place with one central peg and the acromion part is fixated under the acromion using cement. The elongated shape of the prosthesis allows for the surgeon always to find a point of contact to the coracoid for stabilization. The coracoid section of the component is then fixated using a large screw, which is inserted from high to low (through the coracoid) and into the polyethylene. The author only reports on a one and a half year follow-up which showed all prostheses to have "excellent fixation and stability" at that time. Despite this seemingly positive result, the prosthesis is not in widespread use and further follow-ups have not been reported.

McElwain and English (1987) reported on the early results of a porous coated TSA system, see Fig. 2.19. They reported on 13 cases at an average follow-up of 37 months (range of 12 months to 5½ years). The unconstrained system consisted of a metal-backed and porous coated glenoid component. Additional features could be used for increased stability; these included a superior hood for a rotator cuff deficient shoulder and acromial screws for reduced rotation at the joint. Clinically, the early results were good but the author does not distinguish whether acromion pins were used in the reported clinical trials or how many were used. Complications involved radiologic evidence of humeral loosening in one patient at two years. One shoulder dislocated at seven months with eventual loosening of the glenoid component. Loosening of the glenoid plastic insert occurred in one patient. Long-term results are required for a more realistic analysis of the prostheses performance.

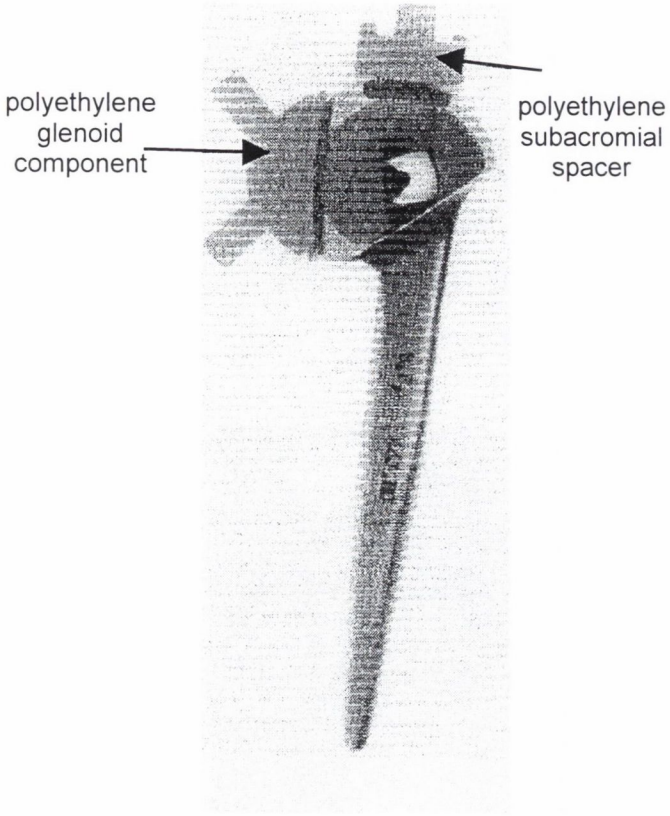

Figure 2.15 *The Beddow Mark III prosthesis with a subacromial spacer (Redfern and Wallace, 1998).*

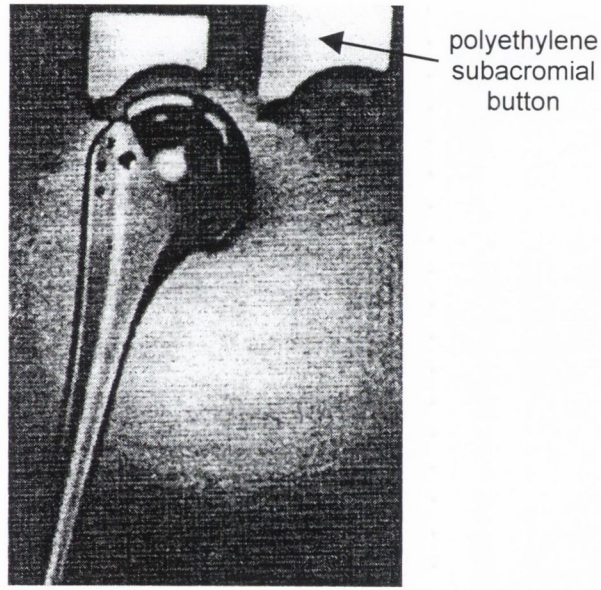

Figure 2.16 *Clayton's subacromial spacers with a Neer humeral prosthesis (Clayton et al., 1982).*

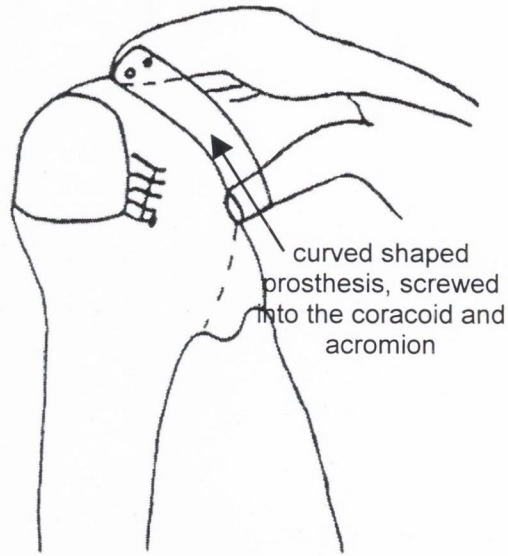

Figure 2.17 *Acropole prosthesis of Grammont. After Wolff and Kobel (1987).*

Laurence (1991) reported on a replacement arthroplasty for the rotator cuff deficient shoulder. The design consisted of a polyethylene cup and humeral component see Fig. 2.20. The humeral head and glenoid components were semi-constrained with a "snap-fit". Surgical implantation involved resection of the glenoid to accommodate the large glenoid cup with the insertion of self-tapping screws to the coracoid and acromion. The lower lip of the glenoid provides the third point of fixation and a small amount of cement was used at each point. Thirty-six patients (38 arthroplasties) were available for follow-up studies with a mean of 6.8 years (range 3 to 15). Postoperatively, pain relief was achieved in 22 of the 71 shoulders; 35 had some minor discomfort. Nine had improved function with still some pain. Two operations failed (neuropathy and ankylosis); three required revision surgery for loosening of the humeral components.

Fassberg *et al.,* (1992) reported on the pre-clinical performance of an acromion fixated design using the finite element method. He was of the opinion that constrained glenoid components are associated with prosthetic loosening whereas unconstrained designs may not be strong enough to support eccentric loads applied by the humeral head. Therefore, his rationale for a glenoid component fixated to the acromian and coracoid is to allow for stress distribution in the scapula, which would reduce the rate of loosening. Unfortunately, no picture of the prosthesis is given but the author describes it as a cup-like prosthesis, comparable to an acetabular component with Ti-6Al-4V alloy material properties. It is fixated to the glenoid, acromion and coracoid using bone screws. A 3D model of the scapula was generated using CT data from an embalmed right scapula and the acromion and glenoid were reamed to fit to the prosthesis. The scapula was restrained below the glenoid neck and two loading conditions were applied. The first was a 500N load and the second was a very large 2175N load (apparently a worse case scenario) and were distributed over a 20 noded area. For the first load case, maximum principal stresses of 3-4 MPa were reached in the bone. The second load case produced similar load patterns but of higher magnitudes (the values are not presented). The author states that non-inclusion of muscles may have caused these conservative results. Finally, his conclusion is that a reduction in bending moments transferred to the glenoid region alone may be reduced by distributing them to the acromion and coracoid also.

Mazas and de la Caffiniere (1977) reported on the poor results of TSA systems and expressed his reservations of their designs, which were not adequate for fixation in limited bone stock. He hypothesised that a new design should be unconstrained yet stable and would use the acromion for fixation to avoid loosening and rupture of the rotator cuff. The author maintains that the supraspinatus is not essential in abduction and that the deltoid is enough. Secondly, the rotator cuff maintains good stability and that a constrained design is not essential. He then describes a new design which has a glenoid component fixated to the glenoid and acromion using three pegs. Due to the size of the polyethylene component, it required that the supraspinatus muscle be removed. There were three sizes of components available depending on the size of the bone. At this stage the prosthesis had been used for three years. Initial conclusions were that fixation to the acromion was good and only two prostheses had loosened; however, the paper does not state how many prostheses were implanted. One case was due to the fact that a prosthesis small enough for the patient was not available. The second was due to the patient's particular history relating to a previous fracture. Stability of the prostheses was successful for all except one patient where anterior wear of the glenoid occurred resulting in the component being placed into anteversion. Range of mobility was close to normal for all patients in abduction and for 75% in flexion.

Mazas and de la Caffiniere (1982) reports on the initial acromial fixated prosthesis design, see Fig. 2.21. With regard to clinical performance, 21 cases were reviewed at the end of 1977 and a further 17 cases which were operated on after that. The placing of the 38 prostheses required a total of 52 operations and 14 reoperations. Reoperations occurred due to paralysis of the deltoid muscle in one patient, two patients received new prostheses and a third was removed. Seven prostheses required reoperation due to instability and one due to a small humeral head being used causing pain. Mazas also reported that eleven shoulders, which were operated on with a posterior approach (more exposure than an anterior approach), were very mobile. Whereas 14 shoulders operated on with an anterior approach had less mobility.

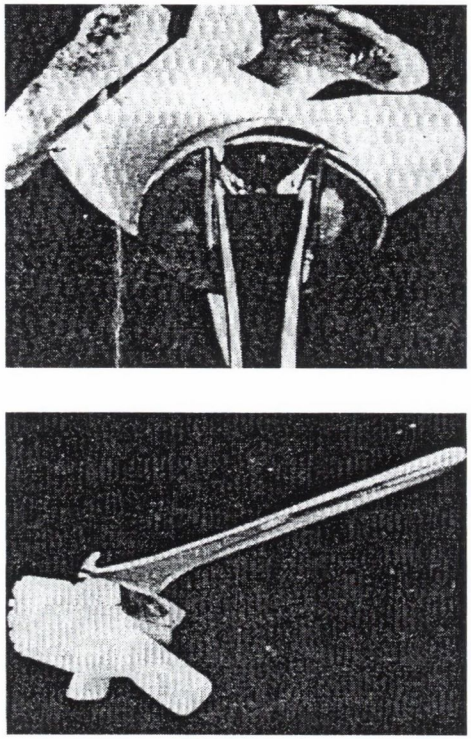

Figure 2.18 *Apoil's semi-constrained glenoid prosthesis consisting of two upward extensions to the acromion and coracoid processes (Apoil et al., 1983).*

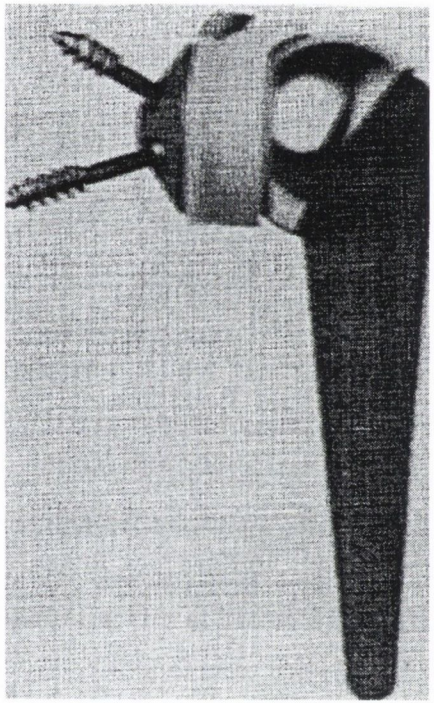

Figure 2.19 *McElwain and English's unconstrained system (Rockwood and Matsen, 1998).*

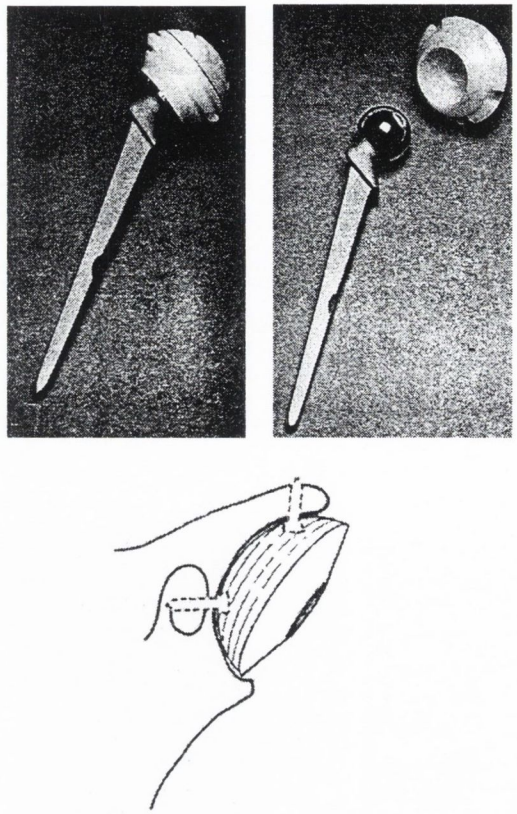

Figure 2.20 *Positions of screws to assist cement fixation of the scapular cup, Laurence (1991).*

Gagey and Mazas (1990) reported on the acromial-fixated design, see Fig. 2.22. Here the author reports on a series of 60 patients showing good clinical results. However, a modification is made to the polyethylene glenoid component which was very large and required removal of the supraspinatus muscle. Therefore, a new prosthesis was introduced in 1985 and consisted of cement and screw fixation, both to the acromion and glenoid. Following on from this, Gagey and Mazas (1990) reported on 36 patients with a mean follow-up of 13 months (range: 6-36 months). A roentenographic analysis showed fixation problems with 15% of the patients. One patient had complete loosening with rupture of the screws, one with acromial loosening, two with complete radiolucent lines and two with partial lucent lines. They also reported on the stiffness of the prosthetic connection between the acromion and the glenoid in relation to the acromion process itself which resulted in large forces being generated and loosening of two prostheses. A reinforcement of the bar led to a reduction in complications. However, long-term results are required before further conclusions can be drawn about the performance of the prosthesis.

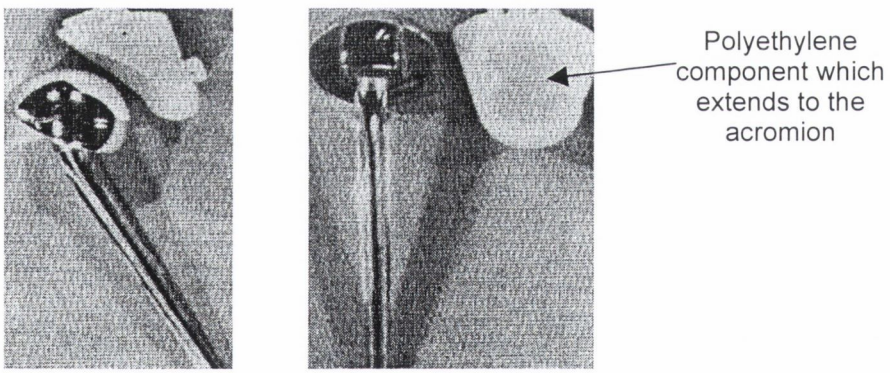

Figure 2.21 *The non-retentive shoulder arthroplasty designed by Mazas and de la Caffiniere (1982).*

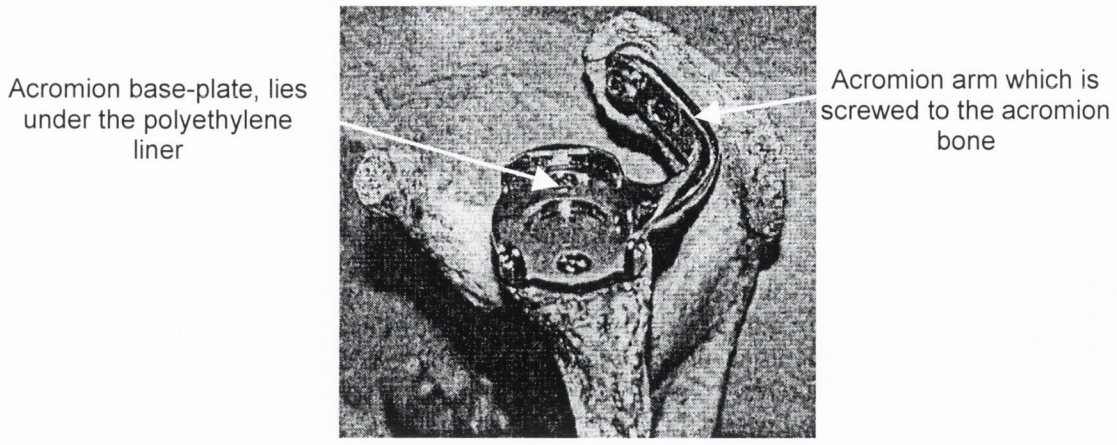

Figure 2.22 *The acromial fixation glenoid prosthesis with the polyethylene base removed (Mazas and Gagey, 1990).*

2.3 Failure scenarios in total shoulder arthroplasty

Wirth and Rockwood (1996) reviewed the main post-operative complications associated with TSA in 41 separate follow-up studies, from 1975 to 1995, see Table 2.4. Clearly from this study we can see that the main complication is glenoid component loosening (33%).

Table 2.4 *Main complications associated with TSA, Wirth and Rockwood (1996).*

Complications	*Frequency (%)*
Glenoid component loosening	33
Instability of the rotator cuff	0-29
Rotator cuff tear	1-13
Periprosthetic fracture	3
Nerve injury	<1
Infection	0.5
Implant	<0.5
Dysfunction of the deltoid muscle	<0.5

2.3.1 Complications associated with the glenoid component

Biomechanical factors affecting the durability of fixation in TSA are numerous. These include the quality and quantity of the glenoid bone stock, the presence of a functioning rotator cuff and proper soft tissue balancing (see Fig. 2.23). Each of these factors plays an

essential role in achieving an optimal result. Furthermore, in the normal joint, i.e. that of no prosthetic fixation, the cartilage and labrum assist in some absorption of forces at the joint. However they are not present in the prosthetic joint. In this case, the amount of humeral head translation depends on the conformity of the glenoid and the humeral components selected. For perfectly conforming prostheses, any amount of translation results in rim loading. This leads to the so-called "rocking-horse" effect, see Fig. 2.24. and may result in glenoid loosening, permanent component deformation, and component wear (Brems, 1993). Franklin *et al.,* (1988) also states that it is this off-centre loading or the rocking-horse phenomenon that is the major cause of loosening. Iannotti *et al.,* (1992) recommend that a diametrical mismatch of 4-6mm of glenoid socket and humeral head is required to avoid this rim loading. In general, for both the normal and prosthetic joint, translation is somewhat dependant on the presence of an intact and well-functioning rotator cuff. When the rotator cuff is deficient the humeral head translation is increased (Ianotti and Williams, 1998) and as a result stability is compromised.

Bone cement is the most popular method of fixation in glenoid replacement and remains, according to Ibarra *et al.,* (1998) it is the "gold standard" from which other methods of fixation can be compared. It is used to provide immediate and secure fixation within the small cavity of the glenoid vault. However, it carries the associated disadvantages of mixing techniques and occurrence of pores, production of uniform cement mantles, radiolucent lines, failure of cement due to high stresses, the risk of loss of bone stock in the event of revision surgery etc.

Much design activity has focussed on radiolucencies found around the glenoid component after implantation. Radiolucencies generally consist of nonmineralised fibrous tissue at the bone-cement interface, occasionally containing cement particles. Lucent lines can be present directly after surgery and are usually made up of blood. Also, their presence can be dependent on surgical technique, see Brems (1993). Most surgeons have suspected that these lucent lines are signs of loosening; however, the absence of long term results (>10 years) can not definitely confirm their suspicions. Furthermore, radiographic assessment of the glenoid is difficult and the variability and non-standardised methods involved in the technique made comparison of studies difficult. Recently, Torchia *et al.,* (1997) reported a five to 17 year follow-up and demonstrated the

progression of these lucent lines to loosening in patients. Definite radiographic loosening has been described as progressive radiolucency or a radiolucent line that is at least two millimetres wide at the bone interface (Havig, 1997). Furthermore, it has been reported that radiolucent lines around the flange of the glenoid component are not associated with loosening but lucencies around the keel are (Barrett *et al.,* 1987).

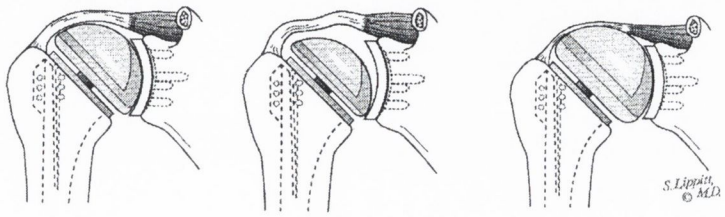

(a) (b) (c)

Figure 2.23 (a) *Adequate soft tissue balancing involves providing the correct size humeral head. Improper selection results in* ***(b)*** *excessive laxity and compromise of the articular surface (humeral head is too small) or* ***(c)*** *overstuffing of the joint tensions the tissues, limiting excursion and decreasing range of motion (humeral head too big). After Rockwood and Matsen (1998).*

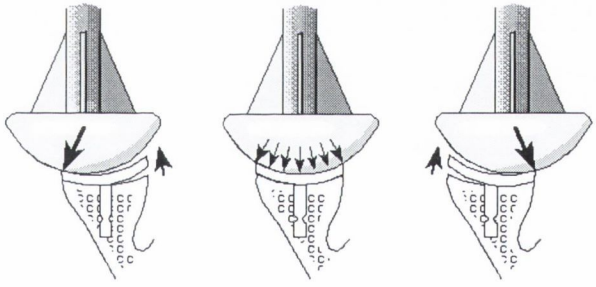

Figure 2.24 The "rocking-horse" effect, after Neer (1990).

The success of TSA using bone cement has been reported on in several short and intermediate follow-up studies. Some of these studies are summarised in Table 2.5 by Torchia *et al.,* (1997). A number of theses authors have agreed that three years follow-up is not sufficient to assess many of the complications associated with TSA. Torchia's study reports with an average follow-up of 9.7 years. They found that 44% of glenoid components showed radiographic evidences of definite loosening (associated with pain).

Controversy also remains as to whether the back of the prosthesis, along with the keel or pegs, should be cemented (Ibarra *et al.,* 1998). Radiographic changes at the cement-

bone interface of the keel portion occur in one-third to one-half or more of patients with increased loosening of the glenoid component with time (Brems, 1993). However, radiographic changes under the flange are less frequent.

Finally, early clinical results for glenoid components fixated by tissue ingrowth are good and radiographically evident changes do not occur as much as for cemented components (Cofield, 1994). However, their disadvantage is that accelerated polyethylene wear occurs (Sperling *et al.,* 1998). Interference or press fit glenoid components have been developed but it is still not clear if they hold any advantage.

Complications related to RA patients: Regarding the success of TSA in RA patients, Frich (1994) reported that complications due to loosening of the glenoid component have been up to 15% in patients with RA. Barrett *et al.,* (1987) carried out a clinical study of fifty total shoulder replacements in 44 patients with an average follow-up of 3.5 years (range, 2.0 to 7.5 years). Thirty-three patients had OA, eleven had RA and six had fractures of the humeral head. Nine of the shoulders had tears of the rotator cuff. The Neer-II system (non metal-backed) was used in all of the shoulders. Four patients required revision surgery, three for loosening of the glenoid component and one for malposition of the components. All had tears of the rotator cuff; the patients requiring revision were treated for OA (one patient) and treatment of previous fractures (2 patients). It was also noted that seven patients with massive rotator cuff deficiencies had superior migration of the humeral head on the glenoid component.

Thomas *et al.,* (1991) reported on the clinical performance of shoulder athroplasty in RA patients. Forty-two DANA prostheses were inserted in 24 patients with a minimum follow-up of two years. Twelve patients (40%) also had significant rotator cuff tears. Four patients were also treated with hooded glenoid components to improve stability in shoulders with rotator cuff tears. Loosening of two glenoid components (7.7%) occurred and revision of one hooded component (25%) was required due to acromial fracture. Furthermore, the author reports on the occurrence of superior subluxation in 50% of the shoulders, which ranged from five to fifteen millimeters from the centre of rotation of the glenoid.

Sneppen *et al.,* (1996) reported on the results of 62 Neer total shoulder arthroplasties in patients with late-stage RA of the shoulder (rotator cuff deficiency and poor glenoid

bone stock). According to the Larsen classification system, 13 were grade III, 23 grade IV and 26 grade V. Follow-up was 92 months (range, 52 to 139). The analysis included an examination of proximal migration and loosening. Thirty-two (51%) showed proximal migration of the humerus before surgery and 55% at follow-up. 40% of the shoulders showed progressive radiographic loosening of the glenoid component. The authors also report that immediately post-operatively, x-ray films showed that eccentric loading on the glenoid surface in 27% of the cases occurred. In ten cases it occurred on the inferior side, resulting in 7 radiographic loose components. In seven patients it occurred on the superior side.

Stewart and Kelly (1997) carried out a long-term analysis of TSA with the Neer II system in rheumatoid patients. They used the Larsen classification system to distinguish their pathological findings in 37 total shoulder arthroplasty pre-operative glenohumeral joints. This showed that all the joints were of Larsen Grade IV or V; i.e. pain source is from the glenohumeral joint, where shoulder replacement should be considered. Twenty-one of the 37 shoulders had deficient glenoid bone stock. All-polyethylene keeled glenoid components were cemented in place. Seven patients had "probable" loosening where loosening was defined as progressive radiolucencies exceeding 2 mm. Three of these so-called loose components had enough pain for a revision surgery. In another study, Kelly (1994) found that all 104 pre-operative patients showed Larsen Grade IV or V destruction at the glenohumeral joint where glenoid bone was said to be deficient in 89 patients at operation. This study also showed that the rotator cuff was normal in 13 shoulders, thin but intact in 6 and torn in 31 shoulders. Furthermore, it was reported that proximal migration of the humeral component due to rotator cuff deficiency led to eccentric glenoid loading and progressive loosening in 42% of total shoulder arthroplasty patients with progressive RA (Søjbjerg *et al.,* 1999).

Bell and Noble (2000) reported on the management of significant glenoid deficiency in TSA. They suggest that grafting should be considered when sizable cysts are present before implantation. The authors also reported on the variability of glenoid tilt (version) present in arthritic cases. Mild glenoid loss can be surgically treated with concentric spherical reaming if sufficient bone is left for glenoid insertion. With deficiencies greater than 30% of the glenoid surface grafting is recommended. The use of bone cement to

compensate for bone loss is not recommended, as it is associated with increased chance of glenoid loosening (Bell and Noble, 2000). Furthermore, if erosion of the glenoid neck is extreme, for example down to the base of the coracoid which can occur in some RA cases, then it is recommended that a hemiarthroplasty is used.

It is clear from these studies that no straightforward solution to TSA in RA patients exists. Furthermore, the relationship between deficient glenoid bone, torn rotator cuffs and superior humeral head migration with glenoid component loosening shows that these factors are essential in any analysis of glenoid component durability.

2.3.2 Complications associated with the humeral component

Long-term results of TSA have been reported by Torchia *et al.,* (1997). In this study a review of 113 shoulders was undertaken between 1975 and 1981. The probability of humeral implant survival alone was 93% after 10 years and 87% after 15 years. This clearly shows that the humeral component performance is good, but only in comparison to glenoid designs, and design improvements should be focused on the glenoid component initially.

2.3.3 Total shoulder arthroplasty versus hemiarthroplasty

Hemiarthroplasty involves insertion of a humeral component without replacement of the glenoid articular surface. Fewer complications are associated with hemiarthroplasty when compared with TSA. However, evidence suggests that the outcome is one of less predictable pain relief and inferior functional gain compared with results achieved with TSA (Boyd *et al.,* 1990) when the rotator cuff is functioning properly. This is especially true for inflammatory arthritis (Skirving, 1999). In 1974, Neer reviewed 47 hemiarthroplasties at an average of six years. Twelve patients had pain relief, functional recovery, and no evidence of degenerative changes after more than ten years follow up. Neer concluded that, for OA, hemiarthroplasty is sufficient as a TSA could lead to complications. Although hemiarthroplasty has been performed for many years, few studies have compared the long-term results of hemiarthroplasty with TSA. However, one study compared the long-term performance of the Neer hemiarthroplasty and the Neer TSA in patients 50 years old or less, (Sperling *et al.,* 1998). It was found that the

estimated survival of the hemiarthroplasties was 92% at five years, 83% at ten years and 73% at fifteen years. Complications were associated with glenoid erosion. For the TSA cases, the estimated survival was 97% at five years, 97% at ten years and 84% at fifteen years. Complications were associated with glenoid component loosening.

2.4 Mechanical testing of glenoid prostheses

Anglin *et al.,* (2001) reported on the loosening performance of cemented glenoid prostheses design pairs (see Figure 2.25) in an *in vitro* bench test. This procedure involved subjecting the components to dynamic edge loading in a biaxial test setup. The test used was subsequently accepted as an industry standard by the ASTM (F2028-00). A humeral head was cycled 100,000 times on the superior and inferior edges of the glenoid using a force of 790 to 940N. The glenoid components were cemented into polyurethane blocks with a Young's modulus of 193 ± 12 MPa. Indication of loosening was determined by measuring the maximum tensile displacement opposite the loaded side. Results predicted that:

(i) a rough-backed design had much lower loosening rates than a smooth-backed design

(ii) a curved back was better than a smooth back

(iii) a less-constrained design was superior to a more-constrained design

(iv) a pegged design was better than a keeled design; threaded pegs were slightly better than cylindrical pegs

(v) an all-polyethylene design was more stable than a metal-mesh-back design.

These mechanical tests provided interesting results, and as the author suggests, could be a useful compliment to a FE analysis of the interfacial and material strains. The results are limited in the fact that the material properties of the bone model used are of average cancellous bone and do not reflect the heterogenous nature and geometric confinement of the glenoid. Furthermore, the effects of destructive RA are not simulated. Finally, the important effects of the three-dimensional muscles are not modelled and the effects of RA are also omitted.

Karduna *et al.,* (1998) report on experimental strain measurement in the keel of an all-polyethylene glenoid component. The objective of the experiments was to determine the effect of altering glenohumeral joint conformity and loading patterns on the strains experienced at the glenoid. Fourteen unpaired fresh frozen human glenohumeral joints, stripped of muscles, ligaments and labrum, were used. Seven were natural joints and seven were prosthetically reconstructed joints (keeled glenoid components). The scapulae were cut to the level of the superior notch and the acromion was removed. They were then potted to the level of the glenoid neck. For the natural joints the humerus was also potted and for the prosthetic joints a humeral head was used for loading. A biaxial rig was used to apply medial-lateral and anterior-posterior translations. For the natural joints, the head size was obviously kept constant and the medial loads were increased (10, 50, 100, 200, 300, 400 N). For the reconstructed joints the effect of joint conformity was tested by altering the radial mismatch of 0, 1, 2, 3, 4 and 5 mm under sequentially increased loads. Results showed that higher forces, for a given translation, were experienced as conformity increased. Rosette strain gages applied to the keel measured highest compressive strains for non-conforming joints with the humeral head centred in the joint. The strains became tensile before rim loading and were greater for conforming joints.

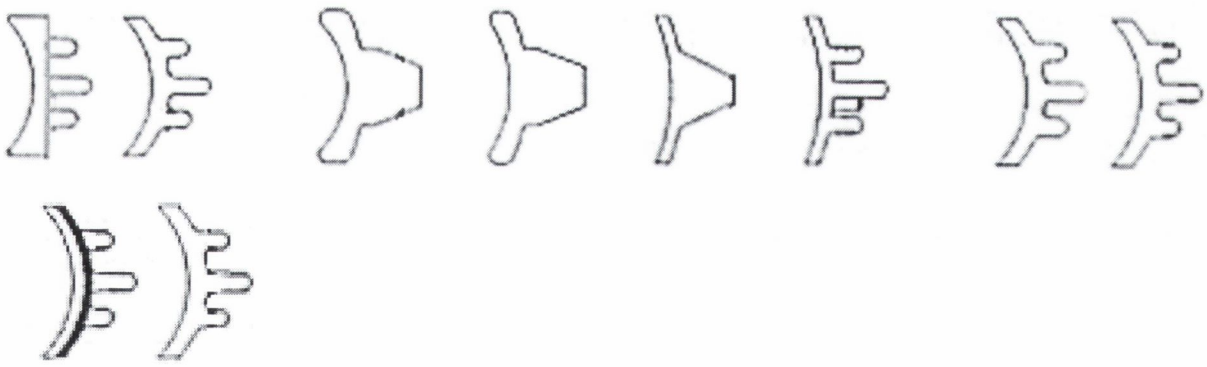

Figure 2.25 *Glenoid component designs mechanically tested by Anglin, (2001).*

2.5 Finite Element Analysis

The finite element method (FEM) has become a widely used tool in orthopaedic biomechanics (Prendergast, 1997). It is a computer-based method suitable for determining stresses and strains at any given point inside a structure of arbitrary geometry and material properties. The model relies on accurate constitutive modelling of the material properties (generalized Hooke's law), 3-D geometric data, loading characteristics, and boundary and interfacial conditions. By using the FEM, pre-clinical testing can be carried out to assess the performance of various prostheses.

The procedure involves discretising a structure into small parts, or elements, whose behaviour can be easily analysed allowing the entire structure to be described when the elements are assembled. Therefore, complex structures can be modelled approximately using various FE procedures. For a fully three-dimensional structure, brick shaped or wedge shaped elements can be used. Elements are connected at discrete points along their boundaries, called nodes. Displacements at each position within the element and on its boundary are defined by interpolating from the nodal positions. These interpolation functions are termed "shape functions". Compatibility of displacements, i.e. continuous displacement, is achieved when the shape functions predict the same displacement on connecting boundaries of adjacent elements. Basic principals of finite element analysis are discussed in Appendix A.

Table 2.5 *Long-term results of total shoulder arthroplasty. After Torchia et al., (1997).*

Author (yr.)	*No. shoulders*	*Mean radiographic follow-up interval (yr.)*	*Components with bone-cement radiolucent lines (no., %)*		*Glenoid component shift in position (no., %)*	*Radiographically "loose" * glenoid components (no., %)*	*Glenoid components revised or removed for aseptic loosening (no., %)*
			Any				
			Area (%)	*Keel (%)*			
Neer *et al.*, 1982	194	3.1	59(30)	23(12)	0	0	0
Cofield, 1984	73	3.8	60(82)	31(42)	8(11)	8(11)	3(4)
Wilde *et al.*, 1984	38	3.0	35(93)	26(68)	NR	NR	1(3)
Bade *et al.*, 1984	38	4.5	25(67)	"most"	NR	1(3)	0
Bell *et al.*, 1986	11	1.3	5(45)	2(18)	0	0	0
Barrett *et al.*, 1987	50	3.5	37(74)	18(36)	4(8)	5(10)	3(6)
Kelly *et al*, 1987	40	3.0	33(73)	25(63)	NR	NR	0
Frich *et al.*, 1988	50	2.3	NR	NR	NR	2(4)	0
Barrett *et al.*, 1989	129	-	106(82)	77(59)	2(1)	12(9)	0
Hawkins *et al.*, 1989	70	3.3	"nearly all"	NR	NR	5(7)	2(3)
McCoy *et al.*, 1989	29	3.1	25(86)	NR	NR	0	0
Brenner *et al.*, 1989	28	5.1	16(57)	6(21)	NR	6(22)	1(3.6)
Boyd *et al.*, 1990	131	3.8	NR	NR	NR	16(12)	1(<1)
Torchia *et al.*, 1997	89	9.7	75(84)	68(76)	34(38)	39(44)	5(5.6)

2.5.1 Challenges of FEA in orthopaedics

The popularity of the FE technique is due to its ability to handle various geometries, loading conditions, and material properties. The FE technique was first introduced to orthopaedic biomechanics in 1972 to calculate the stresses in human bones (Huiskes and Chao, 1983). Applications of this technique in orthopaedics have included understanding the behaviour of healthy bones, prosthetic and fixation devices, failed implants etc. However, the application of this technique in orthopaedics, although well established, differs to normal engineering applications in that the nature of the living tissues is not entirely known. Moreover, it has been stated many times that a balance of accuracy and complexity together with simplicity for ease of analysis are essential. However, over simplification of models can only give qualitative results and design-analysis requires a degree of complexity. Regarding FE modelling of skeletal joints, models of the hip joint are extensive and, as a result of increased computational speed and improved software, more sophisticated models exist (Prendergast, 1997). Again, due to a much larger number of hip arthroplasties performed each year and the less complicated geometry and range of muscle and joint forces of the hip compared to the shoulder joint, a more feasible area of study exists. As a result of this complexity at the shoulder joint, models generated to date have not reached a similar level of sophistication.

In general the quality of a FE solution is based on the accuracy of material property, geometric and boundary conditions input and on the validity of the model. Some authors may focus on one of these aspects with accurate simulation, as it may be difficult and time consuming to include all of them, this is particularly evident in shoulder models. Other factors effecting the quality of results include element types and mesh densities input in the model.

2.5.2 Finite element analysis in total shoulder arthroplasty

For an understanding of the stress transfer at the glenohumeral joint, several 2D FE models of the glenoid region have been developed, these models are summarized in Table 2.6. It is argued that these models do not contain an adequate level of complexity, since only the glenoid region is modelled, random point loads are applied to the glenoid surface and the variability of material property distribution is not modelled. Furthermore, the

basic 2D nature of the models can not incorporate the 3D intricacy of the scapula and its complex range of muscle and joint loads which exist in reality.

Following on from these two dimensional models, preliminary three-dimensional models were created using CT scanning. These modes are summarized in Table 2.7. Again, these models were the first of their type and as a result many simplifications were made. These simplifications including modelling the glenoid region alone, application of point loads rather than a full joint load, no application of muscle loads and finally a homogenous distribution of material properties.

2.5.3 Simulation of rheumatoid arthritis in a finite element model

From previous studies on the measurement of glenoid erosion in arthritis, Neer and Morrison (1988) found that 14.7% of shoulders had enough destruction of the glenoid to make implantation of the prosthesis impossible without bone grafting. McCoy *et al.,* (1989) and Kelly *et al.,* (1987) found that glenoid bone stock was deficient in 20.7% and 62% of the shoulders treated respectively. Mullaji *et al.,* (1994) found that nearly half the available surface of the glenoid was of unsupported bone, mainly posteriorly at the upper and middle levels. Furthermore Mullaji *et al.,* (1994) states that erosion has been reported to occur posteriorly, centrally or superiorly, and anteriorly or centrally by various other authors. We can see from these results that erosion of the glenoid in arthritis is an extremely variable process and that there is no particular accurate way of simulating this destruction.

For the case of RA of the scapula, no previous work has been done to compare the performance of glenoid component designs in both normal and RA scapulae. In the study carried out by Kaufler *et al.,* (1998) a 3D model of a RA scapula was constructed from CT data. Analysis of the performance of three types of components was carried out. These components consisted of an all-polyethylene keel, central cone and two diverging pegs. These were inserted with bonded interfaces (no cement layer) and glenohumeral force of 1.5 BW was applied. They determined that each design had similar stress distributions in the surrounding bone. This may have been due to the application of a "point" load on the glenoid surface. As a result a localized loading occurred. Furthermore, a large osteophyte was included in the model, which was located in the

glenoid vicinity. These two factors would have served as stress concentrators in the model, which may not necessarily occur in the real situation. As a result they may have overshadowed the effects of the design variations resulting in similar results being obtained for each of the components.

Frich (1994) and Frich *et al.,* (1997) examined the material properties of the cancellous bone in the normal state glenoid as well as the glenoid degenerated by RA. Using CT scanning they measured a density for RA reduced by one half to two thirds for compared to the normal glenoid. Dalstra *et al.,* (1996) used this data to analyze the effect of deteriorating bone quality in the glenoid on the load transfer across the glenoid and reduced the bone density for cancellous bone and cortical to one half and one tenth respectively, based on experimental work by Frich.

2.6 Summary

The glenohumeral joint permits the greatest range of movement of any joint in the body. Motion is achieved by the large array of muscles and together with a highly evolved bony structure, resulting in a highly complex system. The human scapula has an intricate shape and only a limited amount of bone is available for glenoid component fixation — this poses a substantial design challenge. In addition, the effects of RA which have been discussed in this chapter, can render the larger problem of component fixation much more intractable. As a result a large range of shoulder arthroplasty systems have been introduced through the years in order to overcome the problem of glenoid component loosening. Shoulder systems begin with the introduction of Péan's shoulder system in 1893. The review clearly shows that, even with this early start in shoulder arthroplasty, the improvement in clinical outcomes comparable to hip and knee devices has not been realized. Adequate pre-clinical tests must be developed prior to clinical introduction if any advances in the success of TSA are to be made. Following on from this, sufficient prospective randomized studies, multicentre studies and registered studies can follow. However, this literature review has shown that clinical introduction and short term follow-up studies are not enough since good prosthesis performance at this early stage may not result in a satisfactory long-term performance.

Table 2.6 *A summary of previously published 2D finite element models of the shoulder region.*

Authors	*Model description*	*Research Question*	*Results*
Orr *et al.*, (1988)	Model of the glenoid region with a central and eccentric load applied.	Is the stress distribution of a prosthetic glenoid similar to that of a natural glenoid?	Metal-backing of a keeled glenoid component may cause a slight improvement in stress transfer to cortical bone, resulting in more physiological bone stresses. Altered fin geometry better stabilized the glenoid component.
Friedman *et al.*, (1992)	Model of the glenoid region with various glenoid joint loads applied.	What effect has prosthesis design and loading on the stress in the surrounding bone?	An all-polyethylene component provides a more physiological stress distribution for loads at an angle to the glenoid surface.
Lacroix & Prendergast (1997)	Model of the glenoid region with various glenoid joint loads applied.	What effect has prosthesis design on cement stresses?	Tensile cement stresses were predicted to be between 7-13 MPa indicating that failure of the cement was likely. Metal-backing of the glenoid component did not reduce the cement stresses by a significant amount.
Stone *et al.*, (1999)	Model of the glenoid region with a central and eccentric load applied.	What is the difference between an all-PE keeled component and an uncemented pegged component with metal-backing compared to the intact glenoid ?	The all-PE design produced an overall trabecular stress pattern similar to that of the intact glenoid. The uncemented metal-backed component produced lower subchondral stresses for both load cases. High PE stresses existed at the PE-metal interface in relation to the all-PE design.

Table 2.7 *Summary of previously published 3D finite element models of the shoulder region.*

Authors	*Model description*	*Research question/aim*	*Results*
Dalstra *et al.*, (1996)	Model of the glenoid region generated using CT scanning. Joint loading is applied and muscle loading is omitted. Effects of RA are not included.	What is the effect of deteriorating bone quality in the glenoid on the load transfer across the glenoid?	Much higher stresses (than the normal case) and larger deformations occur due to the decreased stiffness of the trabecular core.
Kaufler *et al.*, (1998)	Model of a RA glenoid using CT scanning, including large osteophytes close to the area of prosthetic fixation (which will effect the results). A simplified joint load is applied.	What effect has 3 different glenoid component fixation designs on the surrounding rheumatoid arthritic bone in the glenoid?	Different fixation designs for a rheumatoid arthritic scapula had little effect on the stresses in the bone.
Baréa (1998)	Model of a scapula generated using CT scanning. A simplified joint load is applied and muscle loading is omitted. Effects of RA are not included.	How does the load transfer in a normal and prosthetic joint compare? Glenoid prosthesis designs included a Neer II keeled component and an "anatomic" keeled design.	Results showed that the Neer II design produced stresses in the glenoid region similar to the natural case. However, the "anatomic" keeled prosthesis was less susceptible to eccentric loads.
Cattaneo *et al.*, (1999)	Model of the glenoid region generated using CT scanning. Model not used for glenoid component analysis..	To develop a quick method to generate a FE model of the glenoid region from CT data (Patient orientated).	Tool can be used in the future for construction of FE models for other joints in the body.
Gupta *et al.*, (2000)	Model of a scapula generated using CT scanning. Effects of RA are not included.	Stress analysis of cemented and uncemented glenoid prostheses.	Both metal-backing and non metal backing are vulnerable to loosening one way or another.

This review has clearly established that constrained designs were unsuccessful. Many semi-constrained designs have been introduced, some showing good short term follow-up results. This looked promising for semi-constrained designs and poses the question of why continued clinical trials are not reported. Unfortunately to date, clinical studies are small and adequate long-term follow-up studies are generally not available. A definite conclusion as to whether these semi-constrained designs do actually perform well in patients, particularly in patients with RA, still does not exist. Furthermore, with the exception of Anglin (2001), there is little published biomechanical work comparing varying types of unconstrained designs. We suggest, therefore, that it is necessary to carry out a full investigation into the comparative durability of a selection of prostheses in varying patient pathologies.

A pre-clinical testing platform of computational modelling, physical modelling and animal experiments has been recommended to ensure the mechanical durability of new prosthesis designs (Prendergast and Maher, 2001). An investigation into the existing pre-clinical tests carried out on glenoid prostheses was also included in this literature review. Interesting results were obtained from Anglin *et al.,* (2001) from her mechanical bench tests and, as she suggests, could be a useful compliment to a FE analysis of the interfacial and material strains. However, for the shoulder, these bench tests were limited in the fact that the material properties of the bone model used are of average cancellous bone and do not reflect the heterogenous nature of glenoid bone and geometric confinement of the glenoid cavity. Furthermore, the effects of destructive RA were not simulated. Finally, the all-important effects of the three-dimensional muscles were not modeled, with effects of RA and subluxation also being omitted.

The advantages of computer simulation relative to laboratory bench testing are most applicable to the shoulder joint. Regarding the finite element procedure, this technique could be used for an accurate investigation whereby the muscle loads, varying joint loads, complex geometry of the scapula and glenoid, varying material properties and RA properties can be accurately described. Furthermore, parametric variations of glenoid prostheses can be implemented for direct comparison of varying designs. Such studies would be more difficult, if not impossible, to execute in an experimental bench test. Previous finite element studies have been reviewed in this chapter. 2D models of the

glenoid neck with varying glenoid point loads have been used to compare prosthetic durability. Again, because of the complexity of the shoulder joint, 2D models are inadequate. 3D models are few, and a fully 3D model which can fully describe the joint architecture and musculature is required.

It is important to reiterate the point that biomechanical factors affecting the durability of fixation in TSA include the quality and quantity of the glenoid bone stock and the presence of a functioning rotator cuff. Regarding the success of TSA in RA patients, Frich (1994) reported that complications due to loosening of the glenoid component have been up to 15% in patients with RA. It is, therefore, essential that any pre-clinical test of glenoid prosthetic durability must take these patient-specific factors into account. One of the aims of this thesis is to implement a 3D model of the scapula by generating varying component designs and testing both the *normal* and RA joints. This has not been achieved in a 3D FE model to date.

In summary, the author sees a requirement for pre-clinical tests for evaluation of potential component durability in varying patient pathologies, allowing eventual selection of component designs by the surgeon based on the individual patient requirements. If such a model could be shown to be useful, it could eventually reduce the vast quantity of component designs available by highlighting component superiority at an early pre-clinical stage. As a result, fewer designs will reach the costly clinical trials stage, and those that reach this stage would have a higher probability of improving on existing designs.

Chapter 3

Materials and Methods

3.1 Introduction

A pre-clinical testing platform of computational modelling, physical modelling and animal experiments has been recommended to ensure the mechanical durability of new prosthesis designs (Prendergast and Maher, 2001). From Chapters 1 and 2, it is clear that a very complex geometry, three dimensional muscle and joint loading and a complex range of material properties exist at the glenohumeral joint and scapula region. In addition, the complex shape of the glenoid region and the variation of bone properties make laboratory bench testing problematic. Realistic animal experiments would require testing animals with upper extremity motion of a similar nature to humans, and experiments with such animals (primates) would be of dubious ethical merit. Therefore, it is suggested that with a full precise three-dimensional computational model of the system, calculation of accurate stress magnitudes throughout the bone, prosthesis, and cement mantle can be determined. Consequently, the FE methods required to analyse and compare the durability of glenoid components are described in this chapter. A 3D model of the scapula reported by Lacroix (1997) is used as a starting point for this work. A summary of the methods used for the model generation will be described in the following section; a more complete account is given by Lacroix (1997).

3.1.1 Summary of Model Geometry reported in Lacroix (1997)

One embalmed left scapula, of average anthropometric and geometric properties (Mallon, 1992), was immersed in water in a Perspex box. Scans were taken (Siemens Somoton Plus 4) along the sagittal plane and in the coronal direction. Axial images were reconstructed every 1 mm and transferred from a Siemens MAGICVIEW 1000 workstation to a PC via network. Images were used to create a finite element mesh in MARC (Marc, Palo Alto, CA, USA), see Fig. 3.1. Three-dimensional brick and wedge elements were used to generate the mesh.

3.1.2 Mesh generation of glenoid prostheses and reconstruction of the scapula

If a mesh is to be successful then it is has to be specifically customized to the problem under investigation, e.g. refining the mesh in areas of interest. For this analysis, the mesh

was refined around the glenoid neck of the scapula. For incorporation of each prosthesis design, reconstruction of the entire glenoid region was carried out, see Fig. 3.2. Once the existing prosthesis was removed from the model, the outer geometry of the glenoid was kept in-tact and the interior elements and nodes were deleted. The mesh was then manually rebuilt around the prosthesis in order to provide an "optimal fit". As a result distortion of the elements could be minimized and a good aspect ratio maintained. This process is quite tedious and time consuming but was carried out for the various prosthesis designs for optimal results and to maintain quality in the FE solution.

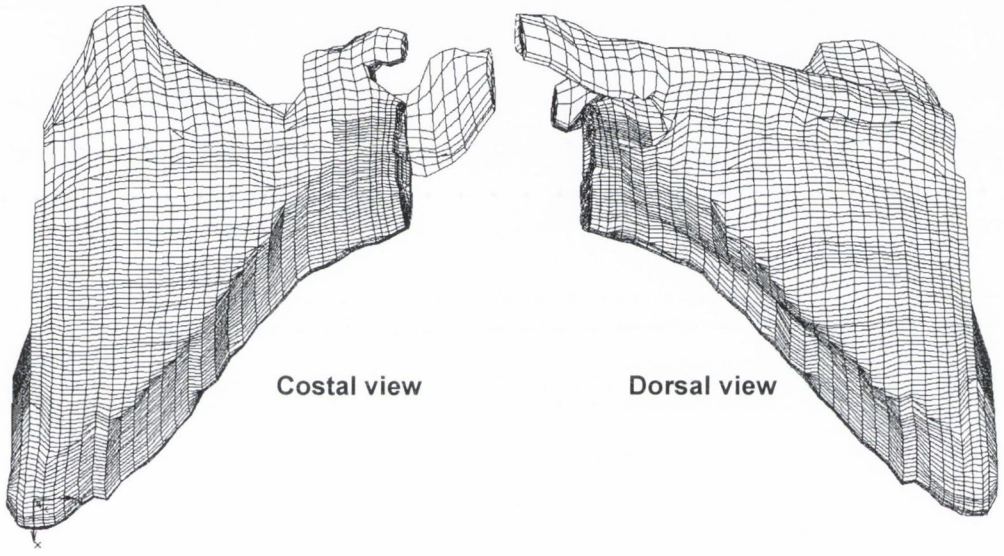

Figure 3.1 *Finite element mesh of the scapula.*

Again, for the fully 3D structure, eight noded brick elements and six noded wedge elements were used for mesh regeneration. Some "tying" of nodes was also required in order to keep mesh regeneration to a minimum. This tying capability is provided by MENTAT (MARC, Palo Alto, CA.) and allows the tying of dissimilar mesh regions together. At the interface between the two regions, see Fig. 3.3, the nodes from the denser mesh region, A, and the elements from the sparser region, B can be tied. The reason for selecting nodes on the finer mesh is that more constraint equations are generated, ensuring a better connection between the sections. The degrees of freedom of region *A* nodes are interpolated with the corresponding degrees of freedom of the nodes on the region *B* elements, using the shape functions of the region *B* elements. Constraint

equations are then written automatically to relate region *A* and *B* nodes at the interface. Fig. 3.4 shows a section through the glenoid region taken in the sagittal plane. This illustrates the differences in glenoid mesh geometry for a keeled and five-pegged prosthesis. Subroutines were also used for specific data output and for data organization.

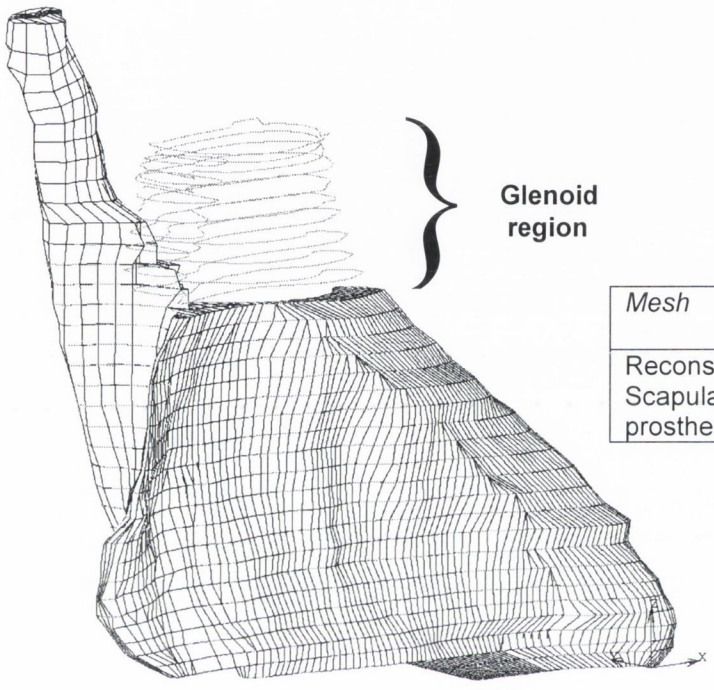

Mesh	*No. of elements*
Reconstructed mesh	~ 4047
Scapula with keel prosthesis	8148

Figure 3.2 *Reconstruction of the glenoid region for insertion of an alternative prosthesis design, corresponding mesh densities are also given.*

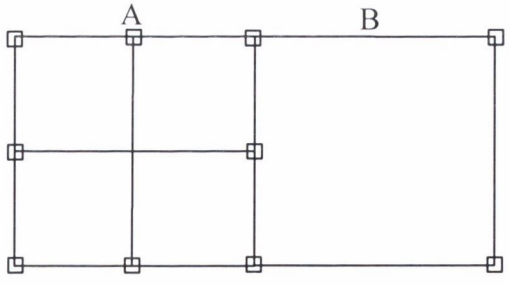

Figure 3.3 *Tying of nodes from denser region of elements A to region B.*

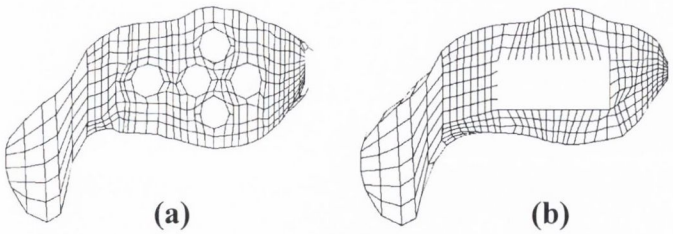

Figure 3.4 *Section through the glenoid bone in the sagittal plane for* ***(a)*** *a keeled prosthesis and* ***(b)*** *a pegged prosthesis.*

The glenoid prosthetic designs were modelled as follows:

(a) an all-polyethylene keeled glenoid prosthesis

(DD 1134-96, DePuy Inc., Warsaw, IN., USA), see Fig. 3.5.

(b) an all-polyethylene pegged glenoid prosthesis

(DD 1134-85, DePuy Inc., Warsaw , IN., USA), see Fig. 3.6.

(c) an all-polyethylene anterior offset keeled glenoid prosthesis

(CPE 649-3-044, Stryker Howmedica Osteonics), see Fig. 3.7.

(d) a metal-backed acormion fixated glenoid prosthesis

(Stryker Howmedica Osteonics, see Fig. 3.8.

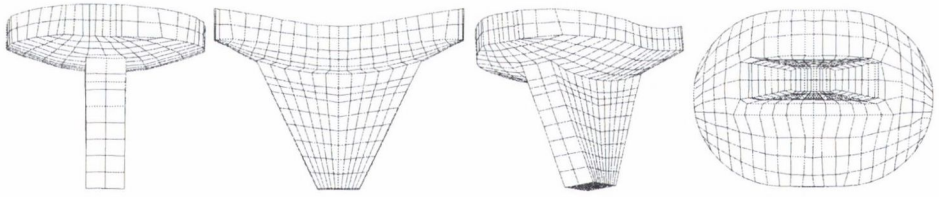

Figure 3.5 *Centre keeled prosthesis mesh* ***(a)*** *inferior,* ***(b)*** *anterior,* ***(c)*** *inferior-anterior views and* ***(d)*** *view from underneath.*

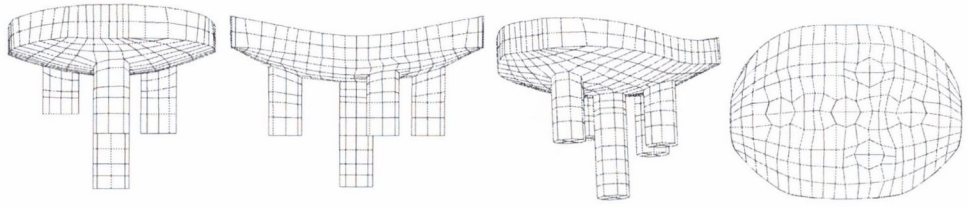

Figure 3.6 *Five pegged prosthesis mesh* ***(a)*** *inferior,* ***(b)*** *anterior,* ***(c)*** *inferior-anterior views and* ***(d)*** *view from underneath.*

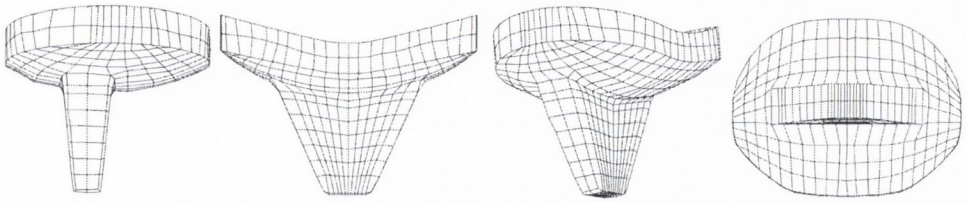

Figure 3.7 *Anterior offset keel* ***(a)*** *inferior,* ***(b)*** *anterior,* ***(c)*** *inferior-anterior views and* ***(d)*** *view from underneath.*

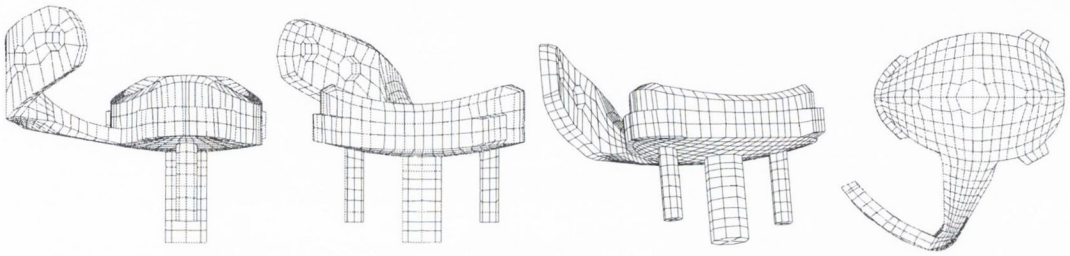

Figure 3.8 *Acromion fixated glenoid design* ***(a)*** *inferior,* ***(b)*** *anterior,* ***(c)*** *inferior-anterior views and* ***(d)*** *view from underneath.*

Insertion of the all-polyethylene prostheses with a cement layer of 1 mm thickness, as advocated by Pearl *et al.,* (1994), was carried out, see Fig. 3.9. For the acromion fixated design a combined cement and screw fixation was used, recommended by Gagey and the HAS system (Howmedica Anatomic shoulder). This involved inclusion of a 1.5 mm cement mantle under the base-plate and a 0.5 mm cement mantle around the glenoid peg. For screw fixation of the baseplate, two cortical bone screws were used. For acromion fixation, two further screws were used see Fig. 3.10. Regarding the acromion fixation screws, it was recommended to allow the screws to break through the acromion bone and to trim them to prevent the sharp tips inserting into the surrounding soft tissue (Gagey, personal communication to Robert Christie, Stryker Howmedica Osteonics).

For analysis of the acromoin fixated design, reconstruction of the glenoid area alone was not sufficient. Reconstruction of the entire acromion was also carried out to incorporate the acromion fixation system, see Fig. 3.11. This figure shows the mesh of the acromion and acromion prosthesis at an intermediate stage. The acromion bone was meshed to fit the acromion arm of the prosthesis. Again the mesh was then rebuilt around the prosthesis in order to provide an optimal fit.

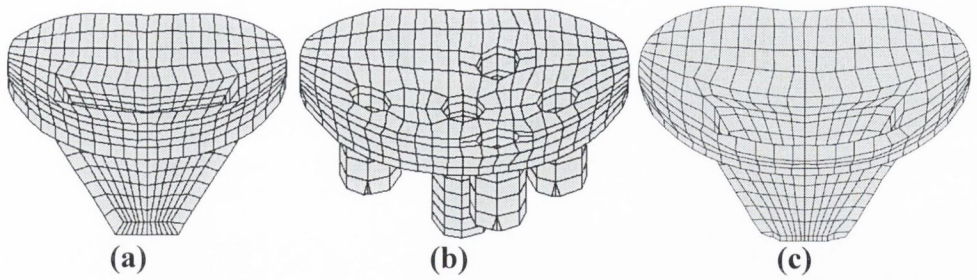

Figure 3.9 *One millimeter thickness cement mantles for* ***(a)*** *the centre-keel design,* ***(b)*** *5-pegged design and* ***(c)*** *the anterior offset keel design.*

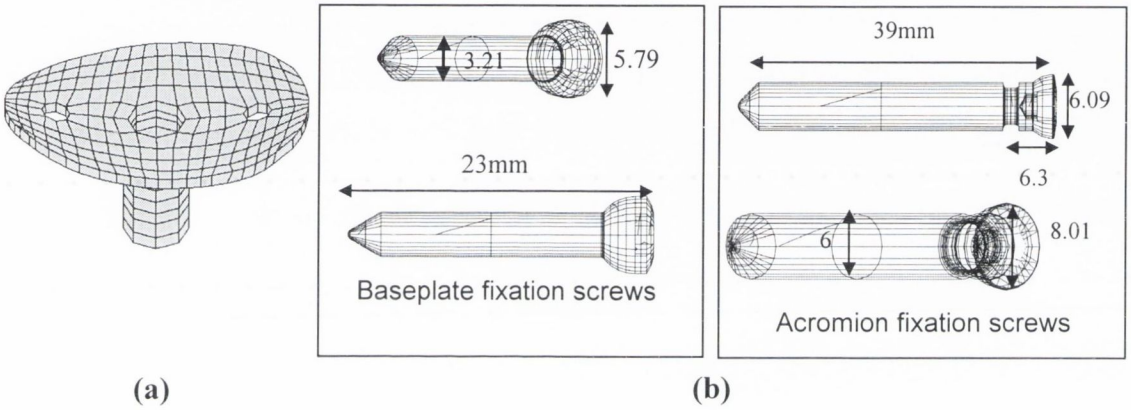

Figure 3.10 ***(a)*** *Cement mantle and* ***(b)*** *screw fixation for the acromion fixated glenoid component.*

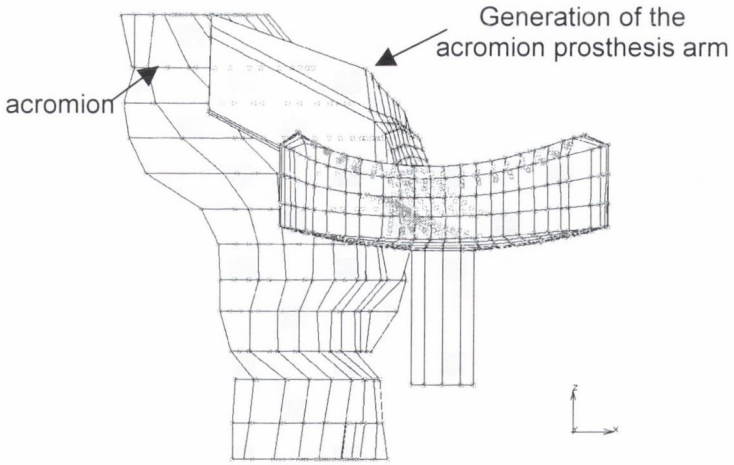

Figure 3.11 *Insertion of an acromial fixated design required rebuilding of the acromion for an optimal fit and to minimize distortion of elements.*

For a better understanding of the entire mesh breakdown, Fig. 3.12 shows the centre keeled and anterior offset keeled glenoid prosthesis meshes as they are inserted into the scapula. Figure 3.13 and 3.14 show insertion of the pegged and acromion fixated designs.

For a comparison of mesh densities, Table 3.1 shows the number of elements for each glenoid component, which allows for comparison of densities for a scapula with no prosthesis inserted and the for the scapulae with the various designs of glenoid components inserted.

Table 3.1 *Comparison of mesh densities for the glenoid components, cement layer and the total meshes.*

Type of prosthesis	*No. of elements Glenoid component*	*No. of elements Cement layer*	*No. of elements Total mesh (including scapula)*
No prosthesis			7251
centre keel	616	484	8148
5-pegged	520	488	8411
offset keel	592	456	8275
acromion design	1157 (polyethylene = 464 metal-backing = 692)	272	8238

As mentioned previously, the mesh in the glenoid region was refined since it is this region which is of particular interest in this study. Refinement of the entire mesh was also carried out in order to investigate if this procedure had any adverse effect on our results, see Fig. 3.15. Table 3.2 shows the number of elements and nodes for the different mesh densities.

Table 3.2 *Comparison of mesh densities for the scapula.*

	No. of elements	*No. of nodes*	*Degrees of freedom*
Mesh 1	8275	11330	33990
Mesh 2	12033	17103	51309
Mesh 3	16501	23901	71703

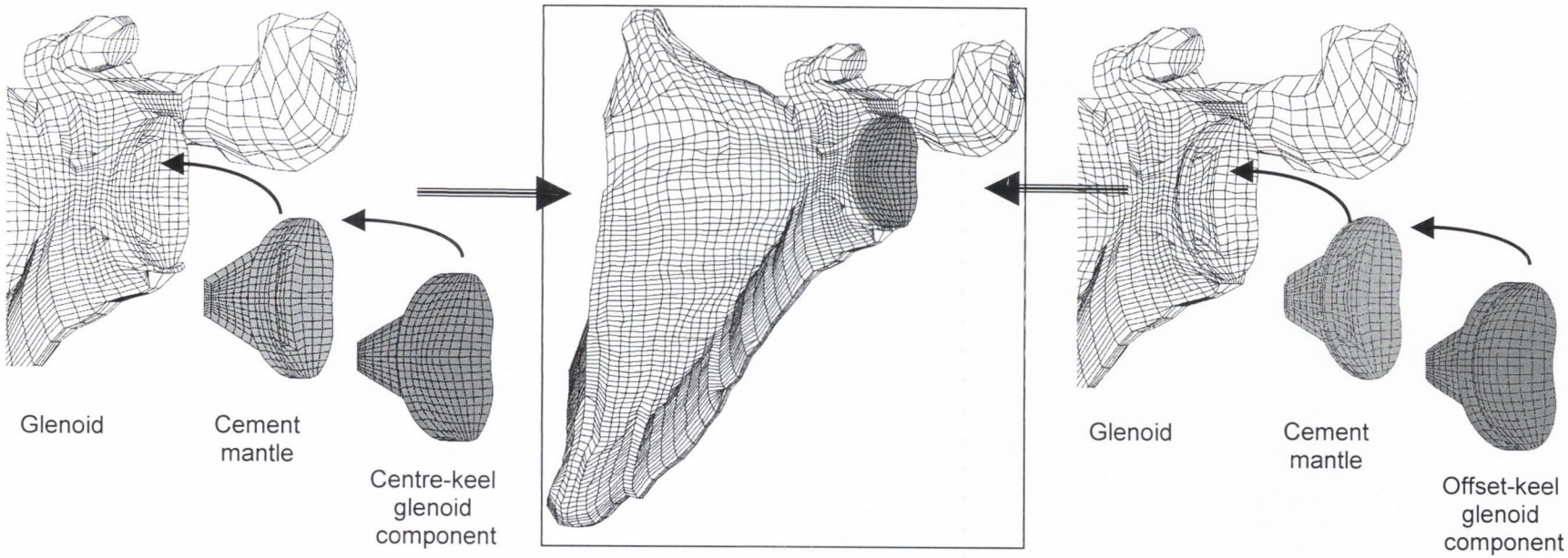

Figure 3.12 Ex*ploded views of the insertion of a centre-keel glenoid prosthesis with a 1 mm thickness cement layer.*

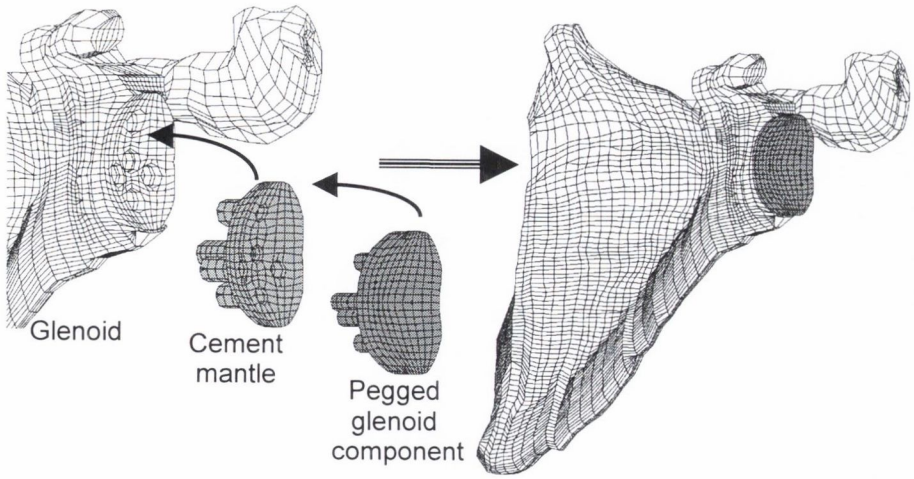

Figure 3.13 *Exploded views of the insertion of a 5-pegged glenoid prosthesis with a 1 mm thickness cement layer.*

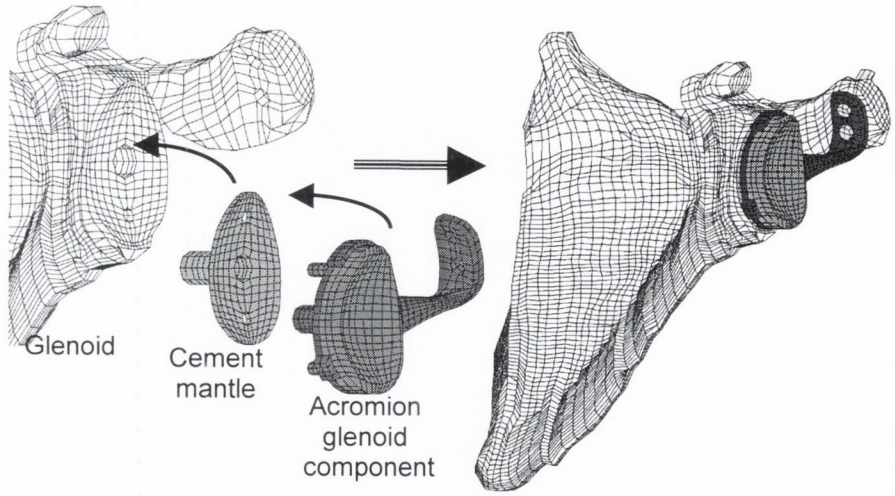

Figure 3.14 *Exploded views of the insertion of an acromion glenoid prosthesis.*

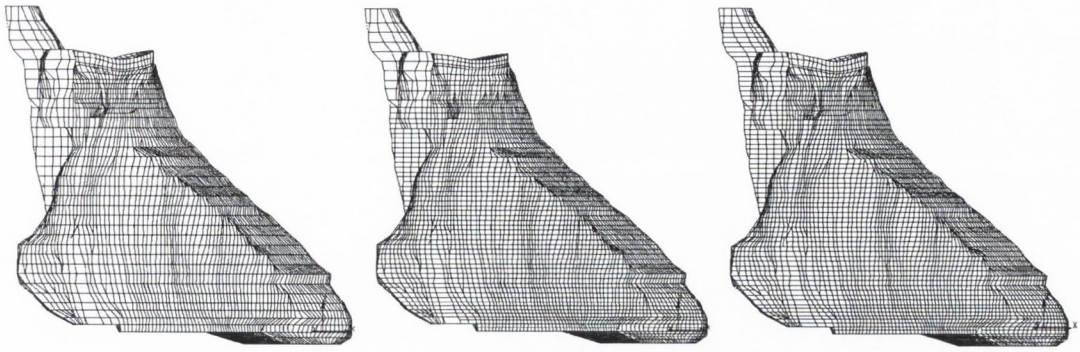

Figure 3.15 *Varying mesh densities for analysis of effect on results.* ***(a)*** *Shows Mesh 1,* ***(b)*** *refined Mesh 2 and* ***(c)*** *further refined Mesh 3. All with a pegged prosthesis inserted.*

3.1.3 Summary of Material Properties reported in Lacroix (1997)

To determine the material properties of the scapula a CT number or Hounsfield number was retrieved for each pixel of the CT scan and correlated to the density of the material by a linear interpolation (Hvid *et al.,* 1989). This CT number is then correlated to the Young's modulus allowing the heterogeneous elasticity of the bone to be defined. The Young's modulus was calculated using the equation developed by Rice *et al.,* (1988):

$$E=0.06 + 0.9\rho^2 \text{ in GPa when } \rho<1.54 \text{ g/cm}^3 \qquad (3.1)$$

and Schaffler and Burr (1988):

$$E=0.09\rho^{7.4} \text{ in GPa when } \rho>1.54 \text{ g/cm}^3 \qquad (3.2)$$

The calculated Young's moduli were rounded to produce 35 absolute values for input into the finite element model. The Young's moduli and Poisson's ratios used for the other materials in the model are given in Table 3.3. These material properties were re-input into the model after glenoid reconstruction.

Table 3.3 *Material properties used for bone cement and the glenoid prostheses.*

Material	*Young's modulus (GPa)*	*Poisson's ratio*
Bone cement (PMMA)	2.2	0.3
Polyethylene (PE)	0.5	0.4
Metal-backing	220	0.32
Cancellous bone screws	220	0.32

3.1.4 Simulation of rheumatoid arthritis in the FE model

From Chapter 2, we can see that erosion of the glenoid in RA is a multifaceted and variable process, and there is no particular accurate method of modelling it. The use of CT data from an individual rheumatoid arthritic scapula would be difficult to justify, as it would be very case specific. In this study, the destructive effects of RA were simulated in the FE model by decreasing the Young's moduli and its corresponding density of the trabecular bone to one-tenth of its normal value. The Young's moduli of the cortical bone were halved to represent both a reduction of its stiffness and a reduction of thickness, see Dalstra *et al.,* (1996), based on experimental work by Frich (1994). This is consistent with the damage associated with a Larsen Grade IV type destruction (Kelly, 1994).

3.1.5 Boundary conditions

The loading of the scapula incorporated in the model was taken from the work of van der Helm (1994). Muscle positions in the study were based on van der Helm's description and also according to the description in Gray's anatomy (Williams, 1995). The muscle locations and areas of application are shown in Fig. 3.16. Muscle and joint load data for 90 degrees of abduction was only available initially. However, the joint reaction force is a maximum of 406N at 90 degrees arm abduction angle (van der Helm and Pronk, 1995), see Tables 3.4 and 3.5, which suggests it may be the most important load angle for analysis. For testing of Hypothesis 2 it was important to include a variable joint load, however, flexion data was not available at the time. Estimations of the joint loading data was carried out using Fig. 2.8, this data is presented in Table 3.5.

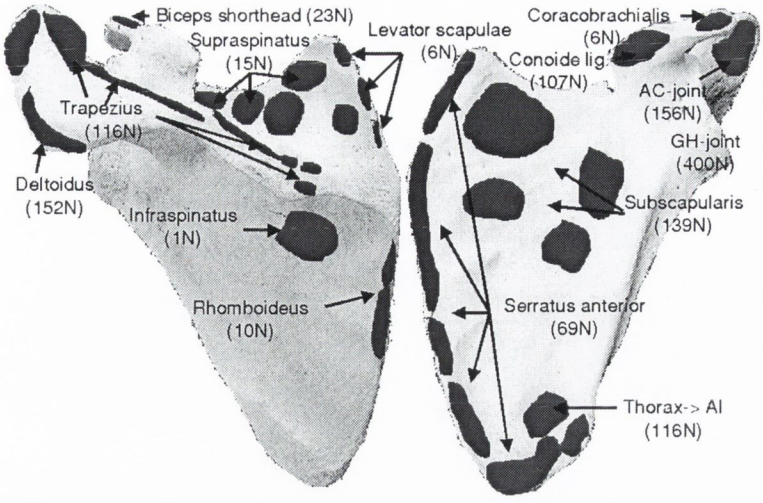

Figure 3.16 *Muscle loads on the finite element model of the scapula at 90 degrees arm abduction. Data from van der Helm (1994).*

Initially, when the directions and magnitudes of the muscles were applied, equilibrium between the forces was not perfectly achieved because of the slight geometric differences between van der Helm's scapula and the one used to generate the CT data for the present finite element model. Therefore, some nodes were restrained to avoid rigid body motion. The resultant reaction force was 118 N indicating that the scapula was almost in equilibrium under the parabolically applied joint force and the muscle loads.

Simulation of the joint load for a closely conforming surface requires that the joint load is parabolically distributed, (Johnson, 1985), this is shown in Fig. 3.17. The contact between the closely conforming surfaces, as a function of the distance from the initial point of contact, is given in the form of a polynomial of degree $2n$, see Johnson (1985). $2n$ is the required order polynomial to describe the initial separation of the contacting surfaces.

For n=1, it is assumed that the load is distributed parabolically with the following load distribution:

$$z = \alpha(x - z_{\max})^2 + \beta(y - z_{\max})^2 + \gamma$$

x and y are the locations of the points on the glenoid surface; z is the load, z_{max} occurs at x=0 and y=0 in the superior-anterior direction, see Fig. 3.17.

α, β, and γ are determined using the following conditions: at $x = 0, y = 0, z = z_{max.}$

at $x = x_{max}, y = 0, z = z_{min.}$

at $x = 0, y = y_{max}, z = z_{min}$

On substitution these conditions give: $\alpha z_{max}^2 + \beta z_{max}^2 + \gamma = z_{max.}$ (3.3)

$$\alpha (x_{max} - z_{max})^2 + \beta z_{max}^2 + \gamma = z_{min.} \quad (3.4)$$

$$\alpha z_{max}^2 + \beta (y_{max} - z_{max})^2 + \gamma = z_{min.} \quad (3.5)$$

Subtracting equation (3.4) from Eqn. (3.5) gives:

$$\alpha = \frac{z_{max} - z_{min}}{z^2_{max} - (x_{max} - z_{max})^2} \quad (3.6)$$

Subtracting equation (3.4) from Eqn. (3.6) gives:

$$\beta = \frac{z_{max} - z_{min}}{z^2_{max} - (y_{max} - z_{max})^2} \quad (3.7)$$

Substituting α and β into Eqn. 3.4 gives:

$$\gamma = z_{max} - \frac{z^2_{max}(z_{max} - z_{min})}{z^2_{max} - (x_{max} - z_{max})^2} - \frac{z^2_{max}(z_{max} - z_{min})}{z^2_{max} - (y_{max} - z_{max})^2} \quad (3.8)$$

A parabolic load can therefore be obtained for different x and y values. The x_{max} and y_{max} values were taken as half the perimeter of the humeral head fitting into the glenoid component (26 mm). Z_{min} was taken as zero, which means that, at the rim, the humeral head exerts no load. The load was calculated so that the sum of the nodal forces

is equivalent to the glenohumeral force found by van der Helm with a maximum joint reaction force in a superior-anterior position (van der Helm, 1994) for 90 degrees arm abduction. Fig. 3.17 shows the intersection of the joint reaction force vector with the articular surface of the glenoid, angled with the frontal and transversal planes. A diametrical mismatch of 6 mm, as recommended by Ianotti *et al.,* (1992) was modelled.

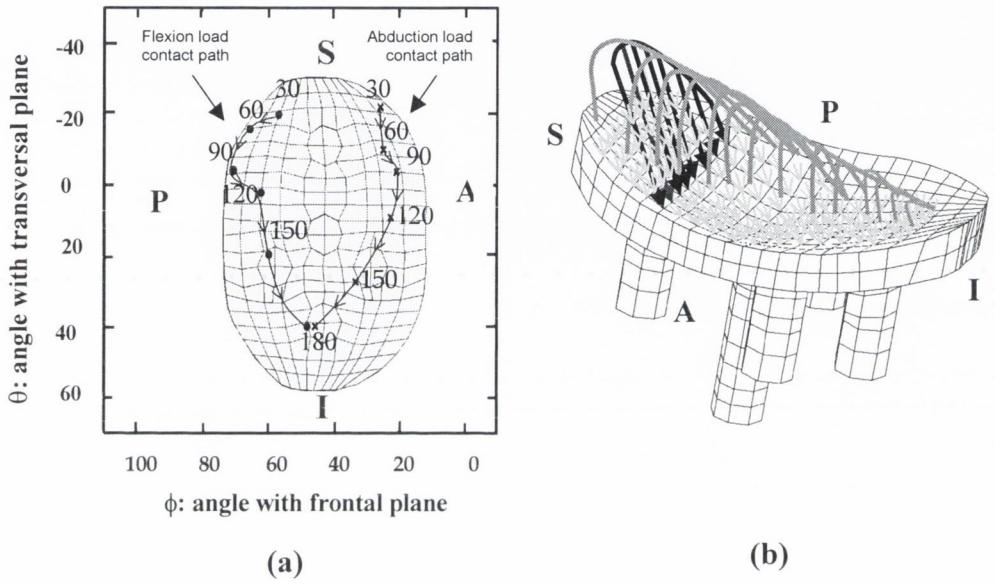

Figure 3.17 ***(a)*** *Schematic representation of the load application on the glenoid surface of a pegged prosthesis mesh (adapted from van der Helm, 1994).* ***(b)*** *The maximum occurs in the superior-anterior quadrant, and the direction of the force is at an angle to the glenoid surface, as shown.*

Table 3.4 *Glenohumeral joint forces for 30 to 180 degrees of humeral elevation in abduction for a right scapula (van der Helm, personal communication).*

Force	*30 deg.*	*60 deg.*	*90 deg.*	*120 deg.*	*150 deg.*	*180 deg.*
x-component (N)	-116.02	-295.89	-355.76	-273.43	-97.19	-19.67
y-component (N)	113.52	28.82	-76.63	-175.08	-156.34	-76.69
z-component (N)	34.01	133.41	148.24	119.61	57.4	24.21
Total force (N)	165.84	325.85	392.95	346.01	192.83	82.79

Table 3.5 *Glenohumeral joint forces for 30 to 180 degrees of humeral elevation in flexion for a right scapula, estimated from Figure 2.9.*

Force	*30 deg.*	*60 deg.*	*90 deg.*	*120 deg.*	*150 deg.*	*180 deg.*
x-component (N)	69.26	101.57	96.19	81.57	40.01	15.39
y-component (N)	-107.73	-96.96	13.85	92.34	25.39	76.95
z-component (N)	-138.51	-265.48	-323.19	-256.24	-136.97	-61.56
Total force (N)	188.65	300.32	337.48	284.33	144.94	99.74

Muscle forces for thirty to 180 degrees of abduction are summarized in Table 3.6 (which became available later in this study) and are detailed in Appendix B.

Table 3.6 *Muscle loads (in Newtons) for 30 to 180 degrees of abduction (van der Helm, personal communication).*

Muscle	*30 deg.*	*60 deg.*	*90 deg.*	*120 deg.*	*150 deg.*	*180 deg.*
Trap scap	86.04	99.244	86.11	68.71	40.46	29.63
trap clav	0	0	0	0	0	0
levator scap	11.18	7.2584	6.75	5.49	0	0
pect minor	0	0	0	0	0	0
rhomb	16.22	10.04	9.9	13.78	8.71	5.71
serr. Ant	69.41	72.59	62.72	53.66	41.16	32.49
delt scap	146.0	153.36	151.02	96.97	40.7	20.71
delt clav	0	0	0	0	0	0
coraco bra	0	0.53	5.94	9.03	4.02	1.15
infrasp	5.784	31.36	1.31	0	0	0
teres minor	0	0	0	0	0	0
teres maj	0	0	0	0	1.27	1.27
supra	11.54	24.52	15.21	6.24	0	0
subscap	25.404	100.97	138.65	108.61	54.18	9.31
biceps L	10.644	29.19	23.57	11.46	0	0
biceps S	0	6.29	22.46	21.85	2.13	2.13

3.2 Investigation of Hypotheses

3.2.1 Testing of Hypothesis 1

For investigation of the first hypothesis, a keeled prosthesis and a five-pegged prosthesis were analysed in both *normal* and RA (Larsen Grade IV) bone under the maximum glenohumeral joint load of 90 degrees of abduction.

3.2.2 Testing of Hypothesis 2

This investigation concentrated on determining the potential durability of a centre keeled prosthesis compared to an offset keeled prosthesis under the effects of the "rocking horse mechanism", see Fig. 2.24. The analysis involved applying various flexion and abduction joint loads on the glenoid surface. Therefore, the stability of the prostheses for different angles of humeral elevation can be compared. Again since the outcome of prosthesis durability is hindered by the effects of RA, the prosthesis performance was also compared in a simulated RA joint. For the RA joint, a Larsen Grade IV type destruction was reproduced and proximal subluxed loads were also applied associated with a deficient rotator cuff for zero to 180 degrees in flexion and abduction. The subluxed loads were simulated by moving the joint load superiorly by 5 mm.

3.2.3 Testing of Hypothesis 3

Since continued interest in new designs is largely due to the fact that when arthritis exists the *unconstrained* system still requires adequate repair of the rotator cuff. These "alternative" designs have used the acromion to aid in fixation of the glenoid prosthesis and to reduce impingement of the humeral head. It has been hypothesised that attachment of the glenoid component to the acromion may minimise loosening rates and possible rupture of the rotator cuff (Gagey and Mazas, 1990). Investigation of this hypothesis involved analysis of the relative motion between the acromion and glenoid under the action of the muscle and joint forces for various arm abduction angles. This procedure is carried out in order to determine if a type of *load sharing* occurred between the acromion and glenoid.

3.3 Methods for analysis of results

From previous studies it is clear that the magnitude of stresses generated in the polyethylene glenoid component are not high enough to cause failure, whereas, stresses produced in the cement mantle were of critical magnitude (Lacroix *et al.,* 2000). In previous studies stresses were calculated for a pre-determined path plot around the interface of the cement layer, see Fig. 3.18 (a), (Lacroix, 1997) or cement mantle stress plots alone were presented (Baréa, 1998). However, this first method is restricted as it only takes into account the particular "line" selected around the interface and may miss other critical stresses throughout the cement layer. Furthermore, this method represents stresses at the interface only and not throughout the entire element. Regarding the second method, in a complex component such as the glenoid cement mantle, the stress distribution plots can be very intricate and difficult to visualize. Therefore, plots of the stress distribution in the cement mantle may be limited. As a result an alternative method will be used which involves calculating a total volume of cement at each stress level throughout the entire cement layer, see Fig. 3.18 (b). This allows for a more quantitative and thorough analysis to be carried out. The procedure involved calculating the volume of each element and by determining the maximum principal tensile stress in each element, the volume of material stressed between 0-1 MPa, 1-2 MPa, 2-3 MPa, etc. was determined. In this way the volume of highly stressed cement in each design could be determined and compared. Stress distribution plots are also presented as they may give important information regarding the location of stress concentrations etc.

To determine the significance and consequences for failure due to the stress produced in the cement layer, we can predict the associated probability of crack initiation. A nonlinear relationship exists between cement stress and probability of failure. As a result the duration of fixation is severely compromised under higher stresses. This has been investigated by Krause *et al.,* (1988) who developed probability of survival curves for the cement. This relationship is further analysed by Murphy and Prendergast (2000), where a relationship between probability of survival Ps and maximum principal stress σ (in MPa) was derived experimentally by for hand-mixed bone cement, for 10 million cycles:

$$P_S = -a\sigma^3 + b\sigma^2 - c\sigma + d \qquad (3.9)$$

where $a = 0.0005$, $b = 0.0202$,

$c = 0.3304$ and, $d = 1.8365$.

The amount of cement material above a given probability of survival can be calculated with this equation. Thus the probabilities of survival of the cement mantle for each design in the various bone stock qualities can be compared. Finally, the various stress distributions in the entire scapula bone were compared for each design against the natural case. As a result the effect, if any, of the natural stress distributions by insertion of various glenoid component designs can be analysed.

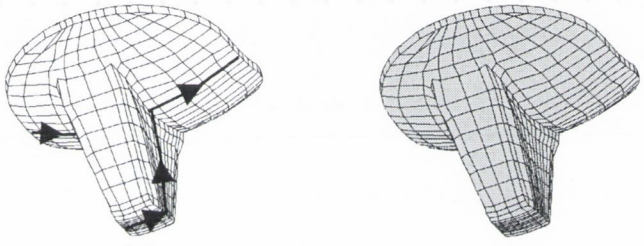

Figure 3.18 ***(a)*** *Method 1 involves taking a path-plot around the cement layer and* ***(b)*** *method 2 takes the stress distribution throughout the entire cement volume.*

3.4 Confirmation of results produced by the FE model

3.4.1 Introduction

Finite element (FE) models in general are only a representation of reality. Results obtained from the model are entirely dependent on how well the model represents reality with respect to the system to be analysed. Similarity of strain data obtained from experimental and FE models is necessary, therefore, to confirm that valid results are being realised.

Experimental methods of validation include strain gauging and the photoelastic technique. Both techniques have been used in the past for bioengineering applications (Orr and Shelton, 1997). However, due to the complex shape of the scapula strain gauging has proved difficult in the past (Lacroix, 1997). Furthermore, strain gauging only gives point measurements and a qualitative stress distribution can only be achieved if a lot of strain gauges are applied which is difficult.

3.4.2 The photoelastic technique

The *photoelastic technique* is based on the property that most transparent materials are *birefringent* when strained. The technique is a visual technique for measuring strains with the capability of measuring a full stress distribution over an entire component. This is particularly useful when analyzing complicated geometries or complicated loading conditions, as it gives a visual *full-field* representation of the stress. Thus critical areas of high and low stress distributions can be identified. The procedure involves making a model version of the component to be tested using a birefringent polymer. The problems of representing a natural material, that of bone for example, by plastics have been addressed in the past by using the photoelastic coating technique. Using this technique, when the model is loaded it becomes stressed and this stress is transferred to the coating. The birefringent coating produces groups of fringes termed isoclinics and isochromatics.

The theory behind production of these fringes suggests that since white light is composed of all wavelengths of the visible spectrum, the relative retardation of a wave (i.e. its change in refraction index) causes the elimination of certain wavelengths or colours. The observer can see a complementary colour of the one that was eliminated. In 1816 Sir Brewster formulated a scientific law, which states "the relative change in the refractive index is proportional to the difference of principal strains". Therefore, the relative change in the light wavelength (colour) observed across the surface is related to the change in strain across the surface (Appendix C shows the isochromatic fringe sequence). This provides information on the direction and magnitude of the principal stress differences as follows:

$$\sigma_x - \sigma_y = \frac{E}{1+\nu} fN \qquad (3.10)$$

where σ_x-σ_y is the principal stress difference, E is the elastic modulus of the test part, ν is the Poisson's ratio of the test part, N is the fringe order and f is the fringe value of the coating. In our study this photoelastic technique was used to attempt to validate an existing FE model of the scapula. This involved coating a set of scapulae (the procedure is discussed in the following section) which were loaded and the fringe patterns viewed using a 030 series reflective polariscope, see Fig. 3.19. Point measurements were taken using the null-balance compensator method, see Fig. 3.19.

3.4.3 Selection of the photoelastic coating

The proper selection of photoelastic coating materials is essential for a successful stress analysis. The coating material must give maximum reliability and accuracy under a given set of test circumstances. Irregular shaped structures cannot be coated with flat sheets and a liquid polymer must be used. This can be applied with the contour sheet method or by spraying. The contour sheet method is preferred because a uniform sheet thickness can be achieved more easily. The birefringent sensitivity of the polymer material is an important factor, since this property is involved in the basic equation of the analysis:

$$\varepsilon_1 - \varepsilon_2 = \gamma_{max} = N(\lambda / 2t_c k) = N.f \qquad (3.11)$$

where ε_1- ε_2 = principal strains, in/in (mm/mm)

γ_{max} = maximum shear strain, in/in (mm/mm)

λ = wavelength of light used in the polariscope, in (m)

t_c = thickness of coating, in (m)

K = strain optic coefficient of the polymer material, dimensionless

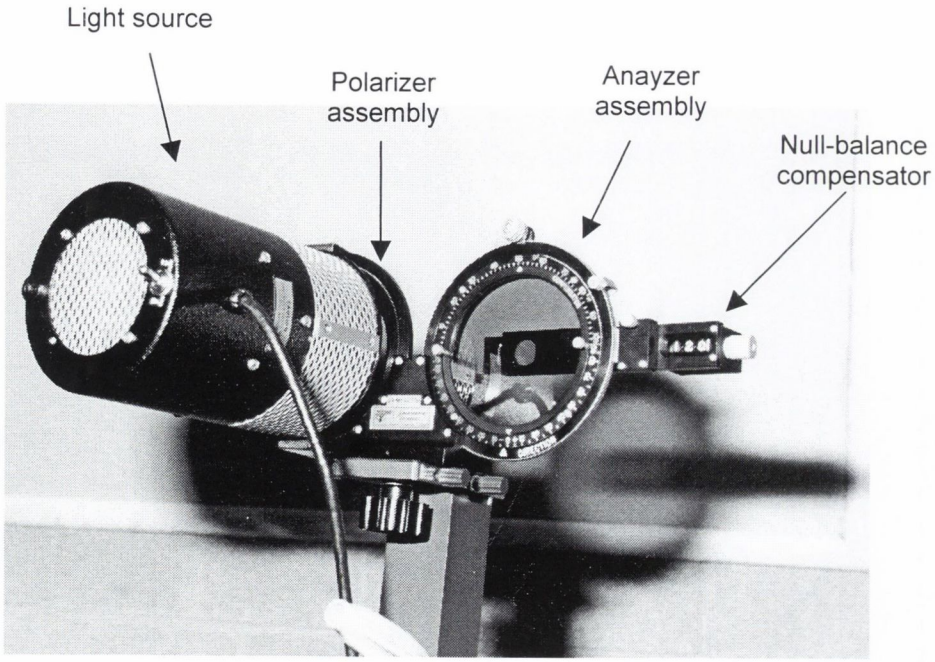

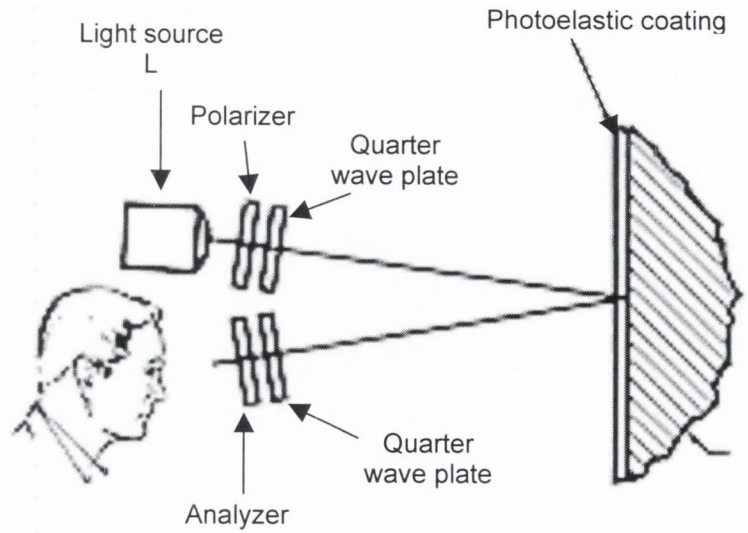

Figure 3.19 *030 series reflection polariscope.*

The overall sensitivity depends, firstly on the sensitivity of the coating, the lower f is the more sensitive the coating and secondly, the sensitivity of the polariscope system for determining N. The polymer is available in three different sensitivities, high, medium and low modulus materials. Since our test piece is bone, which will experience small strains compared to polymer or rubber, we chose a high modulus polymer. Consulting the manufacturers range we chose PL-8 liquid and PC-1 adhesive (see Appendix C). Information supplied by the manufacturer is based on tests being performed at room temperature. The variations of temperature during our tests were approximately 5°C, which will have negligible effects on the properties.

3.4.4 Casting and contouring procedures

For optimal results the coating was cast to conform exactly to the shape of the scapula surface with a uniform thickness.

Materials required for coating preparation

- PL-8 liquid
- PL-1 adhesive
- Teflon coated adjustable coating plate (see Fig. 3.20)
- Silicone rubber, snap together, adjustable frame (see Fig. 3.20)
- Machinists spirit level
- Mould cover
- Stem thermometer
- Acetone
- Gauze sponges
- Releasing agent
- Scissors

Preparing the casting plate

- The casting plate, Teflon sheet and silicone frame, were thoroughly cleaned with gauze sponges soaked with acetone.

- A thin film of releasing agent was applied to the surface of the plate and the parts of the frame in contact with the polymer.
- The casting plate was levelled in two perpendicular directions with the spirit level. This facilitated the flow of the liquid polymer by making it perfectly horizontal.
- The rubber frame was then assembled on the surface to the required sheet size with at least 6mm extra on all sides to compensate for the meniscus that forms during polymerisation of the liquid polymer, see Fig. 3.20.
- The plate was then covered to protect the surface from dust and contaminants.

Preparing the polymer

The polymer was supplied in the form of a resin and a hardener. These were stored in a refrigerator and brought to room temperature before use. The amount of resin and hardener required was determined as follows:

$$W = \rho.A.t \qquad (3.12)$$

where W = mass required (g)

A = area of sheet to be cast (mm^2)

t = thickness (mm)

ρ= polymer density = 1.13E-03 (g/mm^3).

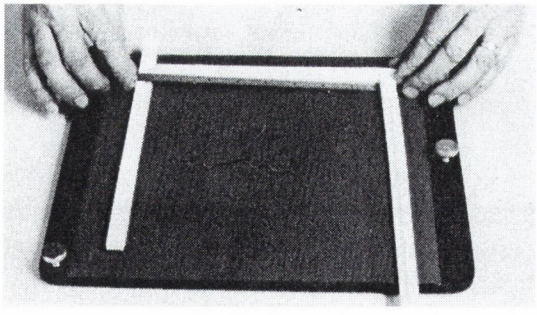

Figure 3.20 *Casting plate with silicone adjustable frame, after the Measurements Group, (1992).*

The resin to hardener proportion was calculated in *parts per hundred* (pph), 10 pph of hardener means 10 grams of hardener for 100 grams of resin. For type PL-8 plastic, the hardener amount is 17 pph.

- The polymer and resin were weighed out carefully and were heated to the recommended 32°C before mixing.
- The hardener was added to the resin and the mixture was stirred slowly, to avoid the introduction of air bubbles, using a stem thermometer.
- The temperature increased during mixing due to an exothermic reaction. When it reached 52°C it was ready for pouring.
- The polymer was poured onto the plate in an "S" pattern and the cup was kept close to improve the flow over the surface, see Fig. 3.21.
- It was recommended that excess mixture was not scraped from the cup sides or bottom as these are the areas of non-uniform mix.
- Bubbles at the surface were removed carefully.

Polymerisation cycle

The liquid polymer passed through several stages before arriving at the contouring stage. At this contouring stage the polymer was highly flexible and it had no geometric or photoelastic memory. The time to reach this stage was dependant on several factors: room temperature, casting plate temperature, type of polymer, thickness and polymer temperature when poured onto the plate. The time for polymerisation was defined using the following stages:

(i) Early stage of polymerisation: When the polymer was probed it was still a liquid, i.e. it stuck to the probe when touched.

(ii) Second stage of polymerisation: The polymer was no longer a liquid, i.e. it no longer stuck to the probe.

(iii) Approaching the contouring stage: The polymer was pressed down with light pressure on the probe and a corner of the frame could be removed

without flow. The edge of the polymer was raised using a "snap-like" flick, the under-surface was sticky and tended to stretch if held too long.

(iv) Optimum stage for contouring: The polymer could be pressed down with moderate pressure on the probe. The corner of the sheet could be lifted up easily with little or no stretching, the under-surface was dry, see Fig. 3.22. The sheet was easily cut with a scissors.

(v) Beyond this: Heavier pressure was needed to depress the polymer. When the corner was lifted it felt stiff. The polymer was cut with difficulty and tended to shatter. At this stage the polymer had an elastic memory and returned to its original flat shape if deformed. Finally, the polymer became a solid flat shape if deformed.

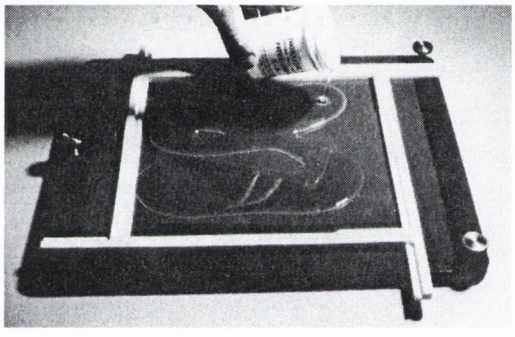

Figure 3.21 *Preparation of the polymer, after the Measurements Group, (1992).*

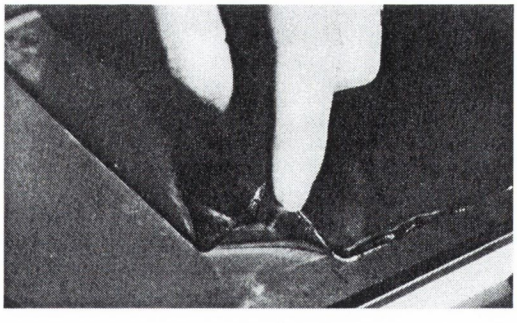

Figure 3.22 *Optimum stage for contouring, after the Measurements Group, (1992).*

Surface preparation

The surface of the scapula was prepared by cleaning it with isopropyl alcohol, as recommended by the Measurements Group (1992). The surface of the polymer coating was prepared as follows:

Removing the semi-polymerised sheet from the mould:

- When the polymer reached the final stage, the rubber was removed from around the sheet.
- Hands, scissors, the surface of the part and the top surface of the polymer were lubricated with mineral oil.
- One corner of the sheet was lifted using a flicking action with one finger and the entire sheet was removed in one motion as removing it slowly would stretch the sheet.
- The sheet was then placed topside down on the casting plate and the mineral oil applied to the upper side.
- A 6mm border was then cut off. A calibration sheet was also cut off and the sheet divided up if required at this stage.
- Calibration of the sheets was carried out by bonding the samples to a bar 318 mm by 25 mm, thickness 6.35 mm, recommended by the Measurements Group (1992). The bar was loaded as a cantilever using dead weights. The fringe value of the coating was determined from the equation of bending of the bar.

Contouring

- The sheet was placed on the part with the original (top) surface in contact with the part. This was important because the bottom part was in contact with the releasing agent, which could affect the eventual bonding.
- One edge of the coating was first brought into contact with the part and the sheet was progressively worked into place. If air pockets formed, the coating was lifted and more mineral oil added and contoured again. The polymer was not allowed to sag under its own weight while being contoured.
- The polymer was then left to polymerise for at least 18 hours.

3.4.5 Adhesion

The adhesive was supplied as a resin and a hardener which had a limited work time once mixed. The surface of the part and coating were fully prepared before preparing the adhesive as follows:

- The surface of the part was degreased using acetone to remove the mineral oil.
- The coating was then cleaned and placed over the surface part. Masking tape was then applied about 5mm from the sheet boundaries, to give a clean boundary.
- The amount of adhesive required was approximately 1 gram for an area of $10cm^2$. This gave a layer of adhesion of 1mm thick. When the sheet was applied, excess adhesive was squeezed out, leaving a layer of about 0.1 to 0.25 mm thick.
- The amount of hardener required with the resin PC-1 was 10pph. The resin was preheated to 32°C while the hardener was used at room temperature. The hardener was added to the resin, and thoroughly mixed using a wooden stirrer. A non-streaked homogenous mixture was reached after approximately five minutes. The adhesive was poured onto the test part and spread evenly with a brush.
- One edge of the polymer was placed on the part and the entire sheet was worked down slowly onto the adhesive preventing air bubbles and extra adhesive developing.
- When the extra adhesive was forced out a thin layer of adhesive was applied around the edges of the polymer to prevent moisture absorption. At the area where the part and the polymer do not meet an adhesive bevel was built up.
- After about 12 hours at room temperature the adhesive was cured fully and the component was ready for testing.
- After testing the coating could be hammered off and the rest of the adhesive could be removed using tetrachloroethans.

3.5 Experimental set-up

Five scapulae were coated and restrained along the medial border in an aluminium box using bone cement. Loading of the scapula was carried out using the modular head of a humeral prosthesis, see Fig. 3.23. Incremental loads of 0.2-1.6 kN were applied in steps of 0.2 kN using the modular head of a humeral prosthesis. These glenohumeral loads were applied for a comparative analysis and were not meant to be reflective of any physiological load. Resulting stresses were then observed using the reflection polariscope and measurements were taken using the null balance compensator.

The FE model of the scapula was also coated with the photoelastic material (E = 2.9 GPa, ν = 0.36), an adhesive layer was not included (usually 0.01 mm thickness) but the coating was assumed to be rigidly bonded to the scapula which is the aim of the adhesive. The scapulae were then restrained along the medial border and the glenoid was loaded parabolically to the same order of magnitudes. Plots of shear stress distributions on the experimental coating and on the finite element coating were then compared.

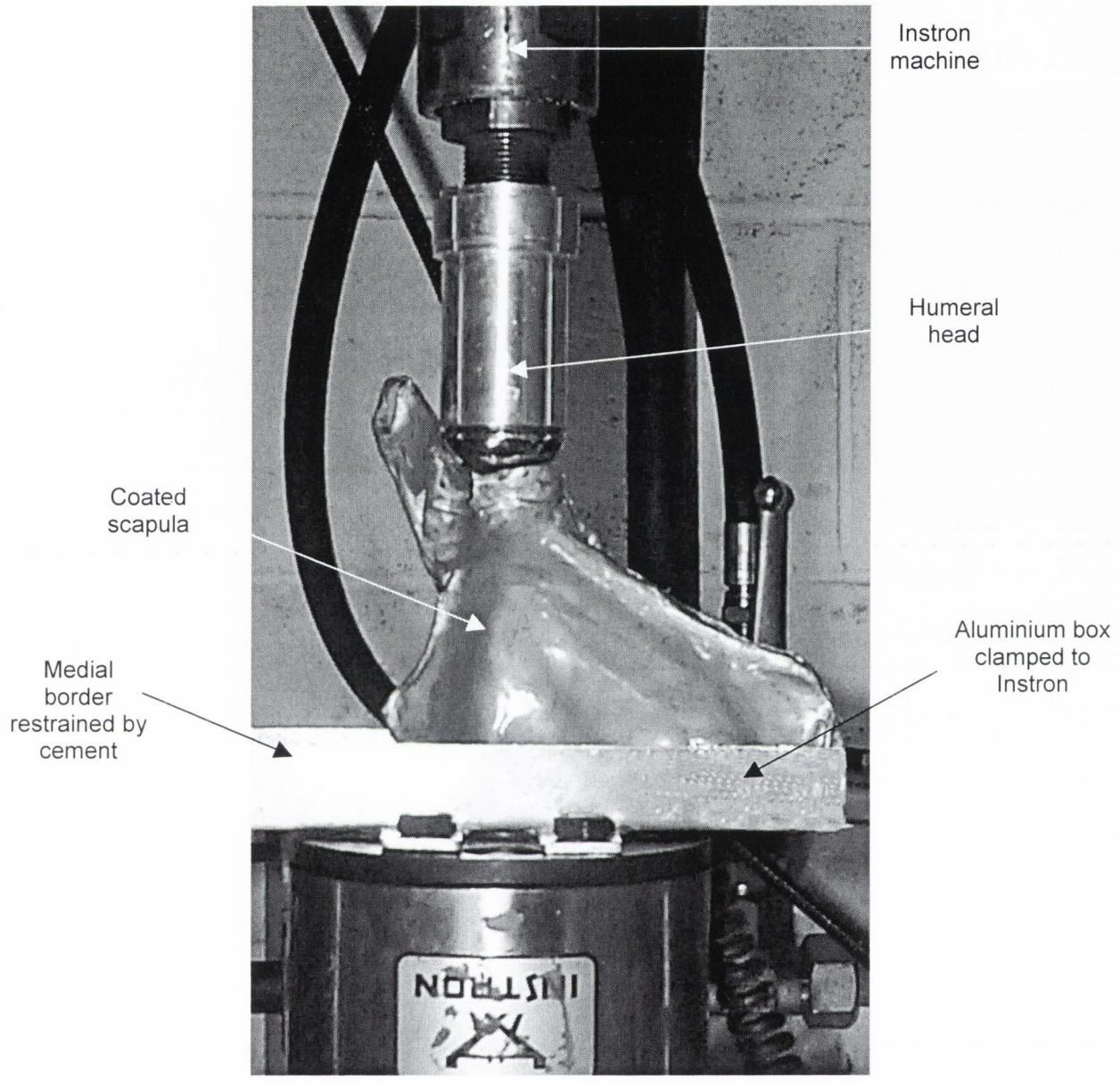

Figure 3.23 *Experimental set-up.*

Chapter 4

Results

4.1 Introduction

The results are presented in this chapter in order to test the three hypotheses posed in Chapter one, Section 1.3. First, however, it must be confirmed that the results obtained with the FE model are reasonable. This is done by comparing them with results obtained using the photoelastic technique.

4.2 Confirmation of the FE results using the photoelastic technique

Figure 4.1 to 4.5 shows the photoelastic fringe patterns for scapula one to five at 1.6 kN glenohumeral load. These plots compare the costal and dorsal views of each individual scapula which can be compared to the FE model of a *coated* scapula. Figure 4.1 shows that high shear stresses occur at the medial border of the scapula (this is where the scapula is restrained by the cement) on the costal side. In particular, high stresses are noted at the junction of the medial border and the superior border. On the dorsal side, high stresses are seen at the junction of the spine of the scapula and medial border and are also noted at the supraspinous fossa. These high stresses are identified by the localised increments of fringe colours. Similarly, for Fig. 4.2, high localised stresses can be identified at the medial border at the supraspinous fossa. Figure 4.3 to 4.5 also show a similar pattern of stress distributions. For comparison to the FE model of the coated scapula, Fig. 4.6 plots the costal and dorsal views of the scapula for a 1.6 kN load.

Calculating the shear stress values at appropriate points which correspond to regions of high stress in the FE model, we find for example, for N=4, a maximum shear stress of 30 MPa was reached experimentally at the superior border. Analysis of the coated finite element model showed that high shear stress distributions occurred along the superior border and supraspinous fossa of the scapula (> 25 MPa). High shear stresses were also observed along the medial border where the scapula is restrained by the cement (> 25 MPa). A plot of these stresses are given in Fig. 4.7 for the maximum glenohumeral load of 1.6 kN and are schematically compared to some of the photoelastic results.

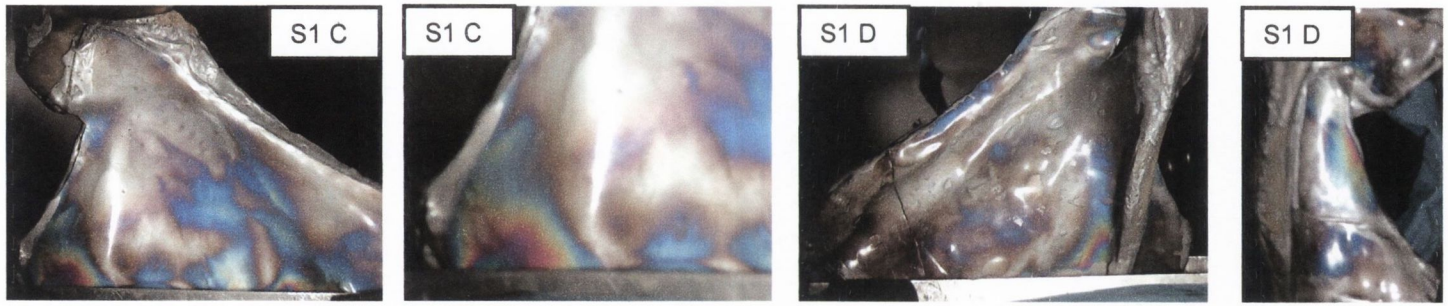

Figure 4.1 *Photoelastic stress analysis plots for scapula 1 at a 1.6 kN load, C refers to the costal view and D refers to the dorsal view.*

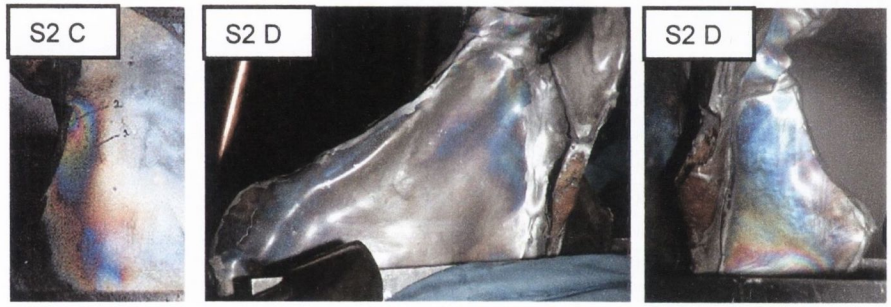

Figure 4.2 *Photoelastic stress analysis plots for scapula 2 at a 1.6 kN load, C refers to the costal view and D refers to the dorsal view.*

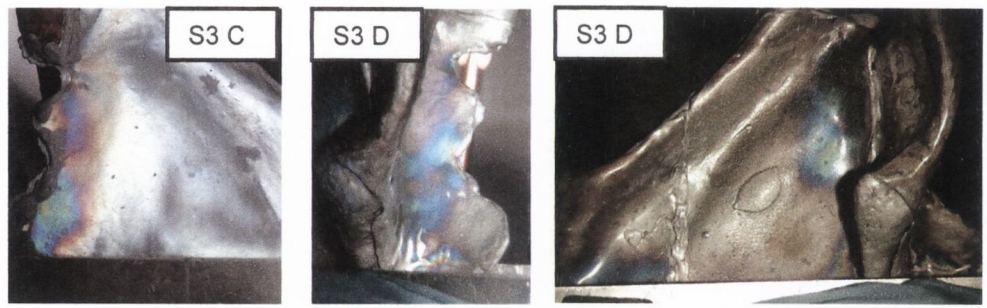

Figure 4.3 *Photoelastic stress analysis plots for scapula 3 at a 1.6 kN load, C refers to the costal view and D refers to the dorsal view.*

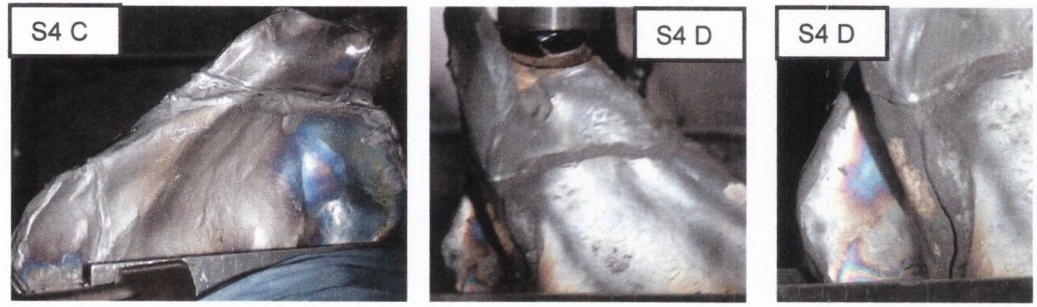

Figure 4.4 *Photoelastic stress analysis plots for scapula 4 at a 1.6 kN load, C refers to the costal view and D refers to the dorsal view.*

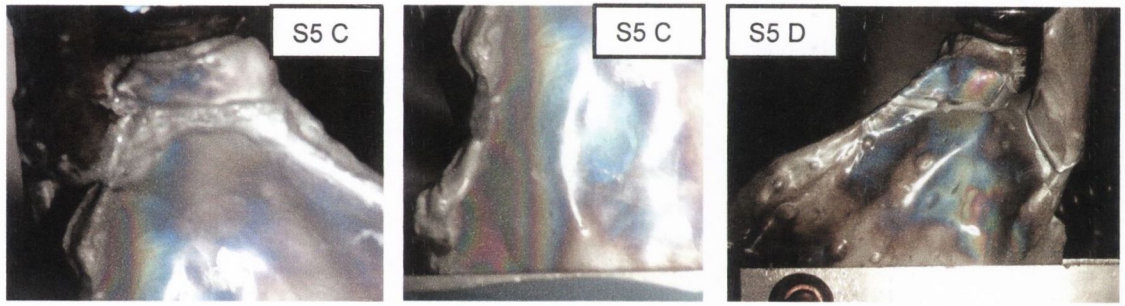

Figure 4.5 *Photoelastic stress analysis plots for scapula 4 at a 1.6 kN load, C refers to the costal view and D refers to the dorsal view.*

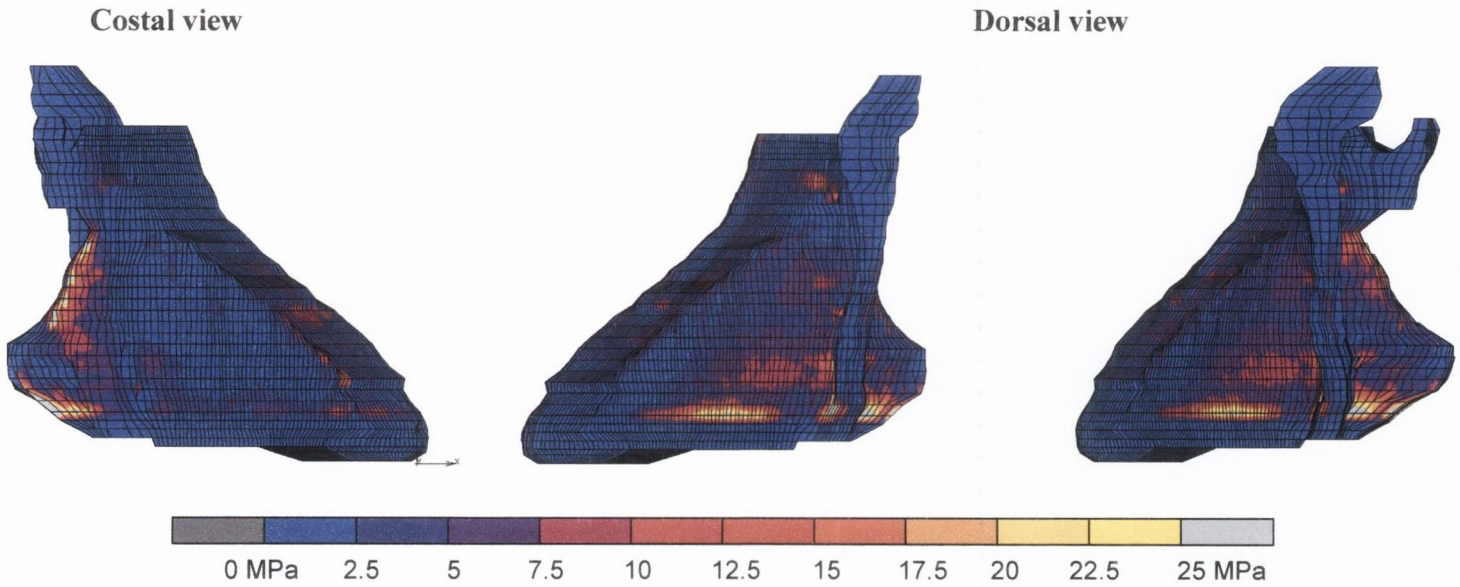

Figure 4.6 *Shear stress plots produced in the FE model of the coated scapula.*

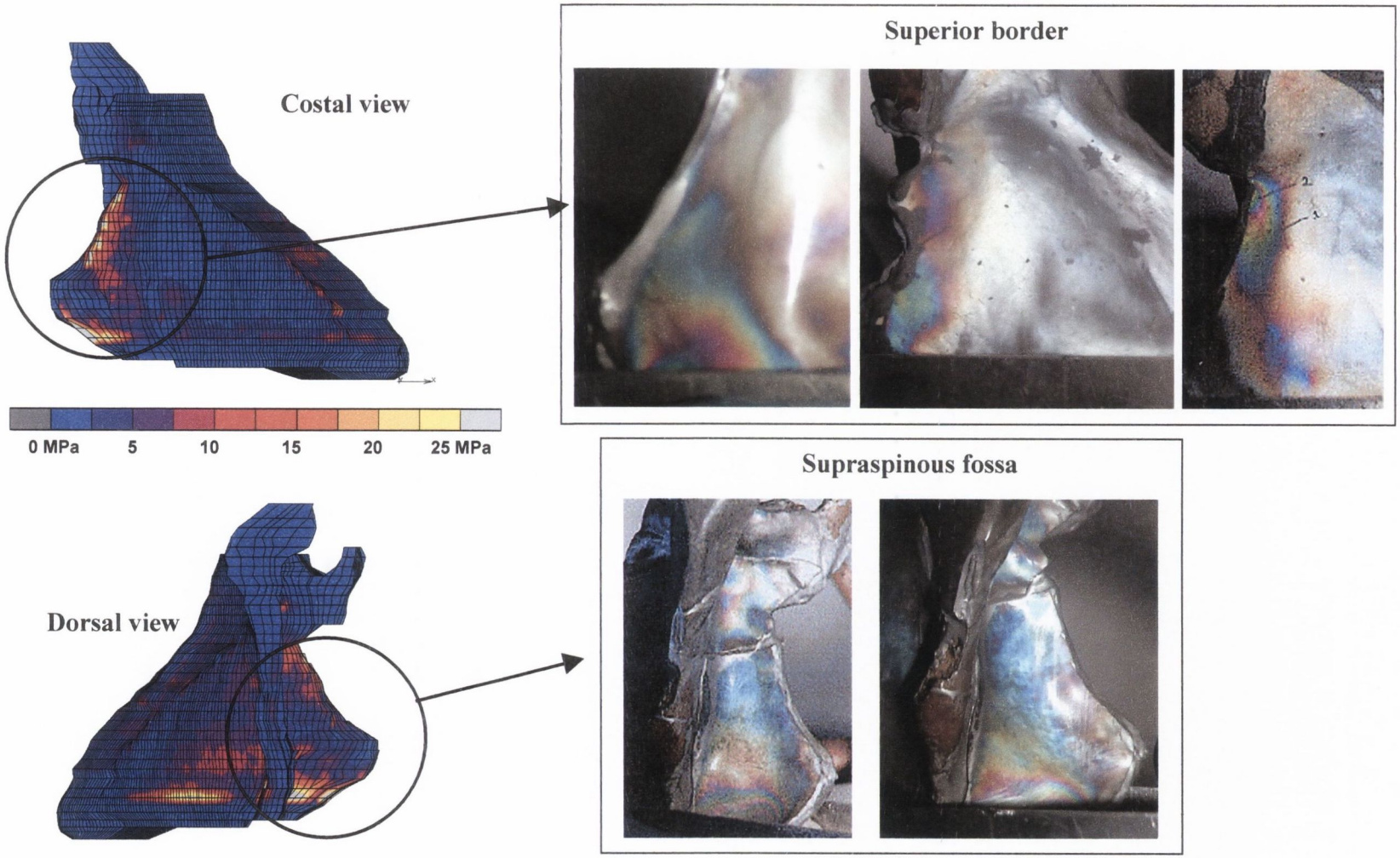

Figure 4.7 *Schematic comparison of the shear stress produced in the FE model of the coated scapula with the photoelasticity results.*

4.3 Comparison of mesh densities

Refinement of the entire mesh was also carried out to investigate if this procedure had any effect on our results. Mesh densities for the entire scapula for mesh 1 (33990 degrees of freedom), the refined mesh (51309 degrees of freedom) and a further refined mesh (71703 degrees of freedom) with a pegged prosthesis inserted are compared. The model was loaded with 90 degrees of abduction muscles and joint load and the resulting maximum principal stress plots are shown in Fig. 4.8 (a). This figure shows that similar stress distributions are achieved for both the original and refined meshes. Using the concept discussed in Chapter 3, the volume of cement stressed to a particular level is plotted for each mesh allowing comparison of the varying densities, see Fig. 4.8 (b).

4.4 Stress distributions in the natural scapula

Stress distribution plots in the natural scapula, i.e. with no prosthesis implanted, showed high maximum principal stresses (mostly tensile) occurring along the spine of the scapula due to the large force of the trapezius muscle and the acromioclavicular joint load acting there, see Fig. 4.9 (a) and (b). For 90 degrees of abduction, the line of the load acts towards the central thinner area of bone. However this is not highly stressed because the thicker borders of the scapula act as "pillars" to take this load. As a result high minimum principal stresses (mostly compressive) occur along the lateral border of the scapula due to the load being transferred there, see Fig. 4.10. Also, large stresses occur below the glenoid due to a narrowing of the neck of the glenoid in this region and due to mesh refinement. These natural scapula stress distribution plots will be used to compare the effects on the scapula distributions of implanting glenoid component prostheses with and without acromion fixation.

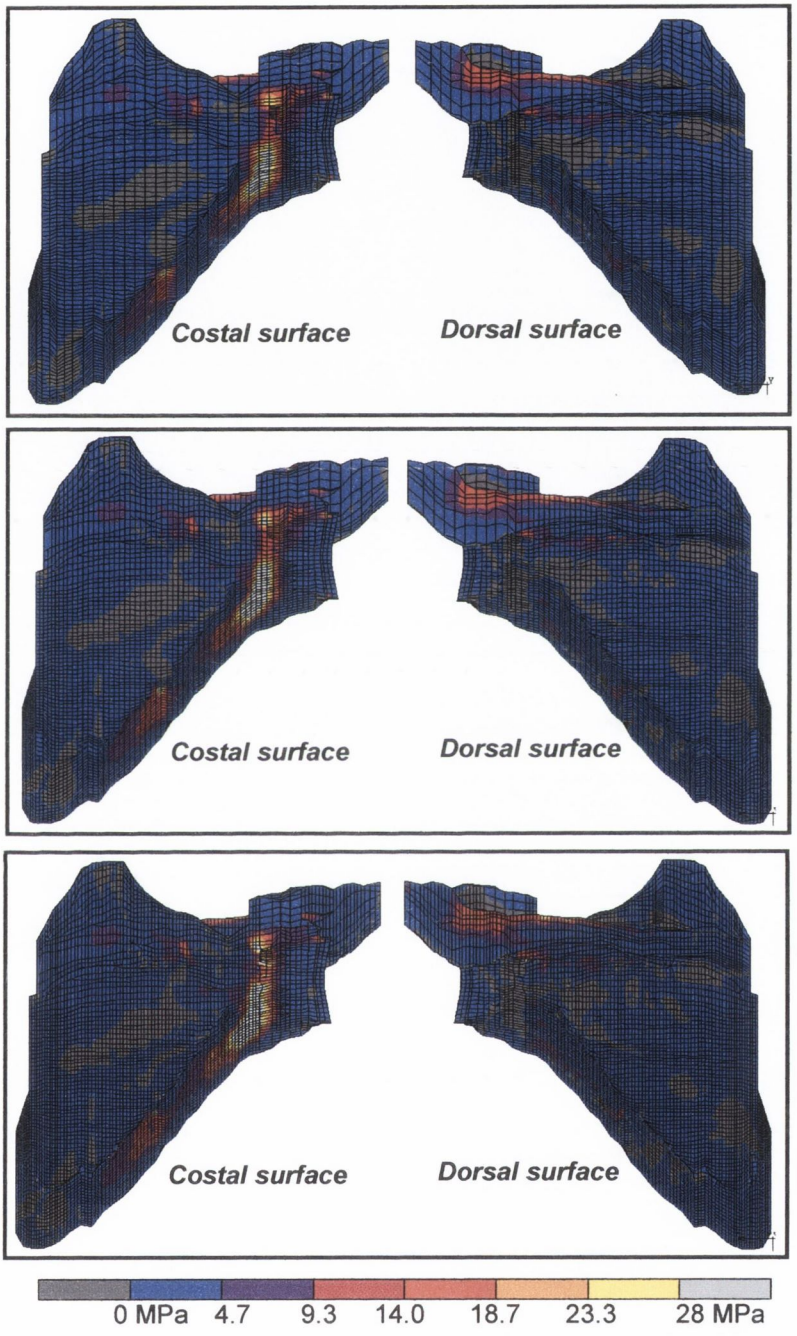

Mesh 1: 33990 degrees of freedom

Mesh 2: 51309 degrees of freedom

Mesh 3: 71703 degrees of freedom

Figure 4.8 (a) *Maximum principal stress distribution in the scapula, a comparison of varying mesh.*

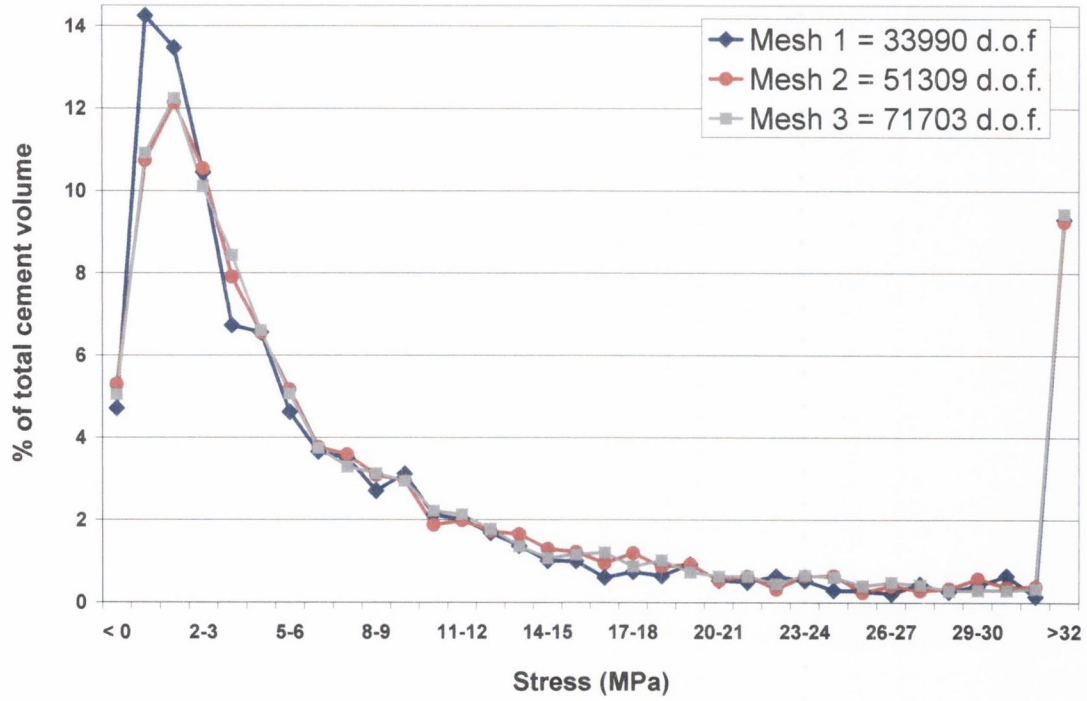

Figure 4.8 (b) *Maximum principal stresses throughout the entire mesh (scapula bone, cement and prosthesis), a comparison of the varying mesh densities.*

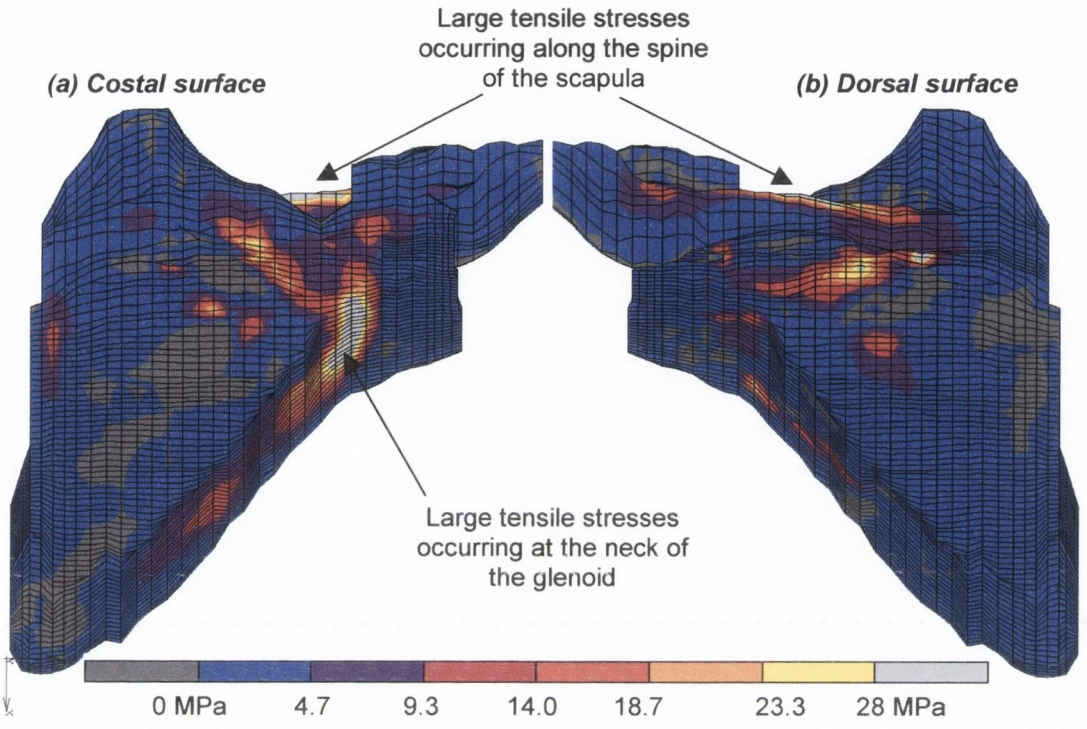

Figure 4.9 *Maximum principal stress plots in the natural scapula (no prosthesis inserted), showing both the costal and dorsal surfaces for 90 degrees of abduction, for normal bone.*

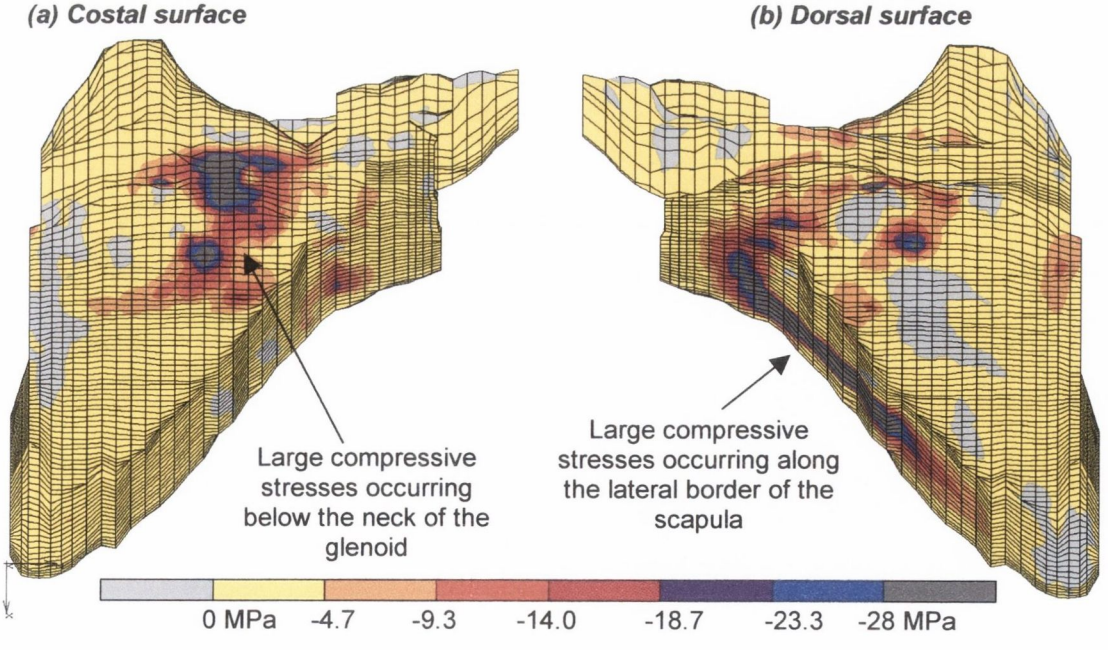

Figure 4.10 *Minimum principal stress plots in the natural scapula (no prosthesis inserted), showing both the costal and dorsal surfaces for 90 degrees of abduction, for normal bone.*

4.5 Testing Hypothesis 1

Hypothesis one states that:

"*A pegged prosthesis provides greater durability to prevent glenoid loosening in normal bone whereas a keeled prosthesis is recommended when there is compromised glenoid bone*", i.e. destruction of the bone due to OA or RA. This hypothesis has been proposed in commercial marketing brochures (Rockwood and Matsen, 1992) but has never been scientifically tested.

4.5.1 Deformation of the prostheses

Deformation of the prostheses is obviously dependent on the surrounding bone quality, the design of prosthesis, and the cement layer. These deformations are presented for the pegged and keeled designs in order to give an understanding of the prosthesis durability in normal bone. Fig. 4.11 shows the displacement of each component mesh for comparison. The deformations are plotted with the same order of magnification for each design thereby allowing a visual comparison. The displacements of keeled and pegged components within the glenoid cavity are different. In each case, compression, shearing, and twisting of the components occur, but the twisting is slightly more significant for the pegged design. This twisting occurs because the joint reaction force (for 90 degrees of abduction) is not acting directly along the centre line of the glenoid and this creates a moment about the anchorage system. As a result, asymmetric stressing of the underlying cement mantle occurs. A keel design best resists this twisting moment, as it is clearly more stable in the superior-inferior plane.

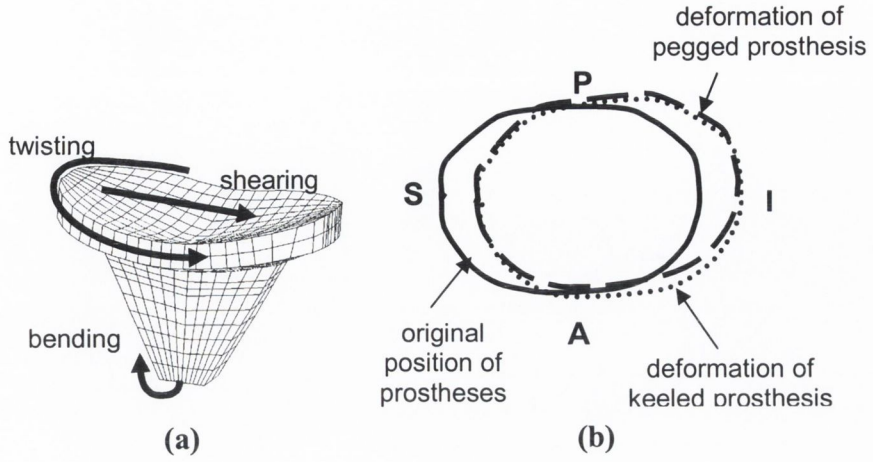

Figure 4.11 *Magnified deformation plot of the polyethylene keeled and pegged components under 90 degrees abduction loading in normal bone* ***(a)*** *shows the twisting, shearing and bending orientation,* ***(b)*** *shows a view looking directly on the glenoid cavity.*

4.5.2 Stress distributions in the scapula with prosthetic fixation

Figure 4.12 (a) and (b) plot scapula stresses for a pegged and centre keeled fixation system. Similar stress distributions exist in the unimplanted scapula and suggests that glenoid component fixation in the scapula does not have a large effect on the overall stress distribution in the bone. However, a general reduction in the magnitude of stresses is noted. This may be attributed to a proportion of the load being absorbed by the polyethylene component and surrounding cement mantle.

4.5.3 Stress distributions produced in the glenoid prosthesis

Stress in the polyethylene at the glenoid cavity is predicted to be very low, generally less than 6 MPa for each type of design. Figure 4.13 compares the maximum and minimum principal stress distributions in the polyethylene pegged and centre keeled glenoid components for both normal and RA bone at 90 degrees of abduction. Highest tensile and compressive stresses are reached for the pegged prosthesis. This may be due to the increased stability of the pegged design compared to the keeled design in the glenoid. Stability is increased in the anterior-posterior direction due to the additional pegs on the periphery. As a result of this stability the polyethylene absorbs the joint load and, as will be shown later, the consequence is that less load is transferred to the surrounding cement mantle.

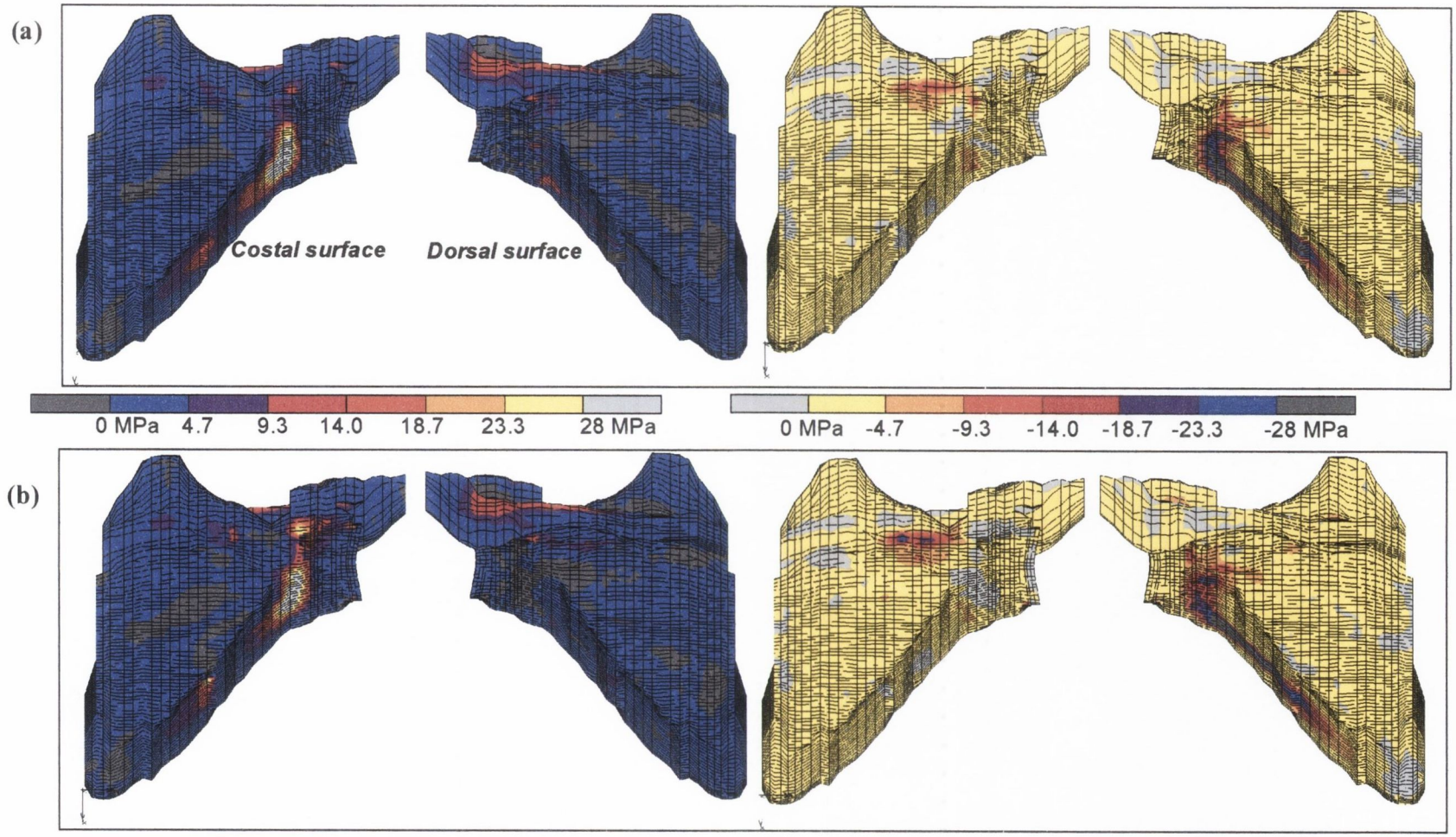

Figure 4.12 *Maximum (0 to 28 MPa) and minimum (0 to –28 MPa) principal stress plots in the scapula, showing both the costal and dorsal surfaces, for* ***(a)*** *a keel prosthesis inserted and* ***(b)*** *a pegged prosthesis inserted, in normal bone.*

4.5.4 Stress distributions in the cement layer around the prostheses

Path plots

Path plots are presented for a comparison of pegged and keeled prostheses in *normal* and RA bone at 90 degrees of abduction in Fig. 4.14. On analysis of the pegged prosthesis, the path plots show that highest tensile stresses occur under the flange on the anterior side (node 1: 2.8 MPa) where the load is located. High tensile stresses also occur at the tip of the larger central peg (node 2: ~2.5 MPa). In comparison, the keeled design exhibits larger tensile stresses at its tip with stresses of approximately 3 MPa (node 3) and greater than 5 MPa (node 4). The stress distribution in the flange is generally of lower magnitude than the pegged case. When analyzing the compressive stresses we can see that for both designs stresses of approximately 3 MPa are reached. The pegged design has a high compressive stress occurring at the tip (node 6: ~8 MPa), whereas the keeled design has a stress of lower magnitude (node 5: ~4 MPa), Fig. 4.14 (a).

Analysis of the pegged design and the centre keel design in RA bone shows that tensile stresses produced by the pegged design are of higher magnitude. These occur at the edge of the flange at node 1 (~3 MPa) as compared to the keeled design, node 4 (<2 MPa), see Fig. 4.14 (b). Also, higher stresses are experienced for the pegged design at the tip of the larger central peg, of magnitude greater than 3 MPa. Compressive stresses show that the pegged design experiences high compressive stresses in the pegs with a stress of 8 MPa in the anterior peg (node 6) and a stress of approximately 9 MPa in the central peg (node 8). The keeled design experiences a lower magnitude of stresses occurring in the keel with approximately 4 MPa at node five and approximately 5 MPa at node 7.

In order to quantify the significance of these path plot results we can calculate the number of cycles to failure for each design, see Table 4.1 using Eqn 4.1 (Murphy and Prendergast, 2000). For *normal* bone, a peak tensile stress of 2.8 MPa occurs for the pegged design (Fig. 4.14 (a), node 1) and 5.3 MPa for the keeled design (Fig. 4.14 (a), node 4). The number of cycles to failure is then calculated as 17.4×10^{10} for the pegged design but only 2.3×10^{10} for the keeled design. Conversely, for RA bone the number of cycles to failure for the pegged design is 12.6×10^{10} and 45.7×10^{10} for the keeled design. This merely emphasizes the non-linear relationship of stress with the number of cycles to failure by showing that even a slight increase in creates a much larger risk of failure.

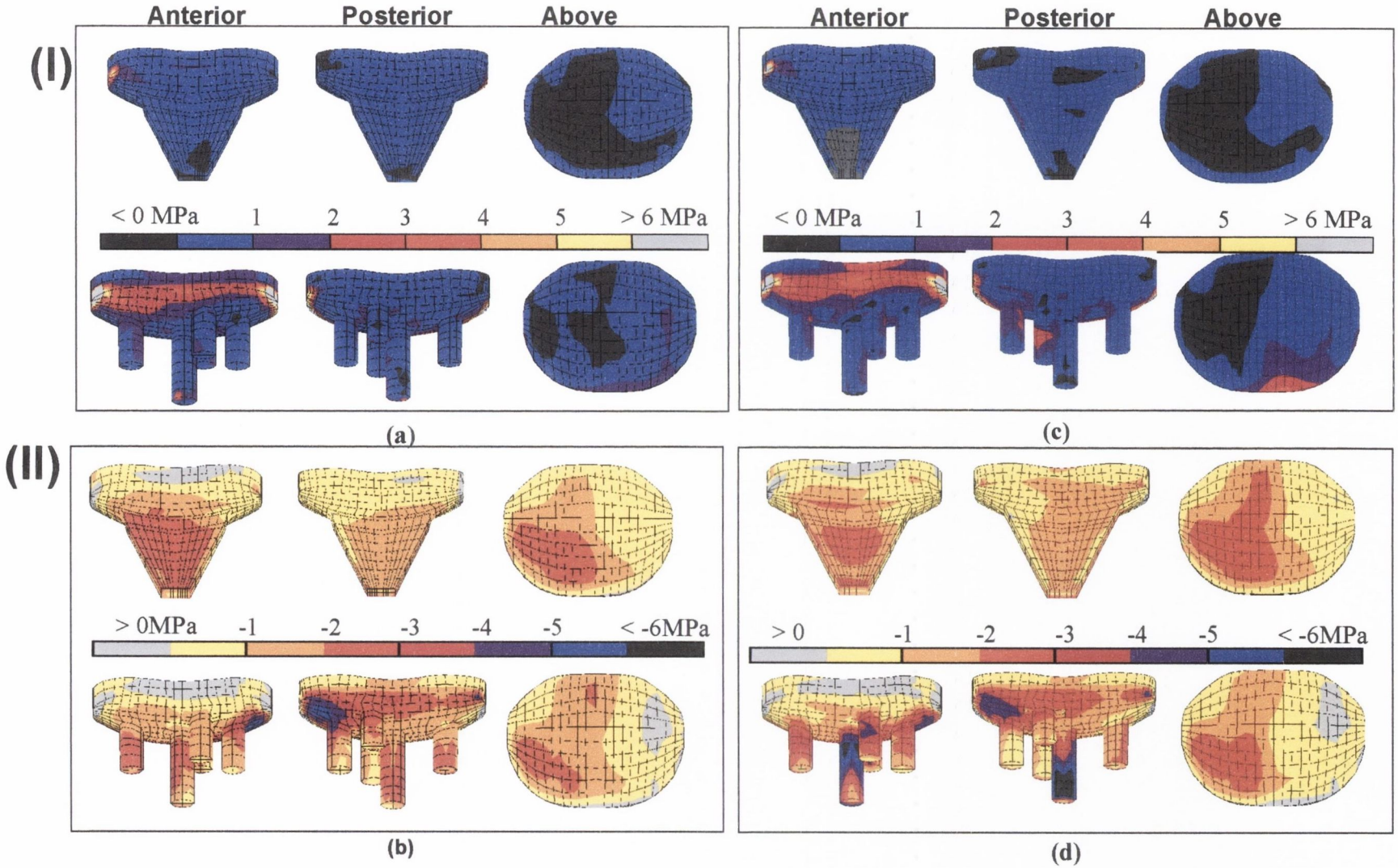

Figure 4.13 ***(I)*** *Maximum (0 to 6 MPa) and* ***(II)*** *minimum (0 to –6 MPa) principal stress distributions in the polyethylene for a pegged and centre keeled prosthesis in* ***(a)*** *&* ***(b)*** *normal bone and* ***(c)*** *&* ***(d)*** *RA bone.*

Fatigue strength of hand-mixed cement in tension:

Failure stress = [-2.86*(number of cycles to failure)]+34.95 (4.1)

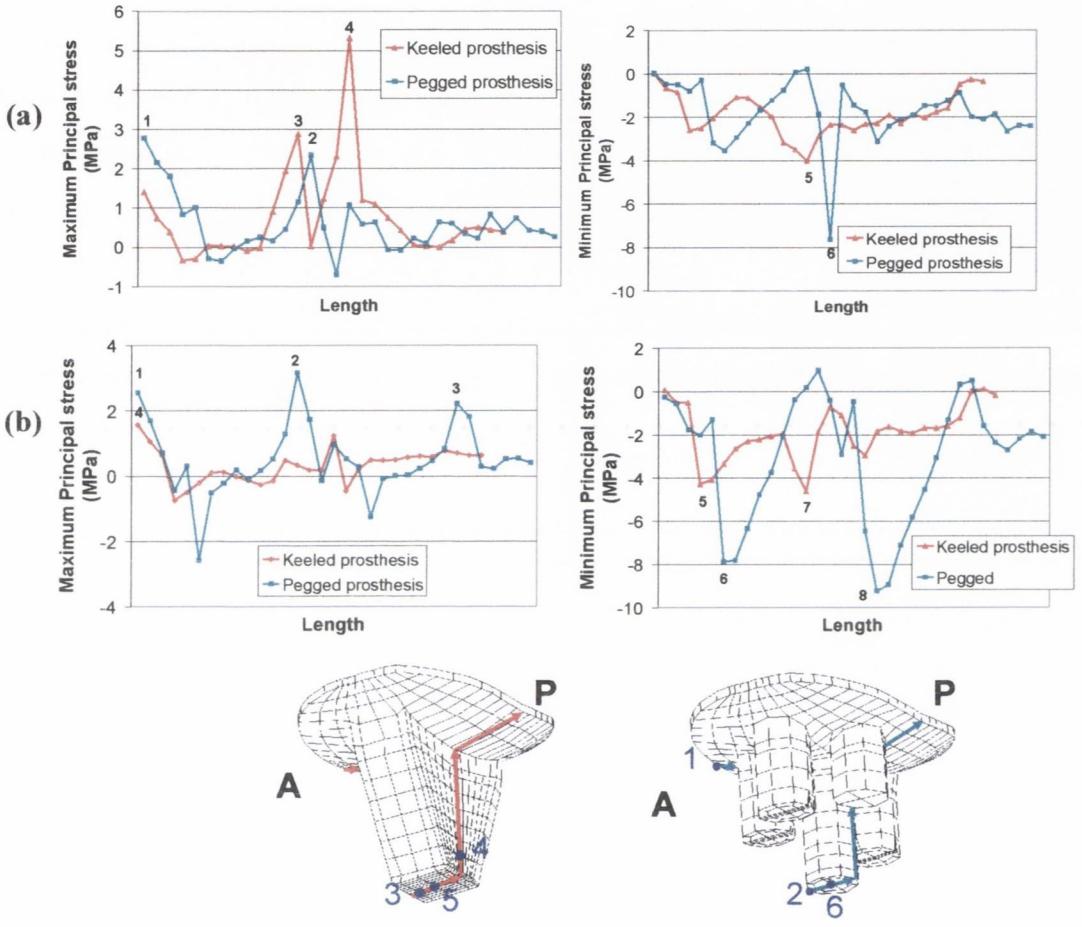

Figure 4.14 *Maximum and minimum principal cement stresses for a path plot of nodes in the anterior-posterior direction - a comparison of pegged and centre keeled designs for* ***(a)*** *normal bone and* ***(b)*** *RA bone. The numbers represent the high stress values for the corresponding nodes shown on the meshes.*

Table 4.1 *Shows the significance of the cement stress values from Fig. 4.13 (a) and (b).*

	Peak tensile stress (MPa)		*Cycles to failure* ($x10^{10}$)	
	Normal bone	*RA bone*	*Normal bone*	*RA bone*
Pegged Design	2.8	3.2	17.4	12.6
Keeled Design	5.3	1.6	2.3	45.7

Pegged does best in normal bone

Keeled does best in RA bone

Details of cement stress distribution:

Plots of the cement mantle will be presented for identification of critical areas of high stress. It is worthy to note here that the tensile stresses are of particular interest as they are associated with crack growth in cement (Lennon *et al.,* 2002). Highest tensile stresses (> 4 MPa) occur under the flange of the pegged and keeled prostheses and at the tip of the keeled prosthesis in normal bone For RA bone, a larger volume is highly stressed (tensile) for the pegged prosthesis in RA bone, see Fig. 4.15. This is due to the "twisting" of the components which is more evident in the region of load application i.e. the superior-anterior region. High compressive stresses occur mainly in the flanges and in the pegs due to the compressive nature of the load being transferred there and also due to the twisting phenomenon which occurs more so for the pegged design. Maximum stresses occur at the edges of the cement flange and also at the tips of the keel and central peg, however, the keeled prosthesis has a larger volume of cement than the pegged prosthesis at the tip, i.e. it has a larger volume which is stressed. In the case of normal bone, both prostheses are more stable due to the support of the surrounding stiff bone. In the case of RA there is less dense bone surrounding the prostheses, therefore the prostheses are more susceptible to the "twisting" deformation, which is more pronounced for the pegged prosthesis and results in higher cement stresses. The pegged prosthesis has more cement volume than the keeled prosthesis just under the flange, and this cement becomes highly stressed in the pegged case.

Quantitative analysis of the stress distribution in the cement layer

The cement mantle surrounding a glenoid prosthesis has an intricate shape and as a result, the stress distributions can be very complex and difficult to visualise. Furthermore, stress contour plots can only show surface stresses and not the stresses experienced throughout the entire mantle thickness. Therefore, the volume of cement stressed to a particular level is plotted for both normal and RA bone (see Chapter 3).

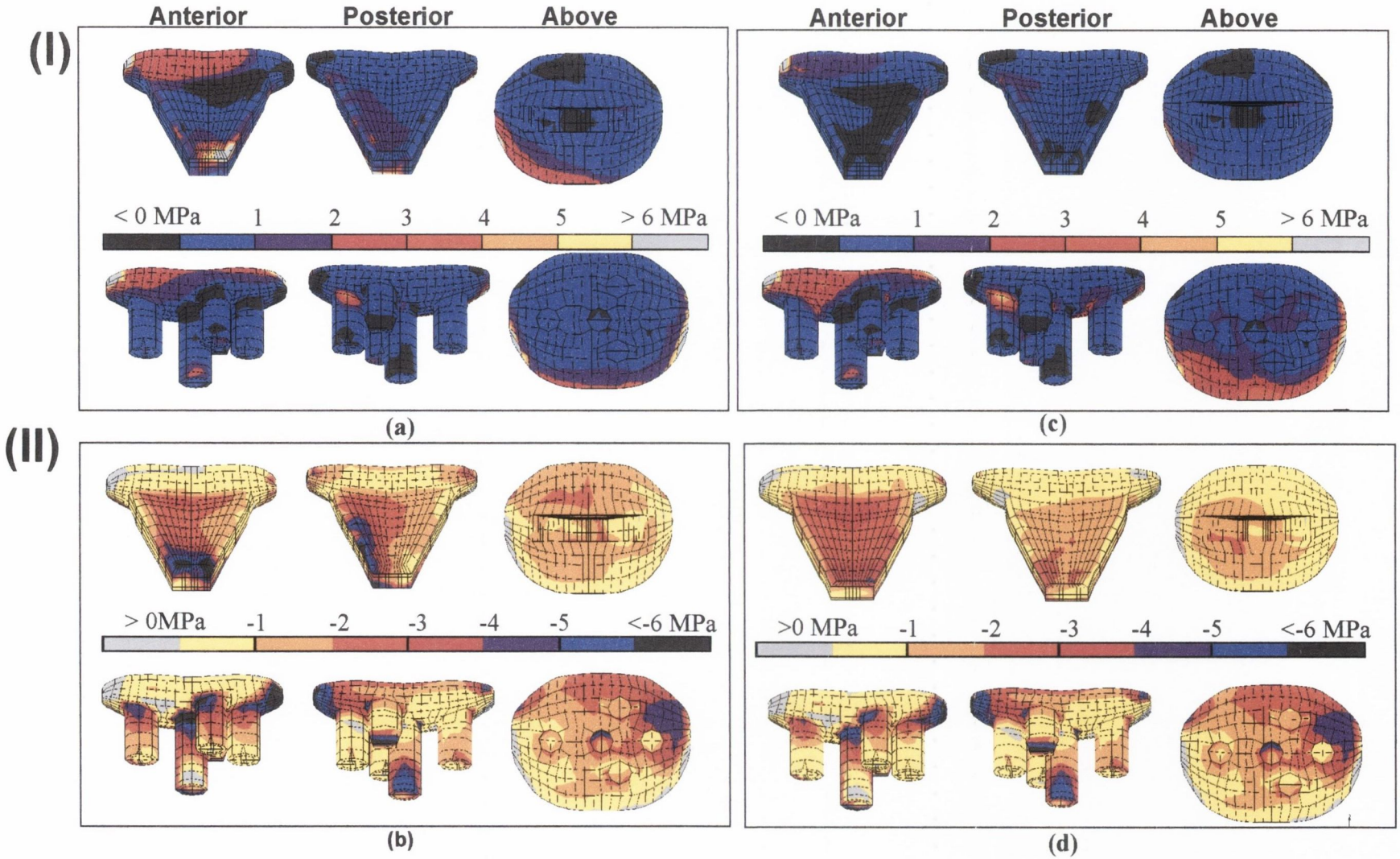

Figure 4.15 ***(I)*** *Maximum(0 to 6 MPa) and* ***(II)*** *minimum (0 to –6 MPa) principal stress distributions in the cement layer for a pegged and centre keeled prosthesis in* ***(a)*** *&* ***(b)*** *normal bone and* ***(c)*** *&* ***(d)*** *RA bone.*

Considering first the situation in normal bone, the prediction is that the keeled design has a greater volume of highly stressed cement compared to the pegged design. For the pegged design, there is a higher volume of cement in the lower stress regions, with over 70 percent of its volume stressed to 1 MPa only, see Figure 4.16 (a). Conversely, for the keeled design, there is a higher volume of cement in the higher stress regions, approximately 50 percent of its volume is stressed over 3 MPa. In fact, there is approximately 10 percent of the cement mantle above 5 MPa with the keeled design compared to less that 1 percent above 5 MPa with the pegged design.

Considering next the RA bone, the situation reverses, the keeled prosthesis has most of its cement volume in the lower stress regions (approximately 80 percent is stressed between 1 and 2 MPa), whereas, the pegged design now has a higher cement volume in the higher stress regions with approximately 20 percent of its total volume over 3 MPa, see Figure 4.16 (b). This indicates the superiority of the keeled design in the RA bone.

Using Eqn. 3.9, the amount of cement material above a given probability of survival is calculated. For example, a cement stress of 3.3 MPa will have a 95 percent probability of survival. Results for a 95 percent probability of survival are reported in Table 4.2. The prediction is that a pegged prosthesis has the highest probability of cement survival for normal bone and a keeled prosthesis has the highest probability of survival for low density bone.

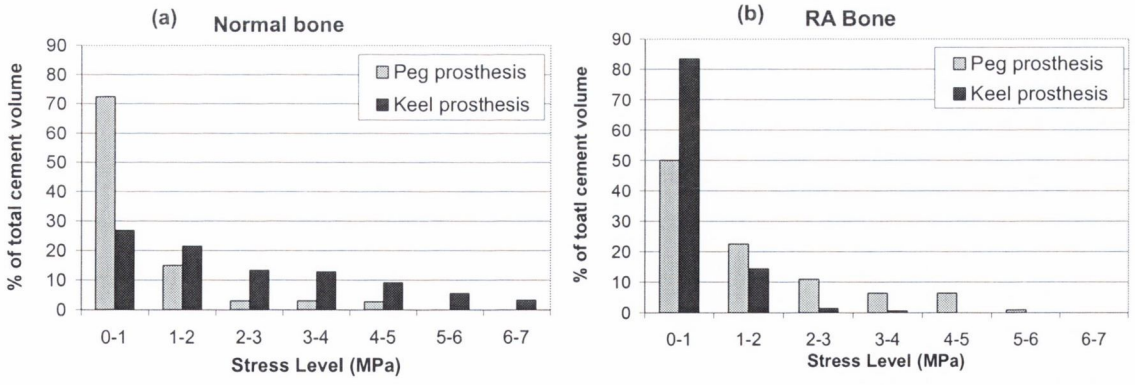

Figure 4.16 *Cement maximum principal stresses for* ***(a)*** *normal bone and* ***(b)*** *rheumatoid arthritic bone – a comparison of designs.*

Table 4.2 *Percentage of cement volume with a greater than 95 percent Probability of Survival (Hypothesis 1).*

Bone Quality	*Pegged Prosthesis (%)*	*Keeled prosthesis (%)*
Normal Bone	94	68
RA Bone	86	99

4.5.6 Stress distributions in the glenoid bone

It is a principal of prosthesis design that the stress distributions in the bone should be as physiological as possible, and should not be of sufficient magnitude to cause microfractures of the underlying trabeculae which might lead to component loosening. When the prosthesis is implanted in normal bone, von Mises stresses under the flange are lower with the keeled design compared to the pegged design, see Fig. 4.17 (a). This is to be expected given the deformation plots in Fig. 4.10 since the pegged design is not as stiff in bending as the keeled design. The corollary of this is that more stress is transferred into the depth of the glenoid with the keeled design, see Fig. 4.17 (a). With the RA bone, this effect is slightly more pronounced, see Fig. 4.17 (b).

However, in the simulated RA bone, the Young's modulus of the cancellous bone was reduced to a tenth and thus becomes weaker. We can take account of this reduction by calculating the reduced density ρ (in g/cm^3) by rearranging Eqn. 3.1 to give,

$$\rho = \left(\frac{E - 0.06}{0.9} \right)^{1/2} \qquad (4.2)$$

where E is the reduced Young's modulus simulating RA bone. From this we can determine the maximum stress σ_{fail} to which the bone would fail (Rice *et al.*, 1988)

$$\sigma_{fail} = 2.45 + 32.66\ \rho^2 \text{ (MPa)} \qquad (4.3)$$

Therefore a stress-to-strength ratio can be calculated using the following equation:

$$\text{Stress - to - strength ratio} = \frac{\text{maximum principal stress}}{\text{failure stress}} \qquad (4.4)$$

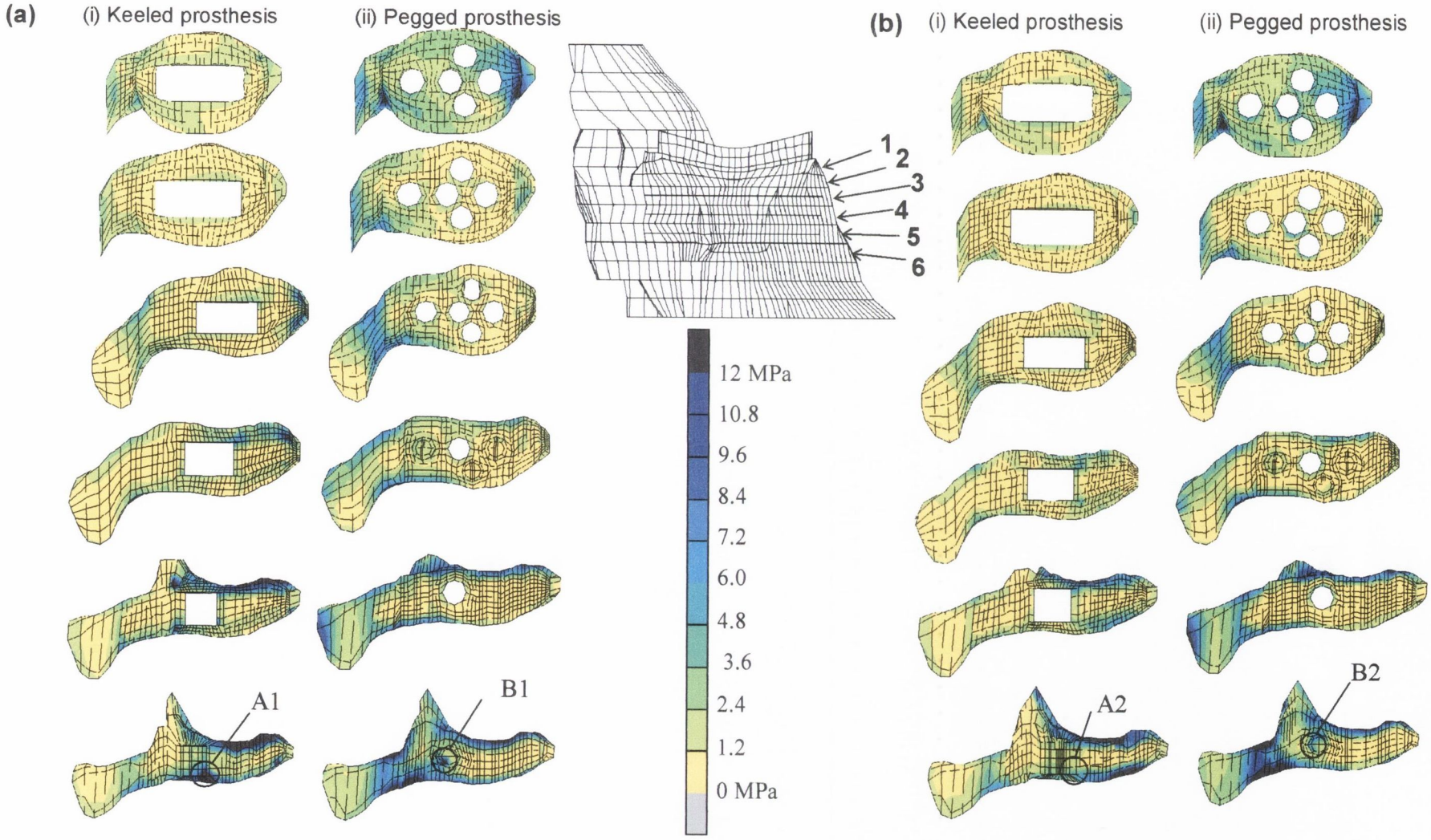

Figure 4.17 *(a) von Mises stresses of the normal bone (i) the keeled prosthesis, (ii) the pegged prosthesis.* ***(b)*** *von Mises stresses of the rheumatoid bone (i) the keeled prosthesis, (ii) the pegged prosthesis. A1, A2, B1, and B2 are regions of high stress.*

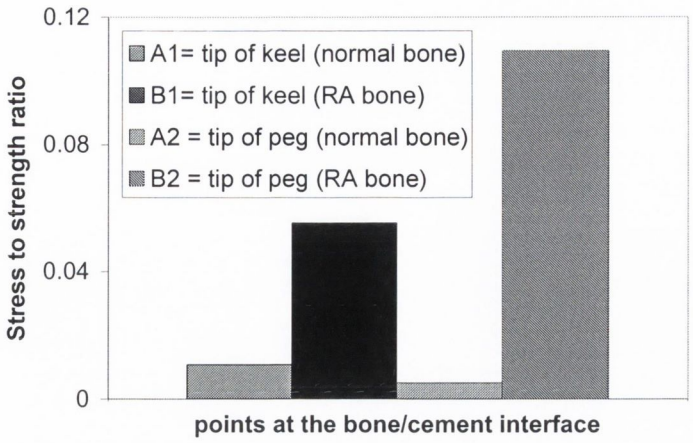

Figure 4.18 *Comparison of the regions of high stress, taking account of the reduction of density in bone due to RA. Each bar represents one point at the bone/cement interface.*

This ratio therefore indicates the actual severity of stress in the bone. A plot of the stress-to-strength ratio versus the points of interest at the interface (at the tip of the keel and central peg) is shown in Fig. 4.18. When comparing the stress-to-strength ratio at the tip of the central peg in both types of bone (normal bone = B1, RA bone = B2) we can see that it is higher for RA bone. When comparing the stress-to-strength ratio at the tip of the keel in both types of bone (normal bone = A1, RA bone = A2) we can see that it is also higher for RA bone. Therefore, we can say not only that prostheses performance, with respect to changes of bone stress, is poorer in RA bone but also that the reduction in performance is greater for the pegged component compared to the keeled design.

4.6 Testing Hypothesis 2

Hypothesis two states that: *"An anterior offset keel provides better durability than a centre keel design due to its more central alignment in the glenoid bone".*

4.6.1 Stress distributions produced in the scapula with prosthetic fixation

Since analysis of Hypothesis 2 does not include the action of the muscle forces, scapular stresses were not included as they cannot be compared to the natural case.

4.6.2 Stress distributions produced in the glenoid prosthesis

For both the normal and RA case at each angle of abduction loading, stress in the polyethylene glenoid component is predicted to be very low. These results are presented in Figs. 4.19 to 4.23. An average of approximately 2 MPa is reached for each design, which is well below the failure limit of this material. Maximum stresses are predicted at the higher loading angles, that of 90 degrees of abduction and flexion. Again these stresses peak at 6 MPa and are not considered to be significant.

4.6.3 Stress distributions produced in the cement layer around the prosthesis

Plots of cement stress distributions

For 90 degrees of abduction, the maximum glenohumeral joint load, tensile stresses underneath the cup of the offset-keel design are predicted to be low, see Fig. 4.24 (a). This is due to the position of the load acting over the offset-keel, placing it in less bending compared to the centre keel design. Highest tensile stresses occur at the superior edge of the cup, of magnitude equal to approximately 3 MPa, but in general are less than 1 MPa. Highest compressive stresses occur along the anterior side (~ 4 MPa) and are higher than the posterior side, indicating that some bending is occurring in the anterior-posterior plane (Fig. 4.24 (b)). A similar distribution, but higher peak stresses, are predicted in the cement around the centre keel design. Again this is due to the keel position with the centre keel design subjected to increased bending due to the load location.

For 90 degrees of abduction for the RA case, low tensile stresses are experienced by both designs, see Fig. 4.24 (c). However, the centre keel design shows higher compressive stresses than the offset-keel design.

At 90 degrees of flexion for the normal case, the offset-keel design experiences highest tensile stresses on the anterior side of the cup with highest compressive stresses on the posterior side, see Fig. 4.25 (a) and (b). This is to be expected due to the loading vector being some distance away from the keel (the position of the loading vector can be seen in Fig. 3.17) placing the keel in more bending than for 90 degrees of abduction. Again, the general trend is that higher stresses are occurring for the centre-keel design.

At 90 degrees of flexion for the RA case, the offset-keel design shows generally lower tensile and compressive stresses than the centre-keel design, see Fig. 4.25 (c).

At 60 degrees of abduction for the normal and RA case, generally low tensile and compressive stresses occur for both designs with similar distributions, see Fig. 4.26.

At 60 degrees of flexion for the normal RA case, high tensile stresses occur at the base of the centre keel design reaching 6 MPa for the RA case. Higher compressive stresses exist also for the centre keel design, see Fig. 4.27.

At 180 degrees of flexion very low tensile and compressive stresses are reached in general, with a peak stress of 5 MPa being reached at the tip of the centre keel design in RA bone, see Fig. 4.28.

Quantitative description of the stress distribution in the cement layer

For the normal joint, at 90 degrees of abduction, the offset-keeled design has a higher volume of cement under lower stress than the centre keel design, with approximately 60 percent of its volume stressed from 0 to 1 MPa only, see Fig. 4.29 (a). Conversely, for the centre keeled design, a greater volume of cement is stressed to a high level with approximately 35 percent of its volume being stressed over 3.3 MPa. Additionally, the centre keel design has over 10 percent of its entire cement volume above 5 MPa, which may result in crack initiation and ultimately failure at the cement layer.

For 90 degrees of flexion, the offset-keeled design has approximately 85 percent of its volume in the 0 to 2 MPa stress level. Similarly the centre keeled design has approximately 85 percent of its volume in this stress range, see Fig. 4.29 (b). Both designs have low volumes of cement stressed above the 3 MPa range, indicating that failure at 90 degrees of flexion is unlikely.

At 60 degrees of abduction joint load, it is shown that both designs have 100 percent of their volumes in the 0 to 2 MPa range, indicating a very low likelihood of failure, see Fig. 4.29 (c).

For 60 degrees of flexion, both designs have approximately 95 percent of their volumes in the 0 to 2 MPa range with the offset-keel having a higher volume above 1 MPa than the centre keel, see Fig. 4.29 (d). Higher stresses are reached in comparison to the 60 degrees of abduction range.

Again, at 180 degrees of flexion, we can see that similarly for both designs, high volumes of cement occur in the 0 to 1 MPa range, see Fig. 4.29 (e). The centre-keel design has a higher volume in the upper range of the band-with approximately 10 percent in the 1 to 2 MPa range. Conversely the offset-keel design has a higher volume in the lower range of the band.

For the RA joint, at 90 degrees of abduction, both the offset-keeled design and the centre keel design have high volumes of cement stressed to low stress magnitudes (<2 MPa), see Fig. 4.30 (a). However at 90 degrees of flexion, the offset-keeled design has approximately 98 percent of its volume in the 0 to 2 MPa stress level whereas the centre keeled design has approximately 80 percent of its volume in this stress range, see Fig. 4.30 (b). This shows that, even in RA bone, the offset keel design is predicted to have a superior performance.

At 60 degrees of abduction and 60 degrees flexion joint loads, again it is shown that both designs have 100 percent of their cement mantle volumes in the 0 to 2 MPa range, see Fig. 4.30 (c) and (d). Finally at 180 degrees of flexion, we can see that similarly for both designs, high volumes of cement are stressed only in the 0 to 1 MPa range, see Fig. 4.30 (e).

Using Eqn. 3.9, the amount of cement material above a given probability of survival is calculated. It is found that the offset-keel design of glenoid component has a greater probability-of-survival under all loading conditions, see Table V. For example, at the maximum glenohumeral joint loading of 90 degrees of abduction, a centre keel design will only have a probability-of-survival of 68 percent compared to an offset-keel design which will have a probability-of-survival of >95 percent, at ten million cycles.

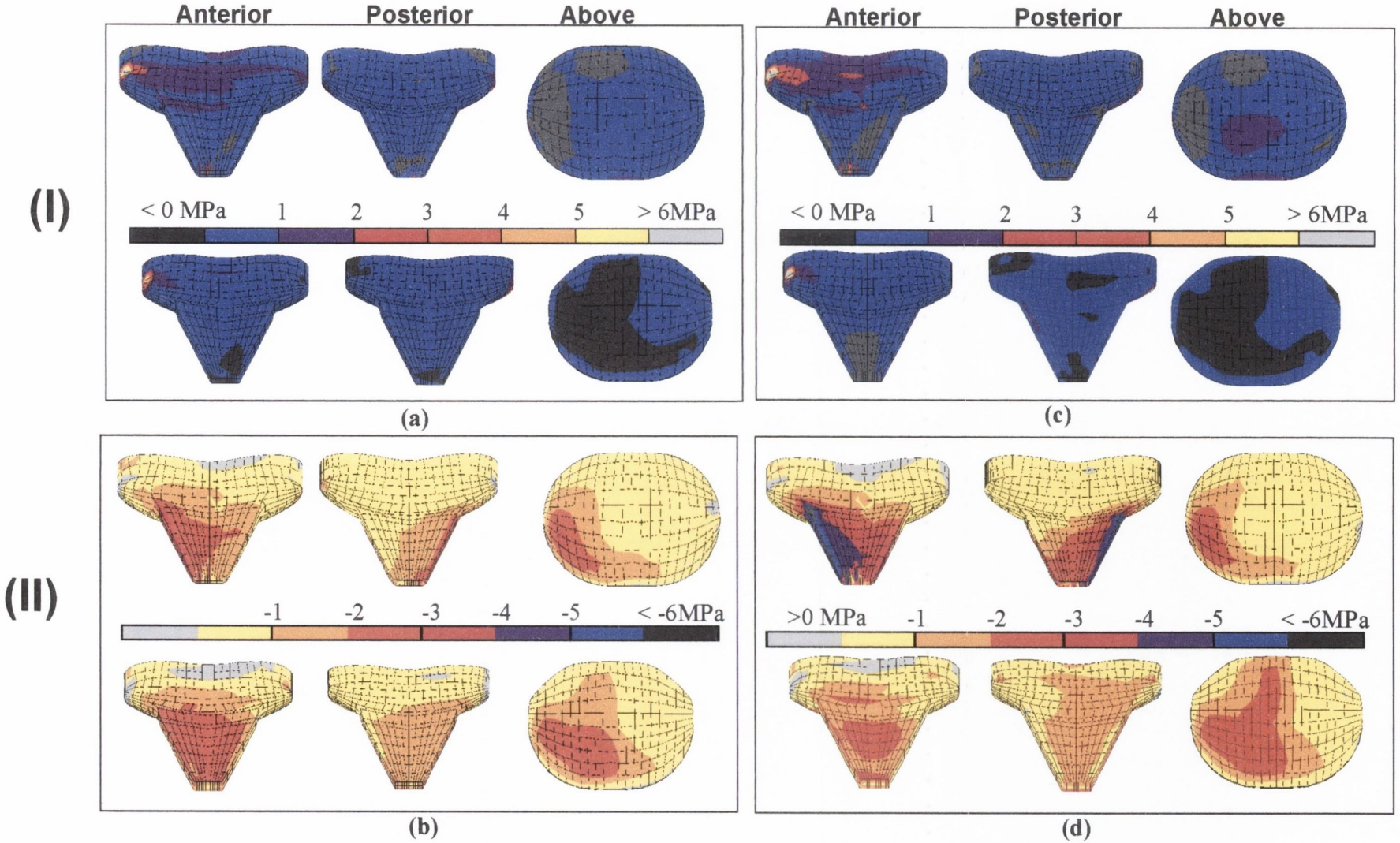

Figure 4.19 90 DEGREES OF ABDUCTION: ***(I)*** *Maximum (0 to 6 MPa) and* ***(II)*** *minimum (0 to –6 MPa) principal stress distributions in the polyethylene for an offset keel and centre keeled prosthesis in* ***(a)*** *&* ***(b)*** *normal and* ***(c)*** *&* ***(d)*** *RA bone.*

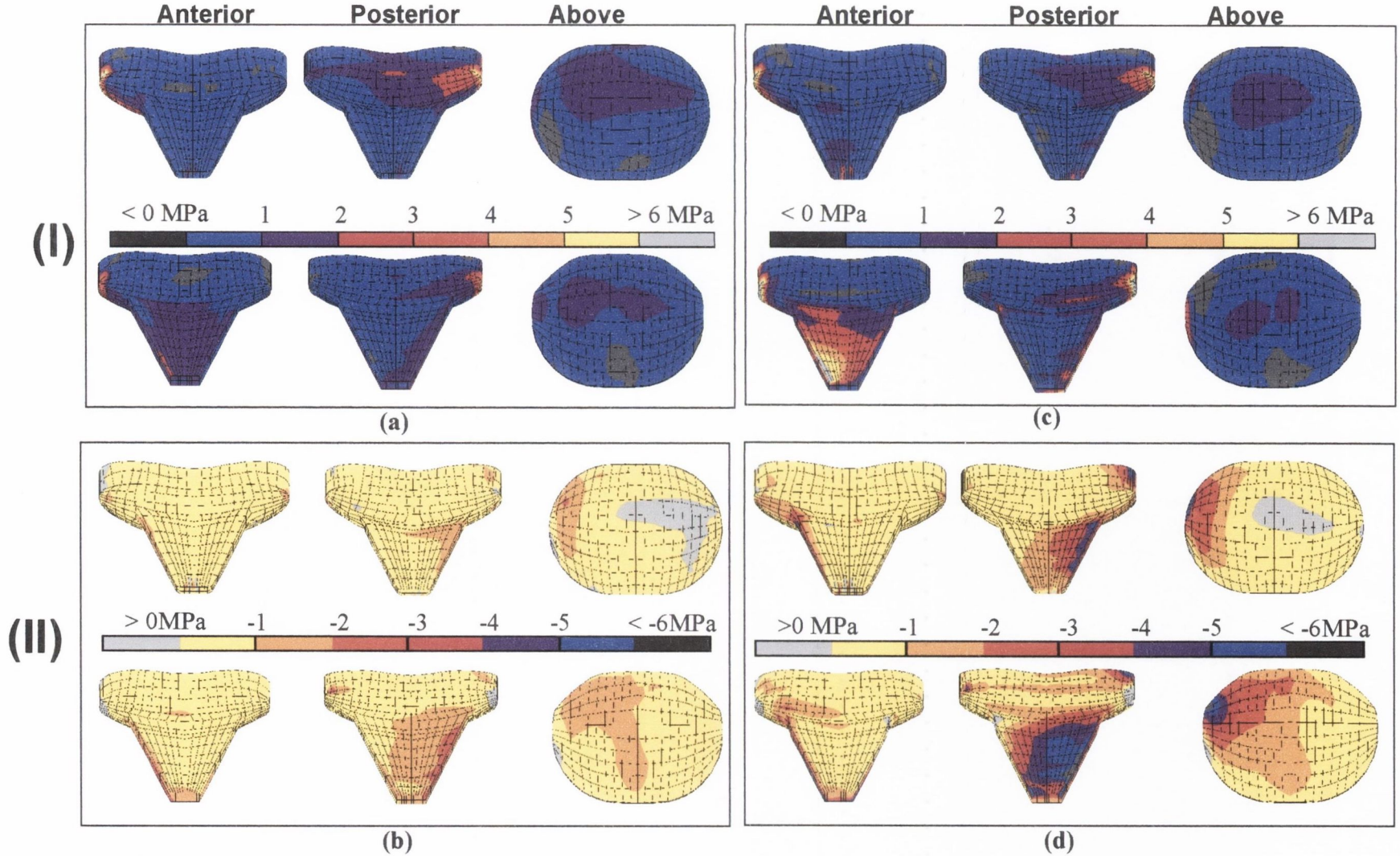

Figure 4.20 90 DEGREES OF FLEXION: ***(I)*** *Maximum (0 to 6 MPa) and* ***(II)*** *minimum (0 to –6 MPa) principal stress distributions in the polyethylene for an offset keel and centre keeled prosthesis in* ***(a)*** *&* ***(b)*** *normal and* ***(c)*** *&* ***(d)*** *RA bone.*

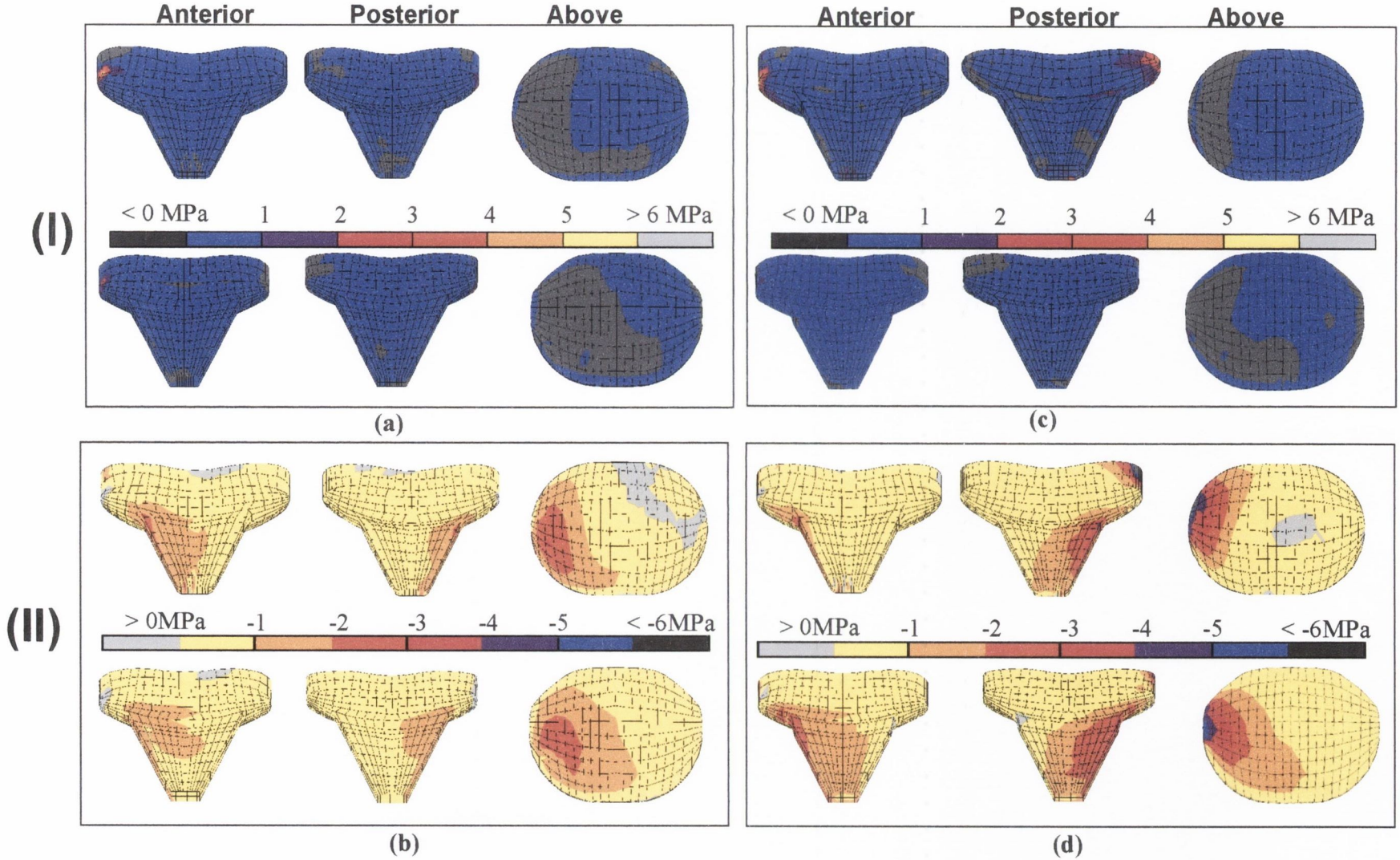

Figure 4.21 60 DEGREES OF ABDUCTION: ***(I)*** *Maximum (0 to 6 MPa) and* ***(II)*** *minimum (0 to –6 MPa) principal stress distributions in the polyethylene for an offset keel and centre keeled prosthesis in* ***(a)*** *&* ***(b)*** *normal and* ***(c)*** *&* ***(d)*** *RA bone.*

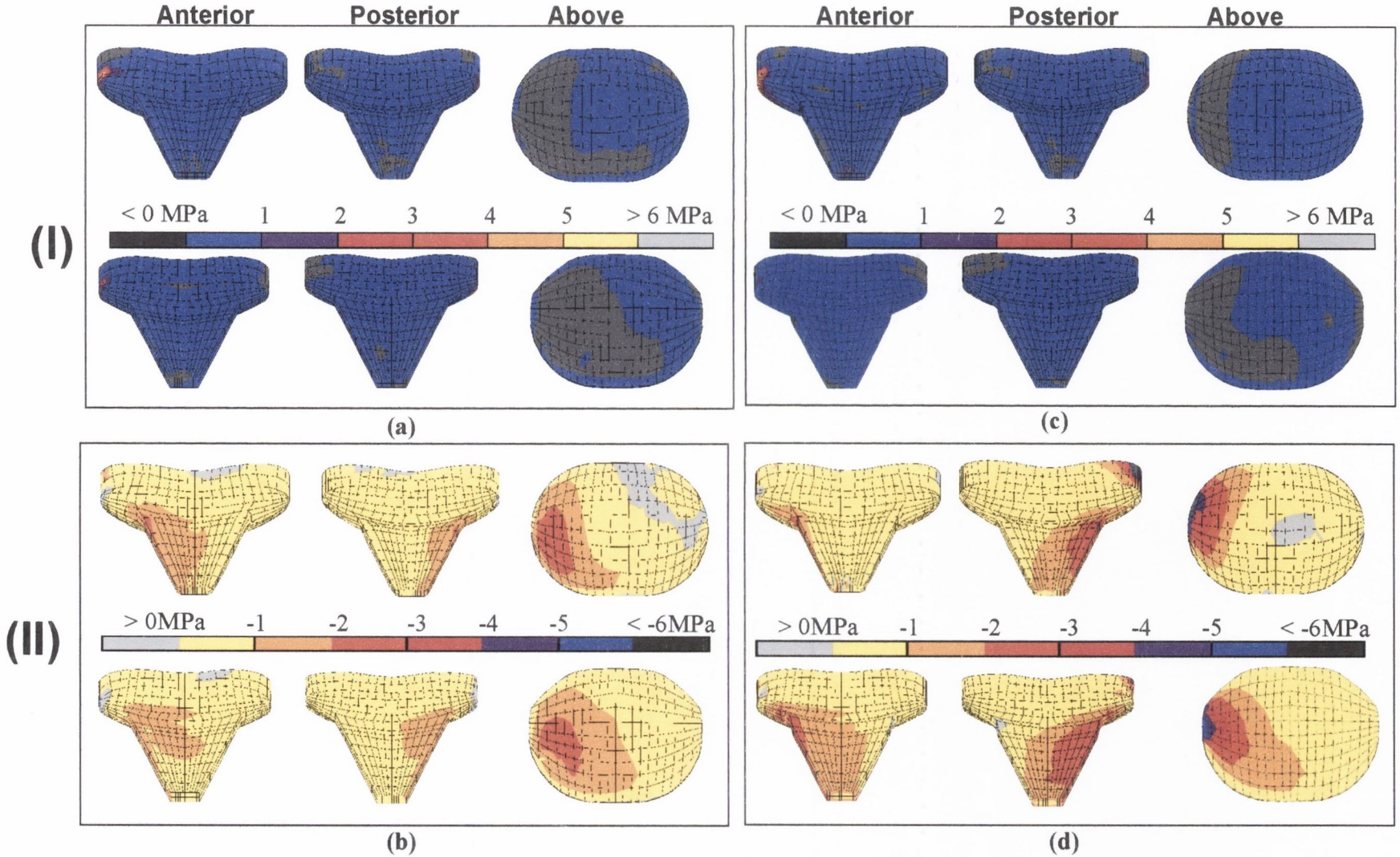

Figure 4.22 60 DEGREES OF FLEXION: ***(I)*** *Maximum (0 to 6 MPa) and* ***(II)*** *minimum (0 to –6 MPa) principal stress distributions in the polyethylene for an offset keel and centre keeled prosthesis in* ***(a)*** *&* ***(b)*** *normal and* ***(c)*** *&* ***(d)*** *RA bone.*

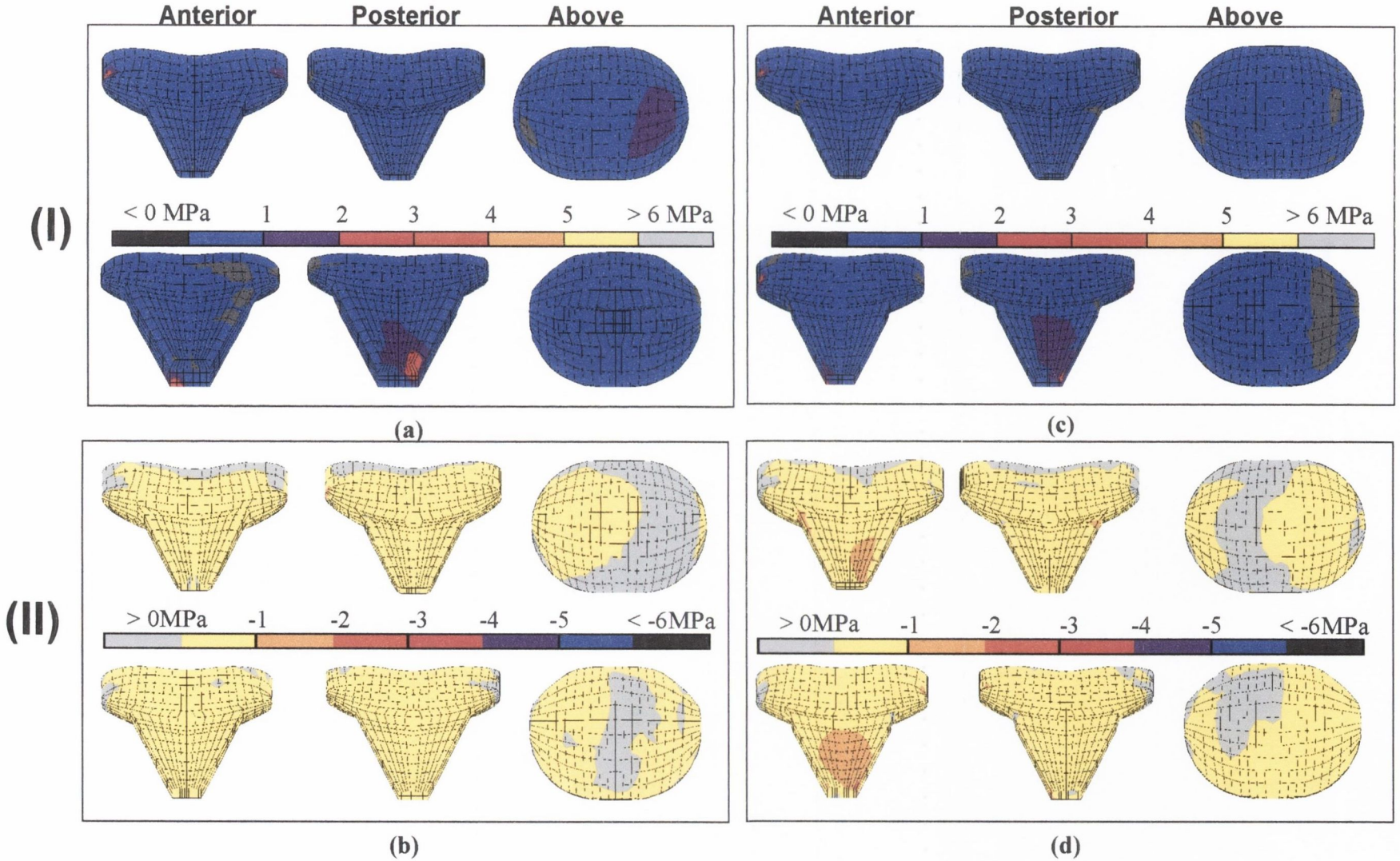

Figure 4.23 180 DEGREES OF FLEXION: ***(I)*** *Maximum (0 to 6 MPa) and* ***(II)*** *minimum (0 to –6 MPa) principal stress distributions in the polyethylene for an offset keel and centre keeled prosthesis in* ***(a)*** *&* ***(b)*** *normal and* ***(c)*** *&* ***(d)*** *RA bone.*

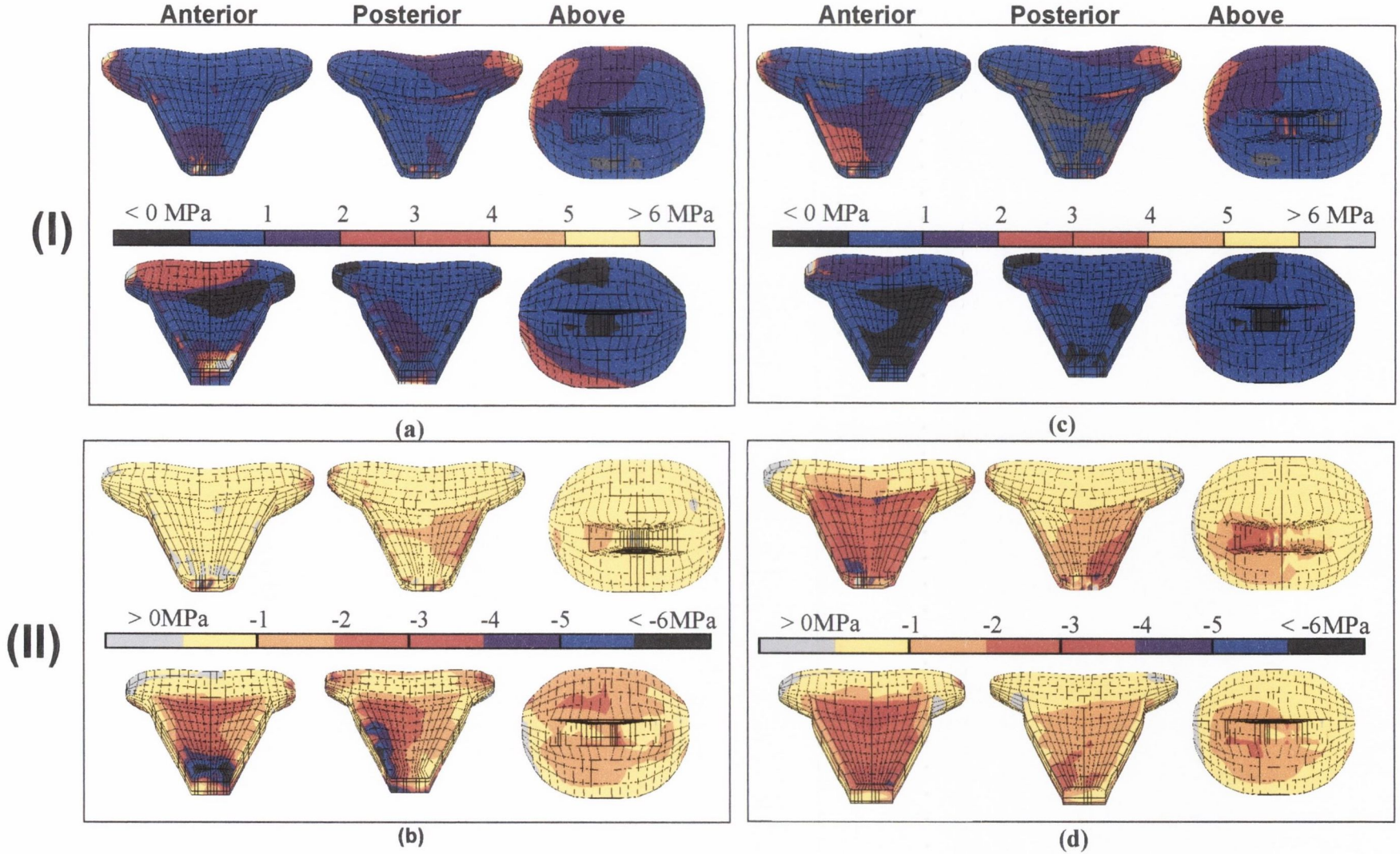

Figure 4.24 90 DEGREES OF ABDUCTION: *Maximum (0 to 6 MPa) and minimum(0 to –6 MPa) principal stress distributions in cement layer for* ***(I)*** *an offset and* ***(II)*** *a centre keeled prosthesis in* ***(a)*** *&* ***(b)*** *normal and* ***(c)*** *&* ***(d)*** *RA bone.*

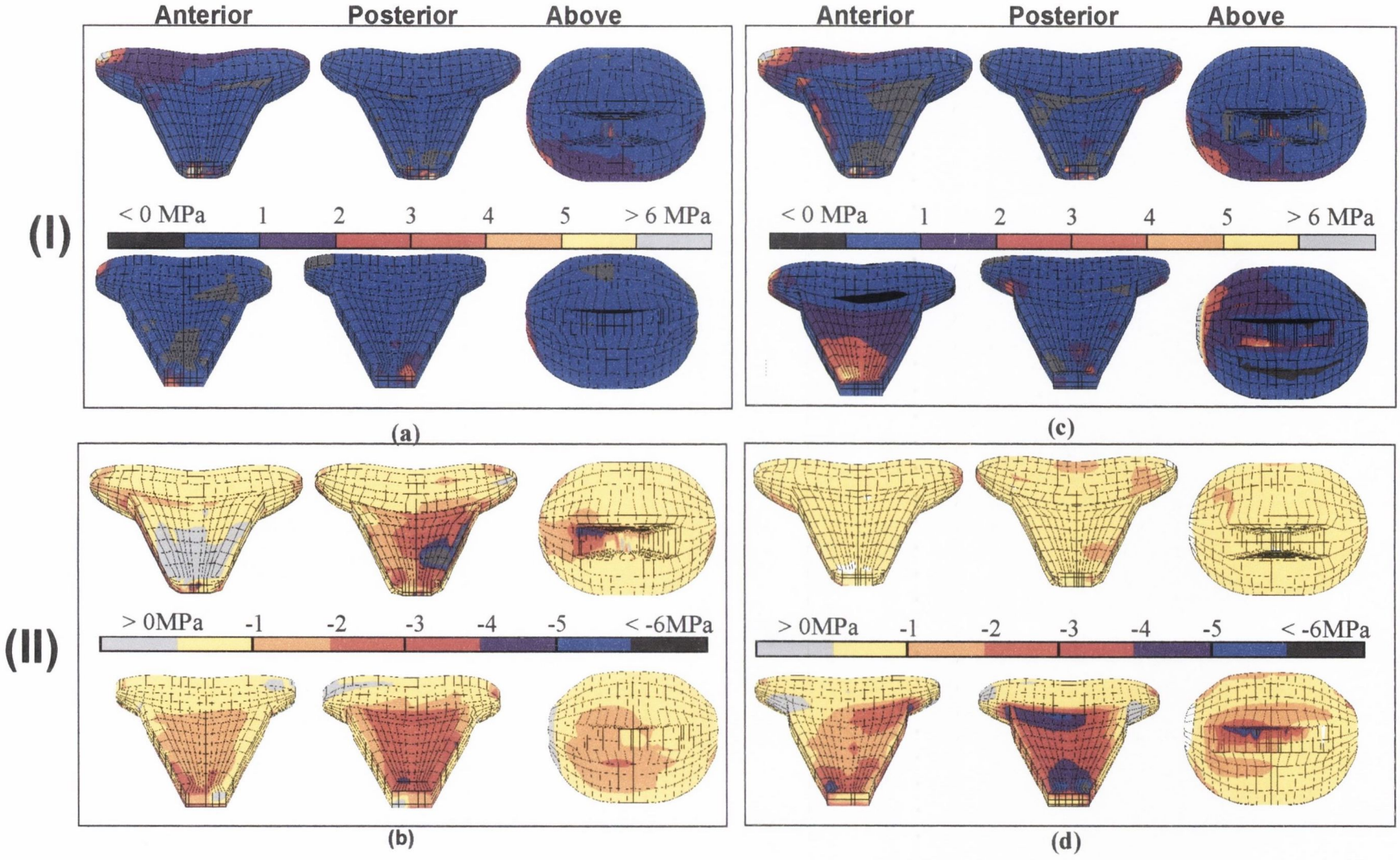

Figure 4.25 90 DEGREES OF FLEXION: *Maximum (0 to 6 MPa) and minimum (0 to –6 MPa) principal stress distributions in cement layer for* ***(I)*** *an offset and* ***(II)*** *a centre keeled prosthesis in* ***(a)*** *&* ***(b)*** *normal and* ***(c)*** *&* ***(d)*** *RA bone.*

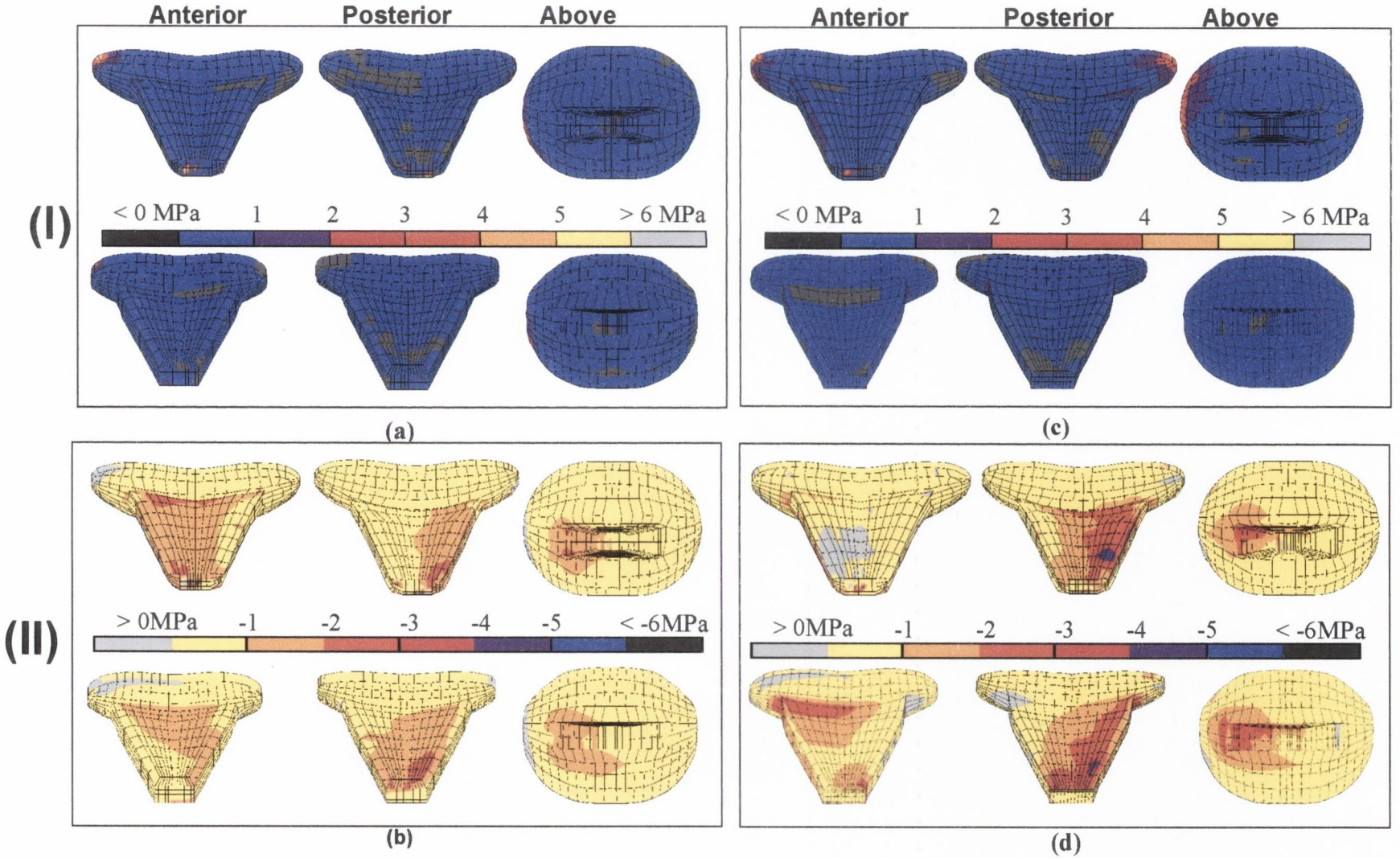

Figure 4.26 60 DEGREES OF ABDUCTION: *Maximum (0 to 6 MPa) and minimum (0 to –6 MPa) principal stress distributions in cement layer for* ***(I)*** *an offset and* ***(II)*** *a centre keeled prosthesis in* ***(a)*** *&* ***(b)*** *normal and* ***(c)*** *&* ***(d)*** *RA bone.*

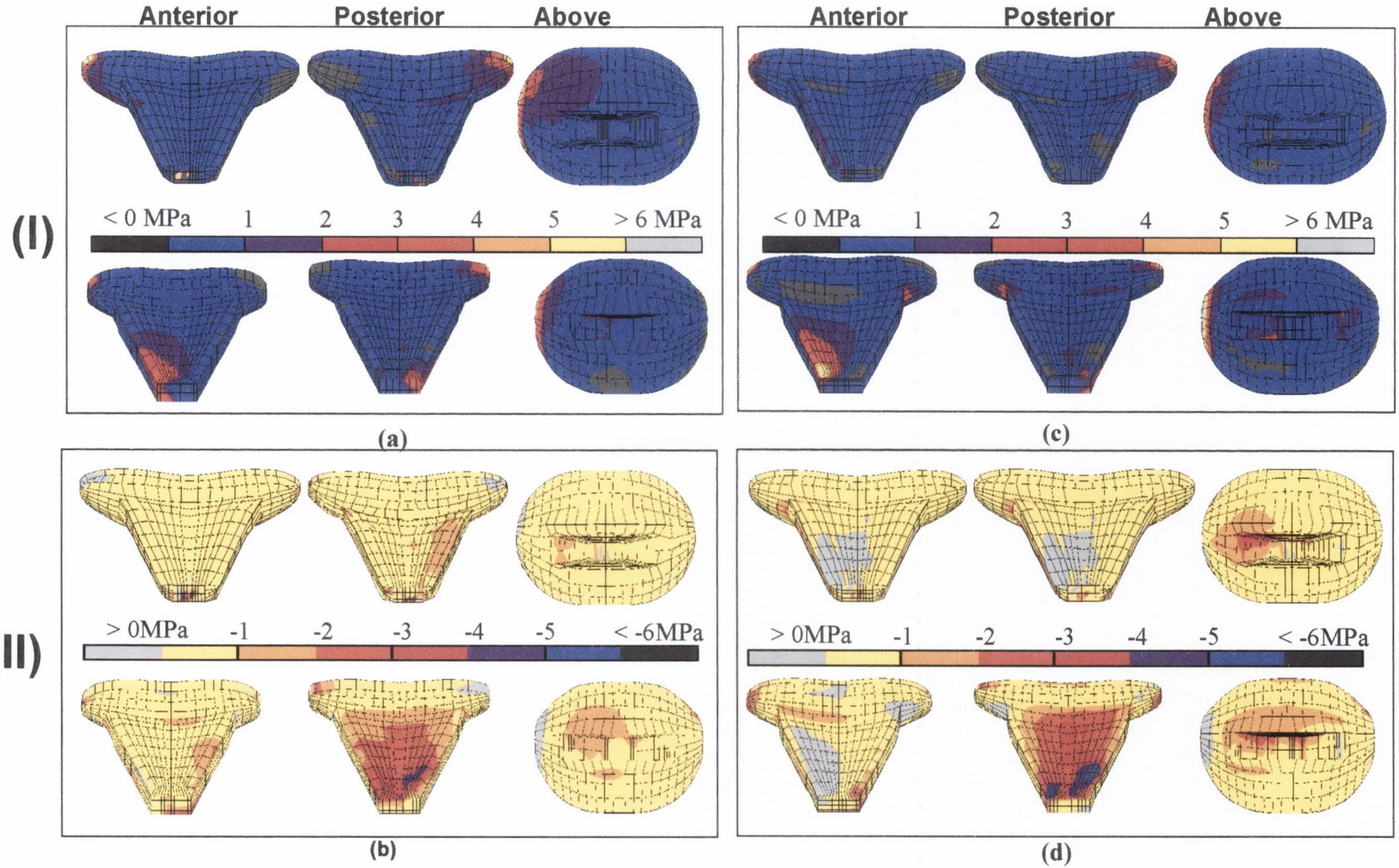

Figure 4.27 60 DEGREES OF FLEXION: *Maximum (0 to 6 MPa) and minimum (0 to –6 MPa) principal stress distributions in cement layer for* ***(I)*** *an offset and* ***(II)*** *a centre keeled prosthesis in* ***(a)*** *&* ***(b)*** *normal and* ***(c)*** *&* ***(d)*** *RA bone.*

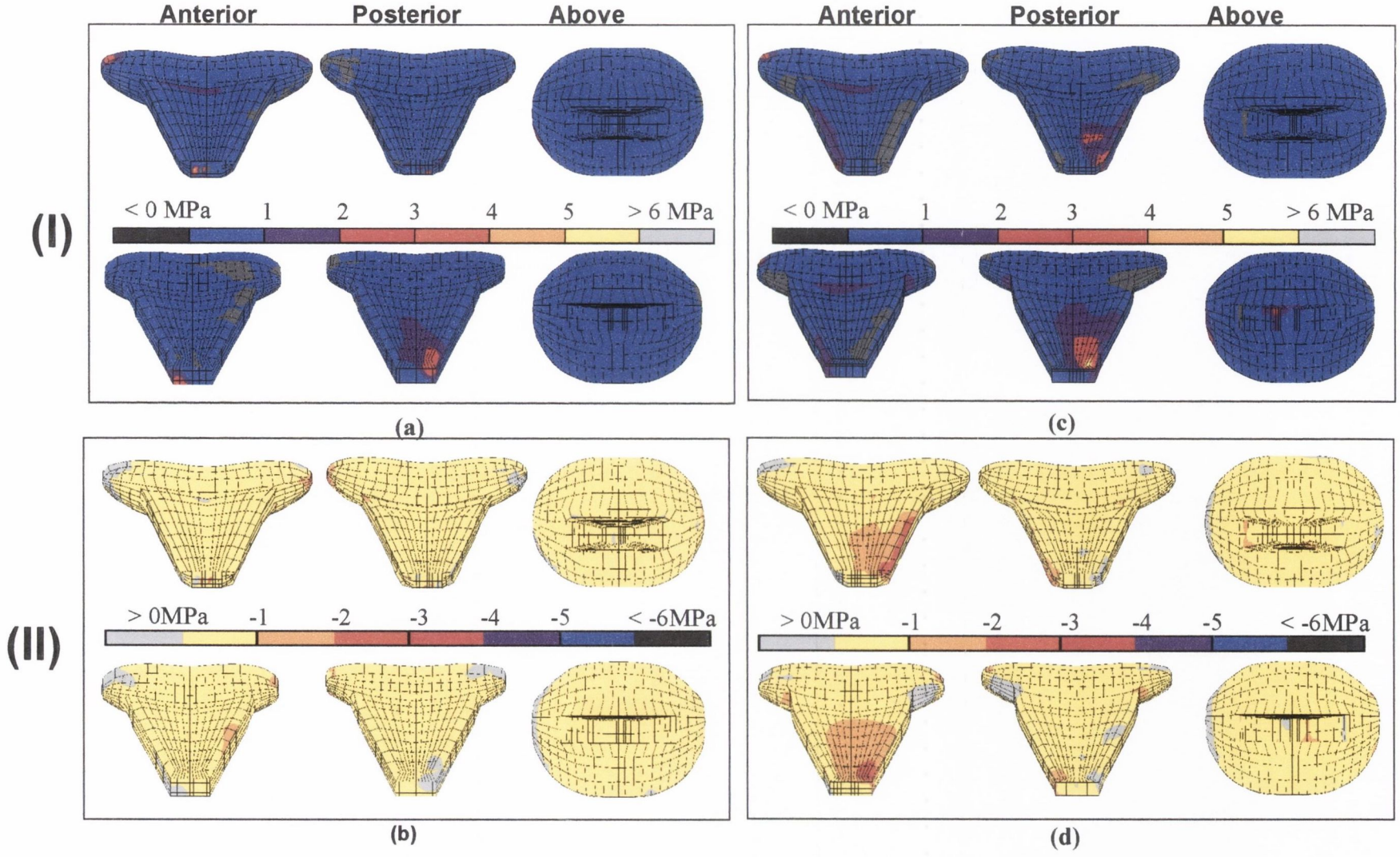

Figure 4.28 180 DEGREES OF FLEXION: *Maximum (0 to 6 MPa) and minimum (0 to –6 MPa) principal stress distributions in cement layer for* ***(I)*** *an offset and* ***(II)*** *a centre keeled prosthesis in* ***(a)*** *&* ***(b)*** *normal and* ***(c)*** *&* ***(d)*** *RA bone.*

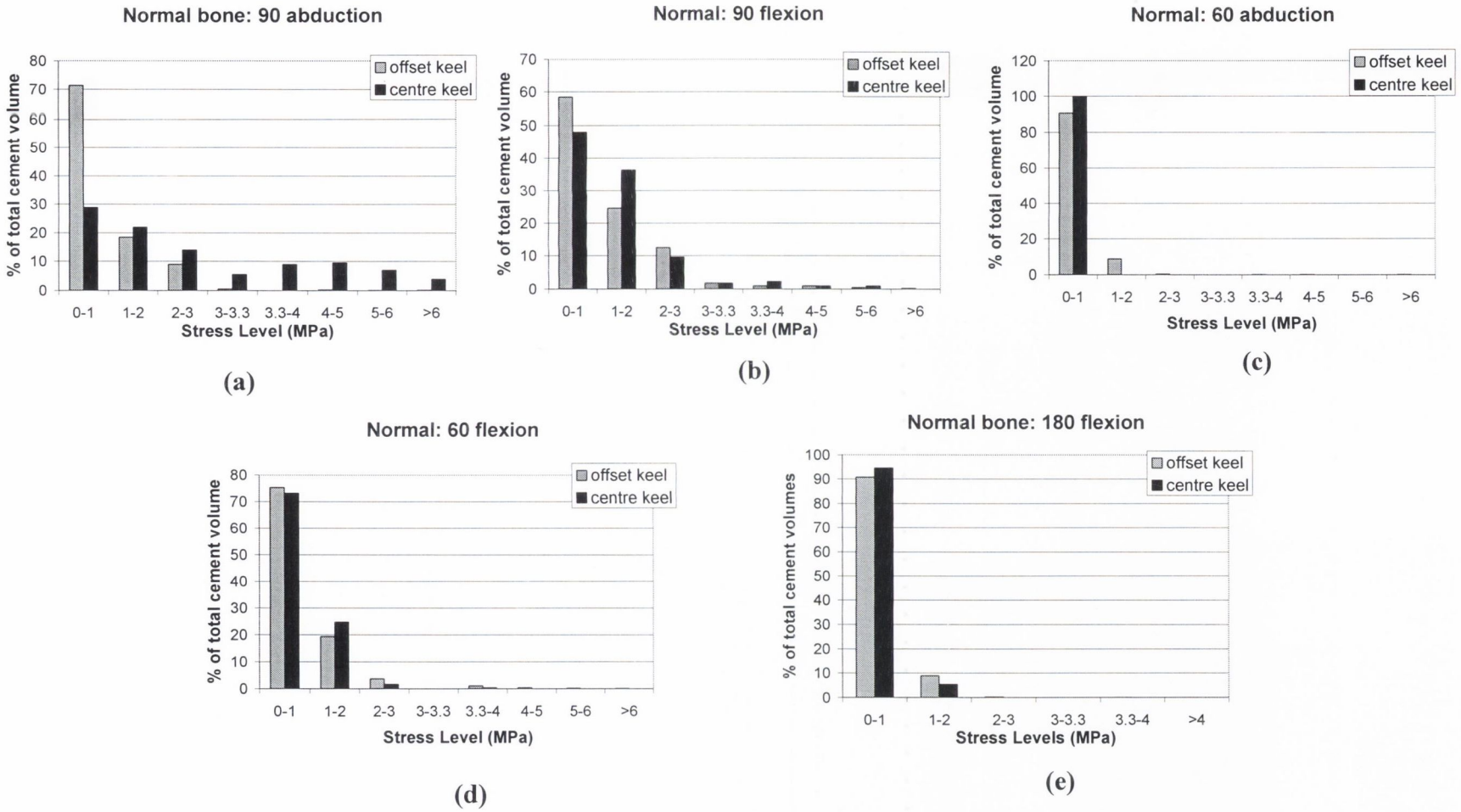

Figure 4.29 *Cement maximum principal stresses for normal bone– a comparison of the centre and offset keel designs for the various joint loading angles.*

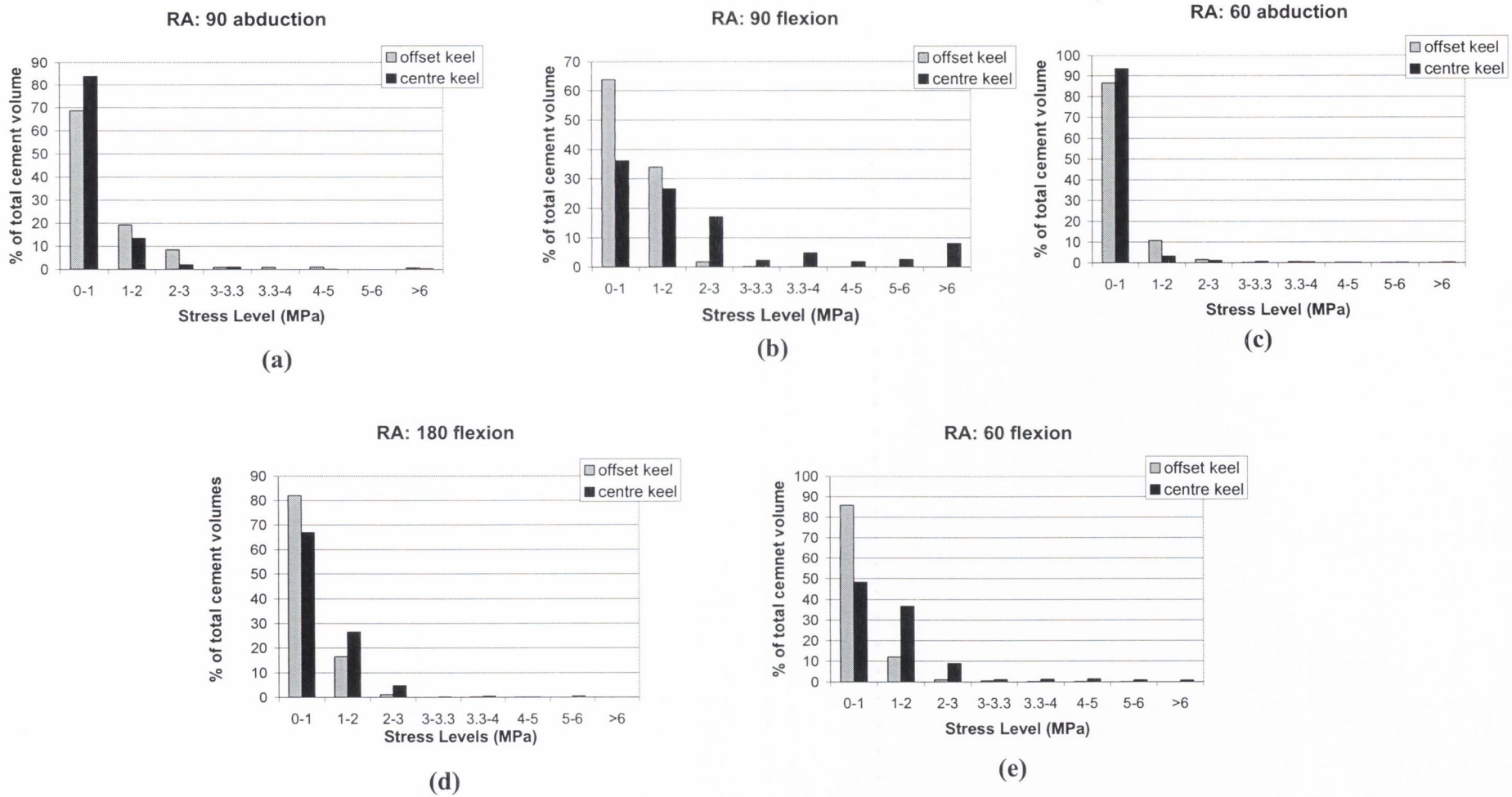

Figure 4.30 *Cement maximum principal stresses for RA bone– a comparison of the centre and offset keel designs for the various joint loading angles.*

Table 4.2 *Percentage of cement volume with a greater than 95 percent Probability of Survival (Hypothesis 2).*

Bone Quality	*Angle of loading*	*Centre Keeled Prosthesis (%)*	*Offset keeled prosthesis (%)*
Normal Bone	90° abduction	70.5	99.2
	90° flexion	94.5	97.5
	60° abduction	100	99.7
	60° flexion	99.1	98.8
	180° flexion	100	100
RA Bone	90° abduction	99.6	98.7
	90° flexion	82	100
	60° abduction	99.2	99.5
	60° flexion	99.4	99.4
	180° flexion	98.2	98.1

4.6.4 Stress distributions in the glenoid bone

Reduction of bone stresses might be expected in the offset keel design because of the greater amount of bone left to bear the load. Results for *normal* bone show that stresses medial to the tip of both prostheses are high, but slightly less for the offset keel design, see Fig. 4.31 (a). Again, as discussed in section 4.4.5, in the simulated RA bone, the Young's modulus of the cancellous bone was reduced to a tenth and thus becomes weaker. This indicates that even though the plots for RA look similar, the actual severity of the stress in the bone is greater.

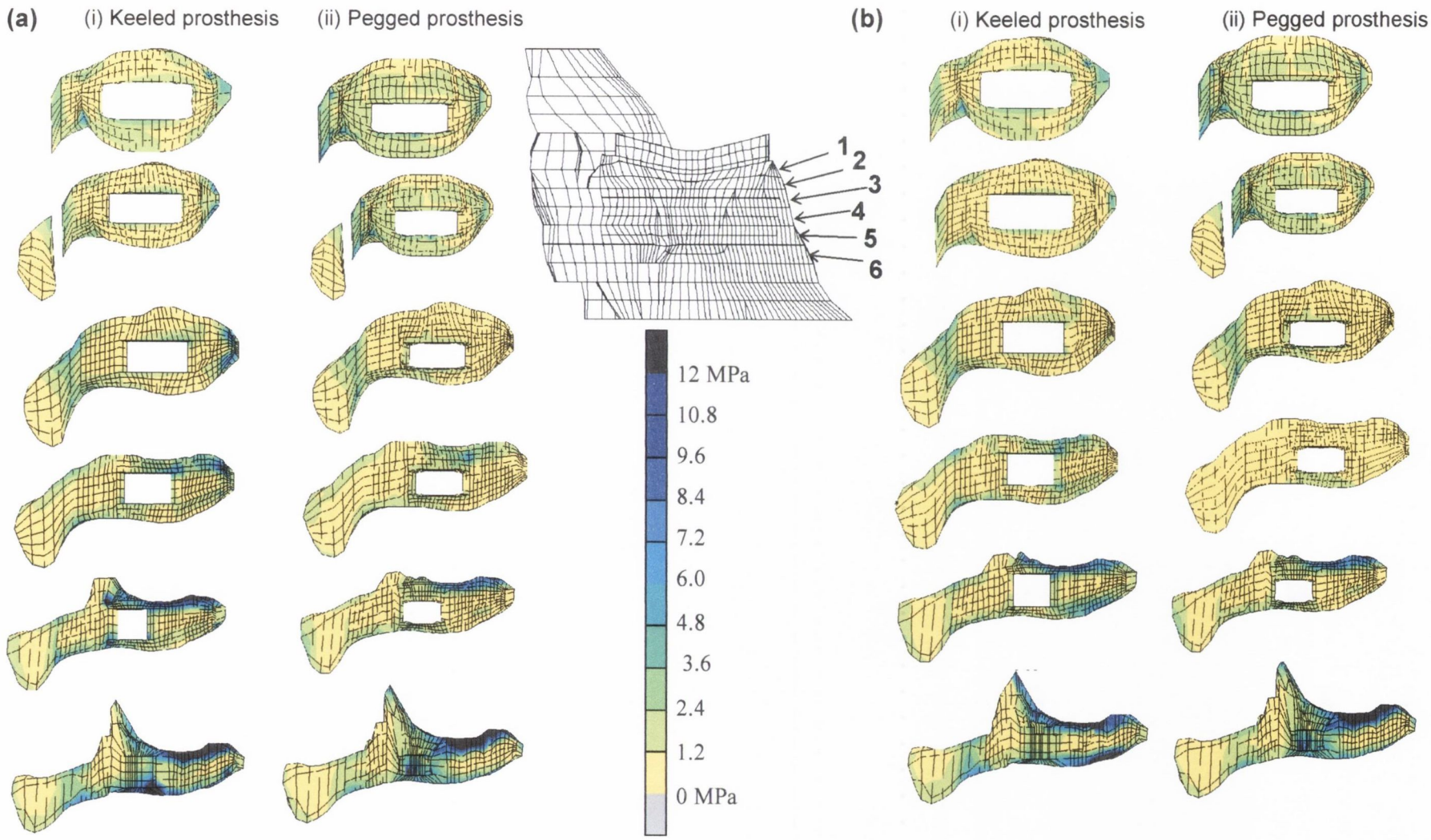

Figure 4.31 *90 degrees of abduction load, von Mises stresses of (i) the centre keeled prosthesis and (ii) the offset keeled prosthesis in* ***(a)*** *normal and* ***(b)*** *RA bone. A1, A2, B1, and B2 are regions of high stress.*

4.7 Testing Hypothesis 3

Hypothesis three states that: *"since secure fixation is difficult to achieve for fixation to the glenoid alone, attachment of the scapular component to the acromion would reduce loosening rates".*

4.7.1 Stress distributions in the cement layer

Plots of maximum and minimum principal stress distributions in the cement mantle for the acromion fixation design are given for 30 to 180 degrees of abduction in the normal and RA case, see Fig 4.32 and 4.33. The predicted stresses are high (> 6 MPa) at the interface of the metal-backing and the cement mantle. They reach magnitudes of greater than 10 MPa at some sites in the mantle. However, stresses in the rest of the cement mantle are generally lower than 1 MPa (see Fig. 4.34).

4.7.2 Stress distributions in the glenoid polyethylene

For Hypothesis 1 and 2, polyethylene stresses were generally of low magnitude (< 6 MPa). However, for the acromion fixated prosthesis high maximum and minimum principal stress polyethylene stresses of 25 MPa were reached. Plots of distributions in the prosthesis polyethylene are plotted for 30 to 180 degrees of abduction in the normal and RA case, see Fig 4.35.

4.7.3 Stress distributions in the metal base-plate

Stresses produced in the metal backing were greatest in the acromion arm, and reached magnitudes of 100 MPa, which is high. Figure 4.36 plots the maximum and minimum principal stresses (0 to 60 MPa) in the acromion base-plate and arm for 30 to 90 degrees of abduction and for (a) the normal case and (b) the RA case. Figure 4.37, then plots the maximum and minimum principal stresses (0 to 60 MPa) in the acromion base-plate and arm for 120 to 180 degrees of abduction and for (a) the normal case and (b) the RA case. The plots are arranged in this way since from Fig. 3.17 we can see that the joint loads of 30 to 90 degrees are positioned on the superior portion of the glenoid whereas 120 to 180 degrees loads intersect at the centre and inferior portion of the glenoid. This results in similar stress distributions for 30 to 90 degrees and 120 to 180 degrees. For superior

loads, highest tensile stresses occur on the posterior face of the acromion arm and highest compressive stresses occur on the anterior arm. For the centre and inferior loads, however, the reverse occurs. For the superior loads, highest overall stresses occur for 60 degrees of abduction, which is not the maximum glenohumeral joint load. However, this may be explained by the fact that at 60 degrees the load is positioned more superior to 90 degrees. This is also true for 30 degrees, but at this angle the joint force is approximately equal to 150 N, whereas at 60 and 90 degrees the magnitude is approximately 320 N and 395N respectively. For the centre and inferior loads highest stresses occur at 120 degrees of abduction, this is to be expected as this angle has the highest joint force.

4.7.3 Stress distributions in the scapula

The generally low cement stresses accompanied with very high peak stresses produced in the cement mantle for acromion fixation and the high stresses produced in the acromion base-plate are investigated further by analysing the load sharing between the acromion and glenoid bone. Stresses in the acromion bone were found to be, on average, 16 MPa greater for the acromion fixation compared to the natural case (no prosthetic fixation), see Fig. 4.38. This may indicate stress transfer away from the glenoid causing cement stresses to be lower there. Plots of stress distributions in the entire scapula show that there is a general increase in tensile stresses in the acromion bone compared to the natural case, see Fig. 4.39. Furthermore, these plots show that there is a general overall increase in tensile and compressive stresses for the RA case compared to the normal case, Fig. 4.40.

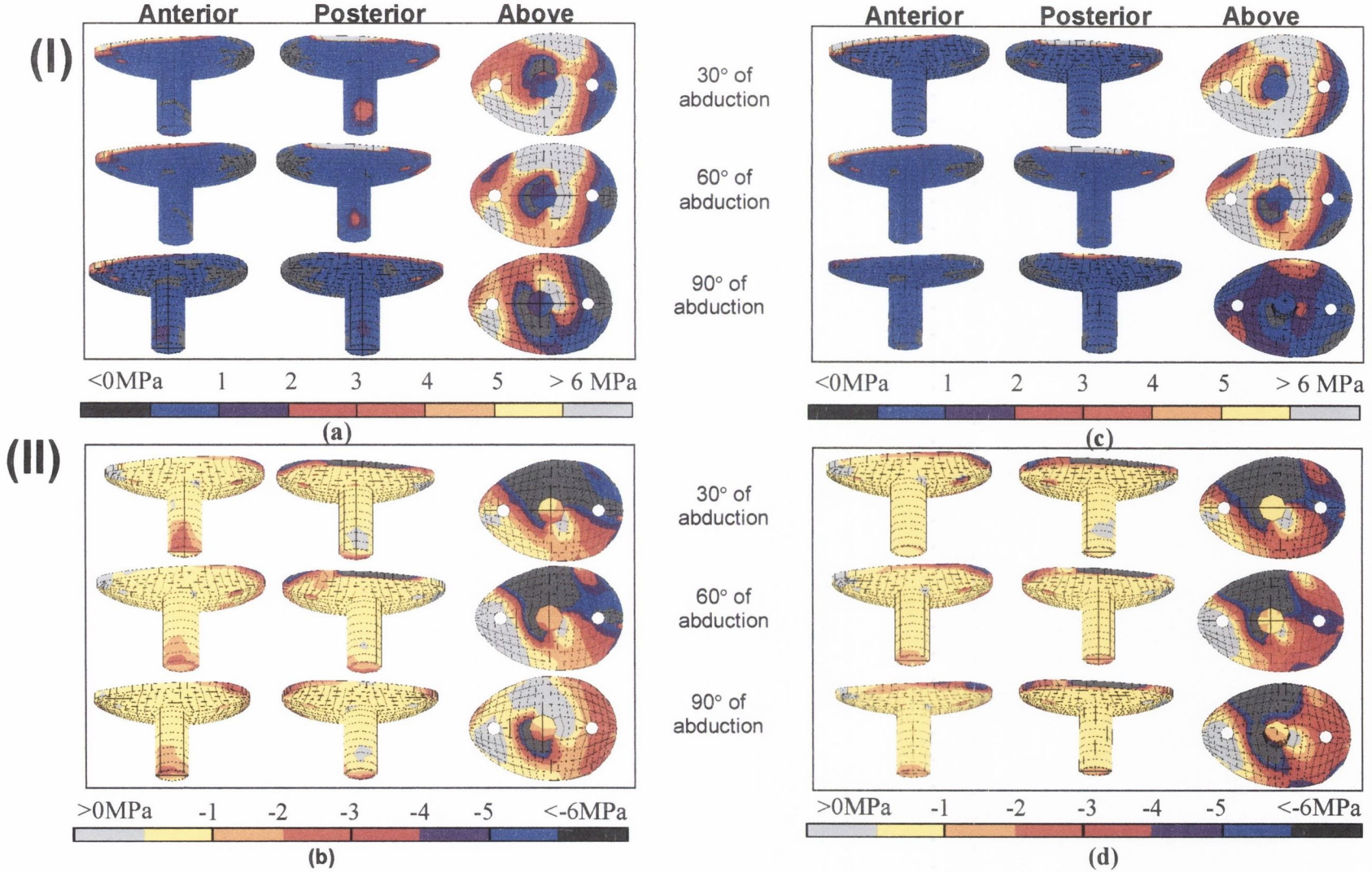

Figure 4.32 ***(I)*** *Maximum (0 to 6 MPa) and* ***(II)*** *minimum (0 to –6 MPa) principal stress distributions in the cement mantle for the acromion design, for* ***(a)*** *and* ***(b)*** *normal bone and* ***(c)*** *and* ***(d)*** *RA bone.*

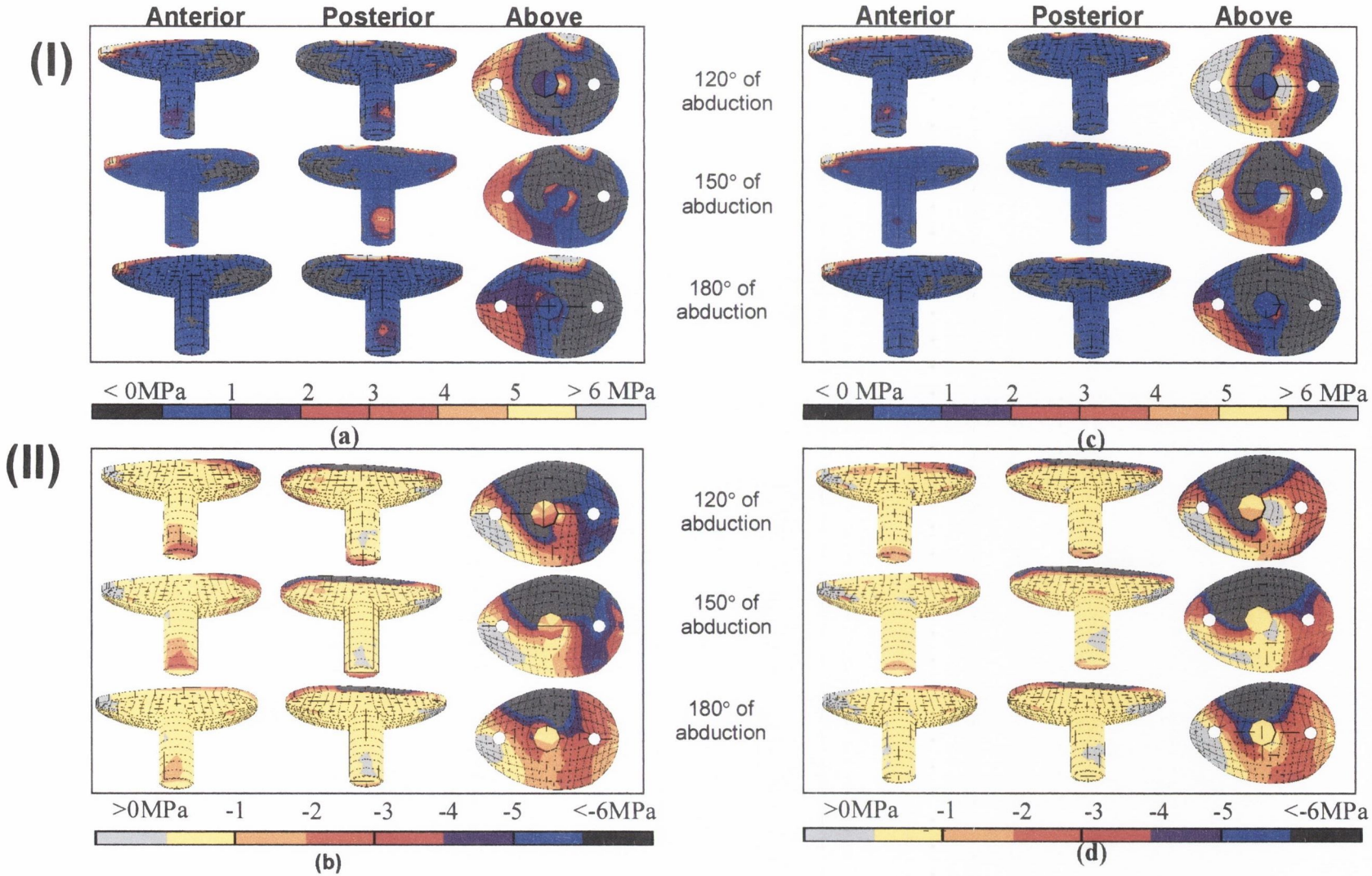

Figure 4.33 ***(I)*** *Maximum (0 to 6 MPa) and* ***(II)*** *minimum (0 to –6 MPa) principal stress distributions in the cement mantle for the acromion design, for* ***(a)*** *and* ***(b)*** *normal bone and* ***(c)*** *and* ***(d)*** *RA bone.*

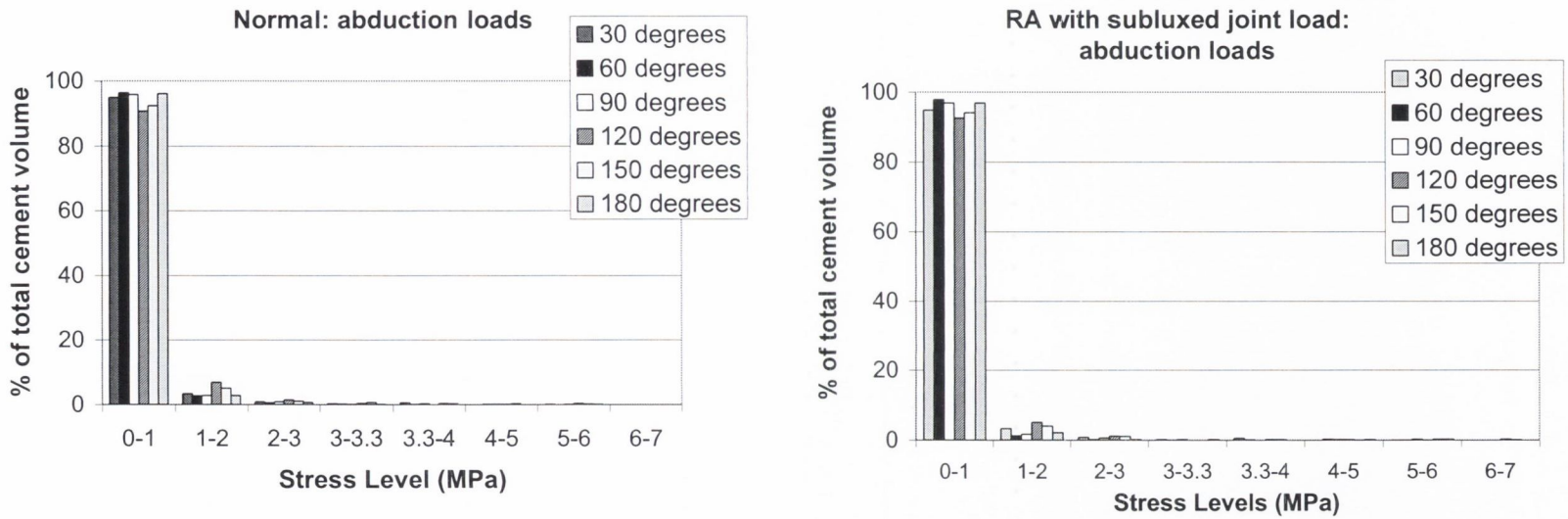

Figure 4.34 *Cement maximum principal stresses for* ***(a)*** *normal bone and* ***(b)*** *RA bone– a comparison of the acromion design at 30 to 180 degrees of abduction.*

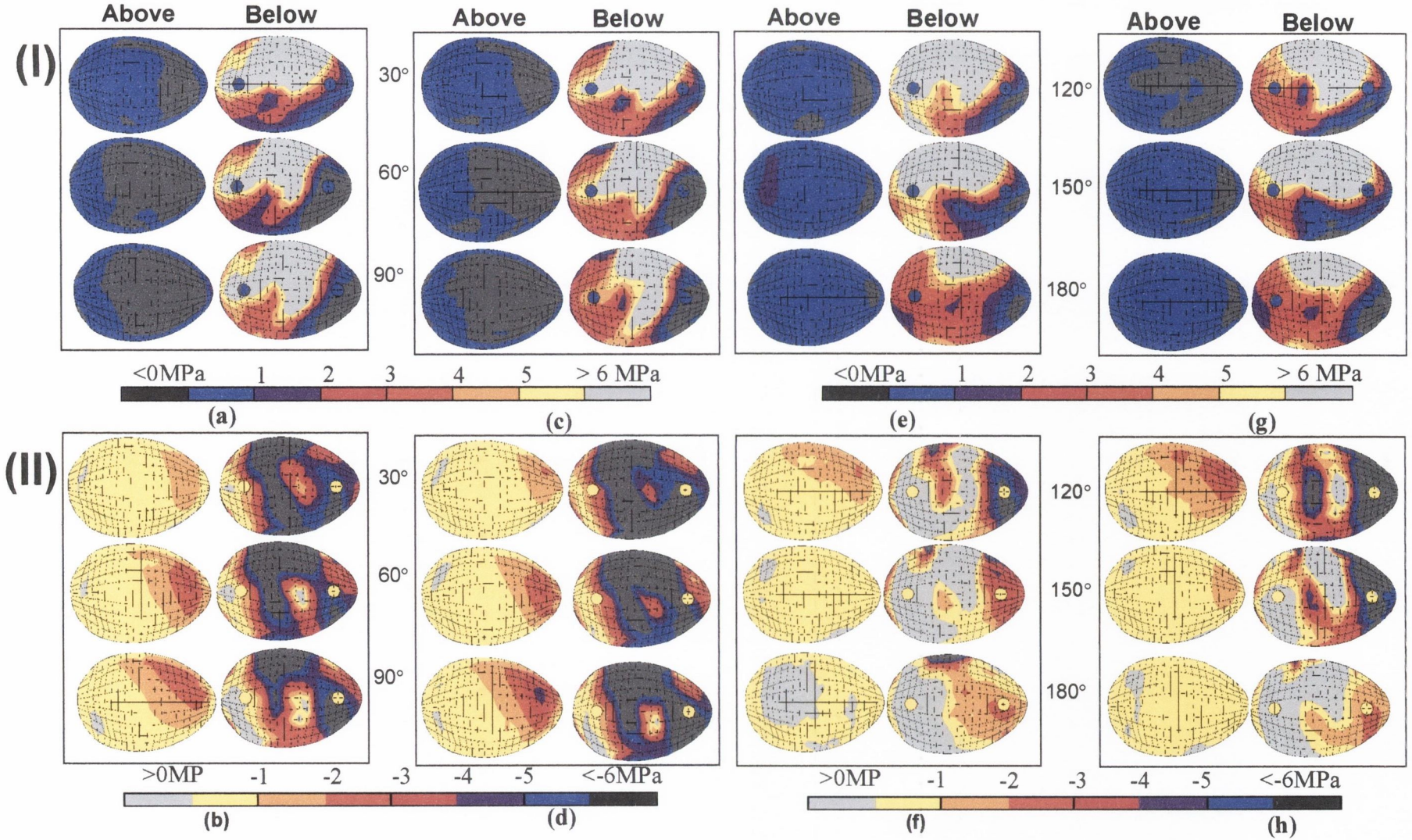

Figure 4.34 ***(I)*** *Maximum (0 to 6 MPa) and* ***(II)*** *minimum (0 t o – 6 MPa) principal stress distributions in the polyethylene for the acromion design, for* ***(a),(b),(e),*** *and* ***(f)*** *normal bone and* ***(c),(d),(g)*** *and* ***(f)*** *RA bone.*

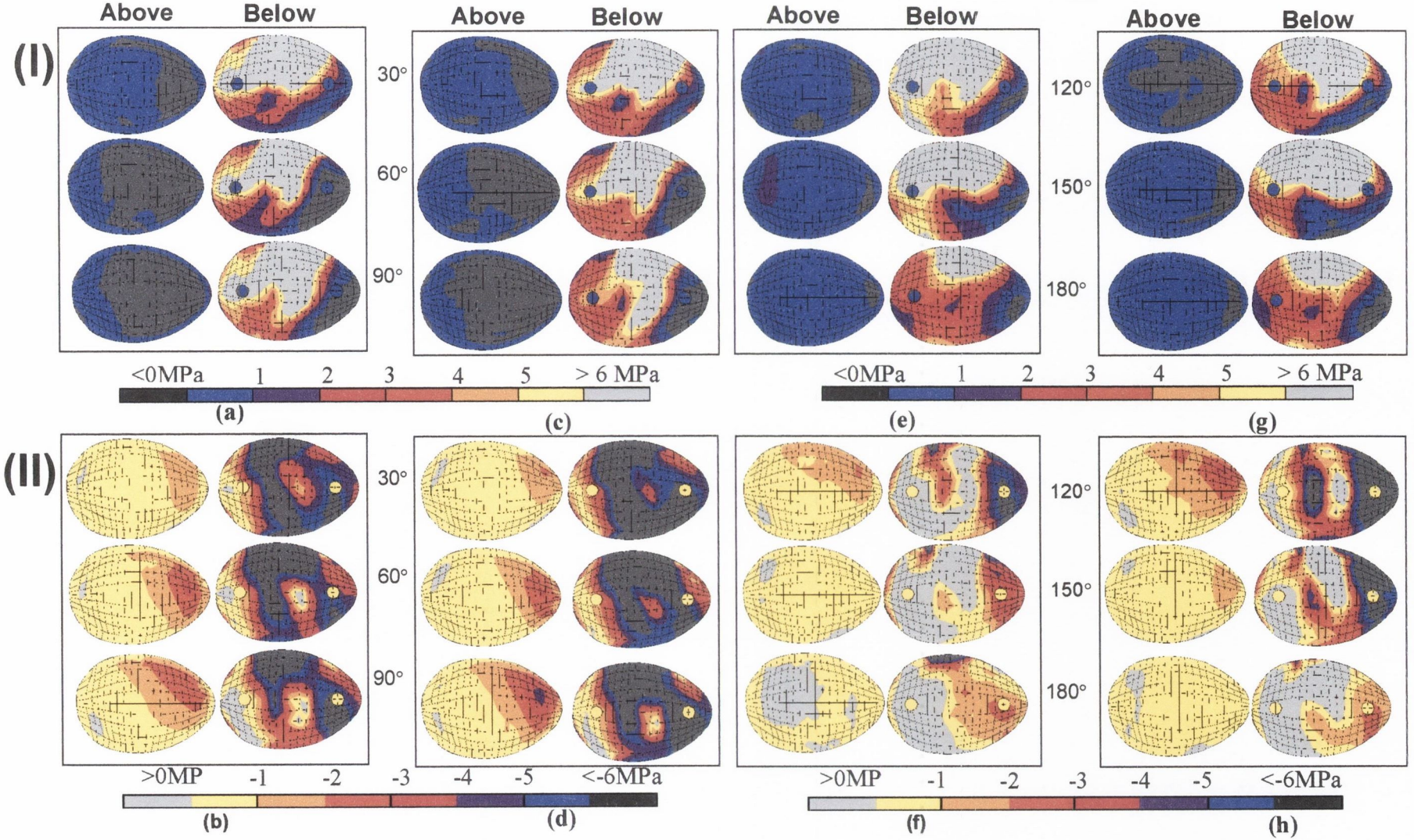

Figure 4.35 ***(I)*** *Maximum (0 to 6 MPa) and* ***(II)*** *minimum (0 t o – 6 MPa) principal stress distributions in the polyethylene for the acromion design, for* ***(a),(b),(e),*** *and* ***(f)*** *normal bone and* ***(c),(d),(g)*** *and* ***(f)*** *RA bone.*

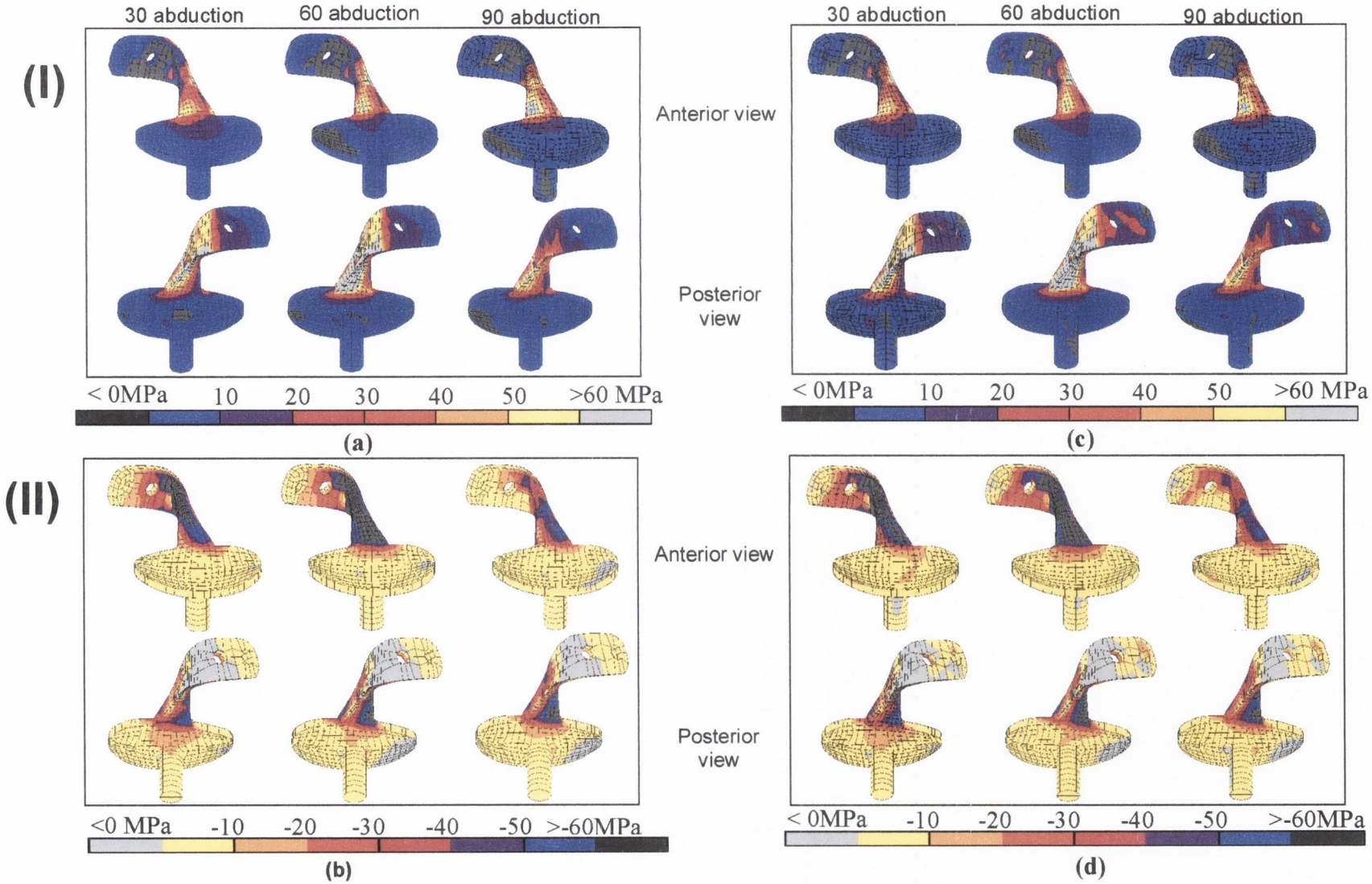

Figure 4.36 ***(I)*** *Maximum (0 to 60 MPa) and* ***(II)*** *minimum (0 to –60 MPa) principal stress plots for the acromion base-plate, 30, 60 and 90 degrees of abduction, for* ***(a)*** *and* ***(b)*** *normal bone and* ***(c)*** *and* ***(d)*** *RA bone.*

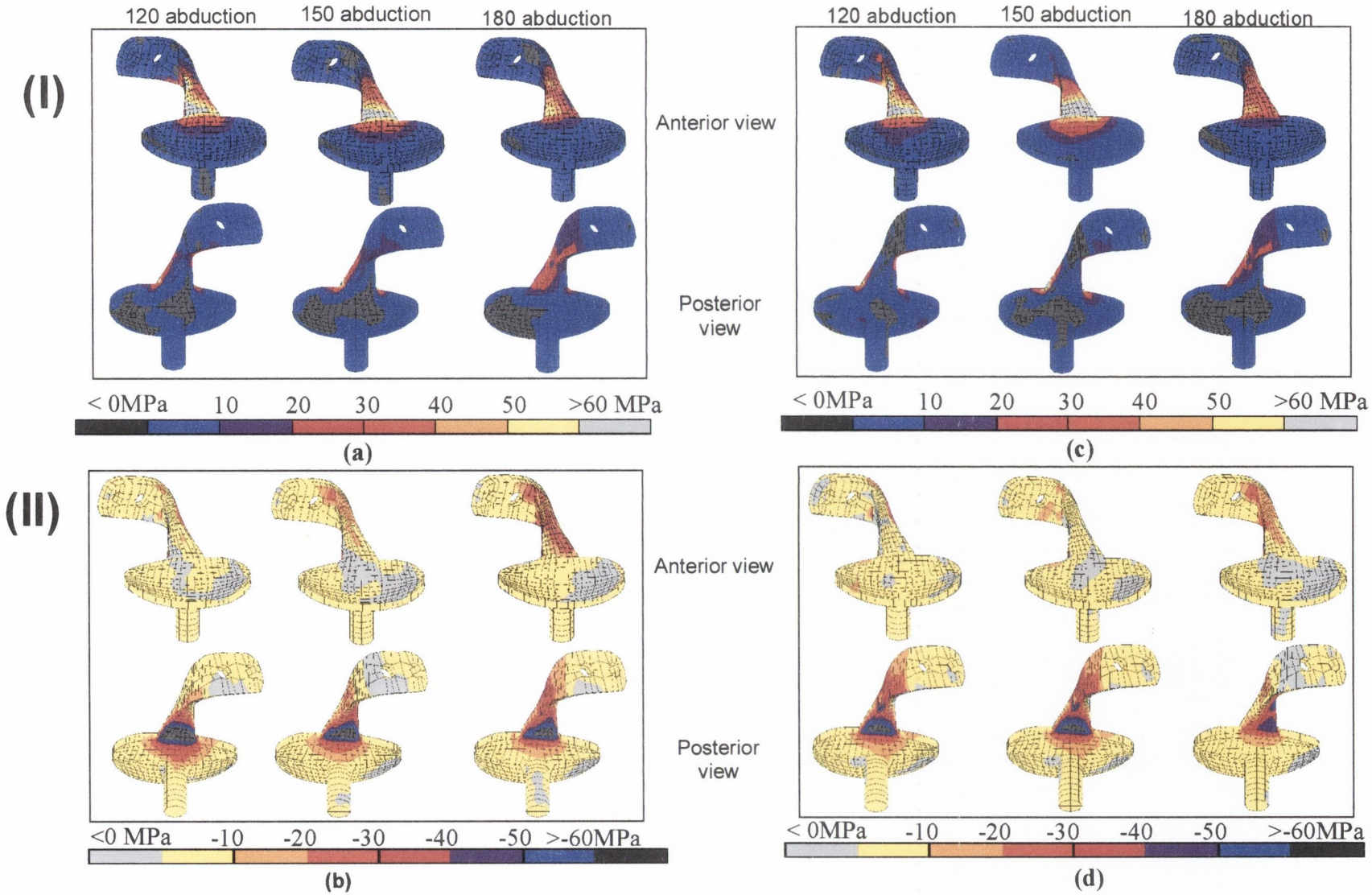

Figure 4.37 ***(I)*** *Maximum (0 to 60 MPa) and* ***(II)*** *minimum (0 to –60 MPa) principal stress plots for the acromion base-plate 120, 150 and 180 degrees of abduction, for* ***(a)*** *and* ***(b)*** *normal bone and* ***(c)*** *and* ***(d)*** *RA bone.*

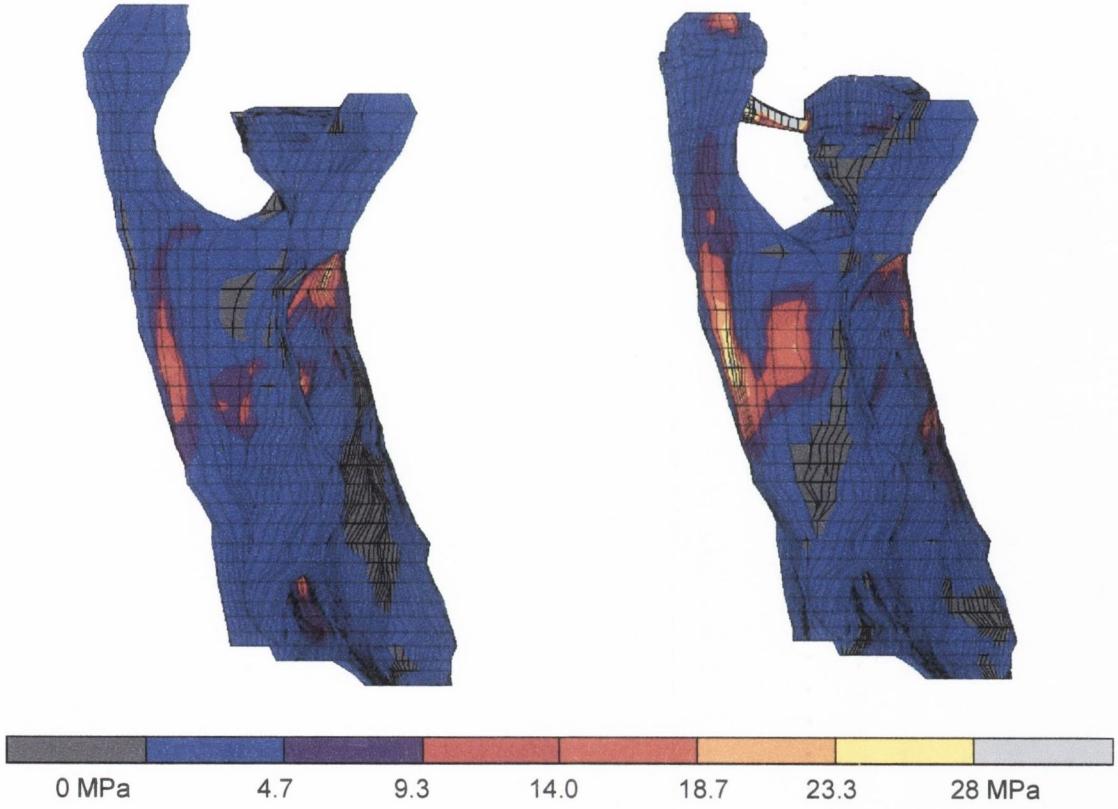

Figure 4.38 *Maximum principal stress plots in* ***(a)*** *the natural scapula (no prosthesis inserted) and* ***(b)*** *with the acromion prosthesis inserted.*

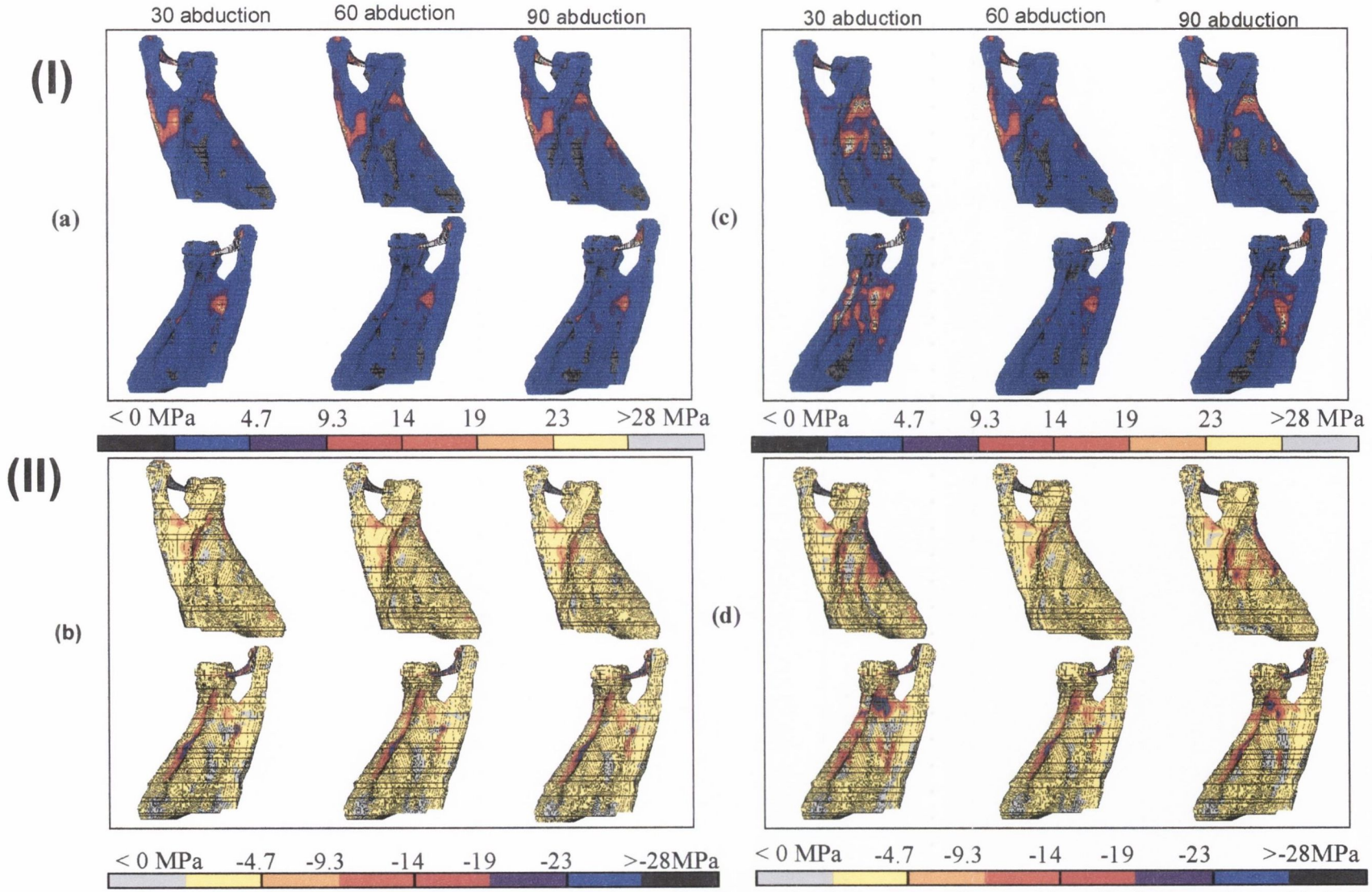

Figure 4.39 ***(I)*** *Maximum (0 to 28 MPa) and* ***(II)*** *minimum (0 to –28 MPa) principal stress plots for the scapula in* ***(a)*** *&* ***(b)*** *normal bone and* ***(c)*** *&* ***(d)*** *RA bone at 30, 60 and 90 degrees of abduction.*

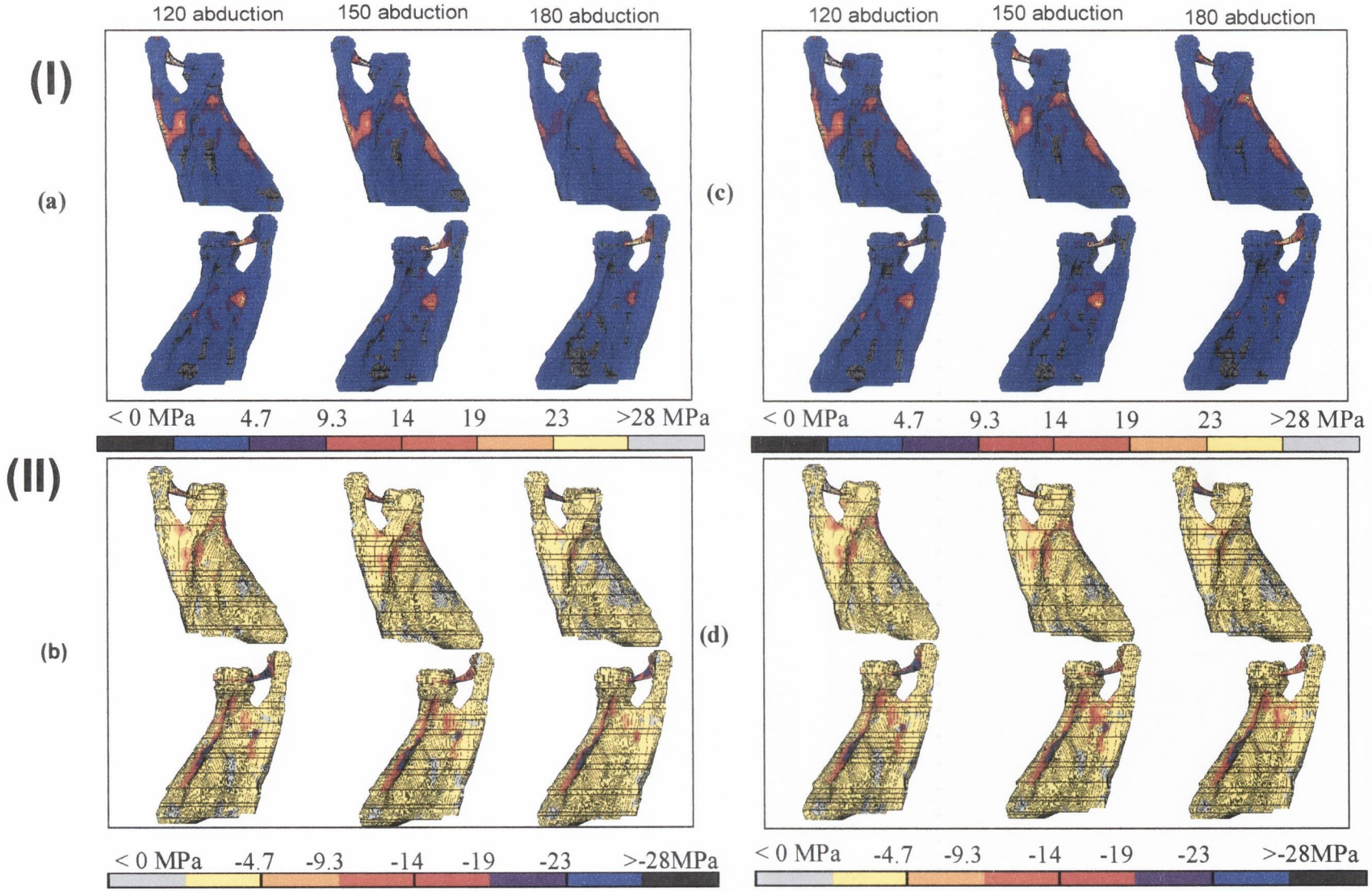

Figure 4.40 *(I) Maximum (0 to 28 MPa) and (II) minimum (0 to –28 MPa) principal stress plots for the scapula in* **(a)** *&* **(b)** *normal bone and* **(c)** *&* **(d)** *RA bone at 120, 150 and 180 degrees of abduction.*

4.7.4 Relative motion between the acromion and the glenoid of the scapula

A relative motion occurs in the unimplanted scapula between the acromion and glenoid due to the action of the trapezius muscle, deltoidus muscle, and the two reaction forces. It may be important, therefore, to determine the extent of motion is with the acromion-fixated glenoid prosthesis. If this motion is large then it will be resisted by the prosthesis and may be the reason why the acromion prosthesis arm is highly stressed.

A small but significant amount of motion occurs between the acromion and glenoid during abduction of the shoulder for acromion fixation, see Fig. 4.41. At the higher magnitude loads (30, 60, 90 degrees of abduction) the highest relative motion occurs (0.8 to 1.2 mm). It is this motion that is resisted by the acromion device and which may cause overstressing of the acromion arm.

At 120 and 150 degrees of abduction, with no acromion fixation, there is a smaller relative motion than for the case of acromion fixation. This is an unexpected result and may be explained as follows: Relative motion between the glenoid and acromion is calculated as a sum of the motion in the *x, y* and *z* directions. With acromion fixation, load sharing is occurring between the glenoid and acromion. However, clearly twisting of the acromion arm is occurring and as a result, motion of the glenoid is not in the same direction as the acromion. This results in a higher relative motion for 30, 60 and 90 degrees and a lower relative motion for 120, 150 and 180 degrees. Why are we getting different results for these two ranges? As we can see from Fig. 4.36 and 4.37, twisting of the prosthetic arm is occurring, however, this twisting motion is different for 30, 60 and 90 degrees of abduction compared to 120, 150 and 180 degrees of abduction. For 30, 60 and 90 degrees, highest tensile stresses occur on the bottom of the arm at the inferior portion, with lower tensile stresses on top at the superior portion. Highest compressive stresses occur on the top of the arm with lower stresses on the bottom at the superior portion. In comparison for 120, 150 and 180 degrees, highest tensile stresses occur on the top of the arm (very low tensile stresses on the bottom) and highest compressive stresses occur on the bottom of the arm (very low compressive stresses on the bottom). These alternative *twisting* motions of the acromion arm may explain the alternative relative motions.

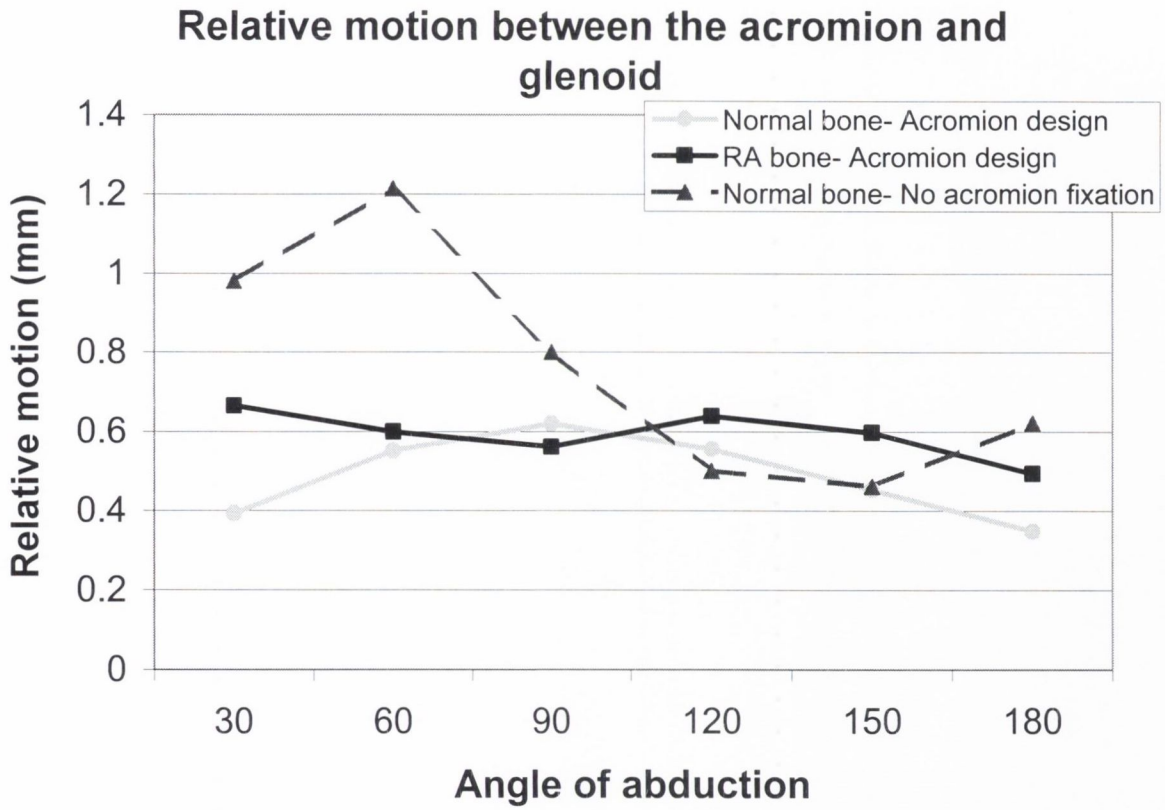

Figure 4.41 *Plot of the relative motion between the glenoid and acromion of the scapula for* ***(a)*** *no acromion fixation and* ***(b)*** *acromion fixation, 30 to 180 degrees of abduction.*

4.8 Concluding remarks

A three-dimensional model of the scapula generated form CT scans (Lacroix, 1997) as used for the basis of this pre-clinical testing protocol. A total of 35 absolute values Young's moduli values were rounded for input into the finite element model. Three-dimensional muscle and joint loads were applied, based on experimental models form van der Helm (1991). The effects of RA were simulated in the FE model, see Dalstra *et al.*, (1996) which is consistent with the damage associated with a Larsen Grade IV type destruction (Kelly, 1994). This model was used to test the three hypotheses stated in Chapter 1. The question of model accuracy was tested using mesh refinement and model validity was also tested using the technique of photoelasticity. When used to test the three hypotheses, the model produced a large array of results. As with all FE models the question of the significance of the results is a major issue. Whether or not the model can be used to refute the hypotheses will be discussed in the next chapter. Furthermore, the extent, if any, of these results on surgical procedure and prosthesis selection are also discussed.

Chapter 5

Discussion

5.1 Introduction

Glenoid component loosening has become a seemingly inevitable part of the TSA service. It is clear from Chapter 2 that only short term clinical follow-up studies are being reported for the shoulder and that the essential long-term studies are missing. Following on from this, few long-term register studies exist for TSA, and therefore improvements of the sort found by Herberts and Malchau (2000) for hip replacements have not been possible. They quote Murray and co-workers that 62 types of hip prostheses are used in the UK, half of which were introduced in the last five years, without any documentation on mid-term results. Furthermore, long term results were only known for one-third of the prostheses, resulting in a revision rate, in the UK, of three times larger than in Sweden. This clearly shows the vast importance of register studies which are only beginning in TSA. Yet, even after rigorous pre-clinical and clinical trials, there is still no guarantee that an innovative device will endure any longer than a traditional device. This is notable for the hip joint where the Charnley has been proven to perform well with 93% of hips still being pain-free after ten years (Huiskes, 1993) where the next step for the hip joint is to increase this durability for over ten years.

The shoulder, however, does not have a traditionally well performing glenoid component to which new devices can be compared. In the attempt to find a well performing device, a plethora of components have been introduced, many of which have no rigorous biomechanical basis. Based on first hand experience, many surgeons have developed their own prosthetic designs. Pointedly Huiskes (1993) queries whether it is fair that patients should participate in experimental development and contribute to a learning curve. Should patients be protected against inventive surgeons? Does this question even need to be asked? Furthermore, a provoking question posed by Sarimento in 1991 is: "If these devices are marketed for the sake of the patient or to keep orthopaedic companies afloat" (see Prendergast, 2001). Of course, public health standards (the EU CE marking and the US FDA regulations) regulate the device market to ensure safety. However, these standards do not ensure that a device is effective. As Coventry states (1992), "Selection of the prosthesis must be carefully made from sound clinical and scientific data". Much work and organisation lies ahead for the improvement of TSA, if

Coventry's objective is to be achieved and an important question, which I will attempt to answer, is how can market flooding of relatively ineffective prosthetic components be best resisted?

An algorithm approach has been proposed to regulate the process of implant innovation (Fig. 5.1), and the lack of adherence to such an approach can partly explain the high failure rate of glenoid components. Before clinical and register studies can be implemented, the first and most important step is to have effective pre-clinical testing procedures. This allows for the identification of weak and strong designs before patient implantation, and can direct investment for further development of high performance devices. Yet, the basic design of glenoid implants lacks widely accepted testing methods that would allow for design superiority to be identified at an early stage. I suggest that pre-clinical testing methods for TSA could be more effective if hypothesis testing is incorporated. As Kuhn and Popper, two contemporary philophosers of science, state science does not progress by accumulation but rather by the refutation of hypotheses (Lakatos and Musgrave, 1970).

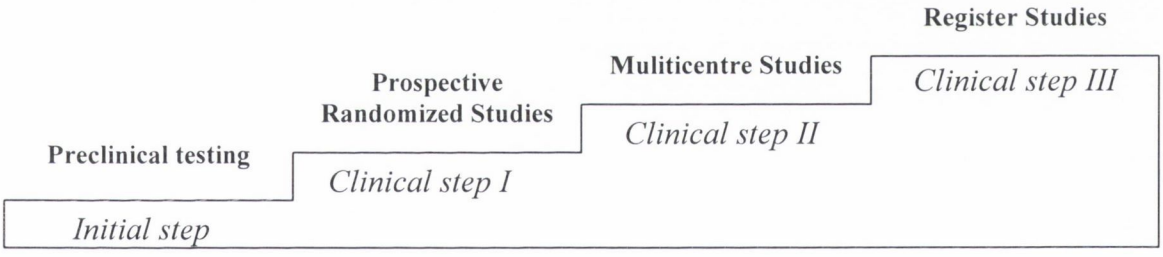

Figure 5.1 *Stepwise introduction of new implants, after Prendergast and Maher (2001).*

5.2 Hypothesis testing for orthopaedic implants

Just as an industrial engineer carries out prototype testing to verify that performance requirements are being met, so to does the empirical scientist construct hypotheses and tests them against experience by observation and experiment (Popper, 1972). The

importance of hypothesis-based research is that the advance in knowledge to be generated by the research is in focus at the outset.

Regarding hypothesis generation, initially, the hypothesis is a provisional description of what we observe. Good scientific hypotheses are statements which can be tested and therefore which can in principle be refuted (Popper, 1972). Failure to confirm a hypothesis can teach us how to better interpret existing observations, and how to improve on these observations by generating and testing further hypotheses as a result. The hypothesis should be relevant, simple and clear and have good predictive power. Additionally, the person who conceives the hypothesis may not know the best methods for testing which may be evident in the area of orthopaedics. The surgeon has a greater understanding of the overall nature of the joint, surgical procedure and the associated problems leading to significant hypothesis generation. Yet it is the engineer who can design the experiment to test these hypotheses.

The idea that glenoid components can be improved to ensure adequate longevity is more of an article of faith than a testable hypothesis. It is a universal statement- a theory. To get a testable hypothesis we must reduce to a particular case. For example, in a study carried out by Anglin (2001), one particular test was applied to a large series of glenoid components. The glenoid components were cemented into polyurethane foam blocks and a cyclic eccentric load was applied and loosening was measured. I suggest that this study lacks a proper hypothesis; as a result it is difficult to remember what the outcome of this study is. Furthermore, I would argue that applying the same test to a large series of implants particularly for glenoid components is a *weak* biomechanical test. Alternatively, I reason that it is less than optimal when surgeons use a particular device with which they have experience and have perfected skills involved for implantation. The reason both these approaches, mechanical and surgical, are lacking is that a huge variability exists at the shoulder joint, it is impossible to imagine that one prosthetic design alone can be used for a wide spectrum of cases. This has been highlighted in Chapter 2 showing that huge variability in the pattern and progression of the degenerative RA shoulder exists. Prosthetic designs for the shoulder should have clearly stated design functions based on surgical observation, these design objectives could be framed as hypotheses. I suggest that hypothesis-based testing can help clear up the "prosthetic surplus" which exists for

TSA. Therefore, three hypotheses are put forward in Chapter 1 which were generated by Orthopaedic surgeons and are tested using engineering methods. It is my thesis that, by challenging these observations or hypotheses and using *strong* biomechanical testing, scientific knowledge can grow and TSA performance can improve.

5.3 Three hypotheses regarding glenoid component design

1) *Hypothesis one states that: "a pegged prosthesis provides greater durability to prevent glenoid loosening in normal bone whereas a keeled prosthesis is recommended when there is compromised glenoid bone".* In order to elude of any vague terms, Hypothesis 1 is refined as follows to compare pegged and keeled glenoid prostheses: *"a pegged prosthesis provides greater durability to prevent glenoid loosening in normal bone whereas a keeled prosthesis is recommended when there is RA bone"*

I believe that strong confirmation of the refined Hypothesis 1 was achieved. The reasons for this are:

(i) Since we are interested in the stress distributions in the area of the glenohumeral joint, precise joint reaction forces, for both the normal case and the RA case, were modelled together with a full description of the muscle forces (van der Helm, 1994). Only with this level of sophistication in the applied loading can the critical question of how susceptible the designs are to the *rocking-horse* loosening mechanism be addressed. Deformations of the prostheses, as presented in Section 4.3, showed that similar deformations occurred for each prosthesis out of the superior-inferior plane. This prediction of the model is supported by a case report on the rotational dissociation of glenoid components in total shoulder prostheses in which two cases of TSA were analysed, both with metal-backed polyethylene glenoid components which failed due to a dissociation of the polyethylene liner from the metal (Feldman *et al.,* 1999). Dissociation occurred due to a twisting of the polyethylene liner out of the superior-inferior plane in a counterclockwise direction. This merely confirms that my study is comparable to the *in vivo* case in that a simulation of the

forces occurring at the glenohumeral joint produces an *in vivo* type of movement at the glenoid interface.

Quantitative analysis of the cement stresses indicates that they are high enough to cause cement failure. Path plots of the cement stresses were included merely to show the non-linear relationship between stresses and the number of cycles to failure. This highlighted how a slight increases in stress can create a much higher risk of failure. However, I would argue that previous studies (Lacroix, 1997 and Gupta, 2002) reporting stresses calculated for selected nodes or a pre-determined path plot around the interface of the cement layer are restricted as a path plot only takes into account the particular "line" or node selected around the interface and may miss other critical stresses throughout the cement layer. Additionally, stress distribution plots can be very intricate and difficult to interpret. Studies reporting these alone can not give a full explanation of what is happening in the mantle (3D studies: Barea, 1998, Kaufler 1998, Lacroix, 1997, Gupta, 2002). I think by reporting the total volume of cement at each stress level throughout the entire cement layer, the associated probability of survival, and with stress distribution plots, a more precise analysis can be made. This is the first 3D FE model study of glenoid component durability which has included such detailed analysis of results.

The maximum stress predicted in the cement mantle for both designs (hypothesis 1) occurs at the tip of the keel with a maximum principal stress (tensile) of approximately 6 MPa. This value may exceed the stress needed to initiate cracks since cracks initiate in PMMA under physiological conditions at about 5-7 MPa (Davies *et al.*, 1987). The prediction of cement failure is even more likely to be true when one considers that the glenohumeral force used in this study was for an unloaded arm. Therefore, results clearly predict that excessive cement stresses are the key factor in glenoid prosthesis loosening and that considerable challenges lie ahead for designers of glenoid anchorage systems.

As previously discussed, we are particularly interested in observing the tensile stress distributions within the cement layer as a prediction of the probability of crack initiation. When comparing the resulting stress outputs for the keeled and pegged prostheses in both *normal* and RA bone, the prediction is that a pegged prosthesis has the highest

probability of cement survival for *normal* bone and a keeled prosthesis has the highest probability of survival for low density bone.

Stress in the polyethylene at the glenoid cavity is predicted to be very low with an average of approximately 2 MPa for each type of design. This may explain the infrequent reports of excessive wear of glenoid prostheses (Wirth and Rockwood, 1996). Karduna *et al.* (1998) report an experimental strain measurement in the keel of an all-polyethylene glenoid component in an *in vitro* bench test. For a load of 400N applied at the anterior rim, a strain of approximately –0.001 is reported on the keel. In this analysis, a force of 406 N for 90 degrees of arm abduction (unloaded) gives a strain between -0.002 and -0.0038. However, the experiment and finite element model are somewhat different. In Karduna's study the scapula is cut to the superior notch (acromion removed) and is potted to the glenoid neck, all muscles are removed and a translational load is applied. Despite these differences, the comparison does indicate that the finite element model is straining the polyethylene to the same order of magnitude as obtained in experimental tests.

Stress distributions in the glenoid bone were also reported and showed that similar von Mises stresses are reported for both designs in normal bone, in general. However, lower stresses are experienced by the keeled design directly under the flange. This is to be expected since the deformation plots showed that the pegged design is less stiff than the keeled design. Regarding the RA bone, by calculating the stress-to-strength ratio, we showed that even though the von Mises stresses are generally lower in RA bone the severity of these stresses is higher. Prosthesis performance was poorer in general in RA bone, more so for the pegged design. However, the present study predicts that the influence of the implant on the stress in the bone surrounding the implant is very small. This suggests that there may be no point in redesigning glenoid components with a view to optimising the stress in the bone; it certainly will not have the same significance as it is suggested to have in hip replacement for example.

Better performance of a keeled prosthesis in RA bone and of a pegged prosthesis in *normal* bone may be explained by the following: the keeled prosthesis has a larger volume of cement than the pegged prosthesis at the tip, i.e. it has a larger volume in the region which experiences the highest stresses. In the case of normal bone, both prostheses are more stable due to the support of the surrounding stiff bone. In the case of RA bone

there is less dense bone surrounding the prostheses, therefore the prostheses are more susceptible to the "twisting" deformation, which are more pronounced for the pegged prosthesis and result in higher cement stresses. The pegged prosthesis has more cement volume than the keeled prosthesis just under the flange, and this cement becomes highly stressed in the pegged case. Furthermore, if we take the case of RA bone within the glenoid, precise reaming of holes (see Fig. 5.2) is surgically difficult as the bone is so weak, i.e. as the holes are being reamed, additional weak bone will be destroyed. Therefore, not only is it easier to insert a keeled prosthesis in the RA case, it also means that most of this *degenerative* bone will be removed. More specifically the low strength material will be replaced with a higher strength material, that of the cement and keeled component. However, when *normal* bone is present within the glenoid, it is better to insert a pegged component as less of this "good" quality bone will be removed and it will provide support to the prosthesis.

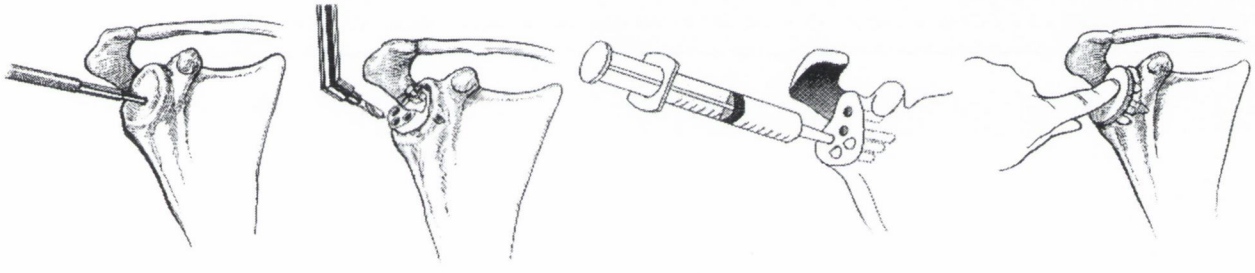

Figure 5.2 *Surgical precision required for a five-pegged glenoid component insertion, from Pearl and Lippitt (1994).*

2) *Hypothesis two states that: "an anterior offset keel provides better durability than a centre keel design due to its more central alignment in the glenoid bone".* This hypothesis was refined to a more testable hypothesis as follows: *"an anterior offset keel provides better durability than a centre keel"* because an anterior keel design may indeed provide greater durability than a centre keel design, but it may not necessarily be because of its central alignment in the glenoid bone.

Strong confirmation of the refined Hypothesis 2 was achieved and the explanations for this are discussed here. When testing the performance of an anterior offset keel compared to a centre keel design, it was anticipated that the offset keel prosthesis would indeed

perform better under an anterior loading due to the anterior placement of the keel. This would result in some absorption of the load before it is transferred to the cement layer. Also, it would be placed under less bending than a centre keel design. However, it was also expected that this prosthesis would perform badly under a posterior loading as the prosthesis would be put under higher bending than a centre keel design. For this reason I believe it was essential to apply both an anterior and posterior load for this test which was not as necessary for the other prostheses due to their symmetry about the superior-inferior plane. However, muscle loading data was not available for flexion and so joint loads alone were applied to test this hypothesis.

At 90 degrees of abduction, in the normal case, tensile stresses in the cement mantle around the offset design were lower compared to the centre keel design, see Fig. 4.29 (a). This was caused by a reduction in bending moment around the keel in the offset design because the point of load application is nearer to the keel. Since failure is associated with high tensile stresses, it can be concluded that the offset keeled design is superior to the centre keeled design in abduction. In RA bone both designs had similarly lowly stressed cement volumes, see Fig. 4.30 (a) showing that under subluxed RA loads, the offset-keel design performs well.

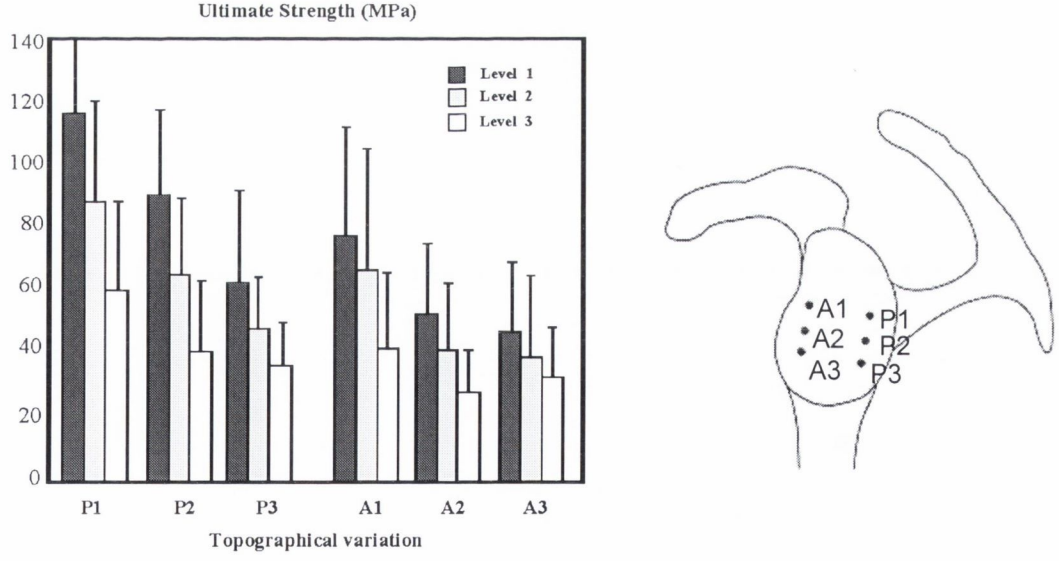

Figure 5.3 *Ultimate strength (MPa) for the anterior and posterior regions of the glenoid, adapted from Frich (1997). Level 1 = 1 to 2.5mm of penetration, level 2 = 2.5 to 3.5mm and level 3 = 3.5 to 4.5 mm of penetration.*

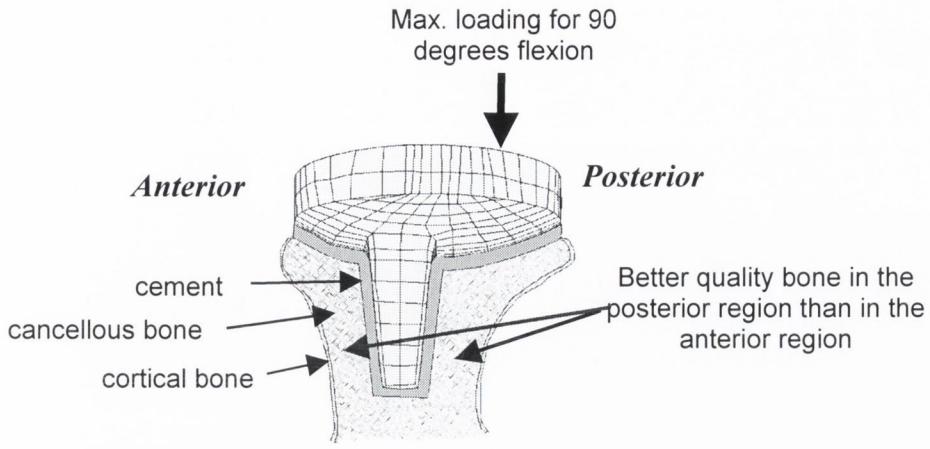

Figure 5.4 *Section through the glenoid bone for an offset keel design.*

Considering the alternative load positions, it was expected that the offset keeled design would perform worse than a centre keel design under flexion loads, *i.e.* when the load was positioned on the posterior side of the glenoid cup (Fig. 3.17). This was because, in such a situation, the offset keel would be subjected to a greater bending moment than a centre keel. However, this expectation did not prove to be true. In fact, for 90 degrees of flexion, for the normal and RA case, the offset keel design was predicted to perform better than a centre keeled design, see Fig. 4.29 (b) and 4.30 (b). Similar results for both designs were found for 60 degrees of flexion. To explain this result, we must look to the material property distribution in the glenoid cavity. From the experimental work of others published in the literature we know that, in general, there is higher strength cancellous bone in the posterior region of the glenoid compared to the anterior region (Anglin *et al.*, 1999, Frich *et al.*, 1997 and Mansat *et al.*, 1998) and this is also the case in the finite element model of this study. Additionally, our model had the highest density in the supero-posterior part of the glenoid, as found by Anglin *et al.*, (1999) Frich *et al.,* (1997) and Mansat *et al.* (1998). To illustrate and further confirm this fact, Fig. 5.3 shows a plot of the ultimate tensile strength against glenoid location where P1, P2, P3 are the posterior positions and A1, A2, and A3 are the anterior locations. Therefore, when comparing P1 (strength ~ 120MPa) to A1 (strength ~ 65MPa) at depth 1, P2 to A2 at depth 2 etc. we can clearly see that indeed there are higher strength values for glenoid cancellous bone in the posterior region compared to the anterior region. Therefore,

inserting an offset keeled prosthesis (with an anterior keel placement) results in removal of lower strength bone and replacement with stronger prosthetic materials, i.e. bone cement and polyethylene. In this way, the better quality higher stiffness bone is left in the posterior region and can provide better support under the cup leading to less bending of the cup and keel than expected in flexion. To further illustrate this point, consider Fig. 5.4 where an offset keel design is shown. Under 90 degrees of flexion (where the distance between the keel and the load vector is large), support of the posterior cancellous bone is required. This will also apply to the RA case, as it has been shown that simulation of RA glenoid bone involves uniform reduction in bone density across the glenoid (Dalstra *et al.,* 1996, Frich, 1994). The offset keel design does not remove the better quality bone in the posterior region. This basically adheres to the desirable fundamental characteristic of glenoid component design, as stated by Rockwood and Matsen (1998), i.e. that preservation of bone-stock is maintained, or in this case *good* bone-stock is maintained and *poorer* bone-stock is removed leading to lower cement stresses for both flexion and abduction loading.

3) *Hypothesis three states that: "secure fixation is difficult to achieve for glenoid components, additional attachment to the acromion reduces loosening rates".*

A concept that has arisen in TSA is that glenoid prostheses would derive greater durability if fixated to the acromion together with the glenoid (Gagey, 1990). As we know, the glenoid vault provides little bone for support of a glenoid prosthesis which undergoes large and complex loads. Furthermore, the glenoid bone may also be compromised by the effects of RA. This leads to the Hypothesis 3 stated above, however, confirmation of Hypothesis 3 was not achieved. Nonetheless refutation of the hypothesis can help us to generate new hypotheses and may lead to better designs eventually.

In general, the stress distributions produced in the cement mantle of the acromion fixated prosthesis are quite low (<3 MPa). However, very high peak stresses are also reached, in the order of 20 MPa, in some areas of the mantle. The relative displacement between the glenoid and the acromion, under the action of the muscle loads, shows that a small but significant amount of motion occurs (~1mm) in the absence of acromion

fixation. If an acromion-fixated prosthesis is used, then this motion is resisted by the prosthetic device and resulted in high stresses being produced in the acromion prosthesis arm (~50 MPa). Furthermore, a type of *load sharing* is to be expected between acromion and glenoid with this device. Consider that, at 90 degrees of abduction, a force of 152 N is applied by the deltoidus muscle, 116 N by the Trapezius muscle and 156 N by the acromion joint (total = 424 N). This implies that an additional load of 424 N together with an existing maximum glenohumeral load of 406 N can be shared which may explain these high stresses. Again, this is for the unloaded arm and higher loads are to be expected during normal daily tasks of lifting objects etc. Prof. Gagey also reported on some preliminary clinical trials with this type of prosthesis (Gagey and Mazas, 1990). However, initially there were problems reported with overstressing of the acromial arm resulting in failure of the device. This led to a reinforcement of the acromial arm by thickening the arm; yet this study suggests that even thickening the acromial arm may not reduce the stresses sufficiently and failure could still occur.

Another negative aspect of acromion fixation is that stresses produced in the entire scapula were altered compared to the natural case, i.e. that of no acromial fixation. Significant global bone stress changes were not found with any of the other glenoid component designs. It is a fundamental design requirement for prostheses to reproduce a natural distribution of stresses. However, for the acromion design the acromion bone stresses show different distributions and are higher than the natural case, i.e. with no prosthesis fixation (~16 MPa higher).

5.3 Comparison to previous work of 3D modeling in TSA

5.3.1 2D versus 3D models

This 3D analysis allows us to model a fully-three dimensional load. This loading is eccentric in nature, in both abduction and flexion, and causes bending and twisting of the keel generating higher cement stresses than are predicted in 2D analyses. Furthermore, the 3D analysis of the scapula gives a more realistic representation of the glenoid component/bone support resulting in a more distributed load on the glenoid cavity.

Therefore peak stresses found at the superior rim of the cement in 2D studies are not predicted here.

In this section a comparison of our results to previous work in 3D modelling of TSA is carried out. As an example of the limitation of 2D finite element analysis Lacroix and Prendergast (1997) used a 2D study to conclude that metal-backing of polyethylene glenoid components produce lower stresses in the cement mantle and an improved stress transfer to the surrounding cortical bone(see also Orr *et al.,* 1988). In a later 3D study it was shown that metal-backing resulted in very high stresses being produced at the cement/bone interface (Lacroix, 1997). In this study we reported very high interfacial stresses produced at the metal-backed prosthesis-cement interface, similar results were reported by Gupta *et al.,* (2000). Clinically, all-polyethylene designs are more traditionally in use as metal-backing of glenoid components is associated with early loosening. Orr *et al.* (1997) found that a two-pegged prosthesis produced a more physiological stress distribution in the surrounding bone than a keeled prosthesis. By introducing a cement layer into the FEM, I obtained more relevant results as it is recommended to insert this prosthesis with a layer of cement (Pearl and Lippitt, 1994). (The cement layer was not included in Orr's study). I found that generally low stresses were found in the surrounding bone for a pegged design, but also for a keeled design, in *normal* bone. These were not of high enough magnitude to cause microfractures in the trabeculae which could lead to loosening of the prosthesis. When analyzing the surrounding cement stresses and comparing both designs probabilities of survival, I could make a clear distinction between the two designs which would not have been possible with a 2D model, see section 5.2.1. Furthermore, stress results were sufficiently quantitative in 3D to allow comparison with failure data. values of 5 – 7 MPa were reached for both designs for the unloaded arm.

This thesis is the first report of an analysis of comparative TSA performances in a rheumatoid arthritic and a normal scapula.

5.3.2 Limitations of the FE model

Finite element analysis is a well established technique for ascertaining stresses in bone prosthesis structures, Prendergast (1997). Element size, element aspect ratio, and mesh

distortion influence the accuracy of the results. However, no model is valid to an infinite degree, and the adequacy of a model can only be judged based on the objectives of the analysis. In this study, a large number of elements were used in the glenoid to accurately predict the stress in the cement mantle. Elements outside the glenoid are, however, slightly distorted in some cases due to the intrinsic geometry of the scapula. Brick and wedge elements were used for model generation, these elements were also used in regions where the scapula was thin, scapula fossas, it was important to maintain a low aspect ratio in these regions for accurate results. To determine the effect of this mesh refinement was carried out where the aspect ratios were reduced even further, results predict that similar stress values to that of the less refined mesh are reached.

A finite element model, such as the one presented here, is limited in its predictive value insofar as we can analyse one bone only. However, the dimensions of the scapula analysed here fall well within those of typical scapulae measured by Mallon *et al.* (1992); hence the results are expected to be representative of scapulae generally. qCT information was used to derive density and Young's modulus. However, beam hardening and partial volume effects are among errors encountered (Crawley, 1990). The average Young's modulus of the glenoid in this study was 330 MPa. In experimental studies, Anglin *et al.* (1999), Frich *et al.* (1997), and Mansat *et al.* (1998) found Young's modulus in the radial direction of 171 MPa , 410 MPa, and 372 MPa respectively. Thus, the material properties of our scapula are within the normal range. Moreover, we also find that the density was highest in supero-posterior part of the glenoid, as found by Anglin *et al.* (1999), Frich *et al.* (1997), and Mansat *et al.* (1998). The present work is only concerned with an analysis of glenoid replacement in the direct post-operative situation; no account was taken of soft tissue formation on interfaces.

Since there is such a large variability in the geometric pathology of the rheumatoid glenohumeral joint, and in the rate of progression of the disease (Kelly, 1994), simulation of a shape changed RA glenohumeral joint was beyond the scope of this study. A general approach to modelling the destructive effects of RA was carried out based on the experimental work of Frich (1993) (to date Frich's study is the only study which has data for RA glenoid bone material property). This consisted of simulating a Larsen Grade IV type destruction with a subluxed joint load. Ideally a large array of scapulae with varying

levels of destruction could be tested for material properties or CT scanned and FE models generated. Again, this is beyond the scope of this study.

Regarding our confirmation of results, due to the complex shape of the scapula strain gauging has proved difficult in the past (Lacroix, 1997, Gupta, 2002). Furthermore, strain gauging only gives point measurements and a qualitative stress distribution can only be achieved if many strain gauges are applied, which is difficult. Strain gauging is appropriate for a femur, for example, as its shape is less complicated. Also, we know how it deforms and moves, i.e. we know that it bends about its long axis and where tension and compression exist. Similarity of strain data obtained from experimental and FE models is necessary, therefore, to confirm that valid results are being realised. Conversely, the photoelastic technique has a full-field capability which allows observation and measurement of strain directions and magnitudes for complex geometries, under varying complex loading modes, regardless of material homogeneity. Point measurements were also calculated and compared to the same regions in the FE mesh. Calculation of the shear stress values corresponding to regions of high stress in the FE model, we find that shear stresses in the same order of magnitude were observed. For example, for N=4, a maximum shear stress of 30 MPa was reached experimentally at the superior border. Similarly, maximum shear stresses of 25 MPa and greater were seen at the superior border of the finite element model. Errors associated with the photoelastic technique include Poisson's coefficient mismatch, incorrect light incidence, uneven coating thickness and, as reported by Cristofolini *et al.,* (1994), the reinforcing effect of the photoelastic coating. However, each of these errors, except for uneven coating thickness and incorrect light incidence, is eliminated in this analysis by applying a coating to our FE model and comparing the results as discussed in Chapter three. The difficulty in creating a homogenous coating thickness experimentally was experienced. However, with much practice and by measuring each coating with a micrometer prior to adhesion, associated errors could be minimised. Furthermore, the scapulae used were different in size and material property distribution to the one modelled in the FE analysis. However, we tried to eliminate this problem by using a set of five scapulae. Finally, it should be noted that the dimensions and material properties of the scapula used for our finite element model fall well within those of typical scapulae measured by Mallon

(1992) allowing our results to be compared. In order to reduce the effects of incorrect light incidence it was important to that the light fell perpendicular to the surface point of interest at all times.

It is important in biomechanical analyses to keep the real research issues at the forefront of your mind. As sometimes these real issues are clouded by the engineering tools used and their implementation. This is why hypothesis based research is constructive as it is totally focused at the outset. The quality of an FE solution is based on the accuracy of material property, geometric (element types, refinement etc.), boundary conditions and confirmation of results. The context in which we use these tools is also important. What I mean by this is, for example, for the anterior offset keel design it was important to use the eccentric abduction and flexion loads in order to determine the effects of prosthesis performance under the rocking horse effect. For analysis of the acromion fixation device it was important to include the effects of RA and a subluxed joint load as this design is recommended to prevent loosening in the presence of a deficient rotator cuff seen in RA patients. Søjbjerg *et al.,* (1999) states that from a clinical review of 500 shoulder prostheses that proximal migration of the humeral prosthesis attributable to rotator cuff deficiency with eccentric glenoid loading and progressive glenoid loosening was experienced in patients with RA. This was achieved by using a variable joint and muscle data set for each angle of abduction and by creating a subluxed load and applying a Larsen Grade type IV destruction. Furthermore, some researchers may focus on one particular modelling aspect, such as reproducing a sophisticated RA scapula mesh but this alone cannot provide a *strong* research tool as it is equally important to include appropriate muscle and joint loads, for example. It is also of utmost importance to provide adequate methods for analysis of results and to obtain results which are of clinical importance, otherwise a highly complicated model is of no use. This analysis has included all these essential aspects for a thorough analysis which I think has provided valuable information regarding glenoid component selection in TSA.

What are the significance of the results and to what extent will they effect clinical practice in terms of everyday use? For many FE biomechanical analyses it may be said that the analysis results will have no real relevance because they will be ignored by clinicians and industrial designers. However, in this case I would argue that this study has

created relevant hypotheses which have been confirmed (or refuted) using strong biomechanical tests. As a result the following clinically significant deductions are made:

- Clearly, large variability exists at the shoulder joint pre-operation compared to the hip. I suggest that, because of this variability, a selection of designs may be required which can be recommended for use based on the pathology of the joint.
- Biomechanically, glenoid material property distribution plays an essential role in glenoid component design and clinically, prosthetic design selection should therefore be based on this material property distribution.
- Since such a small quantity of bone exists for implantation, it is essential to design the fixation so that *good* quality bone is used to its best advantage.
- Removal of *bad* quality bone and replacement with better quality material, that of cement and polyethylene, results in a decrease of cement stresses and essentially a lower probability of failure for the implant. Remaining *good* bone is left to provide good support to the prosthesis.
- Attachment of a glenoid prosthetic component to the acromion may appear to be beneficial, but it does not reduce peak cement stress in the fixation and it may introduce new problems as in RA where fracture of the acromion could result.

Chapter 6

Conclusions

6.1 Conclusions

The conclusions reached are as follows:

(i) Hypothesis-based testing of new designs can help remove the "prosthetic surplus" which exists in total shoulder arthroplasty.

(ii) Pre-clinical tests for evaluation of glenoid component durability must include the varying patient pathologies which are encountered clinically. As a result, at the clinical stage selection of a specific design can be based on the pathological *state* of the joint.

(iii)
- A strong confirmation of Hypothesis 1 was achieved, a pegged prosthesis provides lower stresses and therefore greater durability to prevent glenoid loosening whereas a keeled prosthesis is recommended when there is a tight joint compartment and compromised glenoid bone stock.
- Cement stresses, previously shown to be of a critical magnitude (Lacroix, 1997), were lower for a keeled prosthesis in RA bone and lower for a pegged prosthesis in *normal* bone.
- In *normal* bone, both prostheses are more stable due to the support of the surrounding stiff bone but in RA bone there is less dense bone surrounding the prostheses, the prostheses are more susceptible to a "twisting" deformation; this is more pronounced for the pegged prosthesis and result in higher cement stresses. The keeled prosthesis has a larger volume of cement at the tip, where the highest stresses occur. The pegged prosthesis has more cement just under the flange, and this cement becomes highly stressed in the pegged case due to twisting.

(iv)
- Strong confirmation of Hypothesis 2 was achieved; by virtue of the generally lower cement stresses an anterior offset keel provides better durability than a centre keel design.

- An anterior offset keel provides better durability than a centre keel design under a variable joint load due to the material property distribution in the glenoid vault.
- Removal of *bad* quality bone and replacement with better quality material, that of cement and polyethylene, results in a decrease of cement stresses and essentially a lower probability of failure for the implant. Remaining *good* bone is left to provide good support to the prosthesis.

(iv)
- Confirmation of Hypothesis 3 was not achieved; however refutation of the hypothesis can help us to improve on these observations by generating and testing further hypotheses as a result.
- Stresses produced in the scapula bone for the acromion design were altered relative to the natural case; this did not occur for the non-acromion fixated prostheses. This does not fulfil the fundamental design requirement that prostheses should reproduce a natural stress distribution in the bone as well as possible.
- Due to the load sharing which occurs with an acromion fixation device, overstressing of the acromion arm and critical high stresses are reached in the cement mantle which may result in failure.
- Attachment of a glenoid prosthetic component to the acromion may be detrimental in cases of RA where fracture of the acromion could result.

(vi) Glenoid material property distribution plays an essential role in glenoid component design.

(vii) When an engineer is considering a new design put to her by an orthopaedic surgeon, she should carefully construct a hypothesis which can be rigorously tested using biomechanical methods. This is the way forward for orthopaedic implant innovation.

(viii) This study has created relevant hypotheses which have been tested using strong biomechanical tests, confirmation or refutation has led to clinically significant recommendations for implantation for further future work.

6.2 Future Work

This thesis predicts that the increase of relatively ineffective prosthetic components can be best resisted by coupling hypothesis based research and strong biomechanical preclinical testing. The model used in this study has confirmed and refuted hypotheses regarding glenoid component design. These results can therefore, represent a platform for further research on other aspects of shoulder replacement analysis. Some sophistication could be added to the model, this includes:

- Elastic and isotropic material properties were modelled in this study, viscoelasticity and anisotropy could be included.
- Debonding of the implant in a similar manner as has been done for hip replacement could give a more accurate method to studying component loosening.
- Cemented joint replacements are liable to fail mechanically due to fatigue damage accumulation in the cement mantle. This is associated with high tensile stresses (Murphy and Prendergast, 2000) which are presented in this study. Inclusion of damage accumulation and creep of the bone cement in the model can give more accurate details of the failure mechanisms involved for TSA. Furthermore, further potential failure mechanisms could be analysed.
- More detailed modeling of the cement mantle could be included, in reality it is not uniformly distributed around the prosthesis and a bulk of cement can occur at the tip of the prosthesis. Further information relating to the extent of bonding between the prosthesis and the surrounding cement mantle could lead to a more accurate model.
- Soft fibrous tissue would be expected to develop over time at the cement-bone interface and may compromise the fixation of the prosthesis. Long term prosthesis potential durability should take this into account.
- Simulation of the long-term effects of the remodeling process using finite element codes.
- Most preclinical analyses of glenoid component performance, to date, are carried out in normal or healthy bone, yet in reality the majority are placed in

quite unhealthy RA joints. This study used a general approach to modelling the destructive effects of RA based on the experimental work of Frich (1993). In the future, a large array of scapulae with varying levels of pathology could be tested for improved material property data generation. Furthermore, CT scanning of these scapulae could be used to generate FE models. The ideal solution would be for the generation of patient specific models whereby a series of implants could be tested to suit the particular patients needs.

- Analysis of prosthesis performance under a larger array of loading patterns, for example, dynamic loads for varying patient activities post-operation.
- Loading of the scapula was based on the three-dimensional biomechanical study of van der Helm (1994). Equilibrium between the forces was not perfect because of the geometric differences between van der Helm's scapula and the one used in this study. Restraints were applied in this model to avoid rigid body motion. This resulted in a slightly high reaction force which could be reduced by tuning the force inputs. However, this approach results in altering the loading data file which would be unrealistic. Ideally, the loading data file should be generated for the individual scapulae.
- Further analysis of the photoelastic technique to produce a large array of quantitative results for comparison to our FE model.

In general, increased surgeon and engineer collaboration is necessary to bring TSA design up to date. This will allow for significant hypothesis generation by surgeons for which can then be tested preclinically using appropriate biomechanical tests.

In the near future, glenoid component loosening will continue to be an ongoing problem in TSA, however, hypothesis based testing can help to improve designs and surgical understanding.

References

American Academy of Orthopaedic Surgeons. *Joint motion: method of measuring and recording*. Churchill Livingstone, London, British Orthopaedic, 1965.

American Academy of Orthopaedic Surgeons. *Arthroplasty and total joint replacement procedures 1990 to 1999*. www. Aaos.org/wordhtml/research/arthrop.htm 2001.

American Society for Testing and Materials. *F2028-00: Standard test method for the dynamic evaluation of glenoid loosening or dissociation*. West Conshohocken, PA, 2001.

Amstutz HC, Sew Hoy AL, Clarke IC. UCLA anatomic total shoulder arthroplasty. *Clin Orthop* 155: 7-20, 1981.

Amstutz HC, Thomas BJ, Kabo JM, Jinnah RH, Dorey FJ. The Dana total shoulder arthoplasty. *J Bone Joint Surg* 70A: 1174-1182, 1988.

Anglin C, Tolhurst P, Wyss UP, Pichora DR. Glenoid cancellous bone strength. *J Biomechanics* 32:1091-1097, 1999.

Anglin C, Wyss UP, Nyffeler RW, Gerber C. Loosening performance of cemented glenoid proethsis design pairs. *Clinical Biomechanics* 16: 144-150, 2001.

Apoil A, Koechlin Ph, Augereau B, Hongier J. Total shoulder prosthesis with acromio-coracoidian anchorage. *Acta Orthop Belg* 49 (5):571-578, 1983.

Baréa C, Hobatho MC, Darmana R, Mansat M. 3D finite element study of glenoid implants in total shoulder arthroplasty. In: *Computer Methods in Biomechanics &*

Biomedical Engineering-2 Eds: Middleton J, Jones ML and Pande GN: Gordon & Breach, Amsterdam, 471-478, 1998.

Barrett WP, Franklin JL, Jackins SE, Wyss CR, Matsen FA. Total shoulder arthroplasty. *J Bone Joint Surg* 69A:865-872, 1987.

Bell RH, Noble JS. The management of significant glenoid deficiency in total shoulder arthroplasty: Review article. *J Shoulder Elbow Surg* 9 : 248-56, 2000.

Boyd AD, Thomas WH, Scott RD, Sledge CB, Thornhill TS. TSA versus HA: Indications for glenoid resurfacing. *J Arthroplasty* Dec; 5(4):329-337, 1990.

Brems J. The glenoid component in total shoulder arthroplasty. *J Shoulder Elbow Surg* 2:47-4, 1993.

Cattaneo PM, Dalstra M, Frich LH. The development of a 3D FE model of the glenoid. *Proc 9th Conference of the EORS,* Brussels, 1999.

Clarke IC, Gruen TAW, Sew Hoy A, Hirschowitz D, Maki S, Amstutz HC. Problems in the gleno-humeral relationship- real or imagined? *Eng Med* 8 (3), 1979.

Clayton ML, Ferlic DC, Jeffers PD. Prosthetic arthroplasties of the shoulder. *Clin Orthop Rel Res* 164:184-191, 1982.

Cofield RH. Uncemented total shoulder arthroplasty: A review. *Clin Orthop Rel Res* 307; 86-93, 1994.

Coventry MB. Lessons learned in 30 years of total hip arthroplasty. *Clin Orthop* 274: 22-9, 1992.

Crawley EO, In vivo tissue characterisation using quantitative computed tomography: a review. *J Med Eng Technol* 14: 233-242, 1990.

Cristofolini L, Cappello A, Toni A. Experimental errors in the application of photoelastic coatings on human femurs with uncemented hip stems. *Strain* 95-103, 1994.

Dalstra M, Frich LH, Sneppen O. The loss of load bearing capability in rheumatoid glenoids. *Proc 10th Conference of the ESB,* p. 178, Leuven, 1996.

Davies JP, Burke DW, O'Connor DO, Harris WH. Comparison of the fatigue characteristics of centrifuged and uncentrifuged Simplex-P bone cement. *J Orthop Res* 5: 366-371, 1987.

Davis PR. Some significant aspects of normal upper limb functions. *Eng Med* 1-5, 1977.

Driessnack RP, Ferlic DC, Wiedel JD. Dissociation of the glenoid component in the Macnab/English TSA. *J Arthroplasty* Apr; 13(3):311-9, 1990.

Emery R, Banks M. Shoulder replacement: Historaical perspective. In: *Shoulder Arthroplasty* Eds: Walch G and Boileau P: Springer, Berlin, 3-9, 1998.

Fassberg RI, Downey JA, Keyak JH, Skinner HB. Structural analysis of a new type of glenoid component by three-dimensional finite element analysis. *Orthop Trans* 16: 515-516, 1992.

Feldman AY, Bunker TD. Rotational dissociation of glenoid components in a total shoulder prosthesis: An indication that sagittal torque forces may be important in glenoid component design. *J Shoulder Elbow Surg* 8(3): 279-80, 1999.

Figgie MP, Inglis AE, Figgie HE III, Sobel M, Burstein AH, Kraay MJ. Custom total shoulder arthroplasty in inflammatory arthritis: Preliminary results. *J Arthroplasty* 7(1): 1-6, 1992.

Franklin JL, Barret WF, Jackins SE, Matsen FA III. Glenoid loosening in total shoulder arthroplasty. *J Arthroplasty* 3:39-46, 1988.

Frich LH. *Strength and structure of glenoidal bone.* Doctoral thesis, Århus, Denmark: Arhus University, 1994.

Frich LH, Odgaard A. Bone architecture of the normal and RA glenoid. *Trans ORS* Feb 13-16 pp 683, 1995.

Frich LH, Jensen NC, Odgaard A, Pedersen CM, Søjbjerg JO, Dalstra M. Bone strength and material properties of the glenoid. *J Shoulder Elbow Surg* 6:97-104, 1997.

Friedman RJ, Laberge M, Dooley RC, O'Hara AL. Finite element modelling of the glenoid component: effect of design parameters on stress distribution. *J Shoulder Elbow Surg* 1:261-270, 1992.

Gagey O, Mazas F. A new total shoulder prosthesis with acromial fixation. In: *Surgery of the Shoulder* Eds: Post M, Morrey BF and Hawkins RJ: Mosby Yearbook, St Loius: 282-284, 1990.

Giori NJ, Beaupre GS, Carter DR. The influence of fixation peg design on the shear stability of prosthetic implants. *J Orthopaed Res* 8:892-898, 1990.

Gupta S. *Stress analysis of the scapula: design considerations of glenoid prostheses.* Doctoral thesis, Delft, The Netherlands: Delft University of Technology, 2002.

Gupta S, van der Helm FCT, van Keulen A. Stress analysis of cemented and uncemented glenoid prostheses. *Proc 12th Conference of the ESB,* p. 161, Dublin, 2000.

Havig MT, Kumar A, Carpenter W, Seiler JG III. Assessment of radiolucent lines about the glenoid. *J Bone Joint Surg* 79A:428-432, 1997.

Herberts P and Malchau H. Long-term registration has improved the quality of hip replacement. *Acta Orthop Scand* 71: 111-121, 2000.

Hospital in patient enquiry (HIPE). *Shoulder arthroplasty HIPE data.* The Economic and Social Research Institute (ESRI), Dublin, 1999.

Huiskes R. Failed innovation in total hip replacement: diagnosis and proposals for a cure. *Acta Orthop Scand* 64: 699-716, 1993.

Huiskes R, Chao EYS. A survey of finite element analysis in orthropedic biomechanics: the first decade. *J Biomechanics* 16: 385-409, 1983.

Hvid I, Bentzen SM, Linde F, Mosekilde L, Pongsoitpetch B. X-ray quantitative computed tomography: the relationships to physical properties of proximal tibial trabecular bone specimens. *J Biomechanics* 22(8):837-844, 1989.

Iannotti JP, Williams GR. Total Shoulder Arthroplasty: Factors influencing prosthetic design. *Ortho Clin North Am* 29:377-391, 1998.

Iannotti JP, Gabriel JP, Schneck SL, Evans BG, Misra S. The normal glenohumeral relationships- and anatomical study of 140 shoulders. *J Bone Joint Surg* 74A:491-500, 1992.

Ibarra C, Dines DM, McLaughlin JA. Glenoid replacement in total shoulder arthroplasty. *Orthop Clin North Am* 29:403-413, 1998.

Johnson KL. *Contact Mechanics.* Cambridge University Press, Cambridge, p. 114, 1985.

Karduna AR, Williams GR, Iannotti JP, Williams JL. Total shoulder arthroplasty biomechanics: a study of the forces and strains at the glenoid component. *J Biomech Eng* 120: 92-99, 1998.

Kaufler T, Amis AA, Emery RJH. Analysis of glenoid component fixation designs in the rheumatoid scapula. Abstracts of the 11th Conference of the ESB, Toulouse, *J Biomechanics* 31, 6, 1998.

Kelly IG. Unconstrained shoulder arthroplasty in rheumatoid arthritis. *Clin Orthop Rel Res* 307:94-102, 1994.

Kelly IG, Foster RS, Fisher WD. Neer total shoulder replacement in rheumatoid arthritis. *J Bone Joint Surg* 69B:723-726, 1987.

Kirk PG, Sorger J. Failure of an implant after total shoulder arthroplasty. *J Bone Joint Surg* 79A:597-598, 1997.

Krause W, Mathis RS, Grimes LW. Fatigure properties of acrylic bone cement: S-N, P--N and P-S-N data. *J Biomed Mater Res: Applied Biomaterials* 22(A3): 221-244, 1988.

Lacroix D. *Computer simulation for pre-clinical evaluation of glenoid components for shoulder replacements*. M.Sc. Thesis: University of Dublin, 1997.

Lacroix D, Murphy LA, Prendergast PJ. Three-dimensional finite element analysis of glenoid replacement prostheses: a comparison of keeled and pegged anchorage systems. *J Biomech Eng* 211: 467-74, 2000.

Lacroix D, Prendergast PJ. Stress analysis of glenoid component designs for shoulder arthroplasty. *Proc Instn Mech Engrs* Part H, 211: 467-474, 1997.

Lakatos I, Musgrave A. *Criticism and the growth of knowledge : proceedings of the International Colloquium in the Philosophy of Science, London.* Chicago UP, 1965.

Laurence M. Replacement arthroplasty of the rotator cuff deficient shoulder. *J Bone Joint Surg* 73B: 916-919, 1991.

Lennon AB, McCormack BAO, Prendergast PJ. Implant surface finish affects cement damage accumulation in femoral hip replacement. In submission, 2002.

Lugli T. Artificial Shoulder Joint by Péan (1893). *Clin Orthop Rel Res* 133:215-218, 1978.

Macnab I. Total shoulder replacement- A bipolar glenohumeral prosthesis. *J Bone Joint Surg* 59B: 257, 1977.

Macnab I, English E. Development of a glenohumeral arthroplasty for the severely destroyed shoulder joint. *J Bone Joint Surg* 59B: 137, 1976.

Mallon WJ, Brown HR, Volger III JB, Martinez S. Radiographic and geometric anatomy of the scapula. *Clin Orthop Rel Res* 277:142-154, 1992.

Mansat P, Baréa C, Hobatho MC, Darmana R, Mansat M. Anatomic variation of the mechanical properties of the glenoid. *J Shoulder Elbow Surg* 7: 109-115, 1998.

Mazas F, de la Caffiniere JY. Une nouvelle prosthèse totale d'épaule. *Rev Chir Orthop* 63: 113-115, 1977.

Mazas F, de la Caffiniere JY. Total shoulder replacement by an unconstrained prosthesis. Report of 38 cases. *Rev Chir Orthop* 68: 161-173, 1982.

Mazas F, Gagey O. Prosthèse totale d' épaule.. *Rev Prat* 40: 1021-1025, 1990.

McCoy SR, Warren RF, Bade HA III, Ranawat CS, Inglis AE. Total shoulder arthroplasty in rheumatoid arthritis. *J Arthroplasty* 4: 105-13, 1989.

McCullagh PJ. Biomechanics and design of shoulder arthroplasty. *Proc Instn Mech Engrs* Part H, 209:207-213, 1995.

McElwain JP, English E. The early results of porous-coated total shoulder arthroplasty. *Clin Orthop Rel Res* 218: 217-224, 1987.

Measurements Group. *Technical notes*. Measurements Group Inc, 1992.

Medical Multimedia Group. *A patient's guide to artificial shoulder replacement.* www.medicalmultimediagroup.com 1999.

Miller BF, Keane CB. *Encyclopedia and Dictionary of Medicine, Nursing and Allied Health*. Saunders, Philadelphia-London, 1997.

Mullaji AB, Beddow FH, Lamb GHR. CT measurement of glenoid erosion in arthritis. *J Bone Joint Surg* 76B:384-8, 1994.

Murphy BP, Prendergast PJ. On the magnitude and varability of the fatigue strength of acrylic bone cement. *Int J Fatigue* 22: 855-864, 2000.

Neer CS II. *Shoulder reconstruction.* Saunders, Philadelphia, 143-271, 1990.

Neer II CS, Morrison DS. Glenoid bone grafting in total shoulder arthroplasty. *J Bone Joint Surg* 70A:1154-1162, 1988.

Norweigan register. *National Register for Arthroplasty.* www.haukeland.no/nrl/RAPPORT01.pdf .

Orr JF, Shelton JC. Photoelastic stress analysis. In: *Optical Measurement Methods in Biomechanics:* Chapman & Hall, London, 1-16, 1997.

Orr TE, Carter DR, Schurman DJ. Stress analysis of glenoid component designs. *Clin Orthop Rel Res* 212:217-224, 1988.

Pearl ML, Lippitt SB. Shoulder Arthroplasty with a modular prosthesis. *Techniques in Orthopaedics* 8(3):151-162, 1994.

Pegington J. Anatomy and Biomechanics of the Shoulder. In: *Surgical disorders of the shoulder joint,* Eds: Watson M: Churchill Livingston Press, 3-27, 1991.

Petersson CJ. Painful shoulders in patients with rheumatoid arthritis. *Scand J Rheumatol* 15: 275-9, 1986.

Poppen NK, Walker PS. Forces at the glenohumeral joint in abduction. *Clin Orthop Rel Res* 135:165-170, 1978.

Popper KR. The logic of scientific discovery. Hutchinson, London, 1972.

Prendergast PJ. Finite element models in tissue mechanics and orthopaedic implant design. *Clin Biomech* 12(6): 343-366, 1997.

Prendergast PJ. An analysis of theories in biomechanics. *Engng Trans* 49: 117-133, 2001.

Prendergast PJ, Maher SA. Issues in pre-clinical testing of implants. *J Mater Process Tech* 118 (1-3): 337-342, 2001.

Redfern TR, Wallace WA. History of shoulder replacement surgery. In: *Joint Replacement in the Shoulder and Elbow* Eds: Wallace WA: Butterworth and Heinmann, Oxford: 6-16, 1998.

Rice JC, Cowin SC, Bowman JA. On the dependence of the elasticity and strength of cancellous bone on apparent density. *J Biomechanics* 21(2): 155-168, 1988.

Rockwood CA, Matsen FA. *Global total shoulder arthroplasty system.* DePuy design rationale, 1992.

Rockwood CA, Matsen FA III. *The shoulder.* Philadelphia, Saunders, Vol 2, 1998.

Schaffler MB, Burr DB. Stiffness of compact bone: effects of porosity and density. *J Biomechanics* 21(1): 13-16, 1988.

Shier D, Butler J, Lewis R. *Hole's Human anatomy and physiology.* WCBrown/McGraw-Hill, London, 1999.

Skirving AP. TSA-current problems and possible solutions. *J Orthop Sci* 4:42-53, 1999.

Sneppen O, Freunsgaard S, Johannsen HV, Olsen BS, Søjbjerg JO, Andersen NH. Total shoulder replacement in rheumatoid arthritis: Proximal migration and loosening. *J Shoulder Elbow Surg 5* 47-52, 1996.

Søjbjerg JO, Frich LH, Johannsen HV, Sneppen O. Late results of total shoulder replacement in patients with rheumatoid arthritis. *Clin Orthop Rel Res* 366: 39-45, 1999.

Sperling JW, Cofield RH, Rowland CM. Neer hemiarthroplasty and Neer total shoulder arthroplasty in patients 50 years old or less. *J Bone Joint Surg 80A* 464-473, 1998.

Stewart MPM, Kelly IG. Total Shoulder Replacement in Rheumatoid disease. *J Bone Joint Surg* 79B:68-72, 1997.

Stone KD, Grabowski JJ, Cofield RH, Morrey BF, An KN. Stress analysis of glenoid components in total shoulder arthroplasty. *J Shoulder Elbow Surg* 8(2): 151-8, 1999.

Thomas BJ, Amstuts HC, Cracchiolo A. Shoulder arthroplasty for RA. *Clin Orthop Rel Res* 265:125-128, 1991.

Torchia ME, Cofield RH, Settergren CR. Total shoulder arthroplasty with the Neer prosthesis: Long-term results. *J Shoulder Elbow Surg* 6:495-505, 1997.

Van der Helm FCT. *The shoulder mechanism, a dynamic approach.* Doctoral Thesis: Delft University of Technology, The Netherlands, 1991.

van der Helm FCT. A finite element musculoskeletal model of the shoulder mechanism. *J Biomechanics* 27(5): 551-569, 1994.

van der Helm FCT, Pronk GM. Three-dimensional recording and description of motions of the shoulder mechanism. *J Biomech Eng* 117: 27-40, 1995.

Veeger HEJ, van der Helm FCT, van der Woude LHV, Pronk GM, Rozendal RH. Inertia and muscle contraction parameters for musculoskeletal modelling of the shoulder mechanism. *J Biomechanics* 24: 615-629, 1991.

Waldman BJ, Figgie MP. Indications, techniques and results of total shoulder arthroplasty in rheumatoid arthritis. *Ortho Clin North Am* 19: 435-44, 1998.

Williams PL, Ed. *Gray's Anatomy.* 38th ed., 615-634, 1995 .

Wirth MA, Rockwood CA. Complications of shoulder arthroplasty. *Clin Orthop Rel Res* 307:47-69, 1994.

Wirth MA, Rockwood CA. Current concepts review: Complications in total shoulder replacement arthroplasty. *J Bone Joint Surg* 78A:601-616, 1996.

Wolff R, Kolbel R. The history of shoulder joint replacement. In: *Shoulder Replacement* Eds: Springer-Verlag, New York, 3-13, 1987.

APPENDIX A

Basic principals of Finite element analysis can be explained as follows, (Prendergast, 1996): For one particular element in the model, {P} represents the load acting at a point within the element and {δ} be the corresponding displacement:

$$\{P\} = \begin{Bmatrix} P_x \\ P_y \\ P_z \end{Bmatrix} \quad \text{(A.1)} \qquad \{\delta\} = \begin{Bmatrix} \delta_x \\ \delta_y \\ \delta_z \end{Bmatrix} \quad \text{(A.2)}$$

For the work done:

$$WD = \{\delta\}^t\{P\} \qquad \text{(A.3)}$$

The strain energy is given by product of stress and strain integrated over the volume of the element:

$$U = \left(\int_v \{\varepsilon\}' \{\sigma\} d(vol) \right) \qquad \text{(A.4)}$$

These equations are continuous throughout the element. The displacement at any point within the element {δ} is related to the displacement at the nodes $\{\delta_e\}$ using the shape functions, [N].

$$\{\delta\} = [N]\{\delta_e\} \qquad \text{(A.5)}$$

Strain at any point in the element, {ε}, is related to displacement at any point in the element using compatibility relationships from elasticity with matrix [L]:

$$\{\varepsilon\} = [L]\{\delta\} \qquad \text{(A.6)}$$

Substituting Equation A.5 into A.6 gives:

$$\begin{aligned} \{\varepsilon\} &= [L][N]\{\delta_e\} \\ &= [B]\{\delta_e\} \end{aligned} \qquad \text{(A.7)}$$

This defines the B-matrix, which relates strain at a point in, or on the boundary of an element to the matrix of nodal displacements. Strain is related to stress using a D-matrix, which is determined from the stress/strain constitutive relationship:

$$\{\sigma\} = [D]\{\varepsilon\} \qquad \text{(A.8)}$$

Within the element, for minimization of potential energy (ϕ), is equal to the internal strain energy (U) less the work done by the external loads:

$$\phi = U - WD \qquad \text{(A.9)}$$

In terms of nodal displacements $\{\delta_e\}$, the minimum potential energy condition can be found by differentiating Eqn. A.9 with respect to the nodal displacements and equating to zero:

$$\frac{\partial \phi}{\partial \{\delta_e\}} = 0 \qquad \text{(A.10)}$$

With Eqn. A.3 gives: $\partial U_e - \{\partial \delta_e\}^t \{P_e\} = 0 \qquad$ (A.11)

Where U_e is the strain energy for a given element. By differentiating Eqn. A.4 we get:

$$\begin{aligned} \partial U_e &= \int_V \{\partial \varepsilon_e\}^t \{\sigma\} d(vol) \\ &= \{\partial \delta_e\}^t \int_V [B]^t [D][B] d(vol) \{\delta_e\} \end{aligned} \qquad \text{(2.12)}$$

substituting ∂U_e from Eqn. A.11 into equation A.12:

$$\{P_e\} = \int_V [B]^t [D][B] d(vol).\{\delta_e\} \qquad \text{(A.13)}$$

Hence the stiffness matrix relating nodal loads to nodal displacements is given by:

$$[K_e] = \int_V [B]^t [D][B] d(vol) \qquad \text{(A.14)}$$

The stiffness matrices are then assembled into one entire stiffness matrix for the whole structure.

APPENDIX B

Table B1 *Muscle forces and directions at 30 degrees of abduction.*

Muscle	*fsx*	*fsy*	*fsz*
trapezius, scap part	-0.5794	-0.19476	-0.00166
	-0.91772	-1.97534	0.08367
	-8.12105	-7.55283	0.9587
	-29.23786	-2.30469	-3.51569
	-24.38868	6.145	-2.21449
	-23.26555	6.71617	1.74209
trapezius, clav part	0	0	0
	0	0	0
	0	0	0
	0	0	0
	0	0	0
	0	0	0
levator scapulae	-1.17627	1.86786	-3.0878
	-1.51214	2.32898	-2.57228
	-1.79330	2.69114	-1.91935
pectoralis minor	0	0	0
	0	0	0
	0	0	0
	0	0	0
rhomboideus	0	0	0
	-1.04650	1.14652	-0.89477
	-8.74380	9.09673	-7.00416
serratus anterior	12.65180	-8.8272	-10.75563
	12.44637	-2.31292	-12.43709
	10.83172	1.65558	-11.61917
	6.90269	2.57453	-8.21749
	2.80236	0.63144	-4.18422
	1.23310	-1.78869	-3.3398
deltoidus, scap part	0.90854	-1.45898	-0.37126
	0.33560	-0.55352	-0.10997
	11.27830	-29.37488	-3.73074
	11.69521	-29.30566	-0.75366
	20.53411	-35.59457	1.78923
	19.69160	-34.71724	4.0815
deltoidus, clav part	0	0	0
	0	0	0
	0	0	0
	0	0	0
	0	0	0
coracobrachialis	0	0	0
	0	0	0
	0	0	0
	0	0	0
	0	0	0
	0	0	0
infraspinatus	1.08869	-0.22422	-1.08344
	0	0	0
	1.14754	0.12077	-1.01042
	0.41019	-0.04753	-0.39224
	0.84204	0.28138	-0.67064
	0.83423	0.27646	-0.66487

teres minor	0 0 0 0 0 0	0 0 0 0 0 0	0 0 0 0 0 0
teres major	0 0 0 0 0 0	0 0 0 0 0 0	0 0 0 0 0 0
supraspinus	2.35181 2.42434 1.66672 1.83826 0.81810 0.76666	-0.80795 -0.86917 -0.65518 -0.79556 -0.41159 -0.42254	-1.03821 -0.87594 -0.89768 -0.7438 -0.51349 -0.41186
subscapularis	8.57719 8.78229 0 0 0 0	-0.40507 -0.92333 0 0 0 0	-9.24676 -9.25025 0 0 0 0
biceps longhead	7.82701	-0.48541	-7.19746
biceps shorthead	0	0	0

Table B2 *Passive forces and directions at 30 degrees of abduction.*

Passive forces	*fpasx*	*fpasy*	*fpasz*
gh-joint	-116.0226	11.351762	34.01224
ac-joint	47.45486	-4.01439	24.23066
thorax->ts	0	0	0
thorax->ai	17.35883	9.47339	45.96049
Lig. conoide	0.78322	7.49967	-2.13229

Table B3 *Muscle forces and directions at 60 degrees of abduction.*

Muscle	*fsx*	*fsy*	*fsz*
trapezius, scap part	-3.98794	-11.56978	-0.73951
	-7.6059	-13.66924	-0.54402
	-19.1616	-11.88875	-0.83239
	-23.54183	3.32447	-6.48357
	-20.77872	6.52084	-4.62202
	-20.59557	4.96991	-0.83894
trapezius, clav part	0	0	0
	0	0	0
	0	0	0
	0	0	0
	0	0	0
	0	0	0
levator scapulae	-0.80184	1.8455	-2.12203
	-0.71427	1.66569	-1.57812
	-0.62551	1.47067	-1.12438
pectoralis minor	0	0	0
	0	0	0
	0	0	0
	0	0	0
rhomboideus	0	0	0
	-0.81603	1.00573	-0.38116
	-4.4759	6.5392	-3.6051
serratus anterior	5.70872	-8.29025	-11.06519
	5.89363	-1.63715	-14.88617
	5.48679	4.22001	-14.66578
	4.14939	6.14276	-10.67211
	3.09068	3.52477	-7.71281
	2.69763	-1.10925	-8.30682
deltoidus, scap part	0	0	0
	0	0	0
	17.74283	-15.49603	-4.64854
	14.71033	-12.6765	-1.52998
	41.87601	-37.07658	-2.42394
	40.88693	-35.69482	1.28206
deltoidus, clav part	0	0	0
	0	0	0
	0	0	0
	0	0	0
	0	0	0
	0	0	0
coracobrachialis	0.21201	-0.11985	0.02793
	0.25059	-0.13684	0.03437
	0	0	0
	0	0	0
	0	0	0
	0	0	0
infraspinatus	4.27325	2.41512	-6.02126
	2.00736	0.29273	-3.36276
	3.38808	3.33956	-4.11672
	2.34249	1.74094	-3.36846
	2.32283	3.21632	-2.49925

	2.45329	3.54098	-2.76405
teres minor	0	0	0
	0	0	0
	0	0	0
	0	0	0
	0	0	0
	0	0	0
teres major	0	0	0
	0	0	0
	0	0	0
	0	0	0
	0	0	0
	0	0	0
supraspinus	5.19987	1.0484	-3.52699
	5.36023	0.87136	-3.23424
	3.29013	0.6384	-2.65433
	3.19974	0.3721	-2.1948
	1.56605	0.19521	-1.48894
	1.1682	0.06305	-1.02454
subscapularis	25.99998	18.86304	-35.52964
	29.88148	19.15084	-39.48182
	0	0	0
	0	0	0
	0	0	0
	0	0	0
biceps longhead	14.74033	10.16927	-23.04666
biceps shorthead	5.55798	-2.8586	0.72712

Table B4 *Passive forces and directions at 60 degrees of abduction.*

Passive forces	*fpasx*	*fpasy*	*fpasz*
gh-joint	-295.8906	28.81884	133.40768
ac-joint	95.00634	-69.33487	33.50674
thorax->ts	0	0	0
thorax->ai	66.304	15.65178	69.87326
Lig. conoide	-17.7714	69.94102	-5.7622

Table B5 *Muscle forces and directions at 90 degrees of abduction.*

Muscle	*fsx*	*fsy*	*fsz*
trapezius, scap part	-5.50288	-15.33278	-1.32251
	-10.16819	-17.28285	-1.33263
	-22.06102	-11.58373	-2.28718
	-20.41394	4.47387	-7.04704
	-15.76717	5.38529	-4.75604
	-14.37187	3.23337	-1.81385
trapezius, clav part	0	0	0
	0	0	0
	0	0	0
	0	0	0
	0	0	0
	0	0	0
levator scapulae	-0.73191	1.81395	-1.91269
	-0.61209	1.62295	-1.50041
	-0.45954	1.30072	-1.04306
pectoralis minor	0	0	0
	0	0	0
	0	0	0
	0	0	0
rhomboideus	0	0	0
	-1.19454	1.4481	-0.40162
	-4.00314	6.20455	-3.11501
serratus anterior	2.81397	-7.21111	-8.55329
	2.63426	-1.62013	-13.17416
	2.33953	4.04727	-12.47459
	2.19941	6.14452	-9.06843
	2.42149	4.13992	-7.3927
	3.10652	-0.27766	-9.87832
deltoidus, scap part	0	0	0
	0	0	0
	12.30968	-2.32558	-4.1936
	16.22316	-2.90814	-2.88955
	59.18431	-14.78356	-9.41017
	58.11705	-13.37129	-4.08696
deltoidus, clav part	0	0	0
	0	0	0
	0	0	0
	0	0	0
	0	0	0
	0	0	0
coracobrachialis	1.25258	-0.09279	0.06125
	1.28035	-0.07438	0.07122
	0.9646	-0.0625	0.03459
	1.0034	-0.04567	0.04408
	0.69866	-0.02418	0.02223
	0.72362	-0.01741	0.02647
infraspinatus	0.67111	0.53731	-0.98157
	0	0	0
	0	0	0
	0	0	0
	0	0	0

	0	0	0
teres minor	0	0	0
	0	0	0
	0	0	0
	0	0	0
	0	0	0
	0	0	0
teres major	0	0	0
	0	0	0
	0	0	0
	0	0	0
	0	0	0
	0	0	0
supraspinus	3.65382	1.47505	-3.13575
	3.58768	1.19059	-2.79701
	1.94705	0.78517	-1.90655
	1.66669	0.44652	-1.42306
	0.27491	0.08582	-0.30083
	0	0	0
subscapularis	26.83967	33.58499	-42.69094
	27.49615	30.76163	-42.28091
	2.36043	5.27204	-4.78463
	3.78211	7.90389	-7.97915
	0	0	0
	0	0	0
biceps longhead	3.50676	6.67786	-22.33007
biceps shorthead	22.41597	0.43761	1.34231

Table B6 *Passive forces and directions at 90 degrees of abduction.*

Passive forces	*fpasx*	*fpasy*	*fpasz*
gh-joint	-355.75504	-76.62833	148.24092
ac-joint	126.98706	-84.63385	30.44732
thorax->ts	0	0	0
thorax->ai	92.17575	18.67982	67.38283
Lig. conoide	-33.89642	100.62312	-9.40893

Table B7 *Muscle forces and directions at 120 degrees of abduction.*

Muscle	*fsx*	*fsy*	*fsz*
trapezius, scap part	-3.57066	-9.8701	-0.87454
	-6.67362	-11.26766	-0.94035
	-15.40977	-7.98385	-1.77247
	-15.44441	3.39463	-5.65955
	-12.08729	3.91515	-4.11047
	-10.80875	1.99307	-1.92004
trapezius, clav part	0	0	0
	0	0	0
	0	0	0
	0	0	0
	0	0	0
	0	0	0
levator scapulae	-0.60515	1.47604	-1.51992
	-0.46976	1.28682	-1.2024
	-0.35217	1.09176	-0.92079
pectoralis minor	0	0	0
	0	0	0
	0	0	0
	0	0	0
rhomboideus	0	0	0
	-3.02307	3.42103	-0.70559
	-4.73868	7.1863	-3.43348
serratus anterior	1.06253	-4.98893	-4.98957
	0.75374	-2.07371	-11.09687
	0.5779	3.34639	-10.97006
	1.25702	6.66424	-9.36672
	2.15074	4.60183	-7.82816
	2.55003	-0.06419	-8.22662
deltoidus, scap part	0	0	0
	0	0	0
	5.25889	1.92014	-2.81601
	5.69507	1.98328	-1.84281
	40.29919	8.96807	-13.27754
	39.37654	9.66916	-8.16564
deltoidus, clav part	0	0	0
	0	0	0
	0	0	0
	0	0	0
	0	0	0
	0	0	0
coracobrachialis	1.64161	0.50192	-0.06214
	1.47695	0.48116	-0.04618
	1.26013	0.39035	-0.06048
	1.56842	0.52393	-0.06322
	1.22496	0.41716	-0.06103
	1.39948	0.49557	-0.0634
infraspinatus	0	0	0
	0	0	0
	0	0	0
	0	0	0
	0	0	0

	0	0	0
teres minor	0	0	0
	0	0	0
	0	0	0
	0	0	0
	0	0	0
	0	0	0
teres major	0	0	0
	0	0	0
	0	0	0
	0	0	0
	0	0	0
	0	0	0
supraspinus	1.69898	0.87786	-1.71192
	1.56286	0.63877	-1.43933
	0.65786	0.3576	-0.71629
	0.30164	0.1069	-0.28555
	0	0	0
	0	0	0
subscapularis	12.86265	22.29788	-24.61053
	14.14869	21.73712	-26.1769
	2.60234	12.52464	-8.6313
	3.46138	15.22519	-11.57846
	0	0	0
	0.33558	1.99802	-1.36621
biceps longhead	-1.7303	-0.11579	-11.3281
biceps shorthead	19.71441	9.39381	-0.57026

Table B8 *Passive forces and directions at 120 degrees of abduction.*

Passive forces	*fpasx*	*fpasy*	*fpasz*
gh-joint	-273.42633	-175.08153	119.61259
ac-joint	124.88131	-27.28998	34.77024
thorax->ts	0	0	0
thorax->ai	85.23856	16.79879	45.63993
Lig. conoide	-26.67947	73.05117	-9.61185

Table B9 *Muscle forces and directions at 150 degrees of abduction.*

Muscle	*fsx*	*fsy*	*fsz*
trapezius, scap part	-0.18462	-0.4926	-0.05352
	-1.23337	-1.96506	-0.22978
	-5.68956	-2.38637	-0.91168
	-7.02499	2.19774	-2.9248
	-9.65239	3.79933	-3.82671
	-14.71684	3.46203	-3.5817
trapezius, clav part	0	0	0
	0	0	0
	0	0	0
	0	0	0
	0	0	0
	0	0	0
levator scapulae	-0.07124	0.18658	-0.18173
	0	0	0
	0	0	0
pectoralis minor	0	0	0
	0	0	0
	0	0	0
	0	0	0
rhomboideus	-0.19617	0.17679	0.02492
	-3.03263	3.60523	-0.66499
	-1.84952	3.00348	-1.37713
serratus anterior	0.23568	-1.4597	-1.42792
	0.17423	-1.63468	-9.71721
	0.06519	4.56769	-13.18063
	0.94777	7.50235	-9.53632
	1.37668	3.48666	-5.26472
	0	0	0
deltoidus, scap part	1.1092	1.51453	-1.07075
	1.02986	1.3535	-0.86902
	2.35577	3.48787	-2.8802
	2.30893	2.9632	-1.76508
	8.30339	8.70615	-6.44031
	9.07985	9.32142	-4.95727
deltoidus, clav part	0	0	0
	0	0	0
	0	0	0
	0	0	0
	0	0	0
	0	0	0
coracobrachialis	0.47323	0.42543	-0.10074
	0.48622	0.45445	-0.09826
	0.47415	0.42143	-0.10597
	0.49046	0.45704	-0.10358
	0.49371	0.45767	-0.10913
	0.50252	0.47806	-0.10749
infraspinatus	0	0	0
	0	0	0
	0	0	0
	0	0	0
	0	0	0

	0	0	0
teres minor	0 0 0 0 0 0	0 0 0 0 0 0	0 0 0 0 0 0
teres major	0 0 0 0 0 0	0 0 0 0 0 0	0 0 0 0 0 0
supraspinus	0 0 0 0 0 0	0 0 0 0 0 0	0 0 0 0 0 0
subscapularis	2.86722 3.01457 0.6616 0.7745 -0.21748 -0.32899	6.2008 5.70354 8.50736 8.59804 8.44388 7.82298	-5.99153 -6.05282 -4.49918 -4.96968 -3.68959 -3.77206
biceps longhead	0	0	0
biceps shorthead	5.06697	6.78363	-1.14403

Table B10 *Passive forces and directions at 150 degrees of abduction.*

Passive forces	*fpasx*	*fpasy*	*fpasz*
gh-joint	-97.18999	-156.34033	57.39833
ac-joint	62.46371	18.12464	26.28687
thorax->ts	0	0	0
thorax->ai	45.23466	8.50551	21.72360
Lig. conoide	-8.60231	23.55360	-3.85172

Table B11 *Muscle forces and directions at 180 degrees of abduction.*

Muscle	*fsx*	*fsy*	*fsz*
trapezius, scap part	0	0	0
	-0.03584	-0.05077	-0.00457
	-2.95484	-1.00357	-0.30858
	-4.4012	1.46622	-1.50752
	-7.66912	3.14263	-2.51195
	-12.95017	3.41516	-2.35585
trapezius, clav part	0	0	0
	0	0	0
	0	0	0
	0	0	0
	0	0	0
	0	0	0
levator scapulae	0	0	0
	0	0	0
	0	0	0
pectoralis minor	0	0	0
	0	0	0
	0	0	0
	0	0	0
rhomboideus	-0.34954	0.32202	0.05179
	-2.22045	2.61209	-0.39585
	-0.94889	1.46361	-0.6148
serratus anterior	0.11	-0.85606	-0.8542
	-0.14646	-1.09469	-8.22726
	-0.28922	4.13478	-10.39252
	0.39507	6.33908	-7.42153
	0.73745	2.58009	-3.62217
	0	0	0
deltoidus, scap part	1.02487	3.2263	-2.22119
	1.29202	3.86451	-2.44582
	0.15266	1.60142	-1.20298
	0.47619	2.24008	-1.27824
	0.62803	2.79347	-1.8503
	1.01946	3.38623	-1.72686
deltoidus, clav part	0	0	0
	0	0	0
	0	0	0
	0	0	0
	0	0	0
	0	0	0
coracobrachialis	0.07996	0.15638	-0.04296
	0.08865	0.18136	-0.04591
	0.07609	0.14277	-0.04155
	0.08665	0.17171	-0.04547
	0.08445	0.16213	-0.04505
	0.09133	0.1807	-0.04761
infraspinatus	0	0	0
	0	0	0
	0	0	0
	0	0	0
	0	0	0

	0	0	0
teres minor	0 0 0 0 0 0	0 0 0 0 0 0	0 0 0 0 0 0
teres major	0.03048 0.01919 0.0349 0.0094 0.02138 0	0.34526 0.26055 0.30983 0.10633 0.18365 0	-0.11499 -0.07894 -0.10005 -0.02895 -0.05417 0
supraspinus	0 0 0 0 0 0	0 0 0 0 0 0	0 0 0 0 0 0
subscapularis	0.18949 0.13924 0.114 0.13172 -0.085 -0.13749	0.4036 0.25753 1.7799 1.82203 1.98628 2.06841	-0.41009 -0.29067 -0.88702 -0.98523 -0.75288 -0.8327
biceps longhead	0	0	0
biceps shorthead	0.53206	2.02431	-0.3998

Table B12 *Passive forces and directions at 180 degrees of abduction.*

Passive forces	*fpasx*	*fpasy*	*fpasz*
gh-joint	-19.67327	-76.68541	24.20803
ac-joint	21.66381	13.46658	12.92563
thorax->ts	6.24933	2.99657	9.53133
thorax->ai	18.13156	3.23399	8.01389
Lig. conoide	-1.74797	4.86295	-0.58444

APPENDIX C

Adhesives

All physical and optical properties given are nominal values.

High-Modulus Materials

Cure Time (Hours)	Cure Temperature	Elongation (%)	Elastic Modulus *E* 1000 psi *(GPa)*	Max Usable Temperature °F *(°C)*	Standard Packaging
PC-1 Adhesive: For most applications using PS-1 and PS-6 sheets, and contoured sheets made from PL-1 and PL-8 liquids. Excellent bond strength with absence of creep. Relatively fast curing (12 hours at room temperature). Low viscosity enables very easy handling.					
12	Room	3	450 *(3.1)*	180 *(80)*	1 oz, 3 oz, pt, qt, gal*
PC-1T Adhesive: Same as PC-1 but with thixotropic agent added for bonding sheets to overhead or vertical surfaces. Also used for edge-bonding sheets and for building fillets.					
24	Room	3	450 *(3.1)*	180 *(80)*	3 oz, pt, qt, gal*
PC-8 Adhesive: Formulated and recommended for bonding sheets in post-yield studies where elongation exceeds 3%. Combines high strength and modulus characteristics with high-elongation properties.					
48	Room	5 (typical)	500 *(3.5)*	180 *(80)*	3 oz, pt*
PC-10 Adhesive: Same application as PC-1, except faster curing (3 to 4 hours at room temperature). Because its exothermic reaction is rapid, relatively small amounts should be mixed at one time.					
3 to 4	Room	3	450 *(3.1)*	180 *(80)*	3 oz, pt*

Medium-Modulus Materials

PC-6 Adhesive: A room-temperature, 24-hour-curing adhesive for applications requiring a low-modulus adhesive. Normally used for bonding PS-3 sheets, and coatings produced from PL-2 Liquid Plastic.

24	Room	50	30 *(0.21)*	400 *(200)*	3 oz, pt, qt, gal*

3oz : £23; £62 : 1pt

Low-Modulus Materials

PC-9 Adhesive: An extra-high-elongation material for use with PS-6 sheets, and contoured sheets made from PL-6 Liquid Plastic.

24	Room	>100	0.1 *(0.0007)*	300 *(150)*	3 oz, pt, qt, gal*

PC-11 Adhesive: A high-elongation material formulated for bonding contoured sheets prepared from PL-3 Liquid Plastics.

24	Room	>50	1 *(0.007)*	400 *(200)*	3 oz, pt, qt, gal*

PC-12 Adhesive: A high-elongation adhesive for bonding PS-4 sheets to rubber.

36	Room	>50	1 *(0.007)*	350 *(175)*	3 oz, pt, qt, gal*

*Metric equivalents for 1 oz, 3 oz, pt, qt, and gal are *28 g, 80 g, 0.47 litre, 0.950 litre, and 3.78 litre*, respectively.

For ordering information on all coating materials, refer to price list P-01.

Figure C1 *Adhesive materials (Measurements Group, 1992).*

Photoelastic Coatings

All physical and optical properties given are nominal values.

High-Modulus Materials

Strain Optical Coef. K	Elongation (%)	Elastic Modulus E 1000 psi *(GPa)*	ν	Thickness		Sensitivity Constant to °F *(°C)*	Max Usable Temperature °F *(°C)*
				in *(mm)*	Tolerance		
PS-1 Sheet: An excellent high-sensitivity plastic for accurate analysis in the elastic and elasto-plastic ranges of most metals. Supplied with a processed reflective backing to increase bond strength of the material. Very easy to machine. Exhibits no time-edge effects. Standard size sheets are 10 x 10 in, 10 x 20 in, 20 x 20 in and 20 x 30 in *(254 x 254 mm, 254 x 508 mm, 508 x 508 mm, 508 x 762 mm)*. Tolerance on sheet sizes greater than 10 x 10 in *(254 x 254 mm)* is ±0.004 in *(±0.10 mm)*.							
0.150	5	360 *(2.5)*	0.38	0.120 *(3.05)* 0.080 *(2.05)* 0.040 *(1.00)* 0.020 *(0.500)* 0.010 *(0.25)*	±0.002 *(±0.06)*	300 *(150)*	300 *(150)*
PS-8 Sheet: General-purpose clear plastic for analysis in elastic range of most metals. Slightly lower sensitivity than for PS-1. PS-8 features excellent transparency, and also joins exceptionally well to itself, making it useful for making multi-sheet photoelastic models that require bonding.							
(PS-8) 0.09	3	450 *(3.1)*	0.36	0.120 *(3.05)* 0.080 *(2.05)* 0.040 *(1.00)* 0.020 *(0.50)*	±0.003 *(±0.08)*	160 *(70)*	400 *(200)*
PL-1, PL-8 Liquid: Room-temperature-curing plastics for casting contourable sheets to coat complex shaped surfaces. PL-1 exhibits slightly higher sensitivity. However, PL-8 is recommended for long-term testing (>30 days), since it will not darken with age.							
(PL-1) 0.100 (PL-8) 0.08	3 3	420 *(2.9)* 420 *(2.9)*	0.36 0.36	For casting contourable sheets up to 0.125 in *(3.2 mm)*.		180 *(80)* 160 *(70)*	450 *(230)* 400 *(200)*

Medium-Modulus Materials

PS-3 Sheet: Generally used for analysis of non-metallic materials. Also used for post-yield investigations on metals.

0.02 (typical)	30	30 *(0.21)*	0.42	0.120 *(3.05)* 0.080 *(2.05)* 0.040 *(1.00)*	±0.003 *(±0.08)*	110 *(40)*	400 *(200)*
PL-2 Liquid: A room-curing plastic for casting contourable sheets. Uses are similar to type PS-3 sheet material.							
0.02 (typical)	50	30 *(0.21)*	0.42	For casting contourable sheets up to 0.125 in *(3.2 mm)*.		110 *(40)*	400 *(200)*

Low-Modulus Materials

PS-4 Sheet: Used for analysis of parts made of high-elongation materials such as rubber.

0.009 (typical)	>40	0.5 *(0.004)*	0.500	0.120 *(3.05)* 0.080 *(2.05)* 0.040 *(1.00)* 0.020 *(0.50)*	±0.003 *(±0.08)*	350 *(175)*	350 *(175)*
PL-3 Liquid: For casting contourable sheets. Similar to PL-2, but with higher elongation and lower modulus.							
0.002 (typical)	>50	0.2 *(0.0014)* *After one minute at constant strain.*	0.42	For casting contourable sheets up to 0.125 in *(3.2 mm)*.		90 *(32)*	300 *(150)*
PS-6 Sheet & PL-6 Liquid: Used for application on extra high-elongation materials.							
0.0006 (typical)	>100	0.1 *(0.0007)* *After one minute at constant strain.*	0.500	For casting contourable sheets up to 0.125 in *(3.2 mm)*.		90 *(32)*	300 *(150)*

Figure C2 *Coating materials (Measurements Group, 1992).*

Table C1 *Isochromatic fringe sequence (Measurements Group, 1992).*

Colour	*Fringe order (N)*
Black	0
Gray	0.28
White	0.45
Pale Yellow	0.60
Orange	0.80
Dull-red	0.90
Purple (tint of passage)	1.00
Deep blue	1.08
Blue-green	1.22
Green-yellow	1.39
Orange	1.63
Rose red	1.82
Purple (tint of passage)	2.00
Green	2.35
Green-yellow	2.50
Red	2.65
Red/green transition	3.00
Green	3.10
Green-yellow	3.65
Red	4.00
Red/green transition	
Green	4.15

Figure C2 *Dominant isochromatic fringe colours for full-field interpretation (Measurements Group, 1992).*

Colour	*Fringe order (N)*
Black	0
Yellow	0.6
Red	0.9
Purple (tint of passage)	1.0
Blue-green	1.2
Yellow	1.5
Red	1.75
Purple (tint of passage)	2.0
Green	2.2
Yellow	2.5
Red	2.8
Red/green transition	3.0
Green	3.2

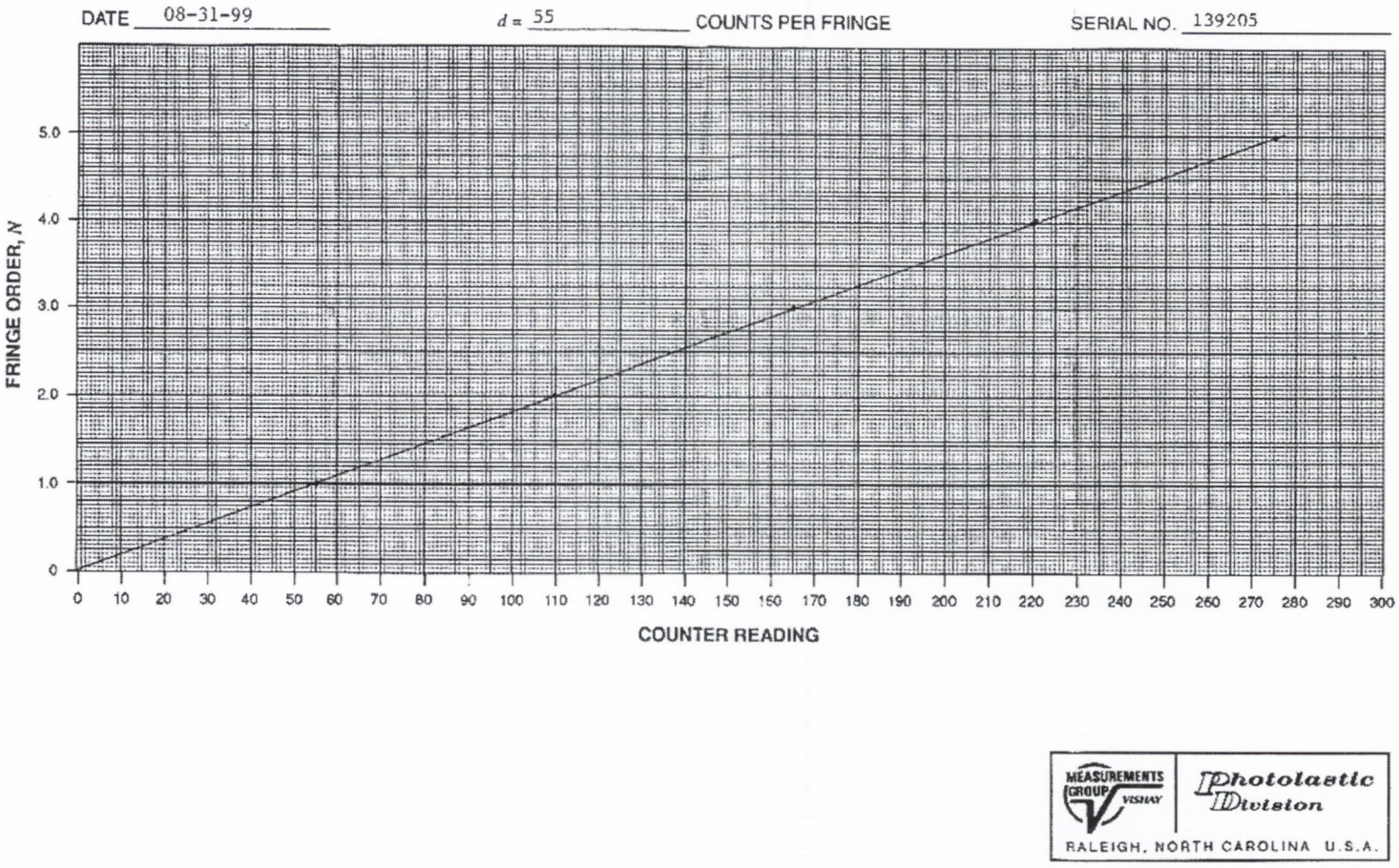

Figure C3 *Model 232 null-balance compensator calibration (Measurements, 1992).*